STUDIES OF THE OXIDATION OF ZINC DIALKYLDITHIOPHOSPHATES

AND RELATED COMPOUNDS

BY

JOHN LEONARD PADDY B.Sc.

A THESIS SUBMITTED FOR THE QUALIFICATION OF

DOCTOR OF PHILOSOPHY

BRUNEL UNIVERSITY

SEPTEMBER 1988

BRUNEL CHEMISTRY

DEPARTMENT

UXBRIDGE

SUPPORTED BY THE

MINISTRY OF DEFENCE

D.Q.A/TS WOOLWICH

ABSTRACT

Raman spectroscopic analysis of $Zn[(RO)_2PS_2]_2$ (ZDDP) and $Pb[(RO)_2PS_2]_2$ (R= ethyl or n-butyl) indicate that four sulphur atoms co-ordinate to each zinc atom whilst only two co-ordinate to each lead atom.

Dialkyl dithiophosphoric acids $(RO)_2P(:S)SH$ exhibit rotational isomerism about P-S and P-O bonds. Temperature-dependence studies of $\nu(SH)$ and $\nu(P-S)$ band intensities indicate ΔH for the equilibria to be 2.5 kJ mol^{-1}, R= iso-propyl ; 3 kJ mol^{-1}, R= n-butyl; $\sim$ 4.5 kJ mol^{-1}, R= n-octyl.

Thin film high pressure DSC analysis of solutions containing ZDDP's or related compounds reveal the following trend with respect to antioxidant effectiveness (R = n-octyl , R' = iso-octyl) :

$$(RO)_2P(:S)SH < [(RO)_2PS_2]_2 < Zn[(RO)_2PS_2]_2 < \text{commercial } Zn[(R'O)_2PS_2]_2.$$

Successive twofold dilutions of 0.08 M organothiophosphate antioxidant in squalane reduce the observed oxidation onset temperatures and increase the heats of reaction ; these tend towards values determined for pure squalane.

Dynamic DSC studies of cumene hydroperoxide (CHP) reduction (0.063 M) by n-butyl ZDDP and notable related compounds (0.04 M) in squalane produce the following trend of reactivity with respect to the decomposition of CHP (R= n-butyl) :

$$Zn[(RO)_2PS_2]_2 > [(RO)_2PS_2]_2 > RSH > R_2S_2 > (RS)_3P{=}S > R_2S > (RO)_2(RS)P{=}S.$$

Detailed investigations by dynamic and isothermal DSC on the reduction of CHP by $[(RO)_2PS_2]_2$ (R= n-octyl , n-butyl) indicate that the mechanism of hydroperoxide decomposition is autocatalytic.

The half-lives determined by P-31 NMR spectroscopic investigations on the oxidation of $Zn[(RO)_2PS_2]_2$ (R= n-octyl) to $[(RO)_2PS_2]_2$ and $OZn_4[(RO)_2PS_2]_6$ (basic ZDDP) by excess CHP (0.12 M) are i) in squalane 10 min ; ii) in cyclohexane 7 min ; iii) in nitrobenzene 46 min. In cyclohexane and squalane the remaining hydroperoxide oxidises n-octyl basic ZDDP to an uncharacterised basic salt that produces a P-31 NMR signal 0.2 ppm lower than n-octyl basic ZDDP, and $[(RO)_2PS_2]_2$. The basic ZDDP salts are more resistant to oxidation by CHP than ZDDP and major products from their oxidation include $[(RO)_2PS]_2S$, an unidentified dithiophosphate (with a P-31 NMR signal of 84.4 ppm w.r.t tributyl phosphate) and an unidentified monothiophosphate (49 ppm).

ACKNOWLEDGEMENT

I would like to take the opportunity to thank Dr. D.N. Waters for guidance provided throughout the course of this project. I am also grateful for the interest shown by Dr. C.M. Jenden , Mr. L. Butcher, Mr. J. Hunt and Mr. R. Williams.

I am indebted to Dr. W. Trott and Mr. P.S. Brook for their help in the fields of NMR spectroscopy and differential scanning calorimetry.

CHEMICAL ABBREVIATIONS

ABBREVIATION	CHEMICAL NAME	CHEMICAL FORMULA
ZDDP	Zinc dialkyl dithiophosphate	$Zn[(RO)_2PS_2]_2$
PbDDP	Lead dialkyl dithiophosphate	$Pb[(RO)_2PS_2]_2$
basic ZDDP	basic Zinc dialkyl dithiophosphate	$OZn_4[(RO)_2PS_2]_6$
DDPA	Dialkyl dithiophosphoric acid	$(RO)_2P(S)SH$
ADDP	Ammonium dialkyl dithiophosphate	$(RO_2)_2PS_2NH_4$
TDTP	Trialkyl dithiophosphate	$(RO)_2P(S)SR$
TTTP	Trialkyl trithiophosphate	$(RS)_2P(S)OR$
TTetTP	Trialkyl tetrathiophosphate	$(RS)_3P(S)$
TTPhate	Trialkyl trithiophosphate	$(RS)_3P(O)$
TTPhite	Trialkyl trithiophosphite	$(RS)_3P$
CHP	cumene hydroperoxide	$Ph(CH)_3)_2CO_2H$
DMA	N,N - Dimethyl acetamide	$CH_3C(O)N(CH_3)_2$
DMSO	Dimethyl sulphoxide	$(CH_3)_2SO_2$

Contents (i)

Contents (ii)

Contents (iii)

Contents (iv)

CHAPTER 1

LUBRICANTS

Lubrication is an essential feature of modern machinery and has been so throughout the ages. The first authenticated use of lubricants is found in the relics of ancient Egypt (1). It is probable that the massive stones of the pyramids were floated into place on thin semi-fluid layers of mortar.

1.1 Classification of Lubricants

Oils can be classified into two main types: mineral oils, and synthetic oils. Mineral oils can be divided into paraffinic and naphthenic oils. Oils, whose character lies between these extremes, are called mixed-base oils. The properties and quality of mineral oils depend on several factors: the source and viscosity range of base oil, the production processes and refining intensity, as well as on the blending and presence of additives. In cases where the requirements are not fully met by petroleum products, a more satisfying solution may be obtained by synthetic fluids with lube oil characteristics. Synthetic base oils are manufactured from relatively pure substances under controlled conditions and may belong to different chemical classes.

Broadly speaking, apart from the ability to lubricate rubbing surfaces, a good lubricant must have most or all of the following attributes:-

1. It should be chemically inert and have good oxidative and thermal stability;
2. It should be resistant to degradation by mechanically shearing forces and preferably be highly incompressible;
3. It should have good viscosity characteristics, ie it must have the correct room temperature viscosity and exhibit a small change of viscosity with temperature (VT behaviour);
4. It should have a low pour point for low temperature application and remain stable and nonvolatile for high temperature applications;
5. It should be compatible with, and have little effect on, materials of construction including metals and non-metallic materials such as seal and flexible hose elastomers;

6. It should be non-corrosive and non-toxic;

7. It should preferably be non-flammable, and for some applications, resistant to nuclear radiation.

1.2 Petroleum-Based Lubricating Oils

Lubricating oils are generally prepared from crude oils according to the following scheme:

Distillation, to adjust the viscosity and flash point;
Refining, to improve the ageing tendency and the VI properties;
Deashphalting of the residue from vacuum distillation ;
Dewaxing, to improve low-temperature properties;
Blending of different base oils and addition of additives, to give the finished product with the required assets.

The naphthenic oils contain significant amounts of cycloparaffins and aromatic hydrocarbons, while the paraffinic oils contain more paraffinic hydrocarbons and have a lower density and viscosity/temperature relationship. They have unfavourable cold properties due to wax separation (at least until they have been dewaxed), and as a rule, lower sulphur content. Base oils of different origin but of the same type are often similar but by no means identical.

1.3 Synthetic Lubricants

Several classes of organic compounds have been developed since 1930 which are used today as base oils for so-called synthetic lubricants. These include phosphoric acid esters, phosphonic acid esters, silicones, silicate esters, polyhalogen hydrocarbons, polyethers (polyglycols, polyphenyl ethers), esters (of mono and polybasic carboxylic acids of mono and polyvalent alcohols), fluorinated compounds (esters), and synthetic hydrocarbons such as polyolefins and alkylaromatics.

A brief description of the principal classes of synthetic lubricants is given here (2,3).

1.3.1 Polyglycol Lubricants

These are based on the following formula :

$$R^1O[CH_2CHR^2-O]_nR^3$$

A large number of different structures can occur, leading to both water-soluble and water - insoluble polymers. The hygroscopic character of the polyglycols is a function of the content of hydroxyl groups. An increase in mass number and ether bonds decreases the hygroscopic property.

The viscosity/temperature characteristics of water - insoluble polyglycols are good and they have low pour points. The oxidation resistance and thermal stabilities of polyglycol lubricants are not especially high. The strongly polar nature of polyglycols, caused by the oxygen atoms, gives the oils a strong affinity for metals. This reduces metal wear. The good dissolving power of polyalkylene glycols prevents the separation of sludge but has unfavourable effects on plastics.

1.3.2 Dibasic Acid Esters

The structural formula of such esters is as follows:-

$$R^1O-C(O)-R^2-C(O)-OR^1$$

R^1 derives from the alcohol used and R^2 from the acid. Two examples of dibasic esters in practical use are dioctyl sebacate and di-iso-octyl azelate. The oxidation stability of such oils is not exceptional but is better than that of petroleum fluids. They have a good thermal stability and viscosity characteristics.

1.3.3 Neopentyl Polyol Esters

These are a group of "hindered" esters formed from organic acids and polyfunctional alcohols such as:-

$$CH_3CH_2C(CH_2OH)_2$$

These have many desirable properties of a good lubricant including good viscosity/temperature characteristics, low pour point and good lubricity, without the use of additives. Oxidation inhibitors are necessary when the esters are used in excess of 200 deg C.

1.3.4 Phosphate Esters

$$(RO)_3P(O)$$

Thermal and hydrolytic stabilities of phosphate esters are structure-sensitive and oxidation stability is good. Phosphate ester lubricants are fire resistant. Good viscosity and VT characteristics give phosphate esters good lubricity properties.

1.3.5 Silicate Esters and Disiloxanes

$$Si(OR)_4 \qquad\qquad [Si(OR)_3]_2\text{-}O$$

The most common types of silicate esters are tetra-alkyl, tetra-aryl and the mixed alkyl-aryl orthosilicates. The esters are liable to hydrolysis. The alkyl derivatives exhibit the best viscosity/ temperature characteristics but branching adversely affects their VT performance. They are more resistant to heat than corresponding carboxylic acid esters. Their low resistance to oxidation is comparatively easily improved by the use of antioxidants. The silicate esters and disiloxanes are not intrinsically corrosive to metals but rust inhibitors are used to deal with any water formed from their decomposition.

1.3.6 Silicones

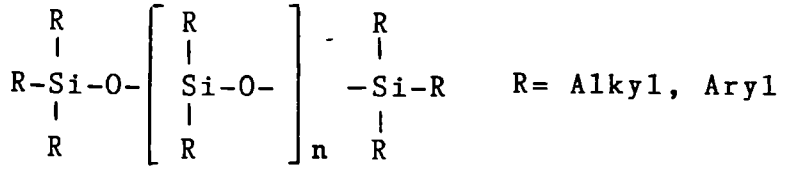

The linear polymers range from low boiling fluids through to gums. They have extreme chemical inertness and heat resistance. The physical and chemical properties of typical silicone fluids fulfil most of the requirements of an ideal lubricant except boundary lubrication. Silicone fluids do not rely on the use of additives for their properties. The fluids owe most of their properties to molecular flexibility, their low intermolecular forces, and their lack of chemical reactivity. Under boundary conditions of lubrication, there is very little physical adsorption onto the metal surface and no chemical interaction between the silicone and the metal surface. A film of the fluid is too compressible to have any appreciable load - carrying capacity. Antiwear additives are generally unsuitable because of their incompatibility with the fluid. Chlorination of the side chain partly alleviates this problem.

1.3.7 Chlorinated Hydrocarbons

Chlorinated hydrocarbons such as the chlorinated biphenyls and chlorinated aliphatics such as hexachlorobutadiene and the chlorinated paraffins have applications as lubricants and hydraulic fluids. The chlorine content of these compounds imparts good lubricating and fire resistant properties, but in the more reactive compounds it can also be a source of corrosion. Chlorinated hydrocarbons have good thermal stability. Their applications are limited by comparatively poor VT characteristics and high pour point.

1.3.8 Chlorofluorocarbons

The low-molecular weight chlorofluorocarbon polymers of interest as lubricants are made by polymerizing $CF_2C1CFC1_2$. They have outstanding oxidative stability and thermal resistance. They have comparatively poor VT characteristics. Their performance in wear tests is comparable with that of conventional gear lubricants containing EP additives.

1.3.9 Polyphenyl Ethers

The properties of these materials may be varied by changing the length of the chain, changing the point of attachment to the benzene ring and incorporating alkyl or other substituents in the phenyl groups. The liquid polyphenyl ethers have higher pour points than most synthetic lubricants but their VT characteristics are reasonably good. They have good resistance to oxidation and very high threshold temperatures of thermal degradation. The high pour point is not considered to be a major disadvantage in their use.

1.3.10

Other types of lubricants are perfluoropoly-alkyl ethers, tetrahydroforan tetrahydrofuran polymers and polythioether oils.

1.4 Chemical Additives

Additives are necessary to satisfy the modern requirements of lubrication technology. Although additives have been used for centuries, it is only since the 1940's that serious development has arisen to enhance or to modify specific natural properties of lubricating oils.

Additives may affect the physical properties of the oil (VT characteristics, crystallization tendency etc), or may have a chemical effect. They can assist each other resulting in a synergistic effect, or they can have antagonistic effects. The additive concentrates are usually 50% active ingredients in a mineral diluent oil.

1.4.1 Additive Types (Crankcase Lubricants)

In the last 40 years additives have been developed to facilitate improvements in particular directions, ie:

1) High temperature properties to control deterioration of the lubricant in service.

2) Low temperature characteristics to prevent the formation of deposits arising from contamination of the oil with partially burnt fuel, etc., as well as to maintain the fluidity of the lubricant at low starting temperatures.

3) Improvement of overall wear properties.

The provision of these essential characteristics depends upon a correct selection of the lubricating oil base stocks, and the use of a combination of additives matched to these base stocks to enhance their natural properties. Oxidation inhibitors are the main concern of this thesis. A brief outline of various antioxidants and their activity is given here. Oxidising conditions are present at many points in any gasoline or diesel engine. The oxidation reactions that occur in a lubricant at elevated temperatures in the presence of atmospheric oxygen lead to ageing of the oil. The oxidation of petroleum hydrocarbons proceeds according to a radical chain mechanism via alkyl and peroxy radicals. A consecutive radical chain mechanism is then started by reaction of these radicals with hydrocarbon molecules. Further reactions of the peroxy radicals or other radicals lead to alcohols, ketones and carboxylic acids.

In mineral oils further oxidation leads to sludge and carbon deposits. Antioxidants interrupt the radical chain mechanism of these autoxidation processes by removal of the radicals and / or by decomposition of hydroperoxides. The build-up of oil oxidation products (acids) enhances corrosion. Metal salts come out of solution causing deposits. Metals catalyse the autoxidation ; therefore, antioxidant combinations used are metal deactivators, radical scavengers, and hydroperoxide decomposers.

1.4.2 Classification of Antioxidants

The following types of compounds are used as antioxidants:

a) Sulphur compounds
b) Phosphorus compounds
c) Sulphur/phosphorus compounds
d) Amines and phenolic derivatives

1.4.2.1 Sulphur Compounds - Elemental sulphur is a good antioxidant but is not used because of its corrosive nature. Sulphurised sperm oil was one of the original inhibitors used. Other sulphur - containing inhibitors are sulphides, disulphides, thiols, phenol sulphides, mercapto-benzimidazoles thiophene derivatives, and thio alkelydes.

1.4.2.2 Phosphorus Compounds - Phosphorus - containing antioxidants include triaryl and trialkyl phosphates. Combined phosphoric acid/phenol derivatives, for example 3,5-di-tert-butyl- 4-hydroxybenzyl-phosphoric acid dialkyl esters, are good antioxidants.

1.4.2.3 Sulphur-phosphorus compounds are more effective than antioxidants containing just sulphur or phosphorus. Zinc dialkyldithiophosphates (ZDDP's) are hydroperoxide decomposers, and free radical scavengers. They are also corrosion inhibitors and extreme pressure additives.

1.4.2.4 Phenol derivatives - Naphthols and sterically hindered dinuclear or trinuclear phenols act as antioxidants. Electron donor substituents increase the efficiency of the compound. These stabilize the phenolic radical produced by hydrogen transfer to a peroxy radical. The phenolic radical is far more stable than the peroxy radical and will not abstract a hydrogen atom from the lubricant.

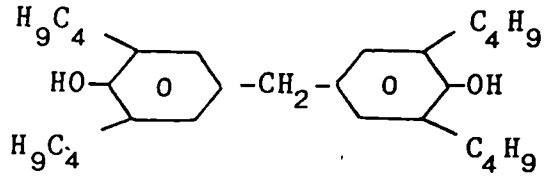

Methylene 4-4- bis
(2,6 tert-butylphenol)

1.4.2.5 Amines - Diphenylamine and phenyl- alpha-naphthylamine have been and are used in highly refined turbine oils. They are most effective at temperatures below 120 deg C. Their own oxidation products are oil soluble.

1.4.3 Metal Deactivators

$$Fe^{3+} + RO_2H \longrightarrow Fe^{2+} + H^{\oplus} + RO_2\cdot$$

$$Fe^{2+} + RO_2H \longrightarrow Fe^{3+} + OH^{\ominus} + RO\cdot$$

Metal deactivators chelate the metal ions and prevent the above reactions. They are added to oils in low concentrations, 5-30 mg/kg. N -disalicyclidene-ethylamine and N,N-disalicylidene -ethylamine are two examples of metal deactivators:-

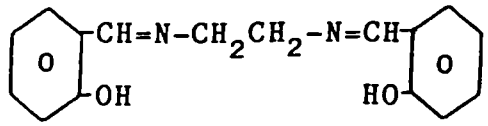

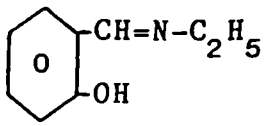

1.4.4 Viscosity Index Improvers

These compounds improve VI characteristics, ie. they reduce the decrease of viscosity with increasing temperature. VI improvers are polymers which are present in oils as colloidal dispersions. The viscosity- modifying effects of these additives can be attributed to the effect of temperature change upon their solvation in the oil. Polymethacrylates and polyisobutylenes are widely used commercially. At low temperature the polymers are curled up. When the temperature is raised the molecules uncurl and act as thickening agents. In a poor solvent the polymer chains attract each other and displace solvent molecules. When choosing a VI improver one has to balance two competing factors: increasing shear stability, viz polyacrylates < polymethacrylates < polyfumarates < polyisobutylenes, with decreasing VI improvement in the same order.

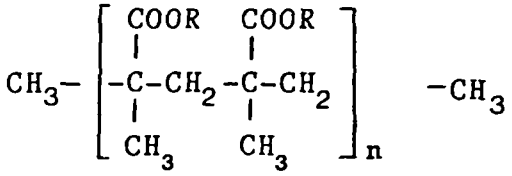

Alkyl methacrylate

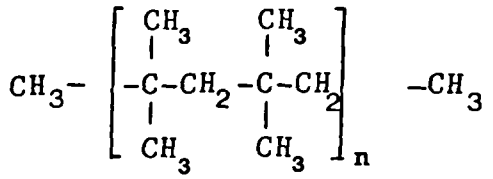

Polyisobutylene

1.4.5 Pour Point Depressants

At low temperatures the viscosity of oils increases and dissolved wax separates from the oil. The pour point depressant deposits a film on the wax crystals, interrupting the crystal growth, and thereby reducing the pour point. Polyalkylnaphathalenes, polyalkylphenols, or polyalkylmethacrylates are commercial pour point depressants and have molecular weights ranging from 2,000 - 10,000.

1.4.6 Detergent and Dispersant Additives

Dispersant and detergents are added to engine oils to suspend and disperse oxidation products, carbon deposits, and resins in the oil. This prevents any varnish or lacquer formation. Crail, et al. (4), give the following definition: "Additives capable of dispersing cold sludge are referred to as dispersants, whilst those for handling higher temperature dirts are referred to as detergents." Detergents must have the following properties to be effective:

a) Hydrophilic (oleophobic) groups ie. sulphonate, hydroxyl, mercapto, carboxylic, or carbonamide constituents.

b) Oleophilic (hydrophobic) aliphatic, cycloaliphatic or alkylaromatic hydrocarbon groups. These improve the detergents' oil solubility.

c) Usually one or several metal ions (aluminium, barium, calcium, magnesium, zinc), or amino groups.

To prevent resin formation detergents can react with hydroxyacids. Hydroxyacids are oil oxidation products. They also neutralize acids of sulphur dioxide and trioxide. They therefore act as corrosion inhibitors. Detergents can be normal, (stoicheiometric amounts of metal), basic, or overbased. Basic and overbased detergents contain a significant excess of metal oxides, hydroxides, carbonates, etc., in colloidally dispersed form. Overbased detergents are necessary in engines where large amounts of acidic compounds are formed. Examples of metal detergents are alkaline-earth sulphonates, salicylates and, thiocarbamates.

"Ashless", that is, metal-free detergents have been more recently developed possessing a special dispersing ability. The acrylated amines are ashless detergents which are moderately effective as detergents but are very good dispersants. Dispersant additives aid the prevention of sludge formation under low temperature operating conditions. Examples of dispersants are polypolar polymers of amides of acrylates, methacrylates and polycarboxylic acids.

1.4.7 Extreme Pressure Additives

These are added to oils to inhibit metal-to-metal destructive contact. Phosphorus, sulphur and chlorine atoms are the primary reaction partners of metals, giving a surface layer which prevents scuffing and welding.

Sulphur Compounds - Disulphides such as butylphenoldisulphide have moderate EP activities. Sulphurised polyisobutene is more effective. These compounds form sulphide layers on the surface of the metal.

Chlorine Compounds - A compromise must be made with EP properties and corrosivity with chlorine compounds. The more reactive the chlorine atom the more easily a chloride layer is formed. However, in the presence of moisture HCl can be formed. Chlorinated aliphatics are favoured more than chlorinated aromatics because they are less stable.

Phosphorus Compounds - Examples of phosphorus EP additives are trialkyl phosphates, salts and amines of dialkyl phosphates, butyl phosphonate, diphosphoric acid esters and trialkylphosphines.

Phosphorus-Sulphur Compounds - Important phosphorus-sulphur EP additives are acidic and neutral alkyl and aryldithiophosphates. ZDDP is a good EP additive as well as being a corrosion inhibitor and antioxidant. The thermal degradation products of ZDDP's also have good EP properties. ZDDP's form at least two layers on the metal surface; a thiophosphate and an iron (II) sulphide layer (5).

1.4.8 Corrosion Inhibitors

A corrosion inhibitor forms a protective layer on the surface of the metal, preventing the access of water or oxygen. Physical inhibitors have long alkyl chains with polar groups which are adsorbed onto the metal to form a hydrophobic layer. Examples of corrosion inhibitors are basic nitrogen compounds such as tertiary amines, fatty acid amides, basic alkaline earth sulphonates, and phosphoric acid derivatives such as thiophosphoric acid esters.

Chapter 1

1) Davidson C., Wear 1957, 1(2), 155-159.

2) Braithwaite E.R., "Lubrication and lubricants", Elesvier Publishing 1967.

3) Klamann D., "Lubricants and related products", Verlag Chemie GmbH, D6940 Weinheim, 1984.

4) Crail I.R.H, J. Inst. Petrol. 1963, 49, 189.

5) Bird R.J. et al., A.S.L.E. Trans 1980, 23, 121-130.

CHAPTER 2

The Role Of ZDDP's In Lubricating Oils

The use of either sulphur- or phosphorus- containing additives in lubricants had its beginning prior to 1920. However, it was not until the late 1930's that metal dithiophosphates, in particular, zinc dithiophosphates began to receive attention as lubricating oil antioxidants, bearing corrosion inhibitors and antiwear agents. In this chapter the function of ZDDP's will be described. In the section dealing with antioxidant action (2.3), the discussion will be extended to include other metal dithiophosphates.

2.1 Anti-wear Properties of ZDDP's

The term wear in internal combustion engines embraces:

1. Corrosive wear of bearings caused by oil decomposition products.
2. Corrosive wear of ferrous parts such as the cylinder bore in the ring travel region, caused by mineral acids originating from the fuel.
3. Abrasive wear caused by air-borne solids.
4. Surface wear, caused by actual rubbing of mating parts associated with conditions of boundary lubrication.

ZDDP's have their greatest effect on the fourth kind of wear.

One popular theory is that ZDDP itself is not substantially chemisorbed on iron but that its decomposition products are adsorbed and these supply the antiwear function (1). Alternatively, or in addition, ZDDP may be initially adsorbed and may then undergo decomposition on the surface. Spedding & Watkins, (2) using ESCA elemental analysis observed that the adsorption of zinc, sulphur and phosphorus occurred at temperatures at which decomposition of ZDDP would be expected. The authors argue that the antiwear function is facilitated by fusible glassy compounds, zinc phosphates or polyphosphates, adsorbed onto the iron oxide surface, and iron sulphides as a ternary eutectic with iron oxide.

However, other authors using various experimental methods suggest that ZDDP's form at least two layers on the metal surface, a thiophosphate layer and an iron (II) sulphide layer (3).

2.2 Corrosion Inhibitory Action of ZDDP's

Various investigators (4) have suggested that both an oxidising agent and an acid are necessary for the attack on the lead phase in copper-lead bearings. ZDDP's inhibit corrosion by decomposing organic peroxides, and by causing film formation on the bearings. The formation of films on metal surfaces suggests that the additive acts at least in part by the elimination of the catalytic effect of metal surfaces or by preventing formation of metal-organic compounds which act as catalysts.

2.3 Antioxidant Action of ZDDP's and Other Additives

Oxidation is the most important process leading to engine oil degradation in internal combustion engines. The process is initiated either by combustion-derived free radicals (5), or by free radicals produced by decomposition of primary oxidation products, for example, hydroperoxides. Both these initiation processes lead to the formation of peroxy radicals which propagate oxidation reactions and form hydroperoxides.

Autoxidation scheme (refs 6 and 7)

	$RH + O_2 \longrightarrow R\cdot + HO_2\cdot$
Initiation	$RO_2H \longrightarrow RO\cdot + \cdot OH$
	$2RO_2H \longrightarrow RO\cdot + RO_2\cdot + H_2O$
Propagation	$RO_2\cdot + RH \longrightarrow RO_2H + R\cdot$
(Chain reaction)	$R\cdot + O_2 \longrightarrow RO_2\cdot$
Termination	$2R\cdot \longrightarrow R-R$
	$R\cdot + RO_2\cdot \longrightarrow RO_2R$
	$RO_2\cdot \longrightarrow$ non radical products $+ O_2$

There are two ways in which antioxidants can function to inhibit autoxidation, (8). Preventative antioxidants act in some way to reduce the rate of initiation, while chain-breaking antioxidants intercept the chain propagating peroxy free radicals and thus terminate the chain reaction. Each type includes a variety of compounds and possible modes of action are indicated in the following classification.

Preventative Antioxidants

1. Light Absorbers (not important in oils)
2. Metal Deactivators
3. Hydroperoxide Decomposers

Chain-Breaking Antioxidants

1. Free Radical Traps
2. Electron Donors
3. Hydrogen Donors

Preventative antioxidants include various organic sulphur compounds, for example alkyl sulphides and disulphides,(7).

Metal deactivators chelate metal ions (eg. Cu,Fe,Mn and Co), thus preventing the catalytic acceleration of autoxidation of lubricants. Compounds such as triethylenediamine, ethylenediamine- tetra-acetic acid, phosphoric acid, citric acid and gluconic acid are effective chelating agents for metal ions and are used at very low concentrations.

Hindered phenols and amines (ashless antioxidants) are chain-breaking antioxidants which act as hydrogen donors to peroxy radicals. The literature often refers to these additives as radical scavengers.

2.3.1 Metal Complexes (Dithiophosphates $[(RO)_2PS_2]_2M$, Dithiocarbamates $[(R_2NCS_2)]_2M$ and Xanthates $[ROCS_2]_2M$ and their Mechanism of Antioxidant Action

The mechanism of antioxidant action of metal DDP's is highly complex and many different schemes are postulated in the literature. However, it is generally accepted that ZDDP's act as both chain-breaking antioxidants (radical scavengers) and preventative antioxidants (hydroperoxide decomposers). There is a large amount of material in the literature that documents the reaction of ZDDP's and related compounds (zinc dithiocarbamates, nickel dithiophosphates, nickel dithiocarbamates and zinc xanthates), with hydroperoxides and peroxy radicals.

Various authors have followed the decomposition of hydroperoxides due to the presence of an antioxidant, by monitoring the disappearance of the 3520 cm^{-1} band in the infra-red spectrum (9,10), by iodiometric titration (11), or by HPLC (12). The distribution of products from hydroperoxide decomposition has been considered to indicate whether the mechanism is homolytic or heterolytic, but there is a certain amount of argument as to which products correspond with which mechanism.

Alkyl radicals can be produced by the thermal or photochemical decomposition of azo-bis-isobutyl- nitrile (AIBN). These alkyl radicals can react with molecular oxygen to form peroxy radicals necessary to initiate autoxidation. Hydrocarbon autoxidation can be monitored by observing oxygen absorption. An antioxidant can prevent oxygen absorption by scavenging peroxy radicals. Bateman and Cunneen (13), describe a method of determining oxygen absorption.

The AIBN- initiated autoxidation of cyclohexene is represented as follows, (14).

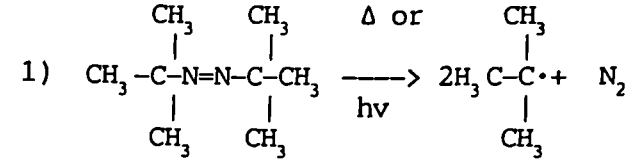

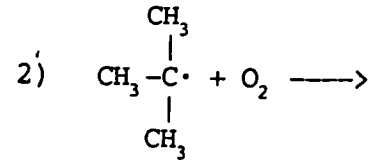

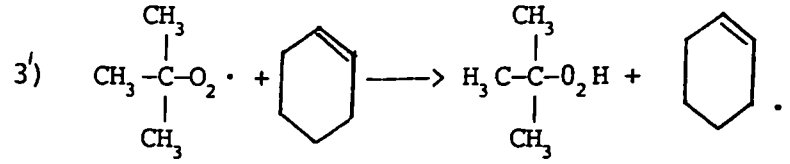

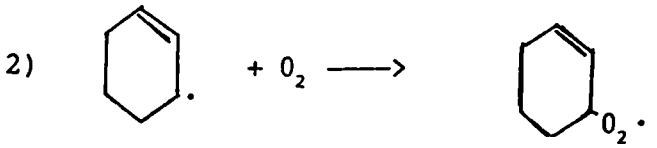

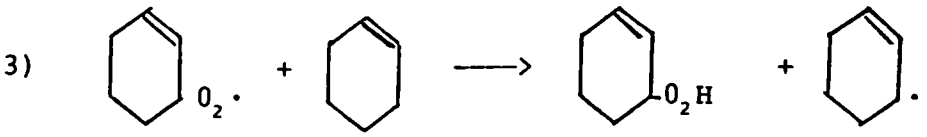

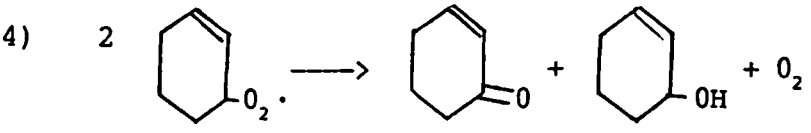

Reactions 2 and 3 make up the main chain propagation sequence. When no antioxidant is present reaction 4 is the inefficient termination reaction, (15).

Metal Complexes as Radical Scavengers

Colclough and Cunneen (16), were the first authors to prove that ZDDP's and similar compounds can act as chain breaking antioxidants as well as hydroperoxide decomposers, described by Larson, (4). When the autoxidation of squalene was catalysed by AIBN the order of reactivity was found to be as follows: phenothiazine > zinc dithiophosphate > zinc xanthate > zinc dithiocarbamate. If uncatalysed by AIBN at 75 deg C the order of reactivity was found to be phenothiazine > zinc xanthate > zinc dithiophosphate > zinc dithioarbamate. The authors suggested that the zinc salts convert the peroxy radicals into peroxy anions by the abstraction of an electron from the electron- rich sulphur atom.

Burn (17), performed azonitrile-initiated oxidation of cumene and indene and observed that a disulphide $[(RO)_2 PS_2]_2$ was a product from the reaction of peroxy radicals with ZDDP. This disulphide was found not to be a radical scavenger. The author states that the mechanism postulated by Colclough and Cunneen is inadequate because the oxidation of indene would not be inhibited by this mechanism. The dithiophosphate radical, Burn argues, would be expected to add to the indene double bond to form an alkyl radical which could promote autoxidation. The author considers this behaviour to be analogous to the radical addition of DDPA $(RO)_2 PS_2H$ to double bonds, (18). Burn therefore assigns scheme B , as the correct mechanism.

Scheme A - Cunneen and Colclough (16)

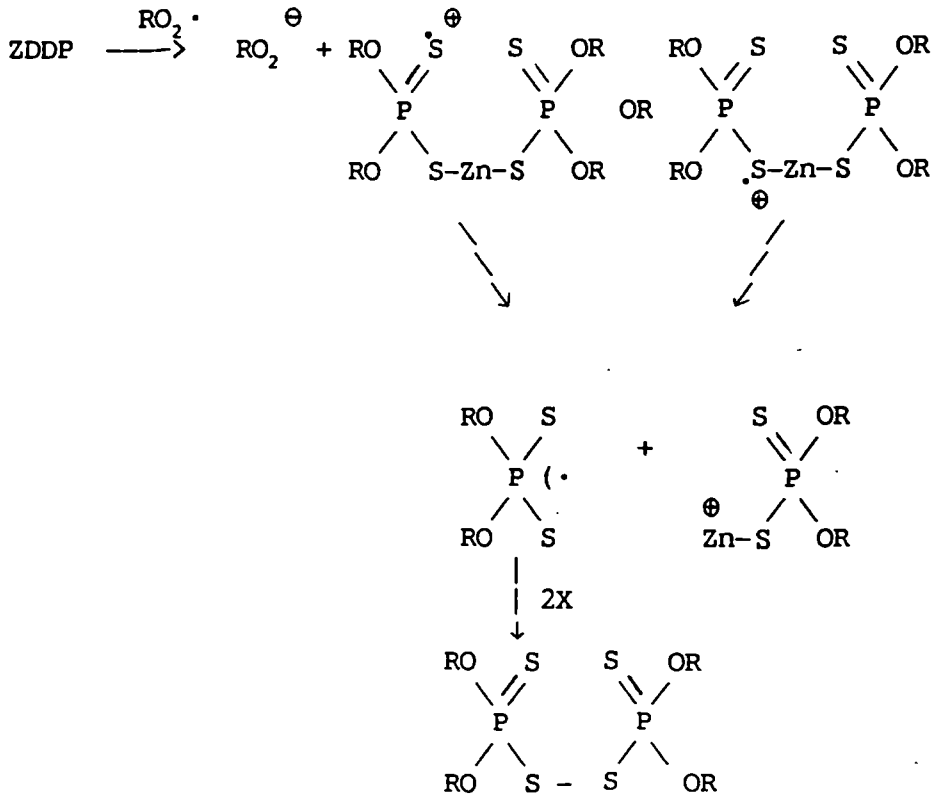

Scheme B - Burn (17)

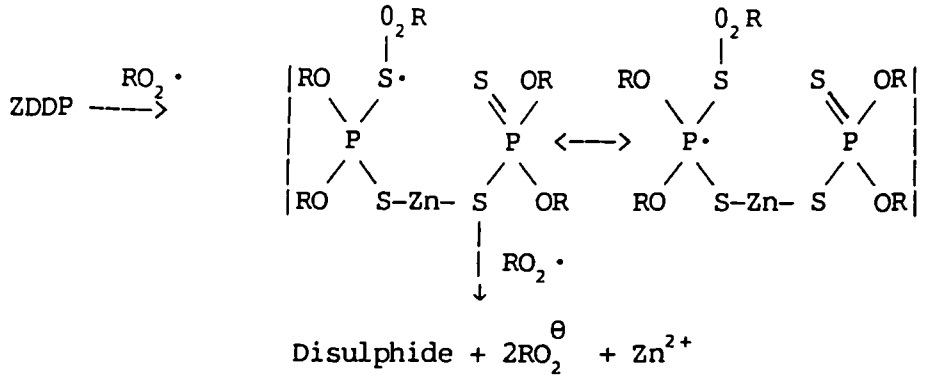

Howard et al (19), analysed the photochemically and thermally initiated AIBN autoxidation of styrene, tetralin, cyclohexene in the presence of ZDDP, zinc xanthate, and zinc dithiocarbamate (ZDTC). The order obtained for radical scavenging activity confirmed Colclough and Cunneen's deductions. The authors stated that: "It is most probable that the reaction of ZDDP's and related zinc complexes with peroxy radicals occur at the metal centre rather than at a sulphur atom". The argument was supported by evidence that $[(iPrO)_2PS_2]_2$ or $(RO)_2P(S)SR$ do not react with peroxy radicals at low temperatures, and the small pre-exponential factors that were calculated for the reaction of ZDDP and peroxy radicals were proposed to be consistent with attack at a sterically protected central atom.

The authors therefore suggested that either an electron transfer reaction or a SN2 process must occur at the zinc centre.

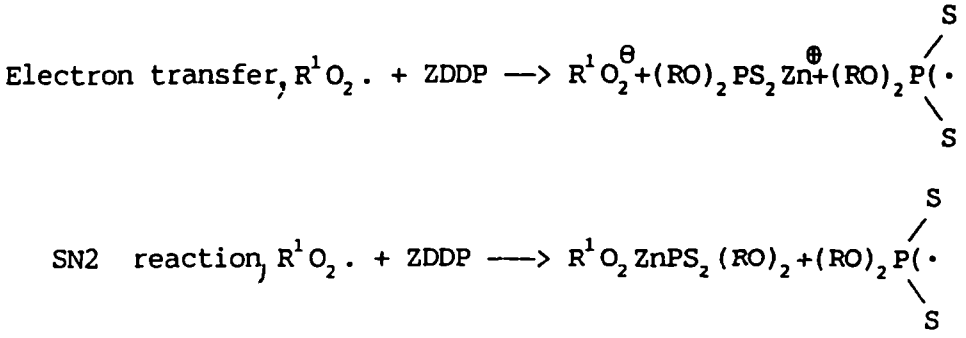

In further work (20), Howard et al performed similar experiments on nickel carbamates and dithiophosphates. The products from the reaction of cumyl peroxy radicals and the antioxidant were analysed. The main product was methyl styrene with smaller amounts of acetophenone and cumyl alcohol. To explain the distribution of products the authors postulated the following mechanism, rather than the electron or SN2 mechanism previously described:-

$$RO_2\cdot + MX_2 \longrightarrow RO_2MX_2 \longrightarrow RO\cdot + OMX_2$$

Cumyl alcohol was reported to be formed by hydrogen abstraction involving cumyloxy radicals. Methyl styrene results from the Lewis acid dehydration of cumyl alcohol. This Lewis acid is formed from the oxidation of the nickel dithiophosphate complex. Acetophenone, the authors argued, is derived also from the cumyloxy radical:-

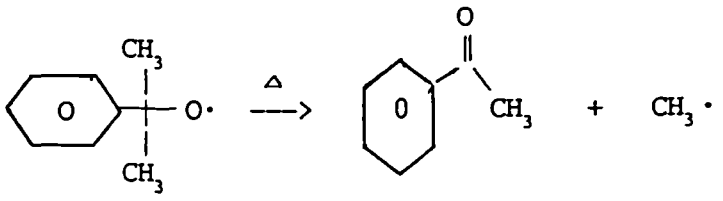

The authors claimed that only a fraction of these alkoxy radicals must escape the solvent cage or the compounds would not inhibit autoxidation.

L R Mahoney et al (14), titrated an antioxidant species with peroxy radicals formed at a constant rate from the decomposition of a free radical initiator. The authors determined that four peroxy radicals reacted with one molecule of 4 ,4 - methylene bis 2, 6- di-tertbutylphenol and three peroxy radicals reacted with one ZDDP molecule to give radical products. However, no mechanism was proposed other than the following simplified reaction scheme:-

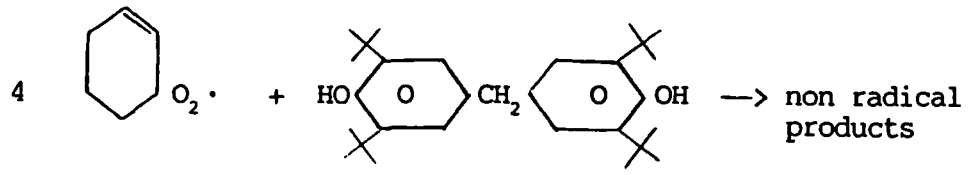

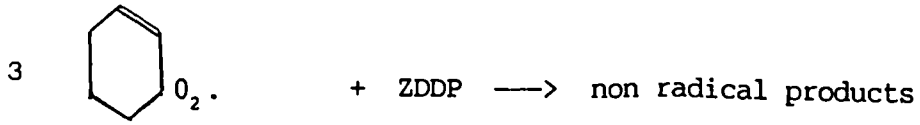

2.3.2 The Reaction of ZDDP's, NiDDP's and NiDTC's etc with Hydroperoxides

Colclough and Cunneen (16), concluded that the efficiency of decomposition of t-butyl hydroperoxide by various studied antioxidants had the following order : zinc isopropyl xanthate > isopropyl ZDDP > isopropyl ZDTC > phenothiazine.

J.D. Holdsworth et al (21), studied the decomposition of hydroperoxides by metal dithiocarbamates and dithiophosphates. The authors observed that the complexes were converted into an effective catalytic non-radical forming hydroperoxide decomposer in a radical generating reaction. It was argued that SO_2 was this catalytic hydroperoxide decomposer. Zinc dithiocarbamates proved to be pro-oxidants initially, before becoming effective hydroperoxide decomposers. This, it was argued was the result of the below reaction:-

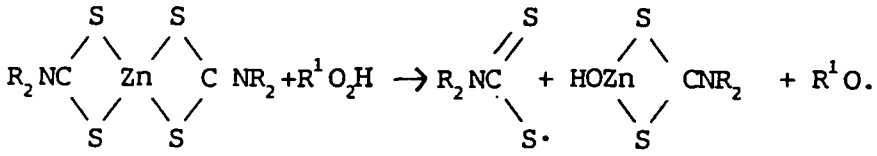

The authors claimed that the thioyl radical is oxidised to give SO_2. ZDDP's however, did not show any initial pro-oxidant activity. It was concluded that depending on the molar ratios of metal complex to hydroperoxide the following hydroperoxide decomposition occurred:

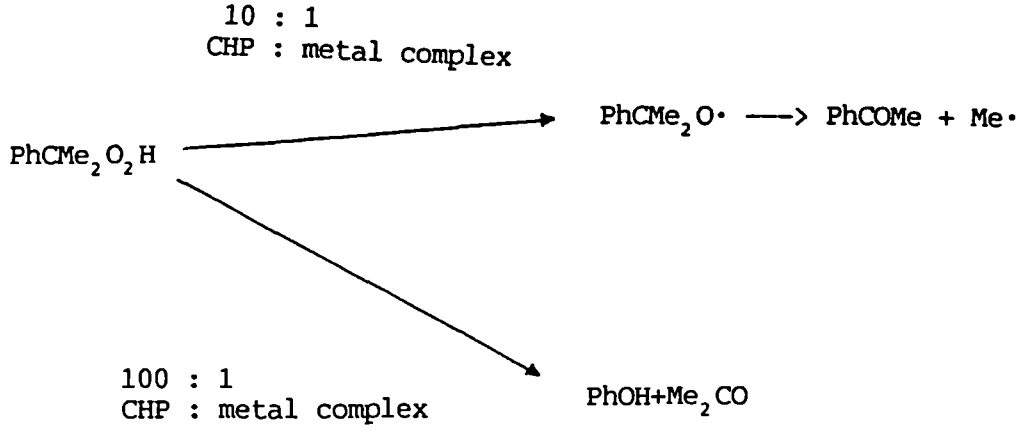

Chien and Boss (22), favoured a mechanism which successively oxidised the sulphurs of a NiDTC complex:

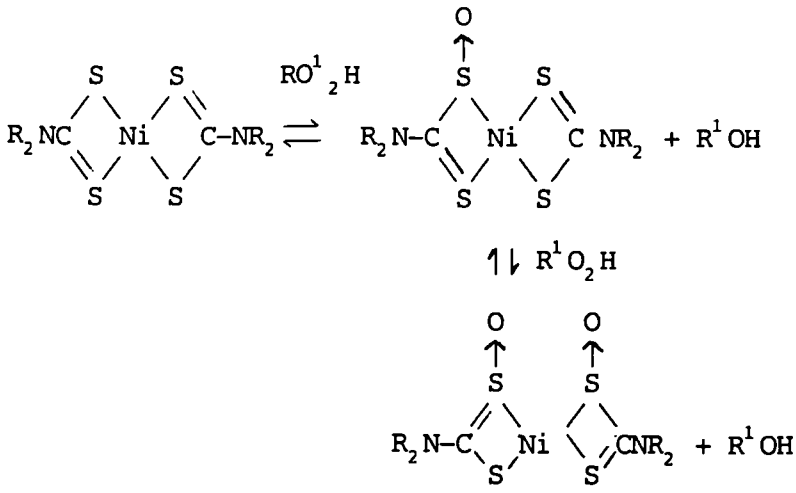

Rossi and Imparato (23), proposed the following mechanism for the reaction of isopropyl ZDDP with cumene hydroperoxide:

$$4\text{ZDDP} + R^1O_2H \longrightarrow \underset{\text{Basic ZDDP}}{[(RO)_2\ PS_2]_6Zn_4O} + \underset{\text{DDDiS}}{\left[\begin{matrix}RO & S\\ & P\\ RO & S\end{matrix}\right]_2} + R^1OH$$

$$\downarrow 15\ R^1O_2H$$

$$1{\cdot}5\ \text{DDDiS} + 1{\cdot}5\ [(RO)_2P(O)S]_2 + \text{Zn O} + 15R^1OH + 3\ \text{Zn SO}_4$$

The authors argued that when these successive reactions are completed a heterolytic decomposition of hydroperoxide occurs producing phenol. Rossi and Imparato observed two pro-oxidant stages in the oxidation of cumene at 60 deg C, (air atmosphere) in the presence of cumene hydroperoxide (CHP) 0.4M and ZDDP 0.05M or basic ZDDP .0125M, by monitoring two separate absorptions of oxygen. The second pro-oxidant stage was prevented by the addition of a phenolic antioxidant. The authors proposed that peroxy or alkoxy radicals were produced from the reaction of hydroperoxide with ZDDP to give the first pro-oxidant stage. The second pro-oxidant step occurred on the complete consumption of dithiophosphate.The authors concluded that because both the second pro-oxidant step and the second stage of hydroperoxide decomposition were blocked by phenolic free radical inhibitors that the agent responsible for the free-radical heterolytic decomposition of the hydroperoxide is formed by an oxidation, via a prevailing radical mechanism, of the products of the decomposition of ZDDP.

Howard et al (10), stated that NiDTC's and NiDDP's cannot be expected to function as preventative antioxidants at ambient temperatures. The authors discovered that Ni DDP's at ambient temperatures react with hydroperoxides to give a pro-oxidant effect. At ambient temperatures a solution of NiDDP absorbed atmospheric oxygen on the addition of hydroperoxide, however ZDDP did not cause the pro-oxidant effect. Addition of a phenolic antioxidant prevented this pro-oxidant behaviour. The mechanism of reaction of NiDDP's and NiDTC's was proposed to be as follows:-

$$M^{n} + RO_2H \longrightarrow M^{n+1} + RO\cdot + OH^{\ominus}$$

$$M^{n+1} + RO_2H \longrightarrow M^{n} + RO_2^{\ominus} + H^{\oplus}$$

The authors concluded that methyl styrene, acetophenone and cumyl alcohol were products from a radical induced decompostion of cumene hydroperoxide. The authors stated that the only antioxidant capability of NiDDP's and NiDTC's at ambient temperatures was their radical scavenging capacity. The zinc complexes however, appeared to be both radical scavengers and preventative antioxidants.

Bridgewater et al (12), studied the mechanism of antioxidant action of ZDDP's and related compounds (ie. basic ZDDP and dialkyl dithiophosphate disulphide (DDDiS)) with hydroperoxides.

Experiments were performed at temperatures in the range of 95-125 deg C on solutions of a 10,000 times excess cumene hydroperoxide over antioxidant. The authors proposed that acetophenone is formed by a free-radical process independent of the promoter used, cumyl alcohol and methyl styrene are formed from cumene hydroperoxide by an ionic mechanism, rather than a free-radical mechanism normally accepted. The ionic decomposition of hydroperoxide takes place via a cationic chain reaction and in the case of ZDDP, BZDDP and DDDiS they proposed that the catalyst may be DDPA (dialkyl dithiophosphoric acid).

Analysis of the products of CHP decomposition by ZDDP and BZDDP were found to be of a very similar distribution and therefore it was deduced that they decompose CHP by the same mechanism. The product distribution was determined to be as follows, 68% phenol, 27% cumyl alcohol, 2% methyl styrene and 5% acetophenone. The authors did not consider that SO_2 is the main catalyst for CHP decomposition.

Bridgewater et al, in previous work observed that a phenolic tetrasulphide decomposes CHP with SO_2 as the catalyst, but the product distribution is not the same as that of BZDDP and ZDDP, (24). The authors suggest that the distribution of products is formed as follows:-

$$RO_2H + H^{\oplus} \rightleftharpoons RO_2H_2^{\oplus}$$

$$RO_2H_2^{\oplus} \rightleftharpoons RO\text{–}OH\ (H^{\oplus})$$

$$RO_2H_2^{\oplus} \rightleftharpoons RO^{\oplus} + H_2O$$

$$RO^{\oplus} \longrightarrow C^{\oplus}$$

$$C^{\oplus} + RO_2 \longrightarrow \text{Phenol} + \text{acetone} + RO^{\oplus}$$

$$C^{\oplus} + H_2O \longrightarrow \text{Phenol} + \text{acetone} + H^{\oplus}$$

$$RO\text{–}OH \longrightarrow R^{\oplus} + H_2O_2$$

$$R^{\oplus} + RO_2H \longrightarrow ROH + RO^{\oplus}$$

$$ROH + H^{\oplus} \longrightarrow \text{2-phenylpropene} + H_2O$$

C =

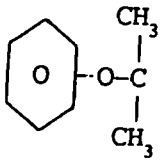

R =

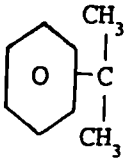

Bridgewater proposed that DDPA is formed from the hydrolysis of ZDDP (12), and from the disulphide, resulting from its homolysis and subsequent reaction with hydroperoxide.

Al-Malaika and Scott (9), followed the kinetics of the reaction of NiDDP and cumene hydroperoxide in chlorobenzene under nitrogen at 110 deg C. Hydroperoxide disappearance was monitored by measuring the band at 3520 cm^{-1} by ir spectroscopy. The concentration of NiDDP was followed by monitoring the (λ = 316 nm) band on a uv/vis spectrometer. The molar ratios were varied and it was deduced that a small molar ratio [CHP]/[NiDDP] (eg 10:1), cumyl alcohol and acetophenone are the predominant products derived from cumene hydroperoxide decomposition. These products, the authors stated, are characteristic of a homolytic process. On the other hand at higher molar ratios (eg. 100:1), the formation of methyl styrene indicates the presence of an acid catalyst and therefore is associated with the ionic catalytic decomposition products, phenol and acetone.

The kinetic studies conveyed the presence of a rapid initial catalytic stage, followed by a secondary induction period, leading into a slower catalytic reation. At the highest molar ratio,([CHP]/[NiDDP] = 500), the decomposition does not achieve the second catalytic stage within the duration of the experiment (three hours), and at the lowest molar ration, ([CHP/[NiDDP]=1), the reaction occurs almost exclusively by the first stage catalyst.

It was proposed that the two-stage catalytic processes were, firstly a homolytic process, favoured by a low molar ratio of hydroperoxide to metal complex, and secondly an ionic decomposition of hydroperoxide occurring at higher hydroperoxide to metal complex ratio. The ionic catalyst was proposed to be an intermediate, dialkyl dithiophosphate disulphide (DDDiS), formed from the oxidation of MDDP's.

In further work a reaction scheme was postulated to account for the reaction profile, (25):

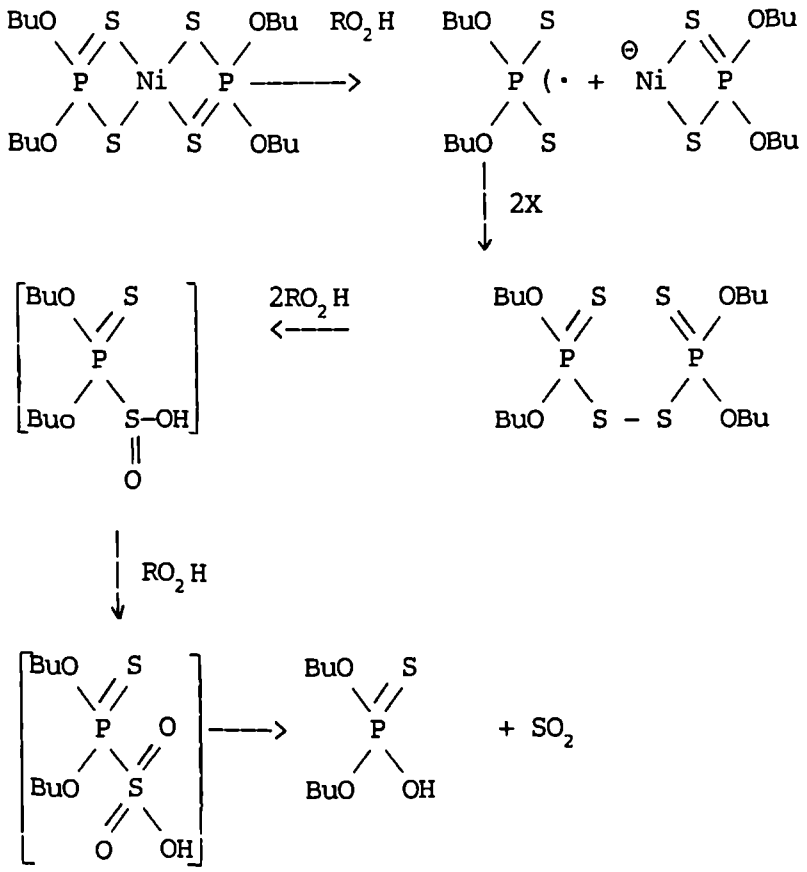

$$SO_2 + RO_2H \longrightarrow SO_3\ (H_2SO_4)$$

2.4 The Thermal Decomposition of ZDDP's

A binary reactor model can be used to describe the oil environment of an engine. The oil is in partitions, between the sump at temperatures of (90 - 100 deg C) and the piston ring zone, where the temperatures are much higher. ZDDP's are likely therefore to undergo decomposition at least in the ring zone, but possibly to some extent, in the sump.

Larson (4), proved using engine performance tests, that the more easily ZDDP is decomposed, the more effective is its antioxidant capability. This implies that the decomposition products of ZDDP are the best long-term oxidation inhibitors.

Coy and Jones (26), analysed the thermal decomposition products of ZDDP's. The authors reported that the final degradation product was $SP(SR)_3$ (S,S,S-trialkytetrathiophosphate).

The intermediate products are O,S,S-trialkyltrithiophosphate, $SP(SR)_2(OR)$ and O,O,S-trialkyldithiophosphate $SP(SR)(OR)_2$. Other compounds charcterized were $OP(SR)_3$, $P(SR)_3$, RSR, RSSR and RSH. H-1 NMR and P-31 NMR were techniques used to characterize the degradation products. Thermal decomposition of ZDDP's also leads to the formation of a white non-crystalline solid precipitate. Compared to the original additive, this solid is high in zinc and oxygen but low in sulphur, phosphorus and alkyl groups.

In further work Coy and Jones postulated a ZDDP decomposition mechanism based on the observed distribution products, (27). Spedding and Watkins (1,2), stated that the mechanism of decomposition of ZDDP is prodominantly hydrolytic. 80% of 1% C5-ZDDP in hexadecane at 170 deg C decomposed after little over an hour when water was present but only 20% of the ZDDP had decomposed after over 4 hours in the absence of water. The distillate from the decomposition was found to be consistent in composition with that observed by Coy and Jones. The residue, the authors stated, were polyphosphates with traces of sulphur. Since ZDDP's degrade in the engine oil environment, it is necessary to consider the hydroperoxide-decomposing capabilities of the ZDDP decomposition products.

Holcik et al (28), performed studies on the reactions of PEDP's with cumene hydroperoxide.

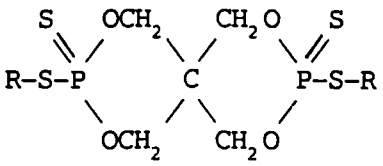

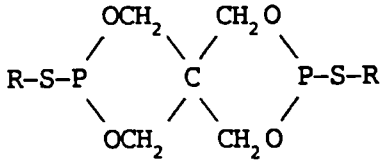

Pentaeaythritol Diphosphates (PEDP's)

The authors showed that 0.0005M PEDP completely decomposed 0.02M CHP in chlorobenzene at 75 deg C. The decomposition took between 3 and 13 hours depending on the structure of the PEDP. The progression of the reaction was followed using Fourier -transform infra-red (FTIR) spectroscopy. Holcik postulated that the PEDP's were oxidised to organophosphorus sulphoxides by CHP. The sulphoxides undergo decomposition at moderate temperatures to give organophosphorus sulphenic acids and an olefin. The sulphenic acid is a weak acid but reacts rapidly with hydroperoxides to produce stronger acids. The remaining hydroperoxide is decomposed in an acid-catalysed reaction to give non-radical products. Shelton et al (7), have studied the reactions of various organic sulphur compounds such as sulphides with hydroperoxides. The authors state that sulphides are oxidised to sulphoxides which when decomposed give a sulphenic acid and an olefin. Successive reactions occur that result in ionic decomposition of hydroperoxides and oxidation of the sulphenic acid. Instability of the sulphoxide appears to be an important requirement for activity as an inhibitor of autoxidation (29).

2.5 Summary

ZDDP's, ZDTC's and zinc xanthates act as hydroperoxide decomposers and radical scavengers. Their radical scavenging ability follows the trend ZDDP > zinc xanthate > ZDTC; and, with respect to hydroperoxide decomposition the trend is zinc xanthate > ZDDP > ZDTC.

Nickel DDP's and DTC's are not as reactive as their zinc analogues and only behave as radical scavengers. When reacting with hydroperoxides at ambient temperatures they are initially pro-oxidants and any antioxidant capacity is the result of radical scavenging.

The initial reaction mechanism of ZDDP with peroxy radicals and hyroperoxides is under a certain amount of dispute, various authors prefer a mechanism in which the sulphur atom is the site of attack. Others favour the metal atom as the active site.

An oxidation product from ZDDP, NiDDP and NiDTC decomposes hydroperoxides by an ionic mechanism. Likely candidates of this species are SO_2, DDPA and acids produced from the oxidation of DDDiS.

Thermal decomposition products of ZDDP play an important role in inhibiting autoxidation of engine oils.

Chapter 2 References

1) Spedding H. and Watkins R.C., Tribology 1982, vol 15, 9-12

2) Spedding H. and Watkins R.C., Tribology 1982, vol 15, 13-15

3) Bird R.J. et al, A.S.L.E. 1980, vol 23, 121-130

4) Larson R., Scientific Lubrication, August 1958, 12-19

5) Mahoney L.R. et al, Ind. Eng. Chem. Prod. Res. Dev., 1980, vol 19, 11-15

6) Bateman L. et al, Trans. Faraday. Soc., 1951, 47, 274

7) Shelton J.R., Rubber Chem. and Techn., 1974, 47, 949

8) Shelton J.R., "Polymr Stabilization", W.L. Hawkins Ed. John Wiley & Sons. Inc. New York 1972., Chp 2.

9) Al-Malaika and G. Scott, Eur. Poly. J., 1980, vol 16, 503-509

10) Howard J.A. et al, Can. J. Chem., 1976, vol 54, 390

11) Mair R.A. and Graupner A.J., Analyt. Chem. 1964, 36, 194

12) Bridgewater A.J. et al., J.S.C. Perkin II, 1980, 1006 - 1016

13) Bateman L. and Cunneen J.I., J. Chem. Soc. 1955, 1596

14) Mahoney L.R. et al., Ind. Eng. Chem. Prod. Res., 1978, vol 17, No 3

15) Ingold K.U., "Free Radicals", Wiley & Sons Inc. New York 1973, vol 1, Chp 2

16) Colclough T. and Cunneen J.I., J. Chem. Soc., 1964, 4790

17) Burn A.J., Tetrahedron 1966, vol 22, 2153-2161

18) Bacon W.E. et al., J. Amer. Chem. Soc., 1954, 76, 670

19) Howard J.A. et al., Can. J. Chem., 1973, vol 51, 1543-1553

20) Howard J.A. et al., Can. J. Chem., 1976, vol 54, 382

21) Holdsworth J.D., J.Chem. Soc., 1964, 4692

22) Chien J.C.W. and Boss C.R., J. Poly. Sci. A-1, Polymer Chem., 1972, 10, 1579

23) Rossi E. and Imparato L., Chem. and Ind. (Milan), 1971, 53, 838

24) Bridgewater A.J. and Sexton M.D., J.C.S. Perkin II, 1978, 530

25) Al-Malaika and Scott, Polymer 1982, vol 23, 1711

26) Coy R.C. and Jones R.D., A.S.L.E. Trans. 1981, vol 24 (1), 77-90

27) Coy R.C. and Jones R.D., A.S.L.E. Trans. 1981, vol 24 (1), 91-97

28) Holcik J. et al., Polymer Degradation and Stability, 1983, 373-397

29) Shelton J.R., et al, Int. J. Sulphur Chem., 1973, vol 8, No 2, 197-220

CHAPTER 3

3.1 Synthesis of Zinc Dialkyldithiophosphates (ZDDP's) and some of their Oxidation, Hydrolysis, and Thermal Degradation Products

This section describes the methods used to prepare ZDDP's and some of their "oil" related derivatives. Techniques to assess the purities of the compounds are outlined and any synthetic innovations over the preparations cited in the literature are discussed.

3.1.1 The Preparation of Crude n-Butyl, n-Octyl and Iso-propyl Dialkyldithiophosphoric Acid (DDPA)

The reaction scheme is:

$$4ROH_{(l)} + P_2S_{5(s)} \longrightarrow 2(RO)_2PS_2H_{(l)} + H_2S_{(g)}$$

The method described by Wystrach et al (1), was basically followed, but a few improvements were made.

One mole of alcohol was heated to a temperature dependent on the alcohol's boiling point, (n-butanol 75 deg C, n-octanol 110 deg C and iso-propanol 55 deg C). 0.28 moles of P_2S_5 was added in a toluene suspension to the agitated alcohol. The addition of P_2S_5 was gauged to prevent excessive rises in temperature which cause DDPA decomposition. An exothermic reaction occurred giving off H_2S gas which was trapped as CuS(s) in a $CuSO_4$(aq) scrubber. The reaction was performed in a fume cupboard with good extraction because of the high toxicity of H_2S gas. The reaction mixture was sustained at the following temperatures, n-butyl DDPA 90 deg C, n-octyl 110 deg C and iso-propyl DDPA 60 deg C, for approximately 90 minutes.

The resulting crude DDPA product was decanted from any residual P_2S_5 and viscous by-product. The decanted liquid was filtered, warmed with activated charcoal to help remove impurities and re-filtered. The toluene was removed during the preparation of the ammonium salt of the acid (ADDP).

3.1.2 The Preparation of Ammonium Dialkyldithiophosphates (ADDP's)

The reaction scheme is: $(RO)_2PS_2H_{(l)} + NH_{3(g)} \longrightarrow (RO)_2PS_2\ NH_{4(s)}$

R = n-octyl, n-butyl or iso-propyl

The cooled crude DDPA and toluene mixture were treated with an excess of gaseous NH_3 admitted beneath the surface of the solution. This reaction was exothermic and the ADDP produced dissolved in the toluene. However, on cooling, ADDP crystals formed which were filtered and washed with 40-60 petroleum spirit under suction in a Buchner funnel. The ADDP was recrystallised from toluene then filtered and washed with 40-60 petroleum spirit at the pump. The salt was air-dried for an hour, at room temperature. The purity was assessed by P-31,H-1 and C-13 NMR (as discussed later) and was found to be of high purity (98%).

3.1.3 The Preparation of n-butyl, n-octyl and iso-propyl ZDDP

The reaction scheme is: $2\ (RO)_2PS_2^{\ominus} + Zn^{2+} \longrightarrow [(RO)_2PS_2]_2Zn$

n-Butyl and iso-propyl ZDDP were prepared by the method described by Dickert (2). Stoicheiometric amounts of ADDP solution were added to an aqueous solution of zinc nitrate. n-Butyl ZDDP is insoluble in water and formed as an emulsion. The n-butyl ZDDP was extracted by shaking with redistilled 40-60 petroleum spirit. The aqueous layer was discarded and the petroleum spirit was removed by rotary evaporation. Iso-propyl ZDDP was precipitated as a white solid which was filtered and air-dried. Due to the insolubility of n-octyl ADDP in water, it was necessary to perform the reaction in a solvent which would dissolve the ADDP and zinc nitrate (the nitrate was chosen because of its high solubility product). Methanol proved to be a suitable solvent, and the zinc nitrate and ADDP were dissolved in the minimum amount of methanol, then mixed. n-Octyl ZDDP proved to have a low solubility in methanol and was easily extracted by shaking with 40-60 petroleum spirit. The petroleum spirit was then removed by vacuum pumping to leave the pure ZDDP.

Zinc sulphate or chloride may be used instead of the nitrate when synthesizing n-butyl and iso-propyl ZDDP from their water-soluble ADDP's. Zinc nitrate must not be used in an acidic environment (ie. when the DDPA is used as a precursor) because nitric acid may be formed which will cause ZDDP oxidation.

The purity of the ZDDP's can be established using P-31, C-13 and H-1 NMR techniques however, a good rough assessment can be made viewing the colour. A clear and not yellow liquid ZDDP indicates good purity (for butyl and octyl ZDDP's), and if yellow crystals of DDDiS are not present in iso-propyl ZDDP, this is a sign of good purity. If the ZDDP's are prepared swiftly and sealed in vessels under vacuum, pure ZDDP's can be prepared without using an oxygen-free atmosphere.

3.1.4 The Preparation of Pure n-Octyl, n-Butyl and Iso-propyl Dialkyldithiophosphoric Acids (DDPA)

Wystrach et al (1), regenerated DDPA's by adding the stoicheiometric amount of H_2SO_4 (aq) to an aqueous solution of ADDP, (in the case of water-soluble ADDP's). Ice was used to keep the temperature down, thereby minimizing acid hyrolysis of the relatively unstable DDPA. The DDPA forms an oily layer on the surface and is extracted by shaking with 40-60 petroleum spirit. The petroleum spirit is then removed to leave the acid. n-Octyl DDPA is less susceptible to acid hydrolysis than n-butyl DDPA which in turn is less prone to hydrolysis than iso-propyl DDPA. Evidence for this statement will be discussed along with the identification of the respective hydrolysis products further in the text.

Much purer acids can be obtained by using an anhydrous protonation technique. The acids are regenerated from an anhydrous solution of ADDP by bubbling HCl(g) below the surface of the liquid. Ammonium chloride is precipitated and then filtered to leave a solution of pure DDPA. Dry chloroform is a good solvent for n-butyl and n-octyl ADDP. However, iso-propyl ADDP is only sparingly soluble in chloroform and therefore dry methanol was used instead.

The methanol or chloroform was evaporated to leave the pure acid. Shaking the methanol/iso-propyl DDPA mixture with 40-60 petroleum spirit to extract the acid and then removing the petroleum spirit tended to cut losses of the volatile isopropyl acid from evaporation, (methanol having a higher boiling point than 40-60 petroleum spirit). The acids were sealed in a vessel under vacuum to prevent hydrolysis and/or oxidation. Analysis of the purity of the prepared acid was performed by C-13, H-1 and P-31 NMR.

3.1.5 The Preparation of n-Octyl, n-Butyl and iso-Propyl Dialkyldithiophosphate Disulphides (DDDiS)

The reaction scheme is:

$$2\ (RO)_2PS_2^{\ominus} + I_3^{\ominus} \longrightarrow [(RO)_2PS_2]_2 + 3I^{\ominus}$$

n-Butyl DDDiS and iso-propyl DDDiS were prepared by oxidising the $(RO)_2PS_2^-$ anion with iodine. KI/I_2 solution was added to a weighed quantity of n-butyl or iso-propyl ADDP in water until a yellow colouration appeared, due to the presence of excess iodine. A "back titration" was performed by adding a few mg of ammonium salt until the yellow colour faded. The butyl DDDiS formed an oily layer on the surface of the solution and was extracted using redistilled 40-60 petroleum spirit. The butyl DDDiS was isolated by evaporating off the petroleum spirit. The iso-propyl DDDiS precipitated as a yellow solid which was washed with methanol and air- dried.

Because n-octyl ADDP is only sparingly soluble in water, methanol was used as a solvent for the oxidation. KI/I_2 solution was added to a 5% solution of octyl ADDP in methanol. The same "back titration" technique was employed to ensure that the complete oxidation of the $(RO)_2PS_2^-$ anion occurs. If any of the ADDP precipitated out on addition of the KI/I_2 solution more methanol was added to redissolve the salt . The methanol was evaporated off leaving a yellow oil on the aqueous layer. The oil was extracted with 40-60 petroleum spirit and the petroleum spirit removed to leave the pure n-octyl DDDiS.

Preparation of the dialkyldithiophosphate disulphides from their corresponding acids was avoided. HI would be produced which could cause acid hydrolysis of the unreacted DDPA, thereby producing impurities.

3.1.6 The Preparation of Basic Butyl ZDDP

The reaction scheme is: $4ZDDP + R^1O_2H \longrightarrow [(RO)_2PS_2]_6Zn_4O + [(RO)_2PS_2]_2$

Basic ZDDP $+ R^1OH$

Equivalent volumes of 1 molar n-butyl ZDDP and 0.5 molar cumene hydroperoxide in squalane were mixed. The solution was allowed to stand at ambient temperature for two hours to allow the reaction to take place and the crystals of basic butyl ZDDP to form.

The crystals were filtered under suction in a Buchner funnel and washed with small aliquots of 60-80 petroleum spirit to remove the residual squalane and n-butyl DDDiS. Any basic ZDDP that dissolved in the petroleum spirit and passed into the Buchner flask was recovered. The purity of the product was assessed by P-31,C-13 and H-1 NMR techniques.

3.1.7 The Preparation of (O,O',S) Tributyldithiophosphate (TDTP)

TDTP was prepared by alkylating the dithiophosphate anion. 1-Bromo-n-butane was the reagent used to facilitate the alkylation. In the literature (3,4), sodium dialkyldithiophosphate is used as a precursor for the alkylation reaction; however, the ammonium dialkyldithiophosphate is more convenient to use and just as effective.

Reaction Scheme:

$$NH_4^{\oplus} + (BuO)_2\,PS_2^{\ominus} + BuBr \xrightarrow{MeOH} (S)P(OBu)_2SBu + NH_4Br$$

Method

5g of n-butyl ADDP was dissolved in 20ml of distilled sodium- dried methanol. 3g of 1-bromobutane was added and the solution was refluxed for 16 hours. The product was extracted from the methanol with 40-60 redistilled petroleum spirit.

The petroleum spirit and any residual bromobutane were removed using a rotary vacuum pump at 80 deg C. Yields of 90% were achieved. The purity was assessed by analytical G.L.C.

3.1.8 The synthesis of O,S,S' Tributyltrithiophosphate (TTTP)

The synthesis was performed in accordance with the literature (5), but with only limited success.

Method

0.03 moles of P_2S_5 suspended in toluene was added dropwise to 0.06 moles of triethylamine and 0.09 mole of 1-butanol (heated to 75 deg C), at a rate needed to maintain reflux. Reflux was continued until there was no further precipitation of copper sulphide in the copper sulphate scrubber indicating that the evolution of $H_2S(g)$ had terminated.

40-60 Petroleum spirit was added to the acid and dry ammonia gas was bubbled under the surface to produce the ammonium salts(s)*. It was found to be necessary to keep the ammonium salt(s) in petroleum spirit because of air-sensitivity. The bulk of the petroleum spirit was decanted and the ammonium salt(s) washed with petroleum spirit. The petroleum spirit was decanted off and the ammonium salt(s) were dissolved in dry methanol. Any residual petroleum spirit formed a layer on top of the methanol and was easily decanted off. In excess of twice the molar quantity of 1-bromobutane was added and the reaction mixture refluxed for 16 hours. The product was extracted from the methanol with 40-60 petroleum spirit and the petroleum spirit was removed by evaporation.

*The composition of the "ADDP" was found to be a mixture of two ammonium salts, a alkyltrithiophosphate and a dialkyldithiophosphate.

Observations

Two layers were not formed after the P_2S_5/ alcohol reaction: this is inconsistent with the literature. Analysis of the products from the alkylation by G.L.C and H-1 NMR indicated that both TTTP and TDTP were main components, (see section 3.2). Therefore the reaction of triethylamine produced a mixture of the mono-acid (DDPA) and di-acid. The literature states that the mono and di-acids should form separate layers: this however, did not occur. The triethylamine is a base added to inhibit diacylation.

Postulated Reaction Profile

$$\text{i)}\quad P_2S_5 + 3BuOH \xrightarrow[\text{Toluene, } 75^\circ C]{\text{Triethylamine}} (S)P(OBu)(SH)_2 + (S)P(OBu)_2SH + H_2S$$

$$\text{ii)}\quad (S)P(OBu)(SH)_2 + 2NH_3 \longrightarrow (S)P(OBu)(SNH_4)_2$$

$$(S)P(OBu)_2(SH) + NH_3 \longrightarrow (S)P(OBu)_2\,SNH_4$$

$$\text{iii)}\quad (S)P(OBu)(SNH_4)_2 + 2BuBr \longrightarrow (S)P(OBu)(SBu)_2 + 2NH_4Br$$

$$(S)P(OBu)_2\,SNH_4 + BuBr \longrightarrow (S)P(OBu)_2(SBu) + NH_4Br$$

3.1.9 The synthesis of Tributyltetrathiophosphate (TTetTP)

Method

8.4g of P_2S_5 in a toluene suspension was added to 25g of 1-thiobutane at 70 deg C. Hydrogen sulphide was removed by a $CuSO_4$(aq) scrubber. The reaction mixture was sustained at a temperature of 70 deg C for two hours. The excess thiobutane was removed by filtration as an ammonium salt after treating the cooled solution with ammonia gas. Toluene was removed by a vacuum rotary evaporator on a steam bath. The yield obtained was approximately 96% and the purity was assessed by G.L.C. and H-1 NMR techniques.

Reaction Scheme:

$$P_2S_5 + 6BuSH \xrightarrow[70^\circ C]{\text{Toluene}} 2(S)P(SBu)_3 + 3H_2S$$

3.1.10 The Preparation of Tributyltrithiophosphate (TTPhate) and Tributyltrithiophosphite (TTPhite)

Method

0.1 mol of trichlorophosphate (Aldrich 98%) or trichlorophosphite (Ventron 98%) were added dropwise to a mixture of 0.3 mol of thiobutane (Aldrich 98%) and 0.3 mol of pyridine, at 70 deg C, in a nitrogen atmosphere. The mixture was agitated and the reaction sustained at a temperature of 70 deg C for an hour. The pyridine salted out the HCl gas produced in the reaction. The product was filtered and any residual thiobutane was precipitated, by treating the liquid with ammonia gas. The ammonium salt was removed by filtration and any traces of pyridine evaporated off. The yields obtained were in excess of 95%.

$$3\ BuSH + PCl_3 \longrightarrow (BuS)_3P + 3\ HCl$$

$$3\ BuSH + OPCl_3 \longrightarrow (BuS)_3PO + 3\ HCl$$

3.2 The Determination of the Purity of TDTP, TTTP, TTPhate, TTPhite and TTetP by G.L.C. (Gas Liquid Chromatography)

Experimental

Analytical gas liquid chromatography was preformed on the synthesised products listed in the table below, using a Pye Unican CD2 instrument. A SE30 (3% stationary phase) column produced good compound separation, using nitrogen as a carrier gas.
0.5 microlitres of sample was injected onto the column and the retention times of the compounds were calculated at different temperatures.

Results (See figs 3.2.1 and 3.2.2)

Table (3.2.1) lists G.L.C. retention times (min), of the synthesized products at different temperatures and their respective G.L.C. determined purities.

Table 3.2.1

The GC retention times (min) of the synthesized products at different Column temperatures and their respective purities in brackets

	Retention times (min)				
	150°C	180°C	200 °C	220 °C	250°C
TDTP	27 (97%)	8	-	-	-
TTTP	27,66 (40%), (60%)	8,17	-	-	-
TTetTP	-	-	21 (96%)	10	5
TTPhate	-	32 (98%)	16		
TTPhite	-	22,32 (86%), (14%)	10,16	-	-

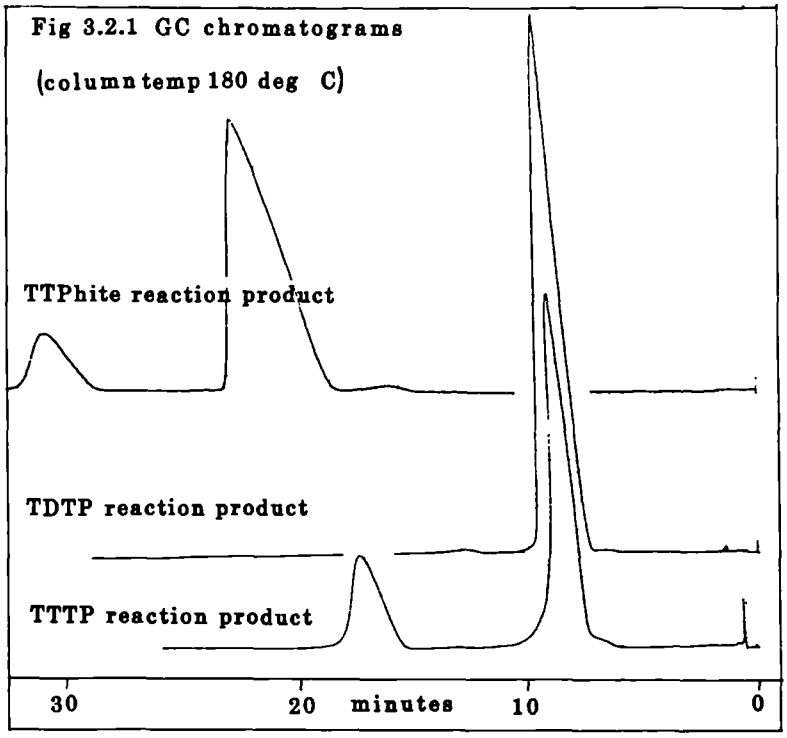
Fig 3.2.1 GC chromatograms
(column temp 180 deg C)
TTPhite reaction product
TDTP reaction product
TTTP reaction product
30
20
minutes
10
0

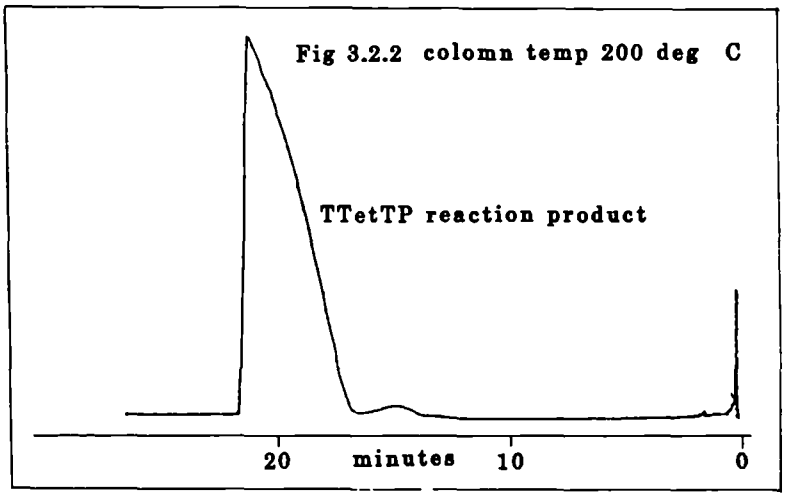
Fig 3.2.2 colomn temp 200 deg C
TTetTP reaction product
20
minutes
10
0

Discussion

The results confirm that the synthesis of TTIP obtained from the literature produced approximately equivalent quantities of TTIP and TDIP. Fractional distillation, preparative G.L.C and T.L.C were techniques used to attempt a separation. T.L.C was the only method to produce some limited success. Preparative G.L.C decomposed the organothiophosphates producing foul smelling thiols. (A preparative SE30 G.L.C column was prepared using 100 grams of Diatomide support and 25 grams of SE30 stationary phase; 100 ml samples were injected onto the column at temperatures found to give a good separation on the analytical columns (at 130 deg C, 150 deg C and 180 deg C). The decomposition was presumably the consequence of a higher percentage of stationary phase necessary to run samples of this size. Fractional distillation left the composition of the mixture practically unchanged. Salame (6) employed a solvent system of 40:1 petroleum spirit: ethyl acetate to purify diethyl-S-isopropyl-mercapto methyl dithiophosphate), a compound similar to TDIP. This solvent proved to give the best separation from the experimentation performed on th large range of other solvent systems; however the spots were too close (Rf's 0.58 and 0.61) to give total separation.

G.L.C of the trialkyltrithiophosphite reaction product indicated the presence of a 14% trialkyltrithiophosphate impurity. The reaction mixture was flushed with nitrogen and therefore it is unlikely that oxidation occurred during the synthesis. It is feasible that trichlorothiophosphate was present in the trichlorothiophosphite precursor. The ambient temperature oxidation of the trithiophosphate to produce the phosphate was monitored by G.L.C, (see fig 3.2.3 and table 3.2.2).

Table 3.2.2 displaying the oxidation in air of TTPhite to TTPhate followed by GC analysis

Compound synthesized	Column temp (°C)	Air exposure (days)	Retention time (min)	Composition (%)
TTPhite	180	0	32	TTPhate 14
			22	TTPhite 86
TTPhite	180	1	32	TTPhate 38
			22	TTPhite 62
TTPhite	180	3	32	TTPhate 60
			22	TTPhite 40
TTPhate	180	0	32	TTPhate 95

Conclusion

The synthesis of (S,S',O) trialkyltrithiophosphate reported in the literature (4), is inadequate; the method produces also a similar amount of (S,O,O') trialkyldithiophosphate. These two organothiophosphates are very similar in chemical nature, thereby causing separation difficulties. Trialkyltrithiophosphites undergo oxidation in air even at ambient temperatures to give the corresponding phosphate.

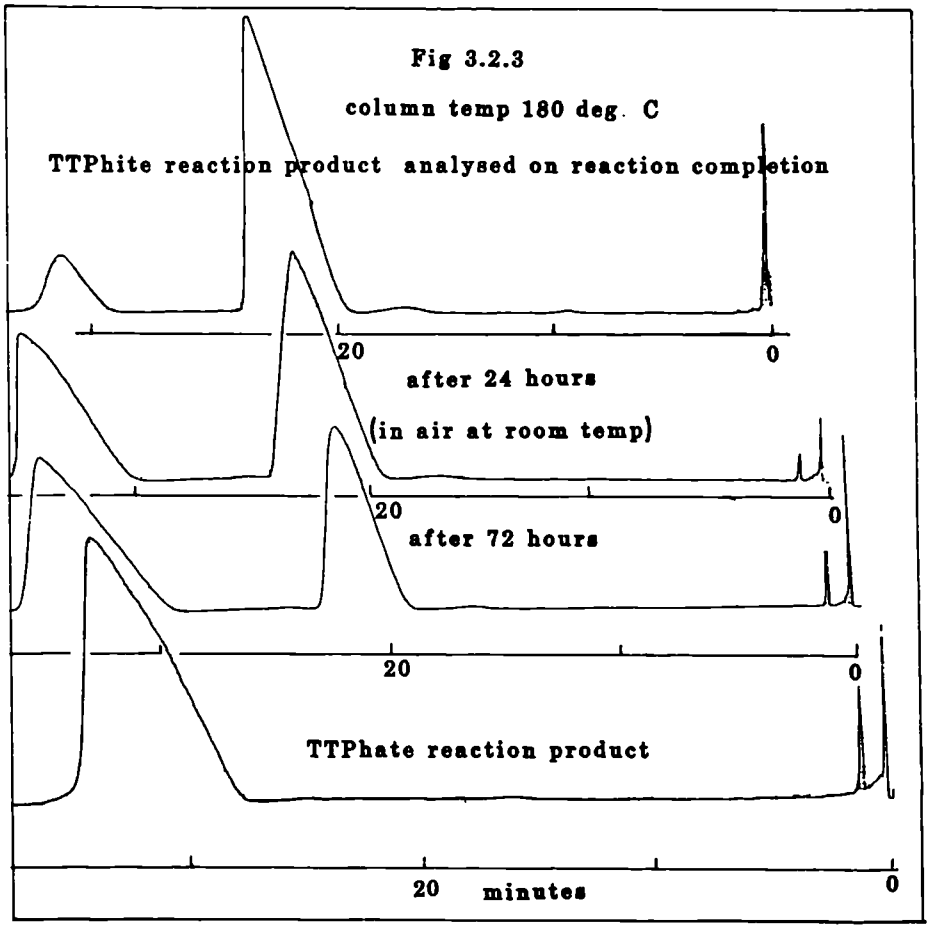
Fig 3.2.3
column temp 180 deg. C
TTPhite reaction product analysed on reaction completion
20
0
after 24 hours
(in air at room temp)
20
0
after 72 hours
20
0
TTPhate reaction product
20
minutes
0

3.3 H-1 NMR Spectra of n-Butyl ZDDP and Other Synthesised Related Organothiophosphates

H-1 NMR spectra of the compounds previously discussed (with relation to their synthetic pathways), were performed in a $CDCl_3$ solution using a Varian T60 NMR spectrometer, (see figs 3.3.1 - 3.3.10)

The following two features distinguish n-butyl dithiophosphoric acid and ammonium n-butyl dithiophosphate:

(1) The DDPA thiol proton has a chemical shift of 3.37 ppm and is a singlet.

(2) The ADDP ammonium ion protons have a chemical shift of 6.8 ppm and are observed as a broad singlet.

The terminal propyl fraction of the butyl group for all the analysed compounds have very similar H-1 NMR spectra, (terminal methyl 0.96 ppm and central methylene protons 1.63 ppm). However, the methylene protons furthest from the terminal methyl exhibit chemical shifts which are more sensitive to their chemical environment,(see table 3.3.1).

Table 3.3.1

Chemical shifts of the methylene protons furthest from the terminal methyl groups for various butyl esters

Compound	Chemical Shift (ppm)		J_{PH} (Hz)		J_{HH} (Hz)	
	OCH_2	SCH_2	OCH_2	SCH_2	OCH_2	SCH_2
ADDP	3.96	-	10	-	6	-
Basic ZDDP	4.08	-	10	-	6	-
ZDDP	4.23	-	10	-	6	-
DDPA	4.25	-	10	-	6	-
DDDiS	4.27	-	10	-	6	-
TDTP	4.2	2.95	10	16	6	8
TTetTP	-	3.10	-	16	-	8
TTPhate	-	2.85	not determined		not determined	
TTPhite	-	2.7	not determined		not determined	

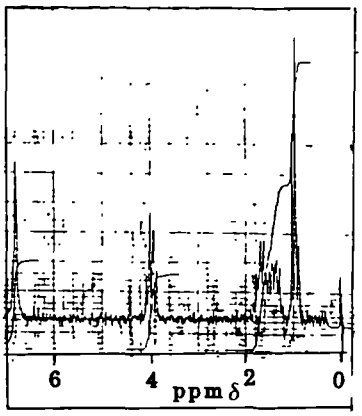

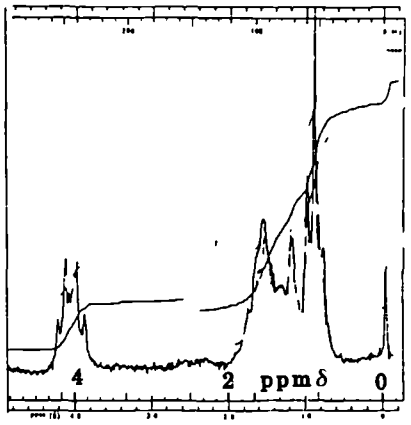

Fig 3.3.1 proton NMR spectrum of n-butyl ADDP

Fig 3.3.2 proton NMR spectrum of n-butyl basic ZDDP

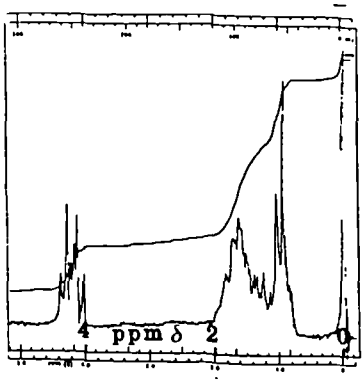

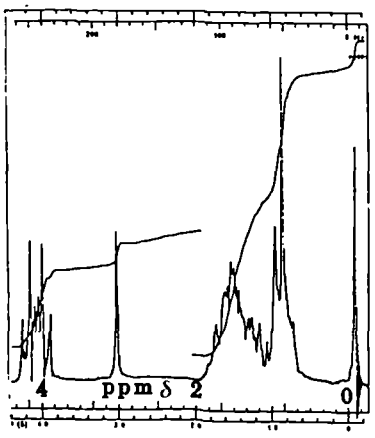

Fig 3.3.3 proton NMR spectrum of n-butyl ZDDP

Fig 3.3.4 proton NMR spectrum of n-butyl DDPA

Proton NMR spectra of n-butyl derivatives

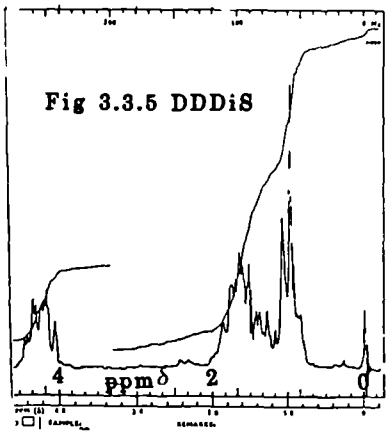

Fig 3.3.5 DDDiS

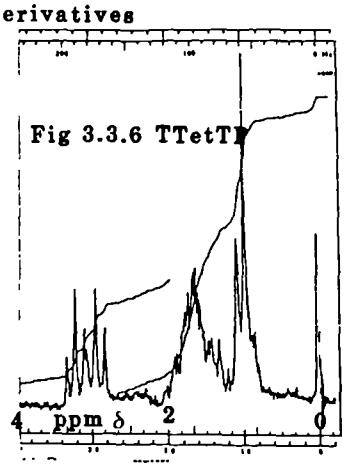

Fig 3.3.6 TTetTP

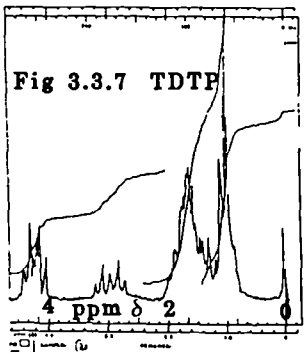

Fig 3.3.7 TDTP

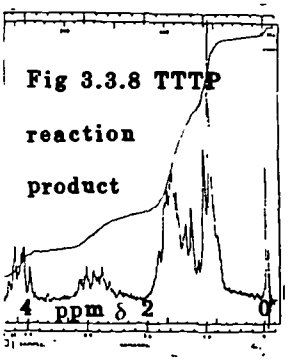

Fig 3.3.8 TTTP reaction product

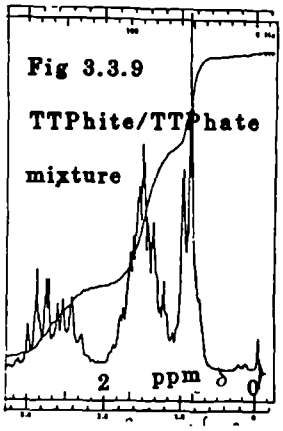

Fig 3.3.9 TTPhite/TTPhate mixture

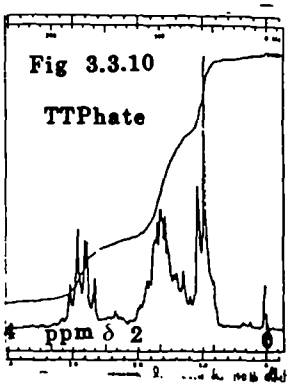

Fig 3.3.10 TTPhate

Discussion

A comparison of the chemical shifts of the oxygen-adjacent methylene protons in dithiophosphates (ADDP, BZDDP, ZDDP, TDTP, DDPA and DDDiS) indicates that the greater the ionic character of the compound, the lower the chemical shifts.

Compounds with more ionic character have more electron density in their phosphorus orbitals, thus inducing greater shielding of the oxygen-adjacent methylene protons. The trend with respect to ionic character (and therefore more shielded O-adjacent methylene protons) is ADDP >> BZDDP, >ZDDP, >DDPA, DDDiS.

Methylene protons adjacent to sulphur atoms are more shielded than those adjacent to oxygen simply because oxygen is a more electronegative atom, and therefore sulphur-adjacent methylene protons have a lower chemical shift.

The sulphur-adjacent methylene protons of tributyltrithiophosphite are shielded to a greater extent than the analogous tributyltrithiophosphate, because the thiophosphite has a phosphorus lone pair. The S-adjacent methylene protons of tributyltetrathiophosphate have a higher chemical shift than those of tributyltrithiophosphate. This is surprising as it seems more logical that deshielding would occur when P=S is substituted for P=O. The O- or S-adjacent methylene protons are split in to a multiplet by coupling from both the two adjacent methylene protons and by the phosphorus atom. The P-H coupling constants are larger than the H-H coupling constants. The coupling constants (J_{H-H} and J_{P-H}) are larger when coupling occurs through sulphur rather than through oxygen.

It is worth mentioning that the O-adjacent methylene protons of DDDiS are poorly resolved. This broadening is caused by the free rotation exhibited around the S-S bond producing different DDDiS conformers.

H-1 NMR was similarly performed on the various synthesised n-octyl and iso-propyl compounds , and similar trends were observed. For example, table 3.3.2 indicates that the more the ionic character exhibited by the molecule, the greater the shielding of the O-adjacent methylene protons.

TABLE 3.3.2

	n-Octyl OCH_2 Chemical Shift	iso-Propyl OCH Chemical Shift
ADDP	4ppm (chloroform)*	4.67ppm (DMSO)
DDPA	4.2ppm (chloroform)	4.88ppm (chloroform)
ZDDP	4.13ppm (chloroform)	4.88ppm (chloroform)
DDDiS	4.23ppm (chloroform)	

*solvent

3.4 P-31 NMR of ZDDP's and Related Organthiophosphorus Compounds

Fourier transform P-31 NMR spectroscopy was found to be the best technique to characterize the purities of the synthesised ZDDP's and their related oxidation, hydrolysis and thermal degradation products. Solutions of the compounds (usually in choroform), were run on a Jeol 90 MHz multinuclear NMR spectrometer at DQA/TS Woolwich. The P-31 nucleus was decoupled and the chemical shifts are referenced against phosphoric acid and according to the IUPAC convention, positive values are to high frequency (low field). However literature published before the 1970's and even some literature published more recently display chemical shifts with an opposite sign, (7). The IUPAC convention however, is used in this thesis. Gorenstein and Kar (8), found that P-31 chemical shifts correlate well with calculated phosphorus electron densities. A more shielded the phosphorus magnetic dipole produces a less positive chemical shift. Integration of a respective P-31 signal does not necessarily determine the relative concentration of the responsible compound. The peak intensity depends on the relaxation time of the particular phosphorus nucleus. If the relaxation times are known, experimental conditions can be set up whereby all the nuclei relax completely and integration is then a direct measure of relative concentration. However, this usually requires long spectrum accumulation times. This is discussed more fully in Chapter 7.

RESULTS Table 3.4.1

Organophosphorus Compound	Chemical Shift	Solvent
Octyl ADDP	109.35	chloroform
Octyl Basic ZDDP	103.11	"
Octyl ZDDP	97.32	"
Octyl DDPA	85.60	"
Octyl DDDis	85.62	"
Butyl ADDP	109.35	"
Butyl Basic ZDDP	103	"
Butyl ZDDP	97.2	"
Butyl DDPA	85.59	"
Butyl DDDis	85.86	"
Iso-propyl ADDP	103.9	"
Iso-propyl Basic ZDDP	not recorded	
Iso-propyl ZDDP	94.3	choroform
Iso-propyl DDPA	81.84	"
Iso-Propyl DDDis	not recorded	
TIPhite	116 *	choroform
TIetTP	92 *	"
TIPhate	68 *	"
TBP	0.7	"

* Literature values (7)

Discussion

There are several factors influencing P-31 NMR chemical shifts in 4- coordinate (tetrahedral) phosphorus compounds and it is not possible to give a comprehensive discussion here. The factors include : the chemical type (i.e. O or S) of the atoms X bonded to the phosphorus , the degree of ionic character of the P-X bonds, including the degree of electron delocalization over the X-P-X grouping , and the X-P-X bond angles. On the IUPAC convention ,the more shielded the P atom ,the more negative (or less positive) the chemical shift. For our molecules the observed trend is as follows (in order of chemical shift):

ADDP> Basic ZDDP > ZDDP > DDDiS

The isopropyl dithiophosphate P-31 nuclei are more shielded than the analogous n-butyl dithiophosphate P-31 nuclei. This is the result of the competition of the greater positive inductive affect of the larger alkoxy chain and the increased ester bond angle of the isopropyl compound.

Successive substitution of oxygen atoms for sulphur atoms increasingly shields the P-31 nuclei, producing a signal with a less positive chemical shift. This is a result , in part, of decreased involvement of the ligand d orbitals in the molecular bonding.

In general, no simple pattern of P-31 chemical shift change with substituent electronegativity or structure change is found.

3.5 C-13 NMR analysis of Octyl DDPA, ZDDP and ADDP

C-13 NMR spectra were produced on a Brüker 200 MHz multinuclear NMR spectrometer at the University of Kent. Samples of n-octyl DDPA, ZDDP and ADDP were run in a solution of chloroform . Table 3.5.1 lists the chemical shifts and assignments of the spectra.

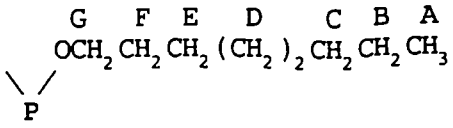

Table 3.5.1

Compound	^{13}C Chemical shifts (ppm)						
	A	B	C	D	F	E	G
DDPA	14.06	22.67	25.62	29.18	29.93 30.10	31.83	68.41 68.55
ADDP	14.08	22.73	26.03	29.42 29.50	30.53 30.69	31.96	67.17 67.33
ZDDP	14.07	22.68	25.65	29.2	29.93 30.10	31.68	68.7 68.83

Discussion

Table 3.5.1 indicates the following interesting points:

a) H-1 NMR has indicated that ADDP, (the most ionic dithiophosphate) has the most shielded P-31 and H-1 nuclei of the dithiophosphates analysed. The G carbon atom (oxygen adjacent) of n-octyl ADDP is also more shielded.

b) The n-octyl ADDP D carbon atoms are inequivalent, unlike the D carbon atoms of n-octyl DDPA and ZDDP.

c) Larger coupling constants are apparent for the C-C-O-P interaction of n-octyl ZDDP and DDPA when compared with the C-O-P interaction, however this is often the case for organophosphorus compounds, tributyl phosphate (TBP), is an example of such a case.

	J(C-O-P)	J(C-C-O-P)
ADDP	8.14 Hz	7.68 Hz
DDPA	6.94 Hz	8.59 Hz
ZDDP	6.55 Hz	8.65 Hz
TBP	6.7 Hz	7.1 Hz

Chapter 3

1) Wystrach V.P. et al., J. Org. Chem. 1956, 21, 705.

2) Dickert J.J. and Rowe C.N. J. Org. Chem. 1967, 32, 647.

3) Norman G.R. et al., J.Amer. Chem. Soc. 1952, 74, 161-3.

4) Mastin T.W. et al., J. Amer. Chem. Soc. 1945, 67, 1662-4.

5) Zh. Obshch. Khim. 1964, 38(6), 1282-6.

6) Salame M., J. Chromatography 1964, 16, 476.

7) Crutchfield M.M. et al., "Topics in Phosphorus Chemistry" 1967, Vol. 5.

8) Gorenstein D.G., Prog. in NMR Spectr. 1983, Vol. 16, 1-98.

9) Carbon-13 NMR Spectra, Sadler Research Laboratories Inc., Vol. 10, No. 1803C.

CHAPTER 4

The Characterization of ZDDP's and related compounds by Raman and ir Spectroscopy

A detailed study of the vibrational spectroscopy of ZDDP's and their oxidation, hydrolysis and degradation derivatives is important to aid the characterization of the compounds prepared and investigated in this work.

This section discusses features of the Raman and infra-red spectra of butyl ZDDP, DDPA, DDDiS, ADDP, basic ZDDP, TDTP and a mixture of TTPhite/TTPhate.

4.1 Background Theory

If a vibration results in a change of dipole moment of a molecule it will absorb infra-red radiation. While the absorption frequency depends on the molecular vibrational frequency, the absorption intensity depends on how effectively the infra-red energy can be transferred to the molecule, and this depends on the magnitude of the change in dipole moment. If a molecule in its equilibrium configuration has a centre of symmetry, the vibrations during which the centre of symmetry is retained will be infra-red inactive.

In order for a molecular vibration to be Raman active, the vibration must be accompanied by a change in the polarizability of the molecule. The locus of points formed by plotting $1/\alpha^{1/2}$ (α = polarizibility) in any direction from the origin yields a surface called the polarizability ellipsoid. For a molecule which is completely anisotropic (polarizability is different in each direction) the ellipsoid has three axes of unequal length.

If the molecule is isotropic (equal polarizability in each direction) the ellipsoid becomes a sphere. If the polarizability ellipsoid is changed in size, shape or orientation as a result of a molecular vibration or rotation a Raman spectrum will result.

Selection rules for ir and Raman spectroscopy are thus different and the activity of a given vibration depends on the symmetry properties of the vibration.

Symmetries are specified by the point group of the molecule. Raman and ir spectroscopy complement each other and are useful tools for determining the structure and bonding of compounds. A simple comparison of the Raman and ir activities of the stretching vibrations of CO_2 (a linear molecule $D_{\infty h}$) and H_2O (a bent molecule C_{2v}) emphasise the points described above.

		Raman	ir
CO_2	νasym	inactive	active
	ν sym	active	inactive
H_2O	νasym	active	active
	ν sym	active	active

Because of the linear structure of CO_2 an asymmetric stretch produces no change in polarizability and a symmetric stretch is not accompanied by a change in dipole, consequently the asymmetric vibration is Raman inactive and the symmetric stretch is infra-red inactive. The asymmetric stretch and symmetric stretches of water are both Raman and ir active, however the symmetric stretch is accompanied by a much larger polarizability change than the asymmetric stretch, therefore the former mode of vibration is stronger in the Raman. Conversely the asymmetric stretch induces a larger change in dipole than the symmetric stretch and therefore the asymmetric stretch is stronger in the ir than the Raman.

Depolarization Ratio

The depolarization ratio ρ_l , for linearly polarized incident light, is defined by reference to planes parallel to, and perpendicular to, the direction of the incident electric vector. Thus, in the notation of figure (4.1.1), is given by

$$\rho_l = I_\perp / I_\parallel = |P_z|^2 / |P_y|^2$$

The Raman intensities $I_\perp$ and $I_\parallel$ are determined in successive experiments by means of a polarization analyser in the scattered light beam. For totally symmetric modes of spherically symmetric molecules $\rho_l = 0$. However, totally symmetric modes of other molecules have ρ_l value greater than zero but less than 3/4, (1). Non-totally symmetric modes have ρ_l equal to 3/4. Therefore, a measurement of the depolarization ratio provides a means of distinguishing totally symmetrical vibrations from the rest.

Fig 4.2.1 Raman spectrum of n-butyl ZDDP

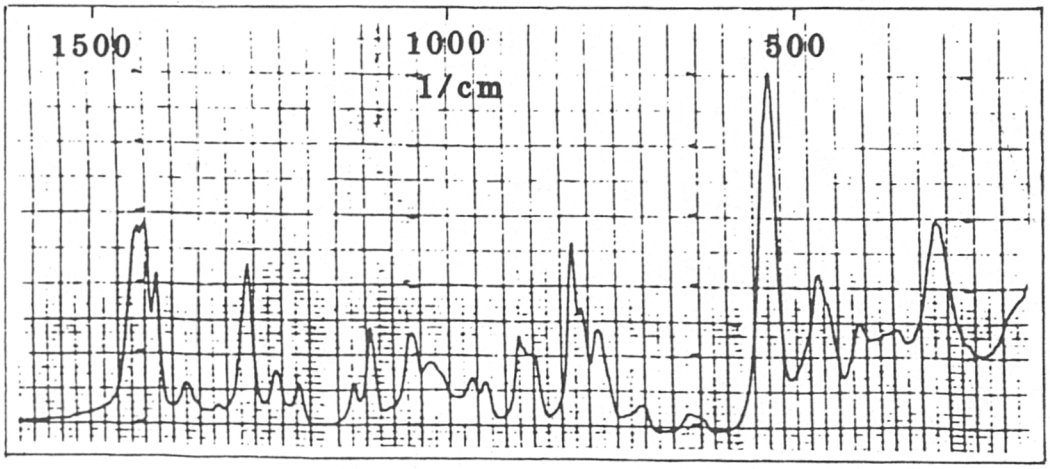

Fig 4.2.2 Raman spectrum of n-butyl ADDP

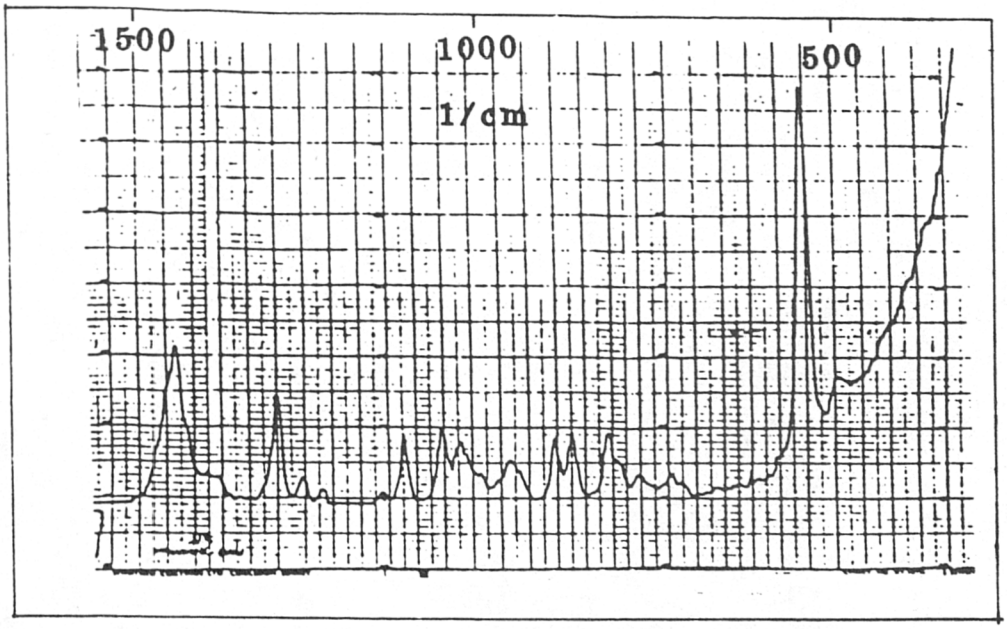

Fig 4.2.3 Raman spectrum of n-butyl basic ZDDP

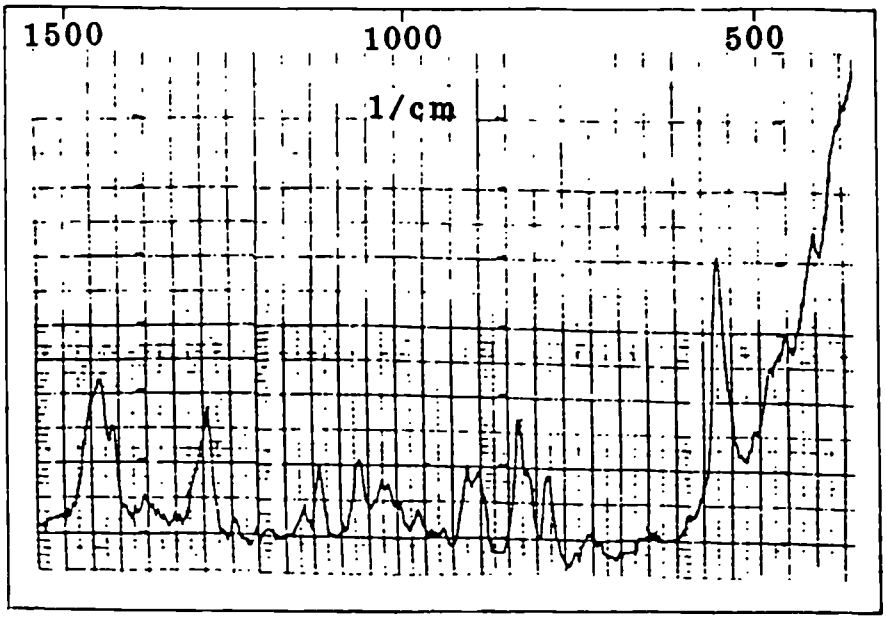

Fig 4.2.4 Raman spectrum of n-butyl DDPA

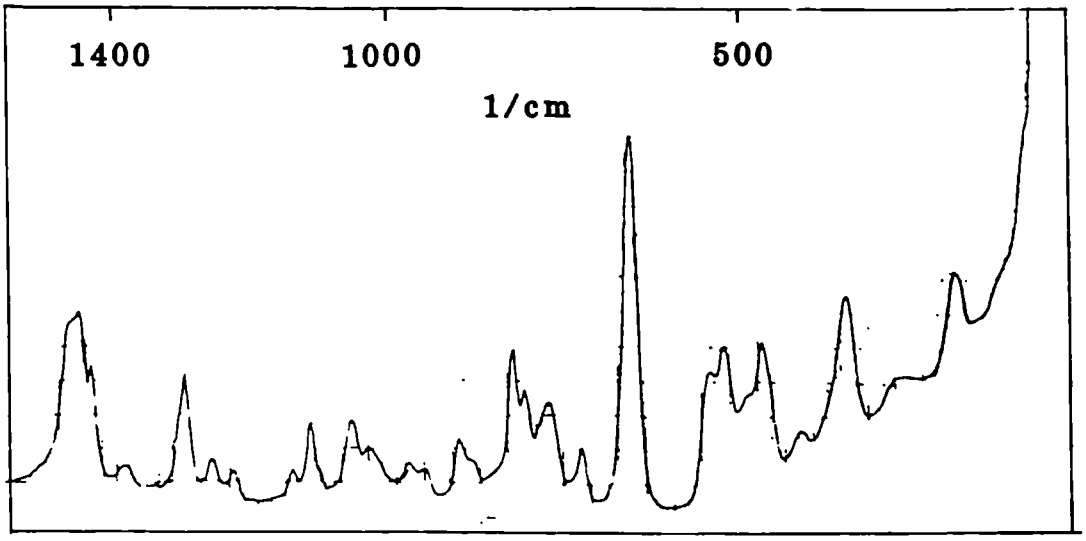

Fig 4.2.5 Raman spectrum of n-butyl DDDiS

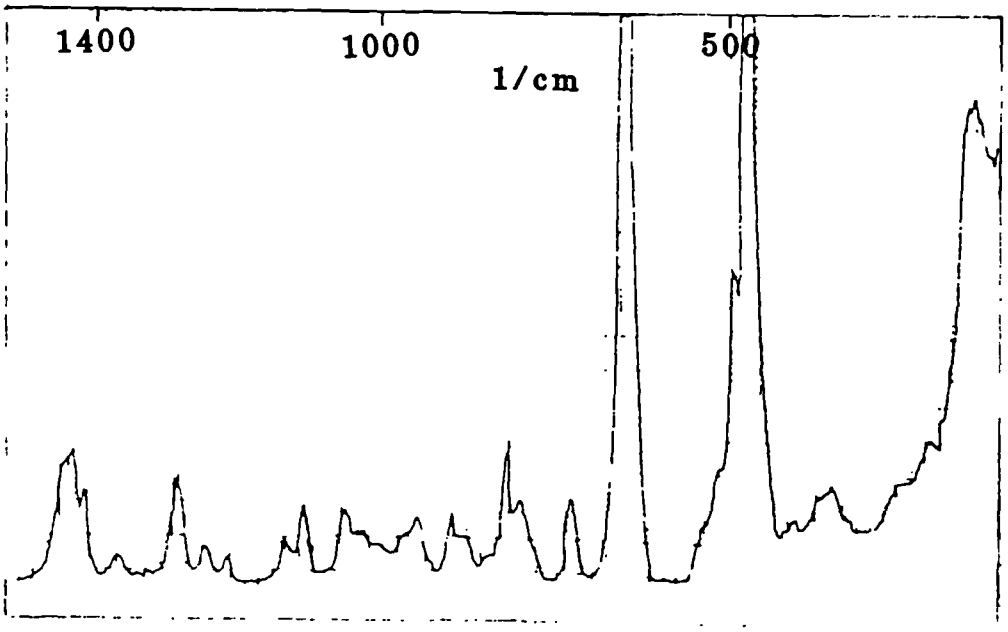

Fig 4.2.6 Raman spectrum of n-butyl TDTP

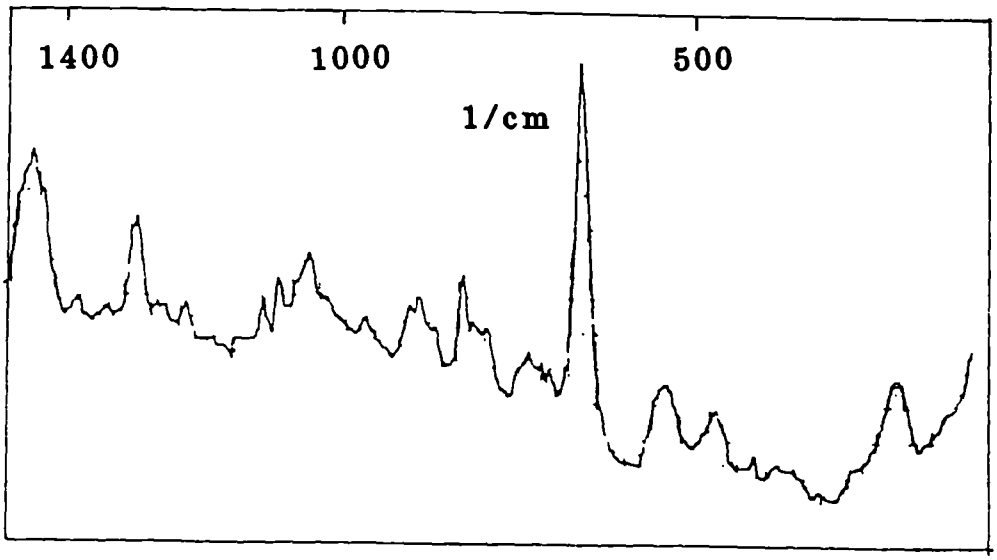

Fig 4.2.7 Raman spectrum of n-butyl TTetTP

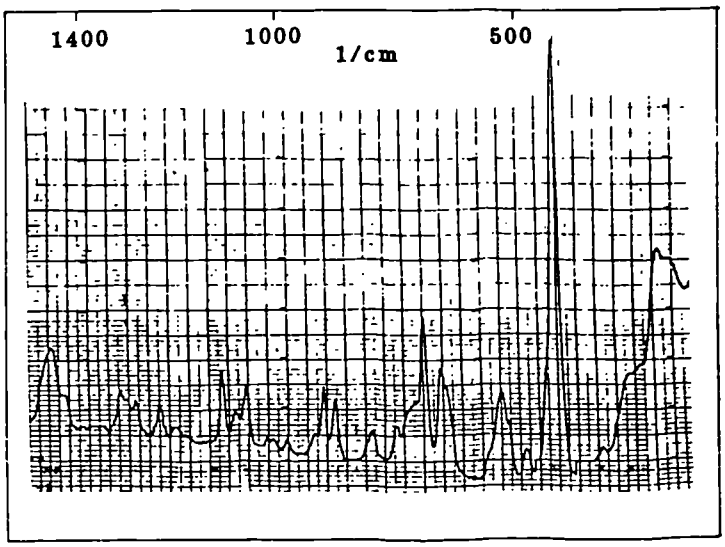

Fig 4.2.8 Raman spectrum of TTPhite with TTPhate impurity

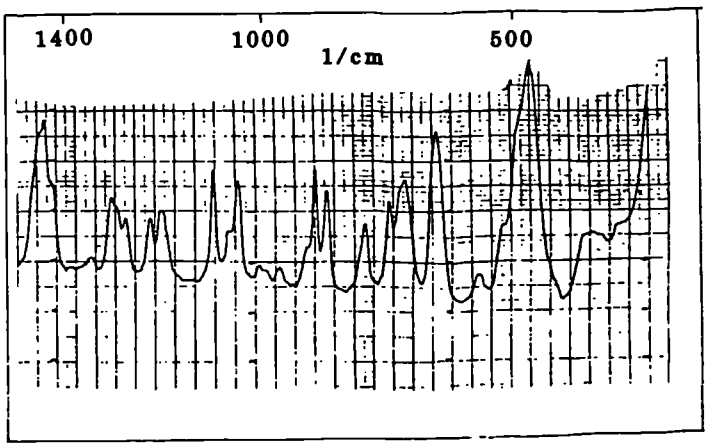

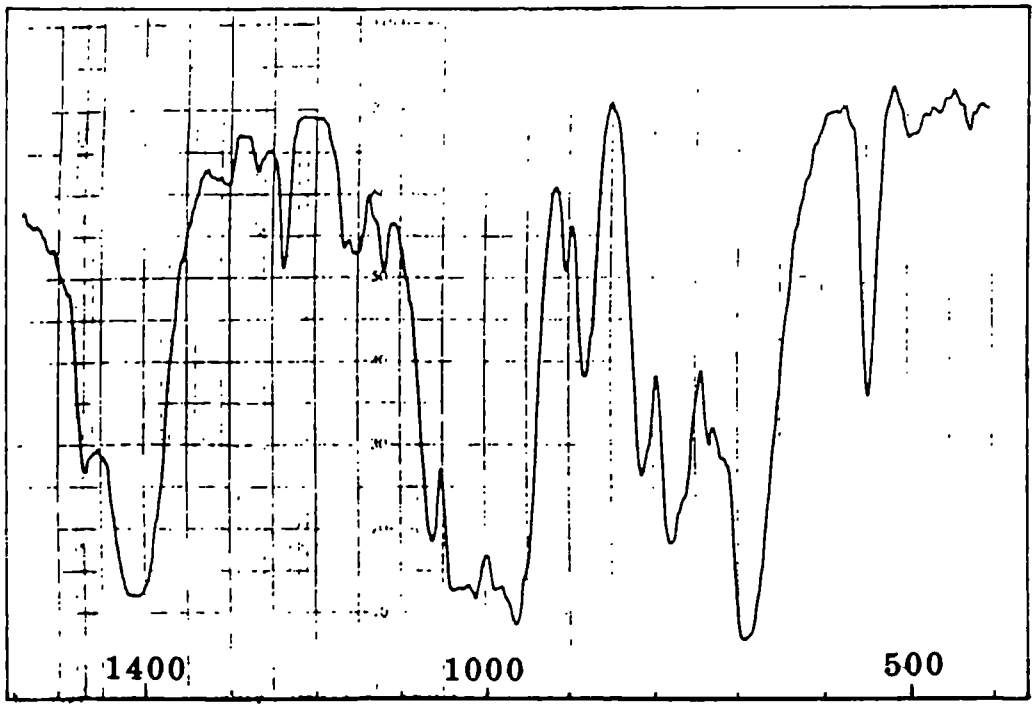

Fig 4.2.9 IR spectrum of n-butyl ADDP

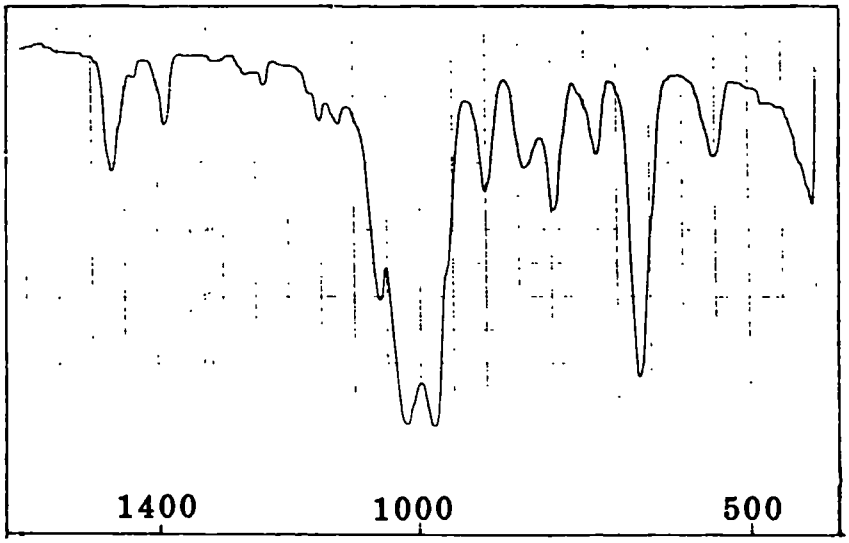

Fig 4.2.10 IR spectrum of n-butyl ZDDP

Fig 4.2.11 IR spectrum of n-butyl basic ZDDP

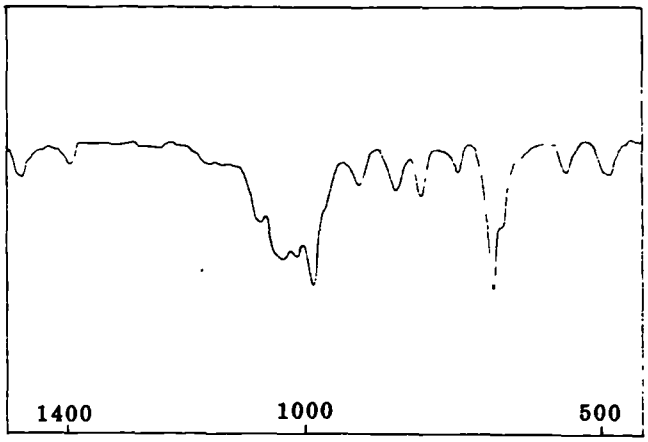

Fig 4.2.12 IR spectrum of n-butyl DDDiS

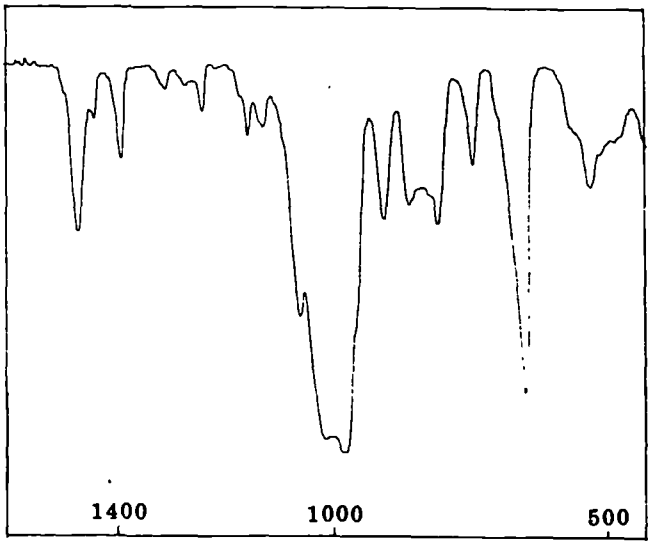

Fig 4.2.13 IR spectrum of n-butyl TTPhite /TTPhate mixture

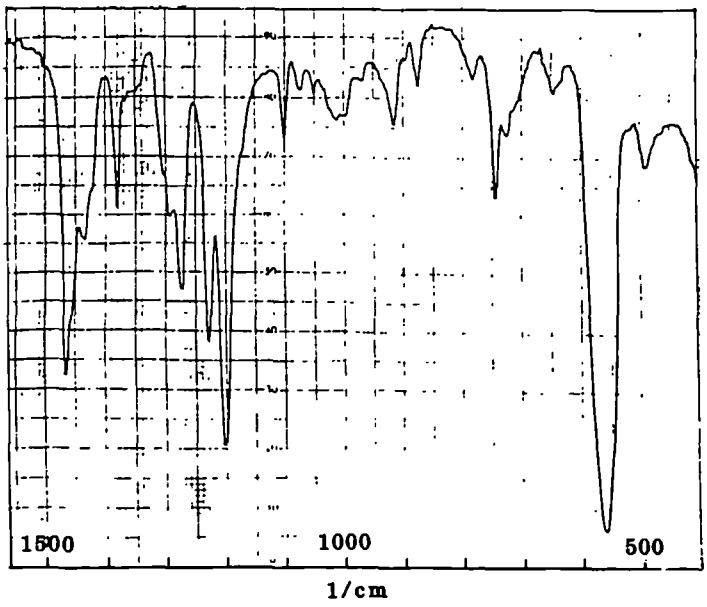

Fig 4.2.14 IR spectrum of n-butyl TTetTP

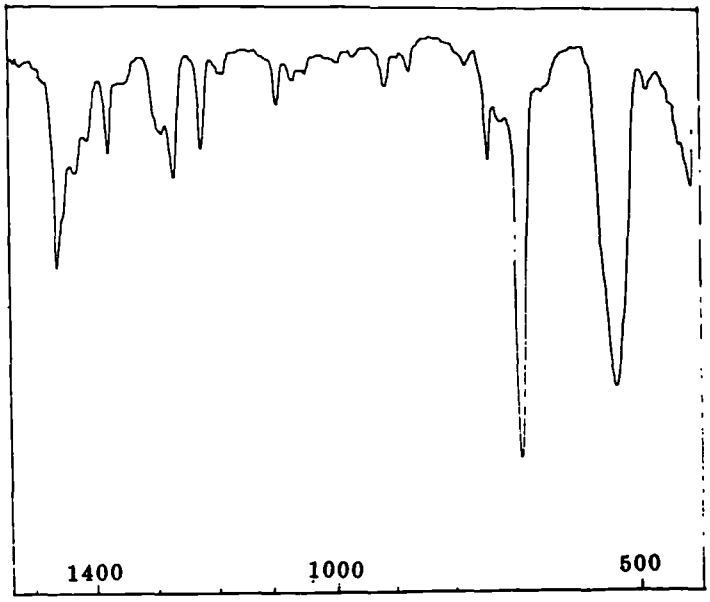

The IR spectrum of TDIP was recorded however it is not displayed here.

The IR spectrum of n-butyl DDPA is given in fig 5.1.4

Fig. 4.1.1

P_x = induced polarisation in the x direction

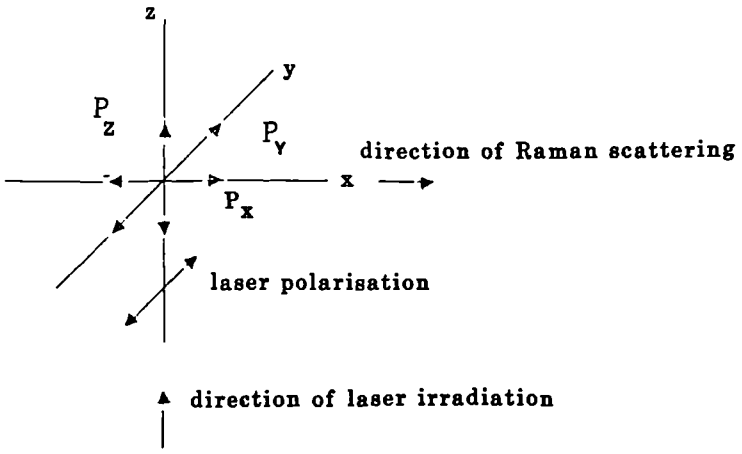

4.2 Experimental

Raman spectra were obtained using a Spex "Ramalab" spectrometer, using the Argon laser excitation line at 514.5 nm. Samples were mounted in the spectrometer in 1mm glass capillary tubes. Ir spectra were recorded with a Pye Unicam model SP 2000 spectrometer. The liquid samples were loaded into the spectrometer as thin films between KBr windows and solid samples were analysed as pressed KBr discs.

Results and Discussion

The spectra of these compounds are shown in figures (4.2.1 - 4.2.14).

a) The Co-ordination of the DDP Ligand to Zinc in ZDDP

The ir spectrum of n-butyl ZDDP is very similar to the covalent dithiophosphate compounds DDPA, DDDiS and TDIP. The mode of dithiophosphate ligand co-ordination to the zinc atom is often incorrectly displayed in the literature, (2-8).

By comparing the Raman and infrared spectra in the region of 500-700 wavenumbers with other dialkyldithiophosphates the mode of ligand co-ordination can be deduced. The table 4.2.1 lists the relative Raman and ir band intensities of n-butyl ADDP, ZDDP, Basic ZDDP, TDIP and DDPA in the region 500 - 700 cm^{-1}.

Table 4.2.1

Butyl	Raman		Infra-red	
ZDDP	650(vw)	550(s)	650(s)	550(m)
Basic ZDDP	660(vw)	550(s)	650(m), 670(ms)	550 m
ADDP	680(vvw)	550(s)	680(ms)	550(m)
DDPA	660(s)	535)(m)	660(s)	535)(mw)
		550)(m)		550)(mw)
TDIP	660(s)	550(m)	660(s)	550(mw)

The dialkyldithiophosphate P=S vibration is observed at approximately 650 cm^{-1} and is strong in the Raman and ir. Although basic ZDDP and ZDDP have ir spectra similar to covalent dialkyldithiophosphates, the Raman spectra resemble the spectrum of ADDP. There is no strong 650 cm^{-1} band present in the Raman spectra of basic and normal ZDDP, however a 550 cm^{-1} intense band exists. In conclusion, both the sulphur atoms of the dithiophosphate ligand are co-ordinated to the zinc atom giving rise to a symmetrical PS_2 stretch at 550 cm^{-1} ,(Raman (s), ir (m)) and an asymmetrical PS_2 stretch at 650 cm^{-1} (Raman (vw), ir (s)). An analogy can be drawn comparing the PS_2 unit of ZDDP with an isolated bent AB_2 molecule (eg. H_2O), whereby all bands are Raman and ir active, but have different relative intensities .

We have performed depolarization measurements of the 550 cm^{-1} band of ZDDP which have confirmed that this band is a symmetric vibration. The bonding of the ligands to the zinc atom of basic ZDDP and ZDDP will be discussed in more detail in the following test; however the structure of n-butyl ZDDP is indicated below:

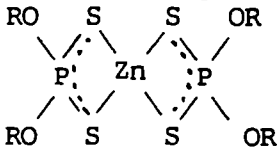

The zinc-sulphur vibration is probably featured at 305 cm^{-1} in the Raman. It is unique to ZDDP and has a comparable frequency to the zinc chloride bond at 280 cm^{-1} of the tetrachlorozincate ion, $ZnCl_4^-$,(9).

b) The assignment of the P=S vibrations

Chittenden and Thomas (10), argued that there are two P=S frequencies (I, 730 - 840 cm^{-1} and II, 580 - 690 cm^{-1}) in dithiophosphates, and these bands disappear on the isomerzation of (O,O',S) dialkyldithiophosphates to (O, S, S') dialkyldithiophosphates. Chittenden et al considered the two bands to be P=S vibrations of different conformers. However in view of the small differences arising from conformational variations in the calculations of Mayants et al (11), this suggestion is not convincing.

Bellamy stated (12), that if the P=S frequency is calculated from the force constant data the low frequency band is more likely to be due to the P=S vibration. Various authors quoted by Bellamy suggest that the P=S I frequency is lower in DDPA's because the P=S bond order is reduced by hydrogen bonding.

The Raman spectrum of ZDDP proves that no P=S stretch is present, however in the ir a band in, the "P=S band I" region, is observed. In a later section the hydrogen bonding of DDPA is analysed and results reveal that the P=S is not involved in hydrogen bonding, therefore dispelling the reduction of bond order, due to hydrogen bonding theory, postulated in the literature. The Raman spectra of covalent dithiophosphates should indicate the existence of a strong band in the region of 760 cm^{-1} - 840 cm^{-1} if Chittenden's assignment of two P=S conformers is correct, however, the same number of bands of similar intensity exist in ADDP in this region.

Nyquist argues that a P=S II band does not exist and suggests that a O-P-O antisymmetric stretch, coupling with some contribution from a C-O stretching vibration, is observed in this region, (13,14).

Nyquist discovered that phosphates had a band in this region which could not be attributed to a P=S vibration. Chittenden et al correctly assigned the P=S vibration of tetrathiophosphates at 690 cm^{-1}, but could not explain the absence of a P=S band I vibration in the infra-red. This is naturally, due to the absence of P-OR substituents.

In conclusion, therefore, only one P=S frequency is observed in the region of 580 - 690 cm^{-1} and is intense in the Raman and ir spectra. The P=S bond of DDDiS is especially strong in the Raman , occurring at 660 cm^{-1}. This is most likely the result of conjugation of the pi orbitals of the dithiophosphate disulphide unit.

c) P-S Vibrations

P-S vibrations are observable in both Raman and ir spectra with medium intensity, between 460 cm^{-1} - 600 cm^{-1} . They are observed as singlets in dialkyldithiophosphates at 550 cm^{-1} with the exception of DDPA, where the P-S vibration is a doublet. The P-S DDPA doublet is caused by the existence of two conformations involving the thiol proton, (see chapter 5)

The PS_3 symmetric vibration of n-butyl tetrathiophosphate occurs at 490 cm^{-1} and is very strong in the Raman but very weak in the infra-red. In contrast however, the PS_3 antisymmetric vibration is intense in the ir at 530 cm^{-1} but weaker in the Raman. Similarly the PS_3 symmetric vibration of the butyl phosphite/phosphate mixture is at 460 - 490 cm^{-1}, and band broadening is present because the sample is a mixture. The PS_3 asymmetric vibration of the phosphate-phosphite mixture is observed at 560 cm^{-1}

Table (4.2.2) summarizes the assignments of the bands observed in the region of 450 - 700 cm^{-1} for the synthesized n-butyl organophosphorus compounds and compares their relative Raman and ir intensities.

Table 4.2.2

	Raman		ir		Assignment
ZDDP	550	(s)	550	(m)	$\nu(PS_2)$sym
	650	(vw)	650	(s)	" (PS_2)asym
Basic ZDDP	480	(vvw)	480	(m)	" Zn-O
	550	(s)	550	(m)	" (PS_2)sym
	650	(vw)	670, 650	(ms)	" (PS_2)asym
ADDP	550	(s)	550	(m)	$\nu(PS_2)$sym
	650	(vvw)	650	(s)	" (PS_2)asym
DDPA	535, 550	(m)	535, 550	(m)	" (P-S)
	660	(s)	660	(s)	" (P=S)
DDDiS	480	(vvs)	480	(w)	ν (S-S)
	550	(m)	550	(m)	" (P-S)
	660	(vvs)	660	(s)	" (P=S)
TTetTP	490	(vs)	490	(vw)	" PS_3sym
	530	(w)	530	(s)	" PS_3asym
	690	(s)	690	(s)	" (P=S)
TTPhite/Phate	460-490	(ms)	460-490	(w)	ν PS_3sym
	560	(w)	560	(s)	" PS_3asym
TDTP	550	(m)	550	(m)	" (P-S)
	660	(s)	660	(s)	" (P=S)

d) The S-S Vibration

The S-S band of DDDiS occurs at 480cm^{-1} and is weak in the ir but a very intense doublet in the Raman.

e) P-O-C Vibrations

There is a general agreement in the literature that the presence of a P-O-C group in a molecule is characterised by a band at 1000 cm^{-1} which is strong in the infra-red, hence the absence in the ir spectra of TTetTP and the TTPhite/Phate mixture. There is however, a marked divergence of opinion when attempts are made to assign this band to either the P-O-(C) or the C-O-(P) vibrations.

Chittenden and Thomas (15,16), argue that the strong absorption band in the ir at approximately 1000 cm^{-1} is characteristic of the P-O rather than C-O vibration of the P-O-C group.

Nyguist (13,14), however disagrees with this assignment, arguing that the solution is more complex. The P-O vibrations and C-O vibrations are, according to Nyquist, coupled. This interpretation is consistent with the disproval of the Chittenden and Thomas band I and II P=S theory. Nyquist postulated that the bands at approximately 1000 cm^{-1} are mostly O-C symmetric and antisymmetric vibrations in character but with some O-P-O symmetric stretch and O-P-O asymmetric stretch character. Analogously the O-P-O asymmetric and symmetric vibration are observable between 860 and 780 cm^{-1} respectively and have contributions from the C-O symmetric and antisymmetric vibrations. Table 4.2.3 compares the bands observed in the Raman and ir in this 780 - 860 cm^{-1} region.

Table 4.2.3

Vibration	DDDiS		ZDDP		BZDDP		ADDP		TTetTP		ADDP in DMA	
	Raman	IR	Raman	IR	Raman	IR	Raman	IR	Raman	IR	Raman	IR
ν(O-P-O)asym		850cm^{-1}		840cm^{-1}		830cm^{-1}		810cm^{-1}				810cm^{-1}
unidentified	825cm^{-1}		830cm^{-1}		830cm^{-1}		830cm^{-1}				830cm^{-1}	
unidentified	815cm^{-1}		820cm^{-1}		820cm^{-1}		810cm^{-1}				810cm^{-1}	
ν(O-P-O·sym	800cm^{-1}	800cm^{-1}	800cm^{-1}	800cm^{-1}	790cm^{-1}	790cm^{-1}	780cm^{-1}	780cm^{-1}	790(w)	790(vw)	780cm^{-1}	780cm^{-1}

All bands are of medium intensity unless stated otherwise.

The higher-frequency P-O vibration is the antisymmetric stretch because it is too weak to be detected in the Raman.

The absence of bands of medium intensity in this region for TTetTP and the fact that the destruction of the ADDP lattices by solvation in DMA does not change the Raman and ir spectrum in this region, enforces Nyquist's assignment.

Analysis of table 4.2.3 reveals an interesting trend. The (O-P-O) symmetric and asymmetric vibrations move to lower frequencies as the degree of covalency of the dithiophosphates is reduced.

f) [(P)-S-R] Vibrations

Chittenden and Thomas (10), identified an ir band (1260 - 1270 cm^{-1}) which is characteristic of the (P)-S-R group. TDTP, TTetTP and TTPhite/Phate all have a band in this region of medium weak intensity in the ir but no band is observed in the Raman. Chittenden and Thomas offered no assignment of this band, however, it is too high for a C-S fundemental vibration and is probably a combination band.

g) P=O Vibrations

The P=O vibration frequency is at 1200 cm^{-1} (10), and is present in the Raman and ir spectra of the TTPhite/Phate mixture. The oxidation of the TTPhite to TTPhate can be monitored by viewing the increase of the P=O band intensity either in the Raman or infra-red.

4.3 The Comparison of the ir and Raman Spectra of ZDDP and BZDDP with Reference to the Crystal Stucture of BZDDP.

The molecular structure of Basic ZDDP is analogous with that established for basic beryllium acetate, (17,18) and basic zinc acetate, (19). A neutral oxygen is surrounded tetrahedrally by four zinc atoms and six dialkyldithiophosphate groups attached symmetrically to the edges of the tetrahedron, (20,21).

The Raman and ir spectra of ZDDP and Basic ZDDP are very similar with the following exceptions.

1) The PS_2 asymmetric vibration of Basic ZDDP is observed as a strong doublet in the ir (650 - 670 cm^{-1}) however, the PS_2 asymmetric vibration of ZDDP is a singlet (660 cm^{-1}). The two sulphur atoms of a BZDDP dithiophosphate ligand bond to different zinc atoms rather than just one, which is probably the case for butyl ZDDP. This more complicated co-ordination may affect the PS_2 asymmetric vibration.

2) The Zn-O vibration is of medium intensity in the ir at 480 cm^{-1}.

3) The BZDDP νC-O region at 1000 cm^{-1} is more resolved than the corresponding region in the ir spectrum of ZDDP.

4) The (O-P-O) symmetric and asymmetric vibrations are slightly lower in the case of BZDDP.

5) Various authors (22), reported the presence of a band at 1200 cm^{-1} in the ir of iso-propyl basic ZDDP, and assigned it to a P=O vibration. We have found however, that both basic butyl and iso-propyl basic ZDDP's do not exhibit this extra band. The authors were probably referring to a band in the 1000 cm^{-1} region that is more intense in basic ZDDP in the ir than the corresponding band of ZDDP.

4.4 A Comparison of the PS_2(sym) and PS_2 (asym) Vibrations and their Relevance to Molecular Structure of n-Butyl, n-Octyl and Iso-propyl ZDDP's and ADDP's

Analysis of the PS_2 symmetric and asymmetric vibrations of octyl, butyl and iso-propyl ADDP and ZDDP's reveal some interesting features (see figures 4.4.1-4.4.8). PS_2 vibrational frequencies are listed in table 4.4.1.

Table 4.4.1

$\nu(PS_2)$ Frequencies

compound	Raman		ir	
	ν asym	ν sym	ν asym	ν sym
iso-propyl ZDDP	655 (vw)	535 (ms)	655 (s)	535 (m)
iso-propyl ADDP	-	560 (m) 590 (m)	670 (s) 685 (s)	560 (m) 590 (m)
n-octyl ZDDP	655 (vw)	555 (ms)	655 (s)	560 (m)
n-octyl ADDP	-	550 (s)	700 (s)	550 (m)
n-butyl ZDDP	655 (vw)	550 (s)	655 (s)	550 (m)
n-butyl ADDP	-	560 (s)	680 (s)	560 (m)

The PS_2 asym and PS_2 sym vibrations of iso-propyl ADDP are both split indicating that there must be two PS_2 environments in the crystal lattice.

Therefore, to compare frequencies it is appropriate to use an average PS frequency or use the νPS_2 frequencies observed when the ADDP is dissolved in DMSO { $\nu(PS)_2$ (sym) = 560 cm^{-1} , $\nu(PS)_2$ (asym) = 680 cm^{-1} }.

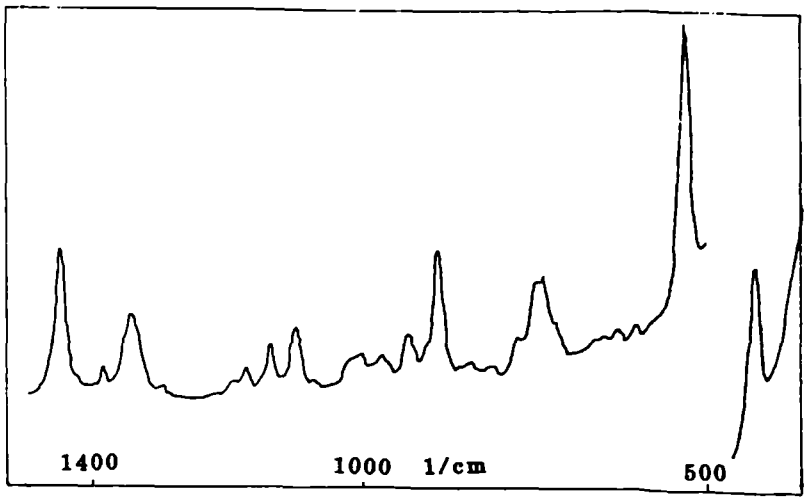

Fig 4.4.1 Raman spectrum of iso-propyl ZDDP

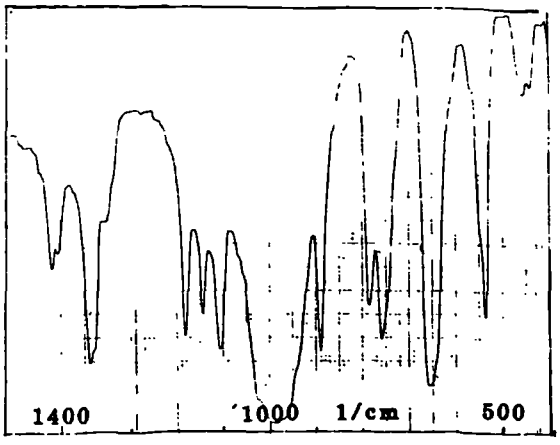

Fig 4.4.2 IR spectrum of iso-propyl ZDDP

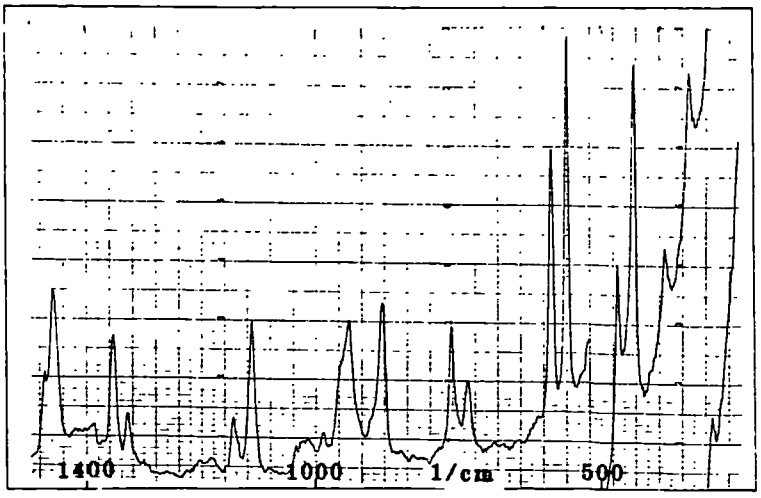

Fig 4.4.3 Raman spectrum of iso-propyl ADDP

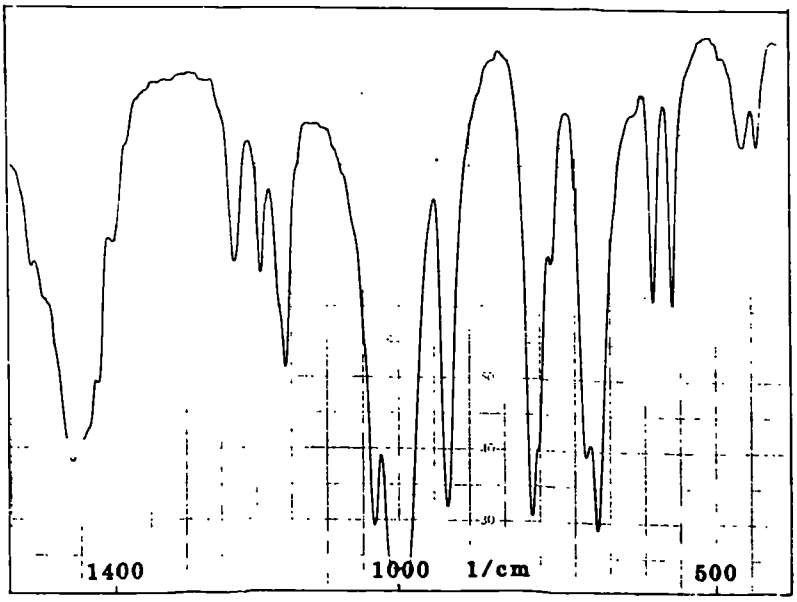

Fig 4.4.4 IR spectrum of iso-propyl ADDP

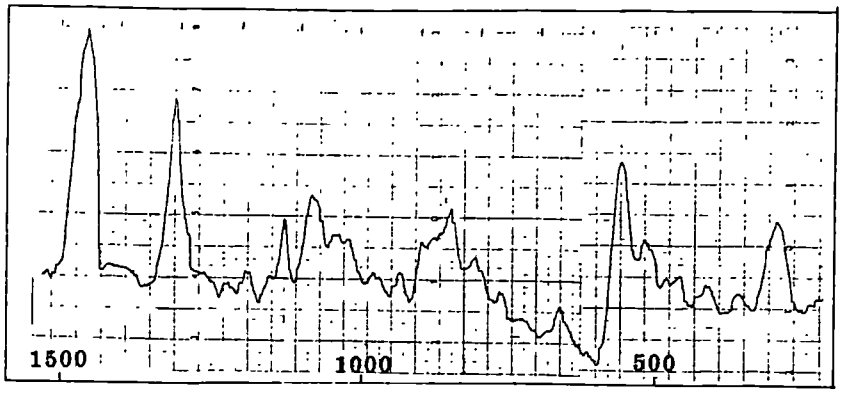

Fig 4.4.5 Raman spectrum of n-octyl ZDDP

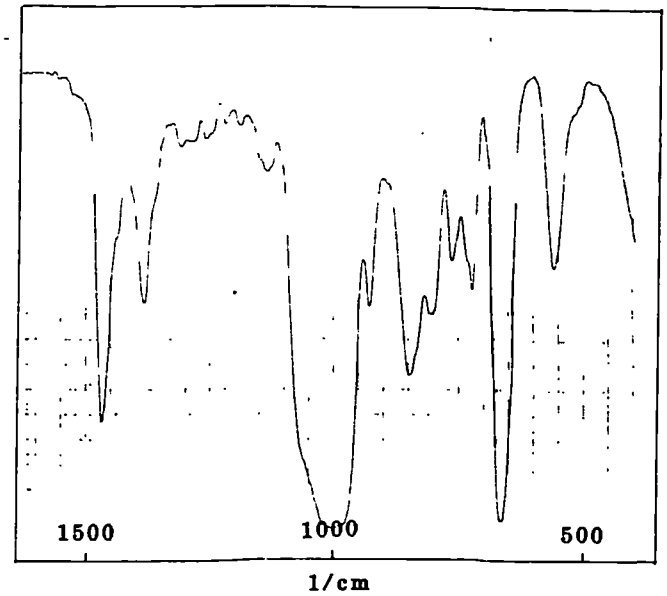

Fig 4.4.6 IR spectrum of n-octyl ZDDP

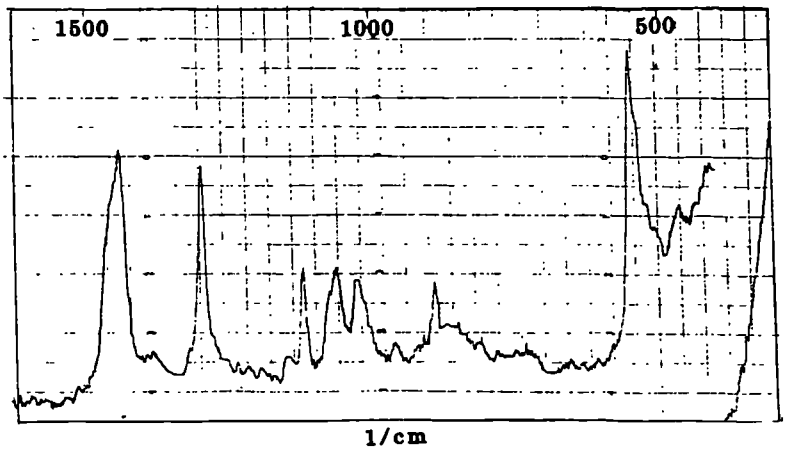

Fig 4.4.7 Raman spectrum of n-octyl ADDP

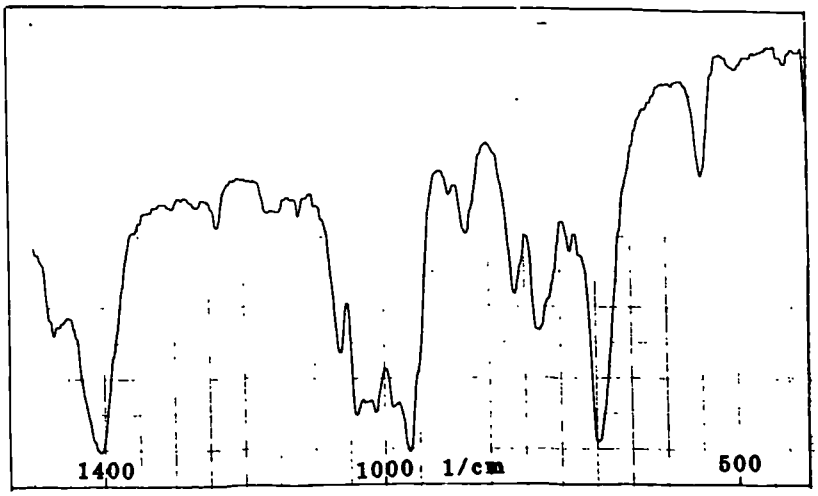

Fig 4.4.8 IR spectrum of n-octyl ADDP

The bonding of the dithiophosphate ligand to the zinc atom reduces the bond order of the PS_2 unit. The lower frequencies of the PS_2 symmetric and asymmetric vibrations reflect this fact. The largest differences are observed in the spectrum of iso-propyl ZDDP. This is expected, as iso-propyl ZDDP is the most stable ZDDP. Iso-propyl ZDDP is a crystalline solid, but n-butyl and n-octyl ZDDP's are liquids. The iso-propyl groups pack more easily allowing a stronger zinc ligand interactions.

Coppens (23), documented the crystal structure of iso-propyl ZDDP and iso-propyl potassium dialkyldithiophosphate. The average P-S bond length of iso-propyl ZDDP is 1.97 Å but it is 1.6 Å for iso-propyl KDDP, indicating the higher bond order of the KDDP PS_2 unit. Iso-propyl ZDDP has four sulphur atoms co-ordinated to each zinc metal atom in a distorted tetrahedral environment. Associated with each metal atom are two dithiophosphate ligands of which one functions as an intrachelating bond wholly to one metal atom and the other functioning as an interchelating group linking two molecules together to form a chain-like structure.

It is difficult to assess whether n-octyl and n-butyl ZDDP have similar interchelating groups but we suspect that this feature is characteristic of a crystalline ZDDP and the liquid ZDDP's have two intrachelating ligands bonded to the zinc atom.

ZDDP's have four zinc-sulphur bonds. Two, we believe are sigma bonds involving both electrons from the zinc 4s shell and an electron from the 3p shell of two sulphurs. The others are dative pi bonds where two sulphur lone pairs are donated into the empty 4p orbital of zinc.

In strongly metal co-ordinating solvents such as DMSO (DN = 29.8, ξ = 46.7, AN = 19.3), the Zn-S bonding is broken and the ir and Raman spectra are identical to the dithiophosphate ion (ADDP in DMSO), (see fig 4.4.9). Intermediate behaviour occurs when iso-propyl ZDDP (20%), is dissolved in DMA (N-N-dimethylacetamide). The following equilibrium is observed:

$$\underset{\nu PS_{2\,sym} = 535\ cm^{-1}}{Zn\,[(RO)_2PS_2]_2} \rightleftharpoons \underset{\nu PS_{2\,sym} = 560\ cm^{-1}}{Zn^{2+} + 2(RO)_2PS_2^-}$$

R=iso-propyl

Two bands are observed in the Raman and ir at 535 cm^{-1} (ZDDP νPS_2 sym) and 560 cm^{-1} (DDP- νPS_2 sym), (see figs 4.4.10- 4.4.11)

Fig 4.4.9 IR spectrum of 30% iso-propyl ZDDP in DMSO

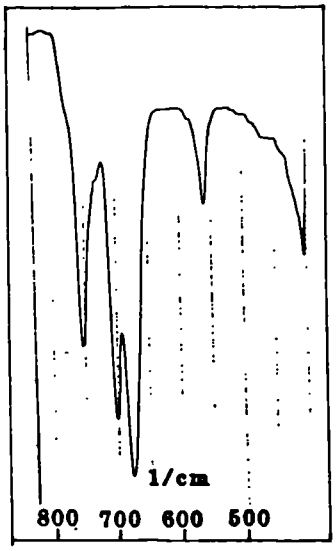

Fig 4.4.10 Raman spectrum of 20% isopropyl ZDDP in DMA

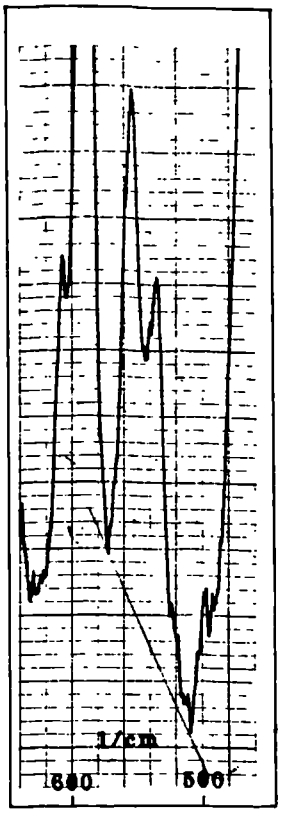

Fig 4.4.11 IR spectrum of 20% iso-propyl ZDDP in DMA

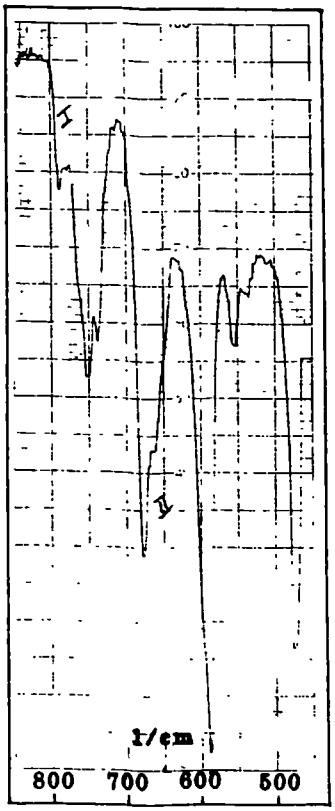

4.5 The Raman and ir specta of Ethyl and Butyl PbDDP

Butyl PbDDP was prepared by mixing stoicheiometric amounts of aqueous butyl ADDP with lead acetate. The white solid precipitate was dried at the pump. Raman and ir spectra were obtained as previously described, (see figs 4.5.1- 4.5.2).

Table 4.5.1 Bands in the Region 500 - 700 cm^{-1} for Butyl PbDDP and ZDDP

PbDDP (Solid)		ZDDP (Liquid)	
Raman	ir	Raman	ir
570(m)	570(m)	550(s)	550(m)
650(vs)	650(s)	660(vw)	660(ms)

In contrast to butyl ZDDP, PbDDP exhibits a strong band at 650 cm^{-1} in the Raman, indicating the presence of a P=S vibration rather than a PS_2 asym vibration. It follows therefore, that only two sulphur atoms are co-ordinated to the lead atom. The 6p orbitals of lead therefore do not accommodate lone pairs from two sulphur atoms to form dative Pb-S bonds. No crystallographic data was found in the literature for n-butyl PbDDP; however, the crystal structure of ethyl PbDDP is well documented, (24). Raman spectra of ethyl PbDDP and ethyl ZDDP were performed and confirmed that the differences occurring in the bonding of ethyl PbDDP and ethyl ZDDP are analogous to those of butyl ZDDP and butyl PbDDP (see figs 4.5.3- 4.5.4). The P-S bond lengths of the interchelating DDP ligands of ethyl ZDDP are more nearly equivalent (25), (a difference of 0.05 Å), than the P-S bond lengths of ethyl PbDDP, (a difference of 0.23 Å), thereby reinforcing the Raman and ir spectroscopic conclusion that two of the four sulphurs encompassing the lead atom are, mainly P=S in character.

Fig 4.5.1 Raman spectra of n-butyl PbDDP

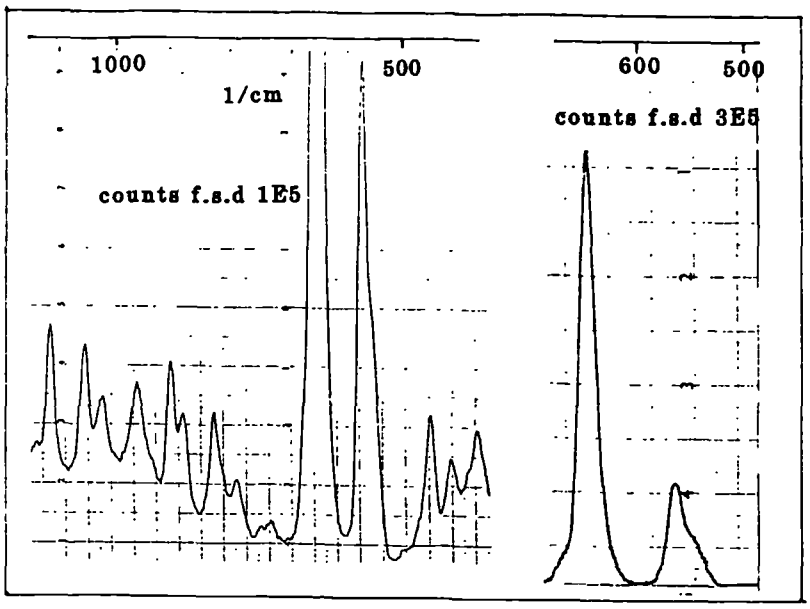

Fig 4.5.2 IR spectrum of n-butyl PbDDP

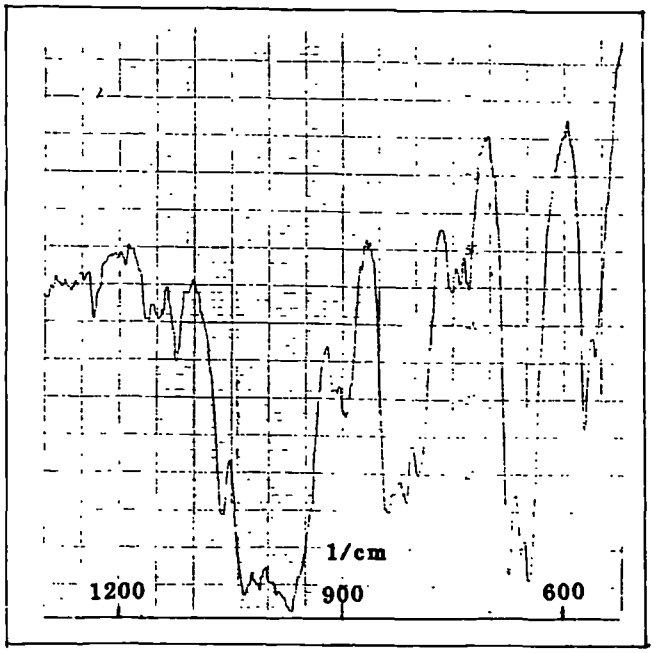

Fig 4.5.3 Raman spectrum of ethyl ZDDP

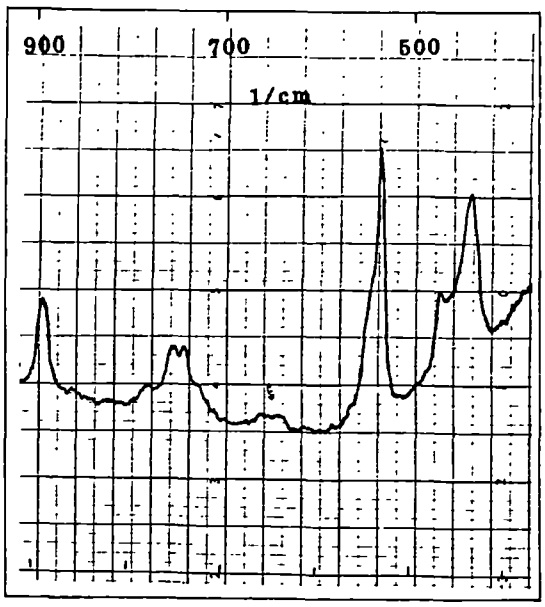

Fig 4.5.4 Raman spectrum of ethyl PbDDP

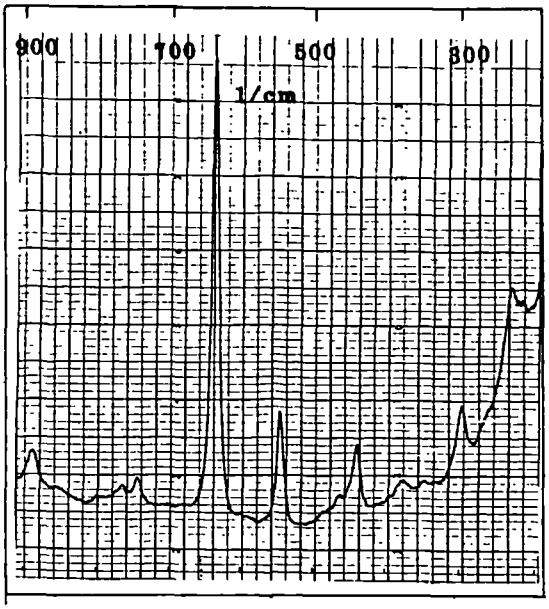

4.6 Solution Behaviour of Butyl PbDDP in DMA

Solid butyl PbDDP has a Raman intensity ratio for the P=S (650 cm^{-1})/ P-S (550 cm^{-1} bands of approximately 4.4. However a 20% solution in DMA has a 650 cm^{-1} /550 cm^{-1} band intensity ratio of 1.0, (see fig 4.6). The band intensity ratio is reduced because the complex, to a certain extent, is dissociated by the DMA solvent. This equilibrium is more easily observed than the ZDDP case where in the Raman the PS_2 asymmetric vibrations of ZDDP and the DDP- ion are very weak and the frequencies nearly coincide with each other.

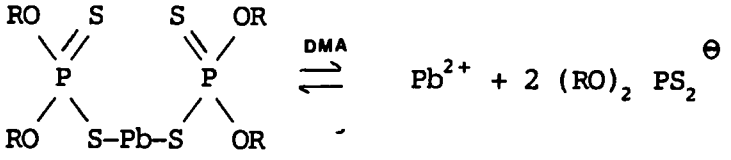

	Raman	ir		Raman	ir
ν(P=S)650cm^{-1}	(s)	(s)	$\nu_{(asym)}PS_2$	(vvw)	(s)
ν(P-S)550cm^{-1}	(m)	(m)	$\nu_{(sym)}PS_2$	(s)	(m)

4.7 Depolarization Measurements of Selected Bands in the Raman Spectrum

Depolarization measurements were performed on the PS_2 sym band of n-butyl ZDDP and on the P=S bands of n-octyl DDPA and DDDiS, (see figs 4.7.1- 4.7.3).

Results

	ρ
n-Butyl ZDDP	
ν PS_2 sym (550 cm^{-1})	0.023
n-Octyl DDPA	
ν P=S (650 cm^{-1})	0.084
n-octyl DDDiS	
ν P=S (650 cm^{-1})	0.29
ν S-S (480 cm^{-1})	0.405

All these vibrations are totally symmetric modes of molecules that are not spherically symmetric. The high degree of polarization of the ZDDP 550 cm^{-1} band indicates that it is the PS_2 sym vibration. The DDPA P=S bond has a higher degree of polarization than the P=S of n-octyl DDPA. Free rotation around the disulphide S-S bond reduces the symmetry of the molecule and therefore reduces its degree of polarization.

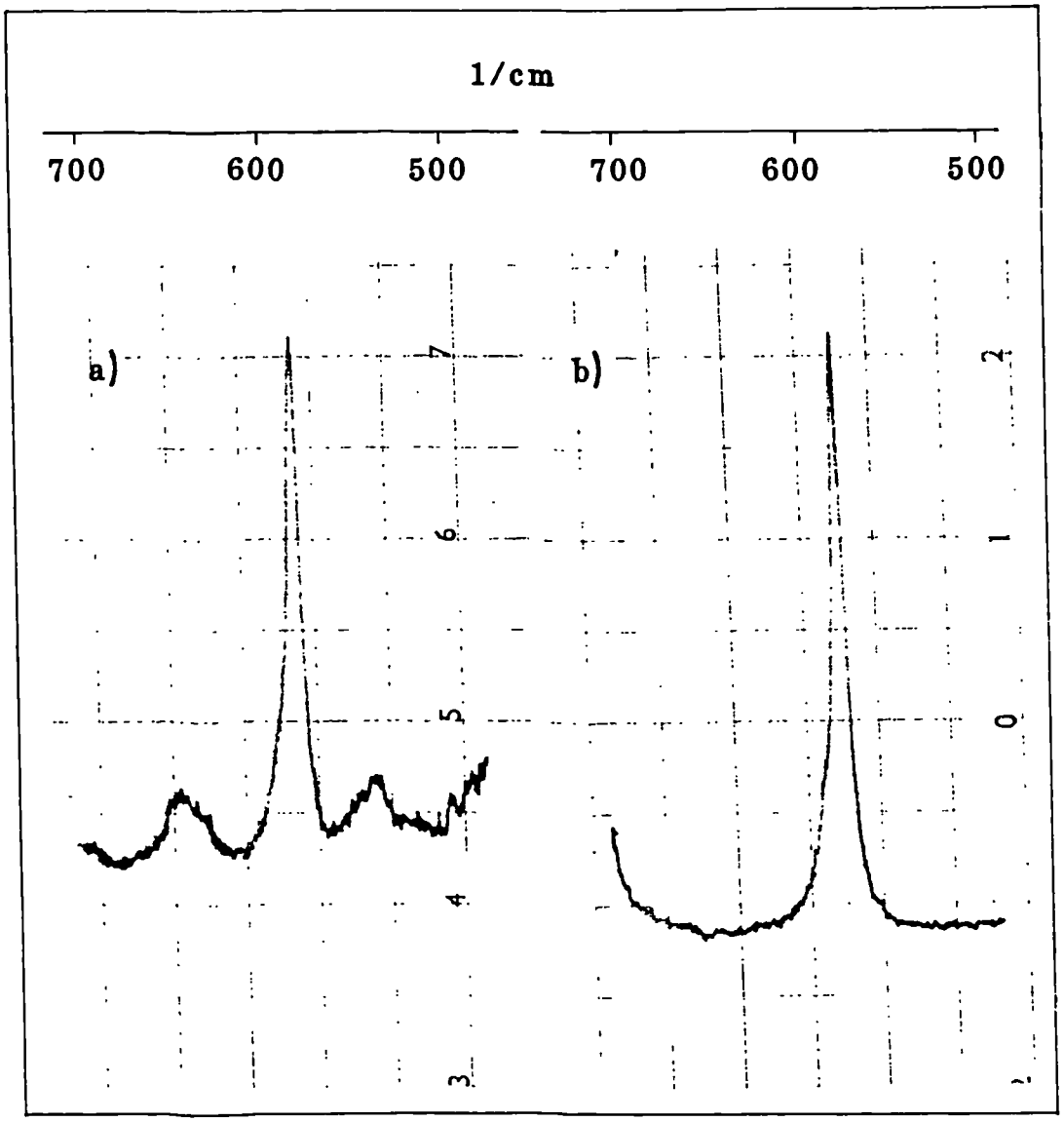

Fig 4.6 a) Raman spectrum of 20% n-butyl PbDDP in DMA

b) Raman spectrum of DMA

Fig 4.7.1 Raman spectra of n-butyl ZDDP a) max b) min settings of polarizer

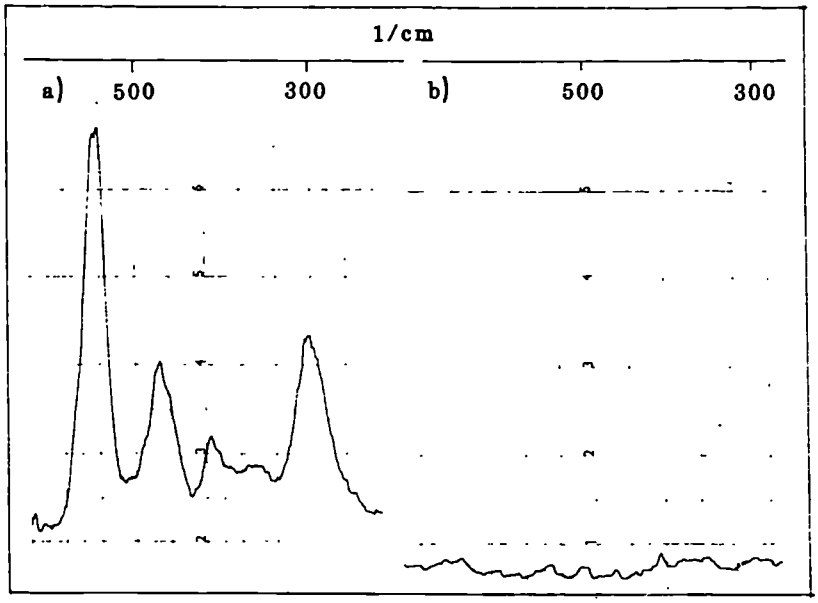

Fig 4.7.2 Raman spectra of n-octyl DDDiS a) max b) min settings of polarizer

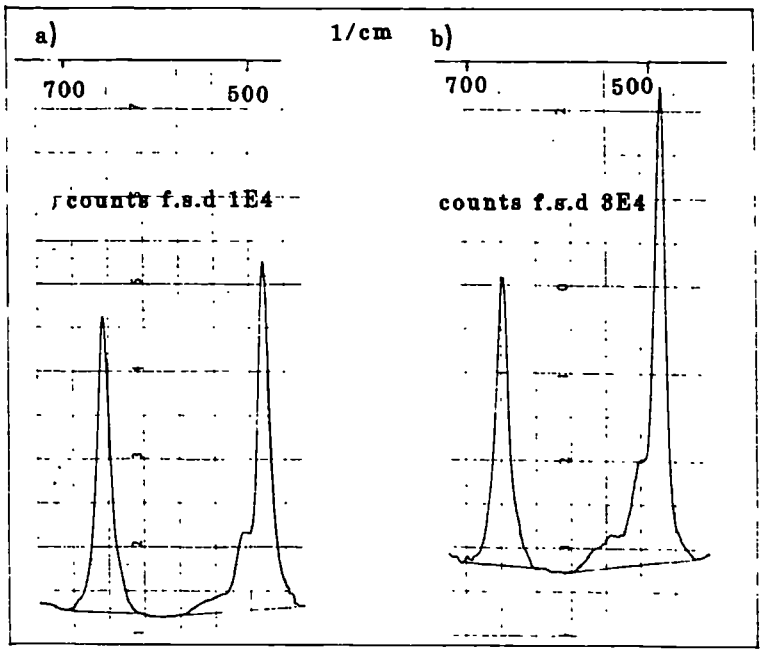

Fig 4.7.3 Raman spectra of n-octyl DDPA a) max b) min settings of polarizer

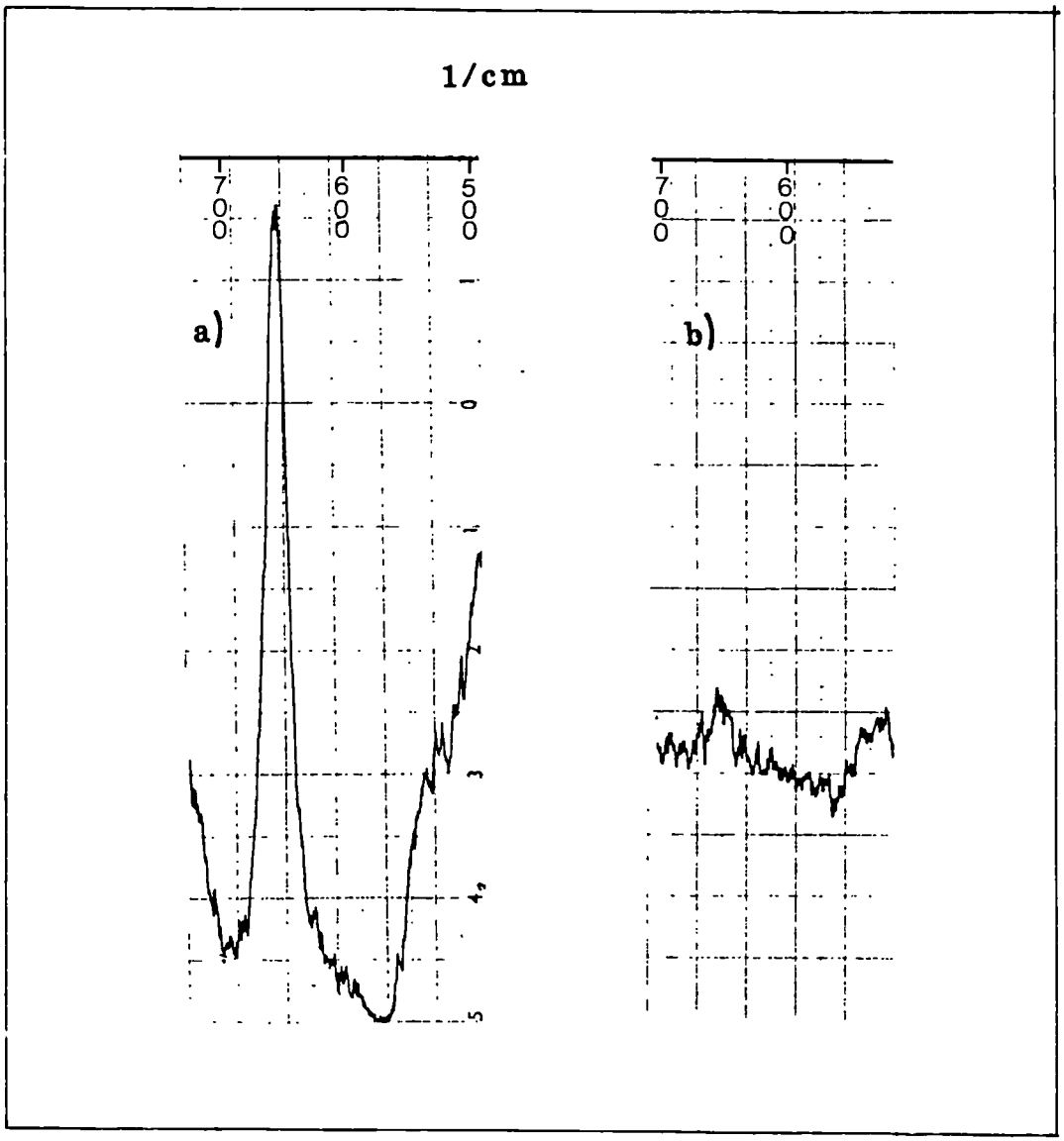

Chapter 4

1) Wilson E.B., Decius J.C. and Cross P.C., "The Theory of Infrared and Raman Vibrational Spectra", McGraw - Hill Publishing Company Ltd., London.

2) Willermet R.A., Mahoney L.R. and Bishop C.M., A.S.L.E Trans. 1980, Vol 23, 3, 217-224.

3) Spedding H. and Watkins R.C., Tribology 1982, Vol 15, 9-12.

4) Dickert J.J and Rowe C.N., J. Org. Chem. 1967, Vol 32, 647-653.

5) Rounds F.G., A.S.L.E Trans. 1975, Vol 18, 2, 79-89.

6) Burn A.J., Tetrahedron 1966, Vol 22, 2153-2161.

7) Ellis R.J., Lake P.J. and Marshall R.A.G, J. Chem. Tech. Biotechnol. 1980, 30, 602-610.

8) Larson R., Scientific Lubrication, August 1958, 12-19.

9) Morris D.F.C., Short E.L. and Waters D.N., J. Inorg. Nucl. Chem. 1963, Vol 25, 975-983.

10) Chittenden R.A. and Thomas L.C., Spectrochim. Acta. 1964, Vol 20A, 1679-1696.

11) Mayants L.S., Optics and Spectroscopy 1959, 7, 108.

12) Bellamy L.J., "Advances in Infrared Group Frequencies", Chapman and Hall, London, 1975, 211.

13) Nyquist R.A., Spectrochim. Acta. 1968, Vol 22A, 1563-1569.

14) Nyquist R.A. and Meulder W.W., Spectrochim. Acta. 1968, Vol 24A, 187-201.

15) Chittenden R.A. and Thomas L.C., Spectrochim. Acta. 1964, Vol 20A, 467-487.

16) Chittenden R.A. and Thomas L.C. Spectrochim. Acta. 1964, Vol 20, 489-502.

17) Bragg W.H. and Morgan C.T., Proc. Roy. Soc. 1923, 104, 437.

18) Morgan C.T. and Astbury W.T., Proc. Roy. Soc. 1926, 112, 441.

19) Koyama H. and Saito Y., Bull. Chem. Soc. Japan. 1954, 27, 112.

20) Burn A.J. and Smith G.W., Chem. Comm. 1967, 17, 394.

21) Normura and Takeshi, Junkatsu 1980, Vol 25, 2, 95-96.

22) McCleverty J.A., et al. J. Chem. Soc. Dalton trans. 1983, 627-634.

23) Coppens P.H. et al., Acta. Crystal. 1962, 15, 765.

24) Tetsuzo I., Acta. Cryst. 1972, B28, 1034.

25) Tetsuzo I., Acta. Cryst. 1969, B25, 2303.

CHAPTER 5

Rotational Isomersion of O-O' Dialkyl Dithiophosphoric Acid (DDPA)

5.1 Introduction

The dimethyl DDPA was investigated by Nyquist (1), who showed that several bands in the ir spectrum of the liquid appear as doublets, due to the presence of rotational isomers. Many other organophosphorus compounds also show ir spectral complexities due to rotational isomersion (2-6), but little informamation on the quantitative aspects of the equilibria between the isomers is available. Raman spectra of DDPA's have not been reported. Raman and ir spectroscopic examinations of n-butyl, n-octyl and iso-propyl DDPA's were performed with a view to studying the rotational isomerisation in these molecules in more detail. A short account of our work has appeared, (7).

Experimental

The acids were regenerated from the ammonium salt using the anhydrous method previously described, (Chp.3). P-31, C-13 and H-1 NMR analysis of the aqueous acid method of preparation revealed the presence of hydrolysis inpurity, possibly $(RO)_2$ P=S (OH). For example, iso-propyl DDPA has a P-31 chemical shift of 82 ppm relative to phosphoric acid, however an impurity signal is observed at 56.5 ppm.

Raman spectra were obtained with a Spex "Ramalab" spectrometer, using Argon laser excitation. Samples for study were contained in a 1mm capillary tube mounted in a heating block where the temperature could be controlled within the region 20 - 110 deg C. Ir spectra were recorded with a Pye Unicam model SP2000 spectrometer, with samples in a Specac model 2000 variable-temperature cell. The samples were enclosed in KBr windows. Temperature variations of relative band intensities (peak heights from Raman spectra; absorbances from ir spectra) were used to estimate ΔH values for the equilibria between the conformers. Writing $I_a = J_a C_a$, $I_b = J_b C_b$ where J_a and J_b are molar intensities of conformers a and b respectively, we have for the equilibrium constant, $K = C_a/C_b = (I_a)/(I_b)/(J_a)/(J_b)$. ΔH may be obtained from the plot of I_a/I_b against $1/T$. Spectra at various temperatures were recorded of solutions at appropriately dilute concentrations in n-tetradecane.

This solvent is sufficiently inert, non volatile and free from spectral interferences so that no problems were encountered in recording the spectra for the range 20 - 110 deg C. (It was not possible to determine ΔG for these equilibria, since the use of the equation $\Delta G = -RT\ln K$ requires a knowledge of the ratio J_a/J_b. This is probably near unity for most cases studied, however; this assumption has not been made).

The DDPA's were deuterated by shaking several times with D_2O, with a view to performing Raman and ir spectral measurements.

Results and Discussion

Figures (5.1.1-5.1.4) present the ir and Raman spectra of the undiluted n-butyl and iso-propyl DDPA's at room temperature. Bands which are important in connection with conformational equilibria are (i)ν(SH) 2400-2600 cm^{-1}, (ii)ν P=S 660 cm^{-1} (iii)ν P-S 520-550 cm^{-1} and (iv) ν P-(O)$_2$ asym 840-860cm^{-1}. Table 5.1.1 summarises these assignments for n-octyl, n-butyl and iso-propyl DDPA and compares them with Nyquists' assignments for $(CH_3O)_2$ P=S (SH) and $(CH_3O)_2$ P=S (Cl), (1,6).

(i) SH (SD)

Deuteration of butyl DDPA produced new bands in the region 1760 cm^{-1} - 1900 cm^{-1}. These are clearly distinguishable in the Raman spectrum and correspond to SD stretches, (See fig 5.1.5). The δS-H band at 780 cm^{-1} for butyl DDPA is more easily observed in the ir and shifts when deuterated to 550 cm^{-1} (approximately the expected shift : 780 x 0.7071 = 552),(See fig 5.1.6). Deuteration therefore helps to assign to (δ)(SH) and (ν)SH frequencies, however the 780 cm^{-1} band only reduces in intensity on deuteration, rather than disappearing, because the δ(SH) vibration coincides with or is very close to the P-(O)$_2$ sym band. The ν(SH) region shows the greatest spectral complexity because of hydrogen bonding. Fig 5.1.7 shows 2300-2600 cm^{-1} region of iso-propyl DDPA. Two sharp bands occur at 2550 cm^{-1} and 2590 cm^{-1} respectively and a broad lower frequency band at approximately 2450 cm^{-1} is present. This broad component is weakened in intensity on heating (fig 5.1.7), and by dilution in tetradecane, and so is ascribed to intermolecular hydrogen bonding. The hydrogen bonding of octyl, butyl and iso-propyl DDPA's is effectively absent for concentrations of <20% in tetradecane at ambient temperature. Variation of the relative Raman intensities of the 2550 and 2590 cm^{-1} bands of butyl (20%) and iso-propyl DDPA (20% in tetradecane) are depicted in figs. 5.1.8 and 5.1.9. The 2590 cm^{-1} band becomes relatively more intense at higher temperatures, and this supports the assignment analogous to that of Nyguist for the dimethyl ester (1), that this higher-frequency component belongs to the rotational conformer, (a) (p. 61). Here the S-H proton is cis to the P=S bond. For this conformer intramolecular hydrogen bonding (to oxygen) is absent. The 2550 cm^{-1} component is correspondingly assigned to the intramolecularly hydrogen bonded (to oxygen) trans conformer, (b) (p. 61).

Fig 5.1.1 Raman spectrum of iso-propyl DDPA

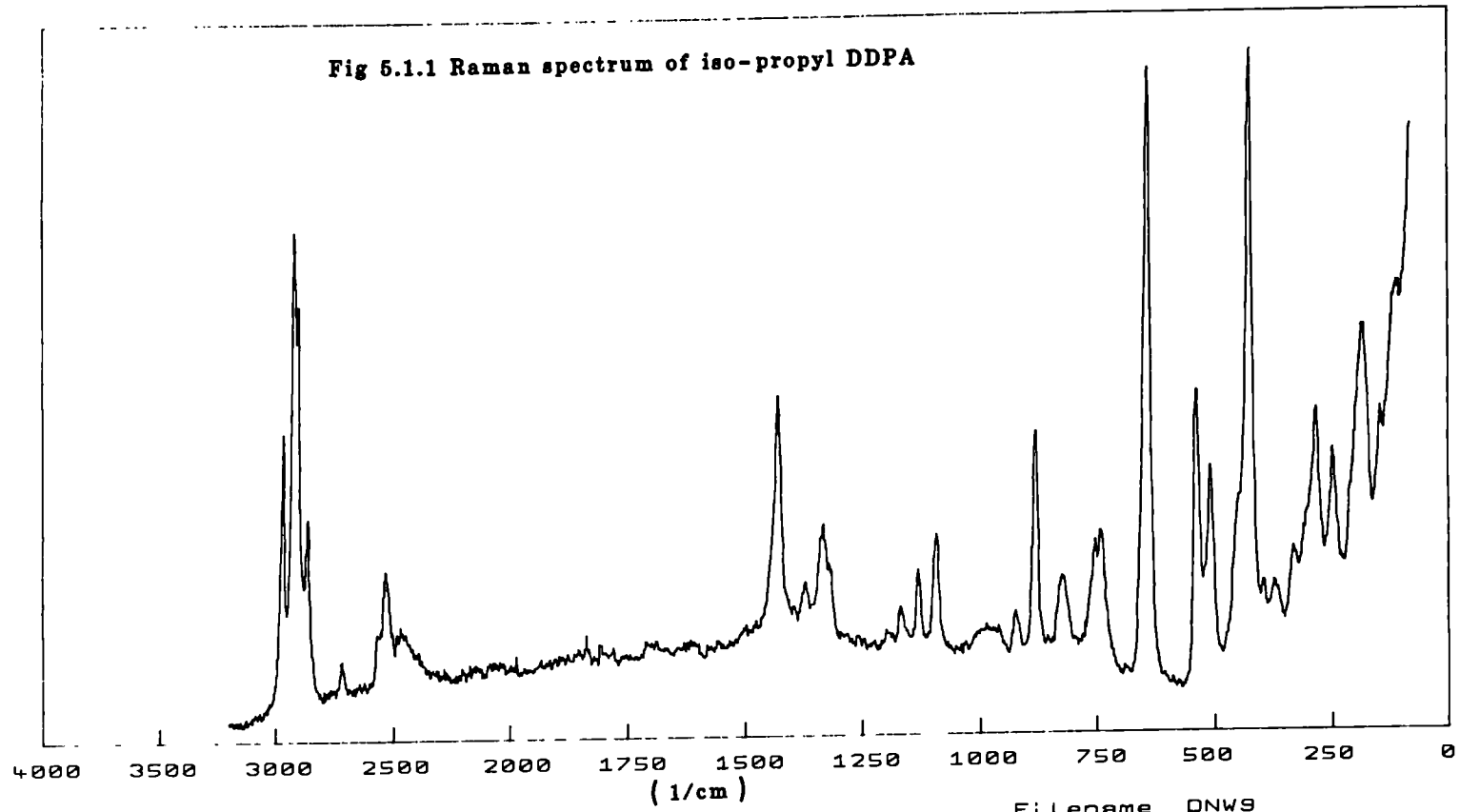

Fig 5.1.2 Infrared spectrum of iso-propyl DDPA

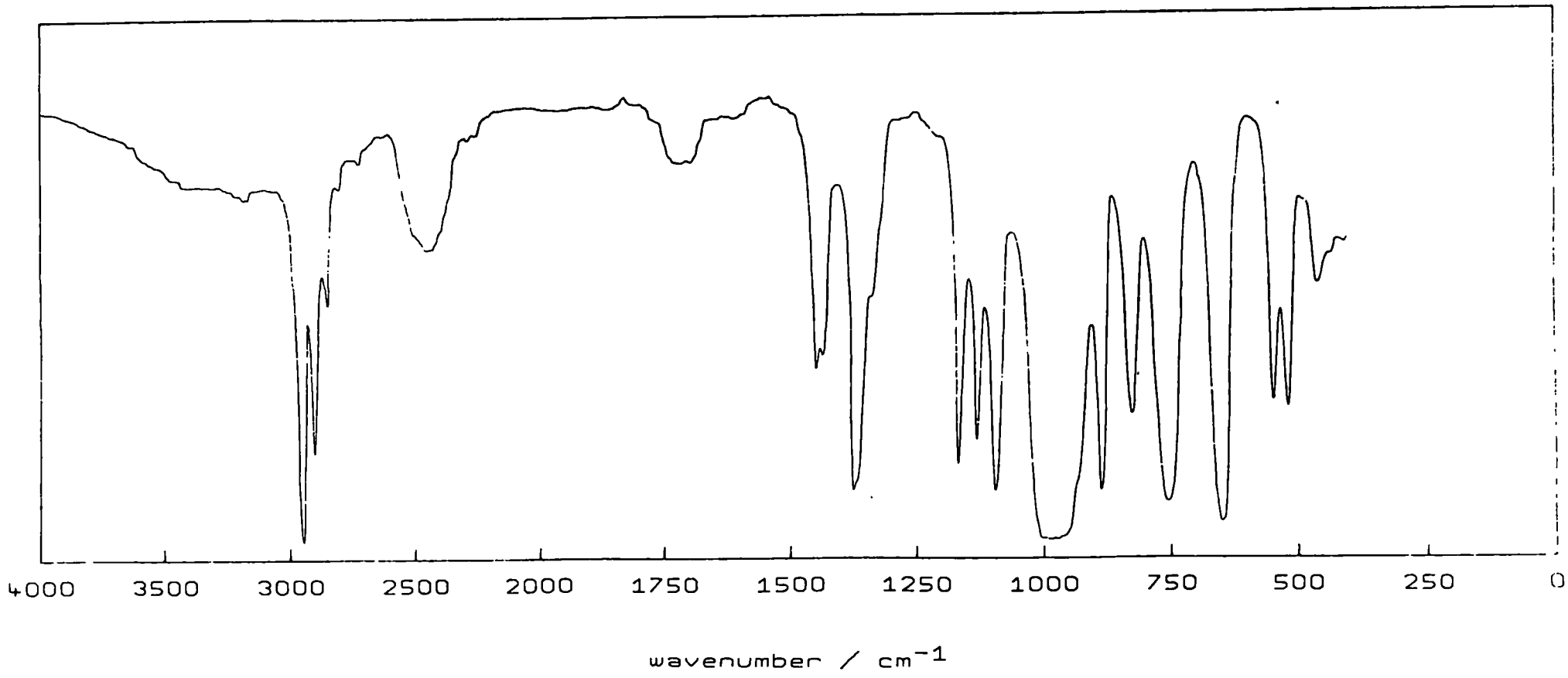

Fig 5.1.3 Raman spectrum of n-butyl DDPA

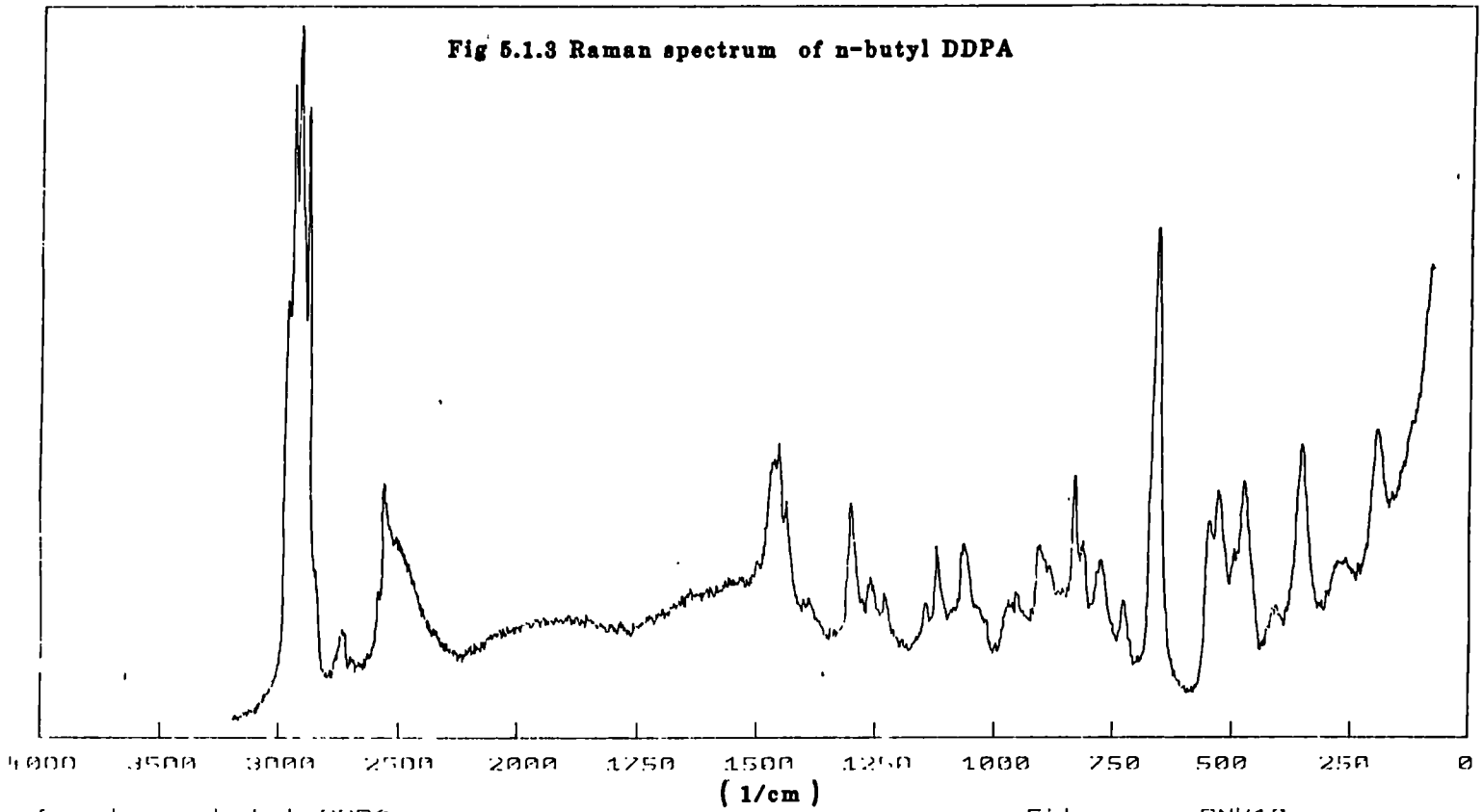

Fig 5.1.4 Infrared spectrum of n-butyl DDPA

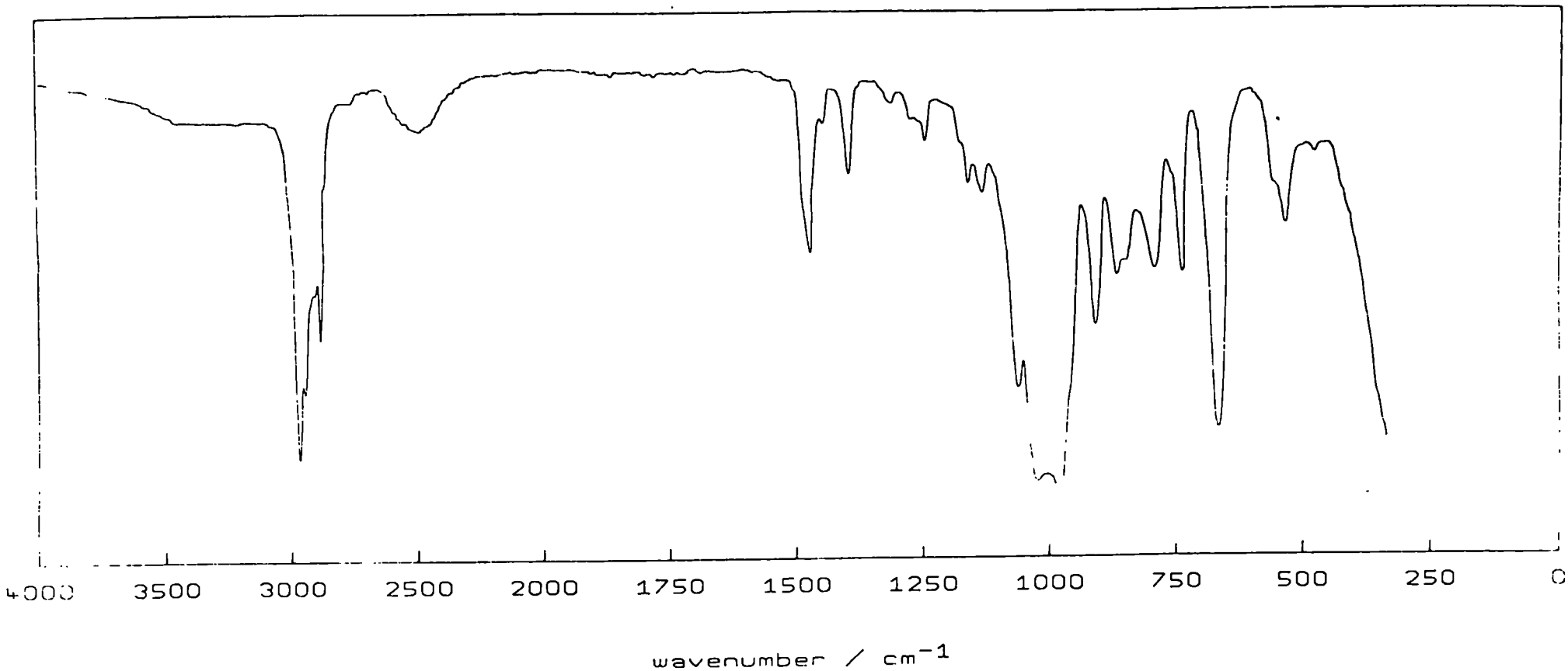

Table 5.1.1

$(MeO)_2P(S)SH$			$(MeO)_2P(S)Cl$			$(i\text{-}PrO)_2P(S)SH$			$(n\text{-}BuO)_2P(S)SH$			$(n\text{-}OctO)_2P(S)SH$			Assignment
Band	Intensity		Band	Intensity		Band	Intensity		Band	Intensity		Band	Intensity		
(cm^{-1})	Rn	ir	(cm^{-1})	Rn	ir	(cm^{-1})	Rn	ir	(cm^{-1})	Rn	ir	(cm^{-1})	Rn	ir	
2588	nr	(w)		-		2590	(m)	(w)	2590	(m)	(w)	2590	(m)	(w)	)
2550	"	(w)		-		2550	(m)	(w)	2550	(m)	(w)	2550	(m)	(w)	) ν(SH)
2450	"	(w)		-		2450	(m)	(w)	2450	(m)	(w)	2450	(m)	(w)	)
857	"	(m)	845	nr	(m)	840	(vw)	(m)	860	(vw)	(m)	870	(vw)	(m)	$\nu(PO_2)$asym
									840	(vw)	(m)				
810	"	(m)	836	"	(m)	760	(m)	(m)	780	(m)	(m)	790	(mw)	(mw)	$\nu(PO_2)$sym
782	"	(m)		-		760	(m)	(m)	780	(m)	(m)	760	(w)	(mw)	δ(SH)
660	"	(s)	666	"	(ms)										) ν(P=S)
670(shld)	"	(ms)	655	"	(s)	660	(s)	(s)	660	(s)	(s)	660	(s)	(s)	)
524	"	(m)	525	"	(m)	550	(m)	(m)	550	(m)	(m)	550*	(m)	(m)	) ν(P-S)
490	"	(m)	486	"	(m)	520	(m)	(m)	530	(m)	(m)	520*	(m)	(m)	) or ν(P-Cl)

* not well resolved

Fig 5.1.5 Raman spectrum of deuterated n-butyl DDPA (1750-1900 1/cm)

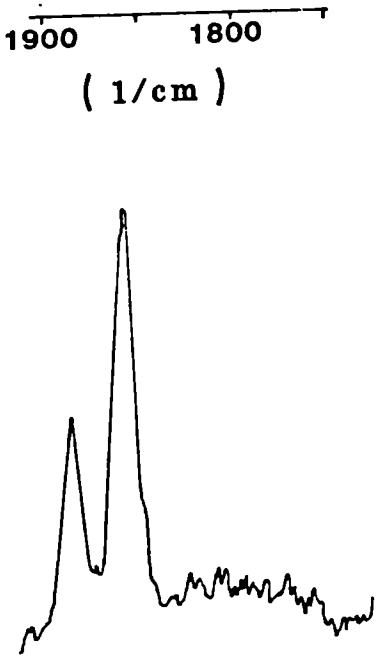

Fig 5.1.6 Infrared spectrum of deuterated n-butyl DDPA (400-1200 1/cm)

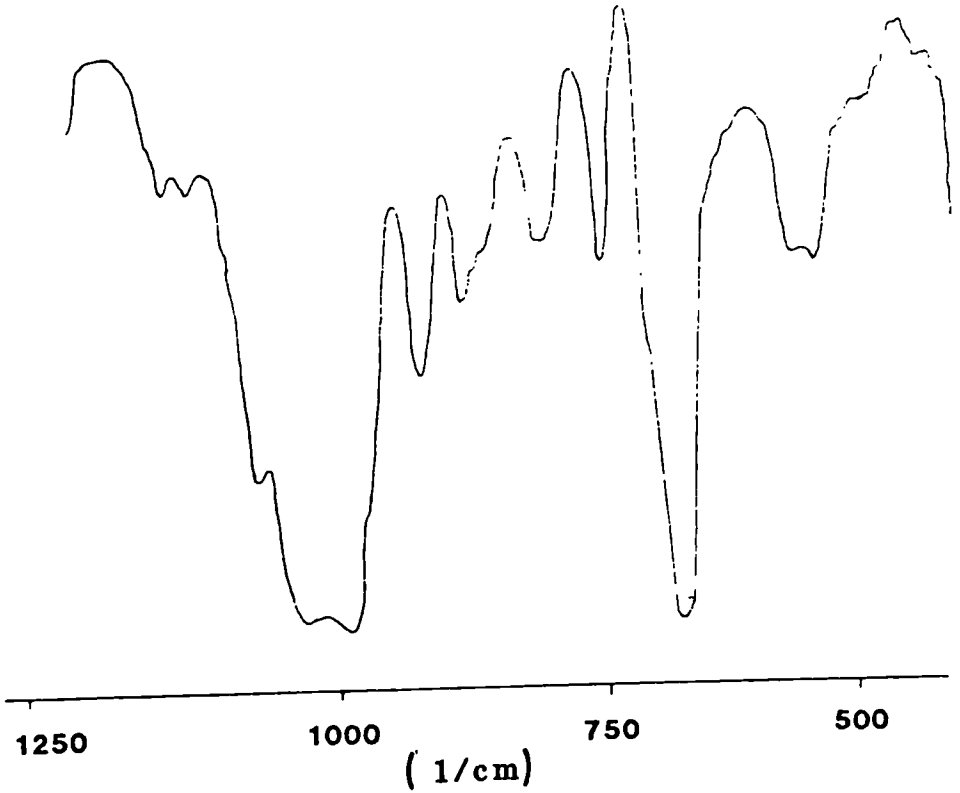

Fig 5.1.7 Raman spectra of iso-propyl DDPA (2300-2600 1/cm) at 1) 25 2) 60 3) 80 deg C

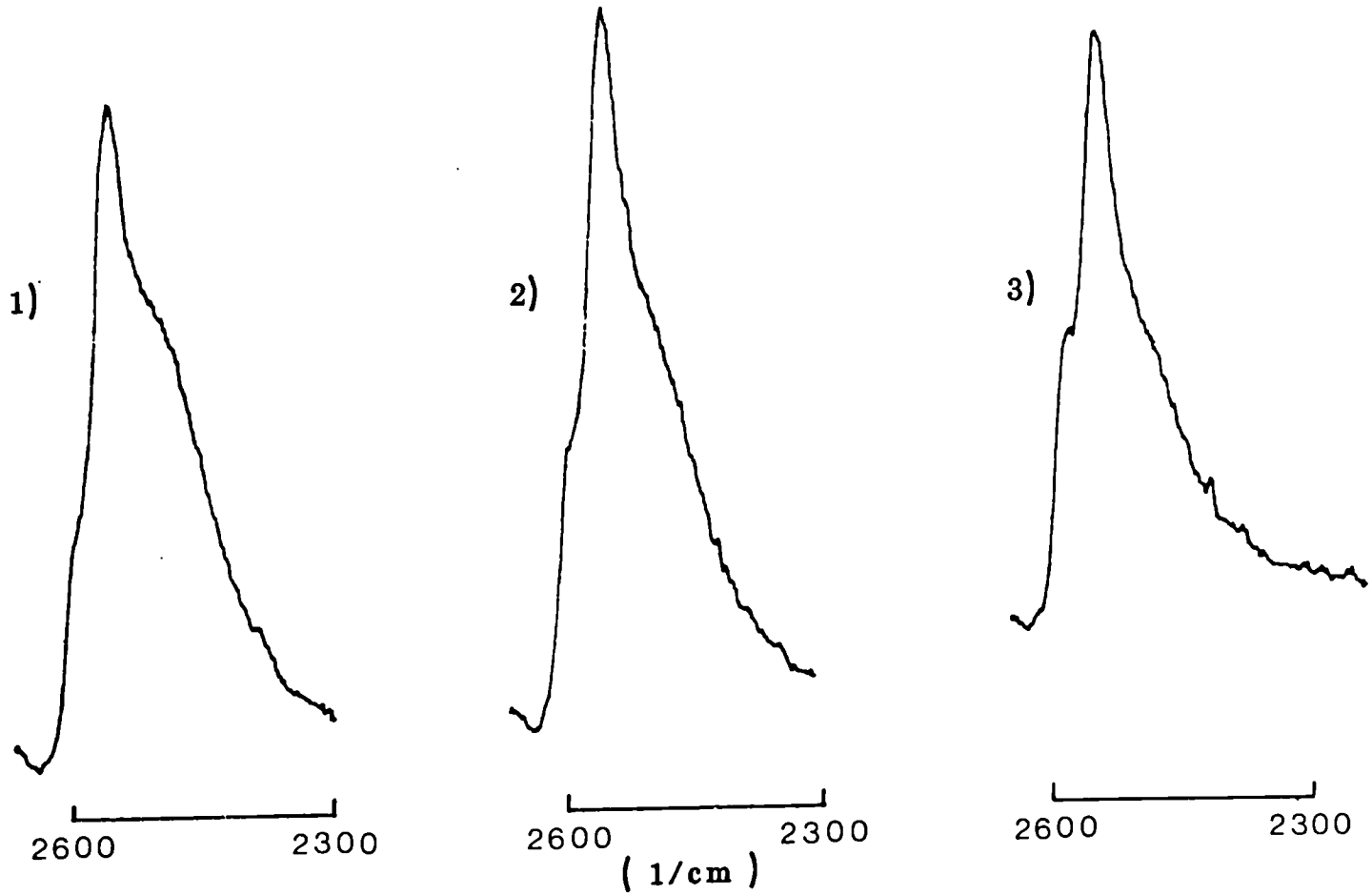

Fig 5.1.8 Raman spectra 20% iso-propyl DDPA in tetradecane

(2500-2700 1/cm) 1) 22 2) 40 3) 60 4) 80 5) 100 deg. C

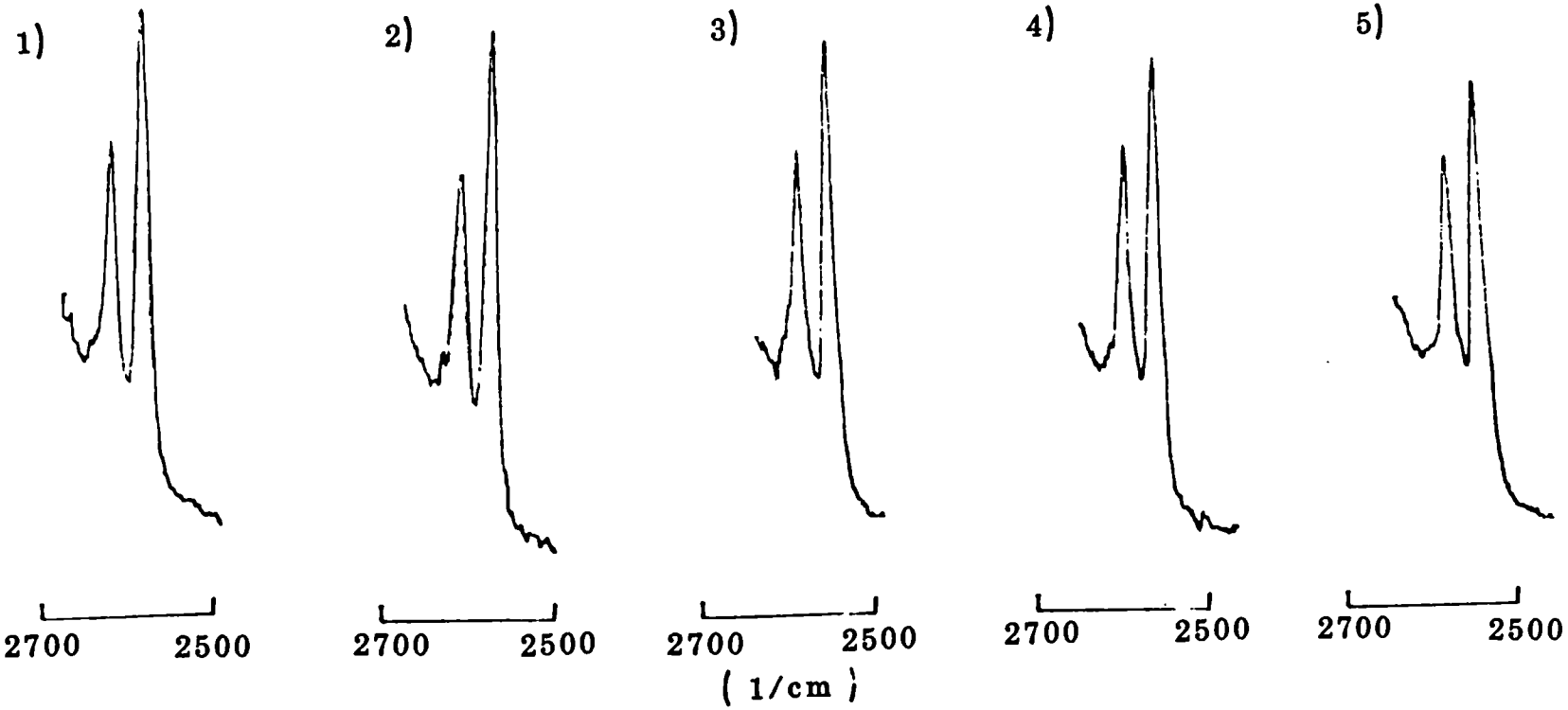

Fig 5.1.9 Raman spectra of 20% n-butyl DDPA in tetradecane (2500-2700 1/cm)

1) 22 2) 40 3) 60 4) 80 deg C and 5) cooled to 35 deg C

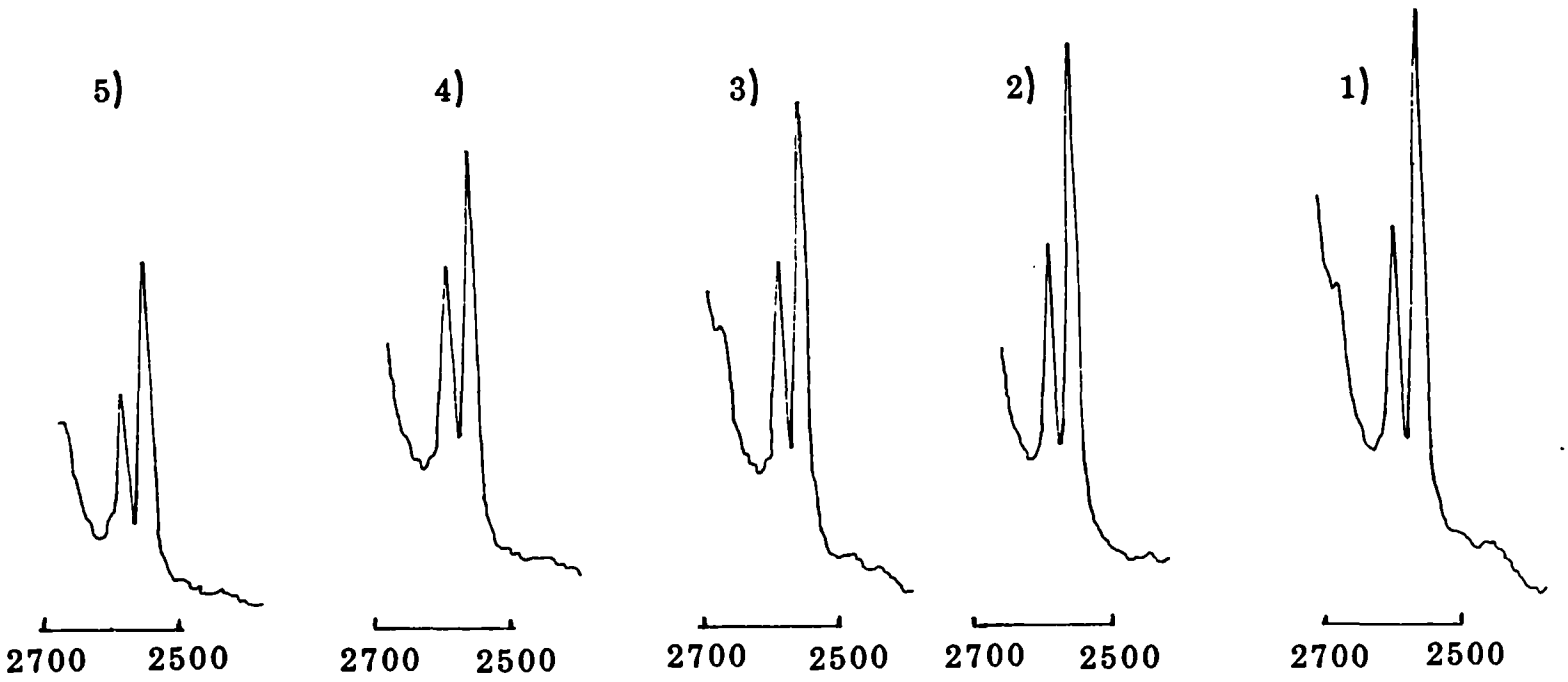

a 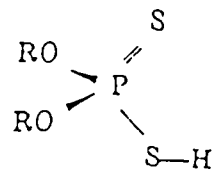

b 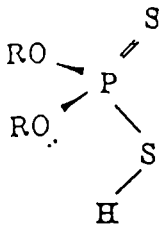

Nyquist (1), by referring to work performed by Popov et al. (8), deduced that the thiol proton was H bonded to oxygen not sulphur, because $(SBu)_2$ P=S(SH) studied by Popov et al. only had a single SH vibration. These assignments are in fact supported by dilution measurements. It is observed that, as intermolecular hydrogen bonding is progressively removed by dilution in tetradecane or by heating, it is the 2590cm^{-1} band which gains more intensity than the 2550 cm^{-1} band: this suggests that the hydrogen atom of the conformer responsible for the 2590 cm^{-1} band is more accessible for intermolecular hydrogen bondong than is the hydrogen of the conformer responsible for the 2550 cm^{-1} band.

ii) P-S and P=S Bands

For $(CH_3O)_2$ P=S(SH) two bands at 489 and 523 cm^{-1} are assigned to P-S stretching vibrations of isomers arising as a result of rotation about the P-O bonds . Nyquist (1), has suggested that this rotation is concerted with the hydrogen atom rotation about the P-S bond, in such a way that conformer (a) is associated with one of the P-S rotational conformers, and conformer (b) with the other. The hydrogen bonding in conformer (b) of course requires an oxygen lone pair to be suitably orientated, so this suggestion seems plausible. The P-S doublet frequencies for the studied DDPA's are for (iso-PrO)$_2$P=S(SH) 518, 549 cm^{-1}, (BuO)$_2$P=S(SH) 535, 550 cm^{-1} , and for (OctO)$_2$-P=S(SH) 515, 550 cm^{-1} . The two components of the octyl DDPA are poorly resolved and appear to be partly overlapped by another band, so that only a qualitative indication of their temperature dependence could be obtained. In all cases the higher-frequency band increased in intensity as the temperature was raised, indicating that this band is associated with conformer (a), see figs 5.1.10-5.1.13. Dilution in tetradecane causes an increase in the 550 cm^{-1}/520 cm^{-1} P-S intensity ratio, for example, the Raman P-S 550 cm^{-1}/520 cm^{-1} intensity ratio for neat iso-propyl DDPA increases from 1.4 to 1.8 on dilution to 20% in tetradecane. Therefore possibly more of conformer (a) is involved in hydrogen bonding intermolecularly to other DDPA molecules. This may well be expected because conformer (a) has a SH free from intramolecular hydrogen bonding and is therefore more available for intermolecular hydrogen bonding. The P=S vibrations occur at about 650 cm^{-1} and are not resolved into doublets like the P=S band of $(CH_3O)_2$P=S(Cl). The P=S vibrations of the two conformers must be very close in frequency. Nyquist reported a shoulder on the strong 650 cm^{-1} P=S band at 670 cm^{-1} of $(CH_3O)_2$ P=S(SH) in the ir, but it is so slight in the published spectrum (1) that its presence is arguable.

Fig 5.1.10 Raman spectra of 20% iso-propyl DDPA in tetradecane at 1) 22 2) 40 3) 60 4) 80 deg C

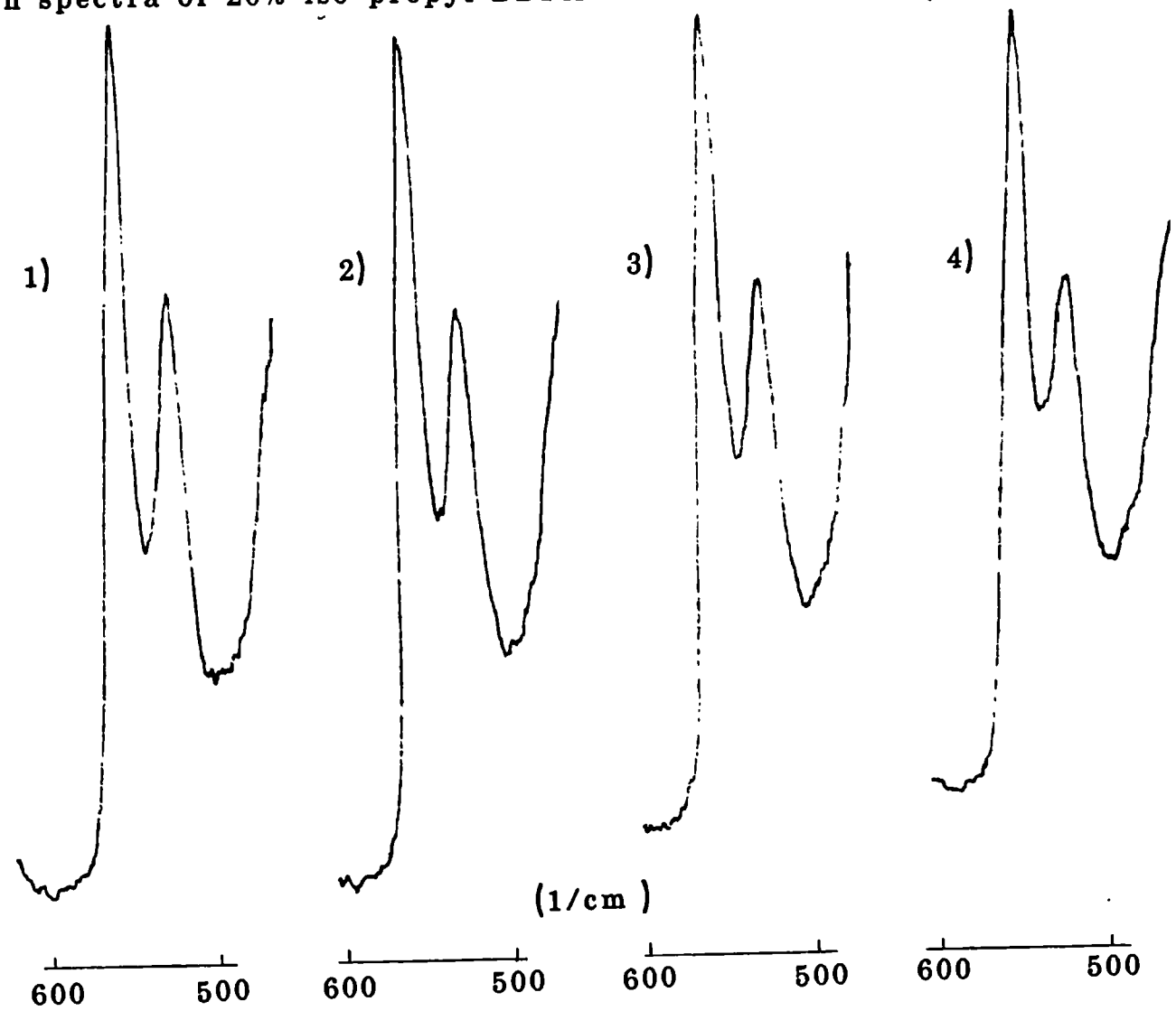

Fig 5.1.11 Infrared spectra of 20% iso-propyl DDPA in tetradecane at 1) 22 2) 35 3) 50 4) 70 deg C

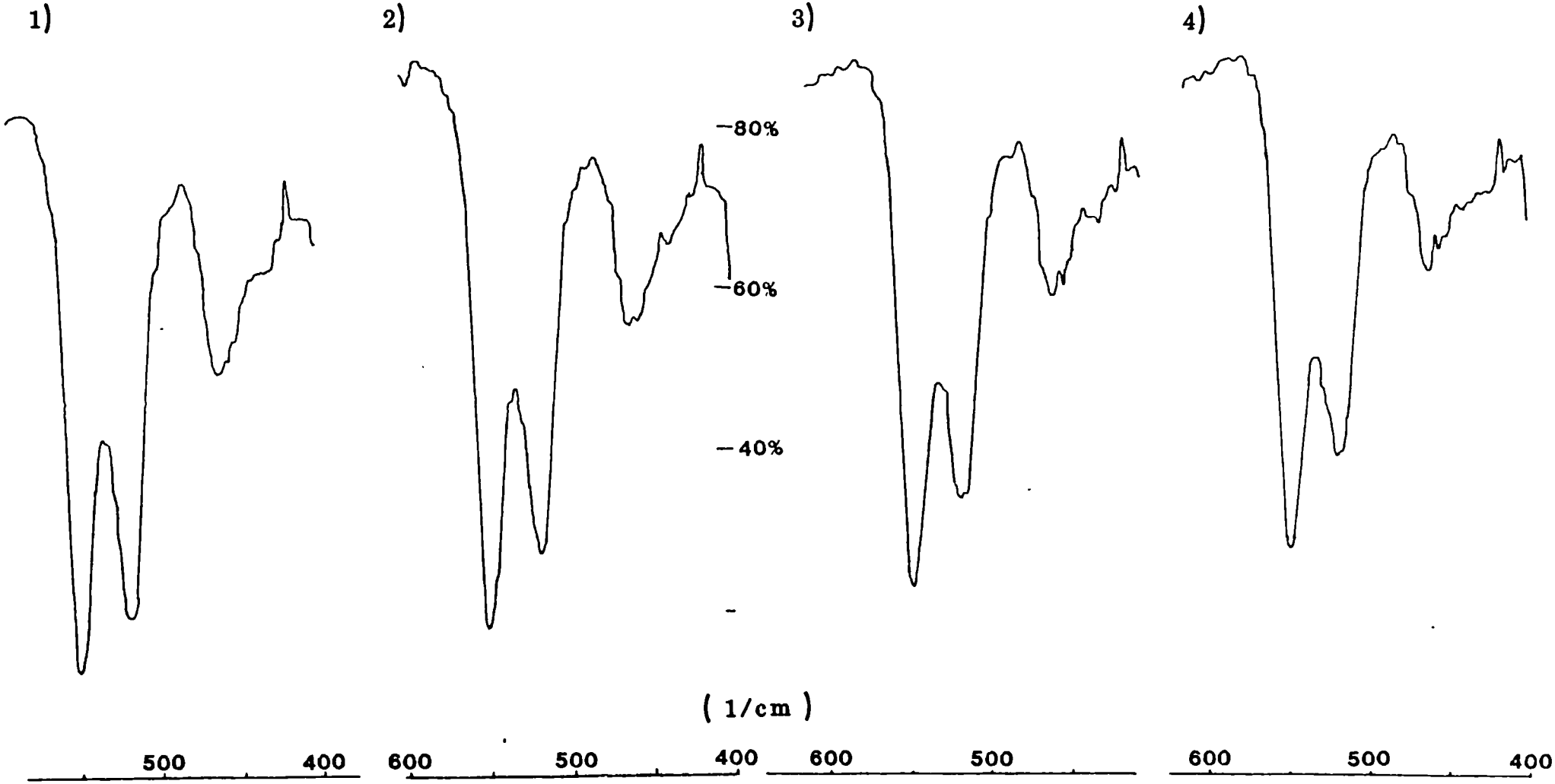

Fig 5.1.12 Raman spectra of 20% n-butyl DDPA in tetradecane at 1) 22 2) 35 3)and 4) 80 deg C

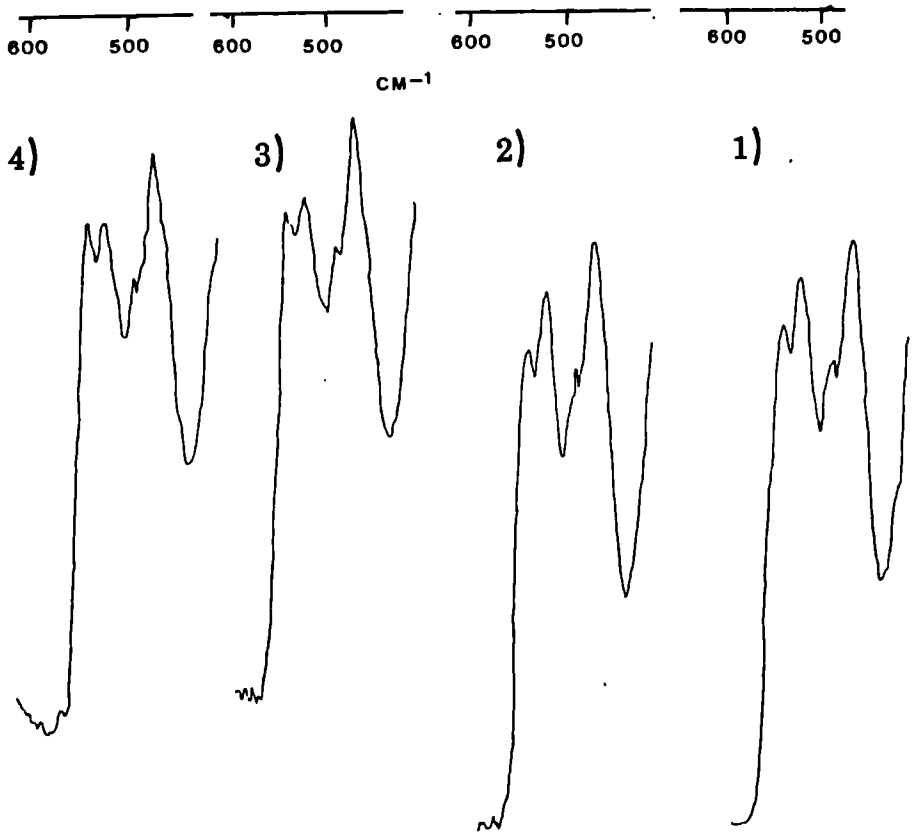

Fig 5.1.13 Infrared spectra of 20% n-butyl DDPA in tetradecane at 1) 40 2) 50 3) 60 4) 70 deg C

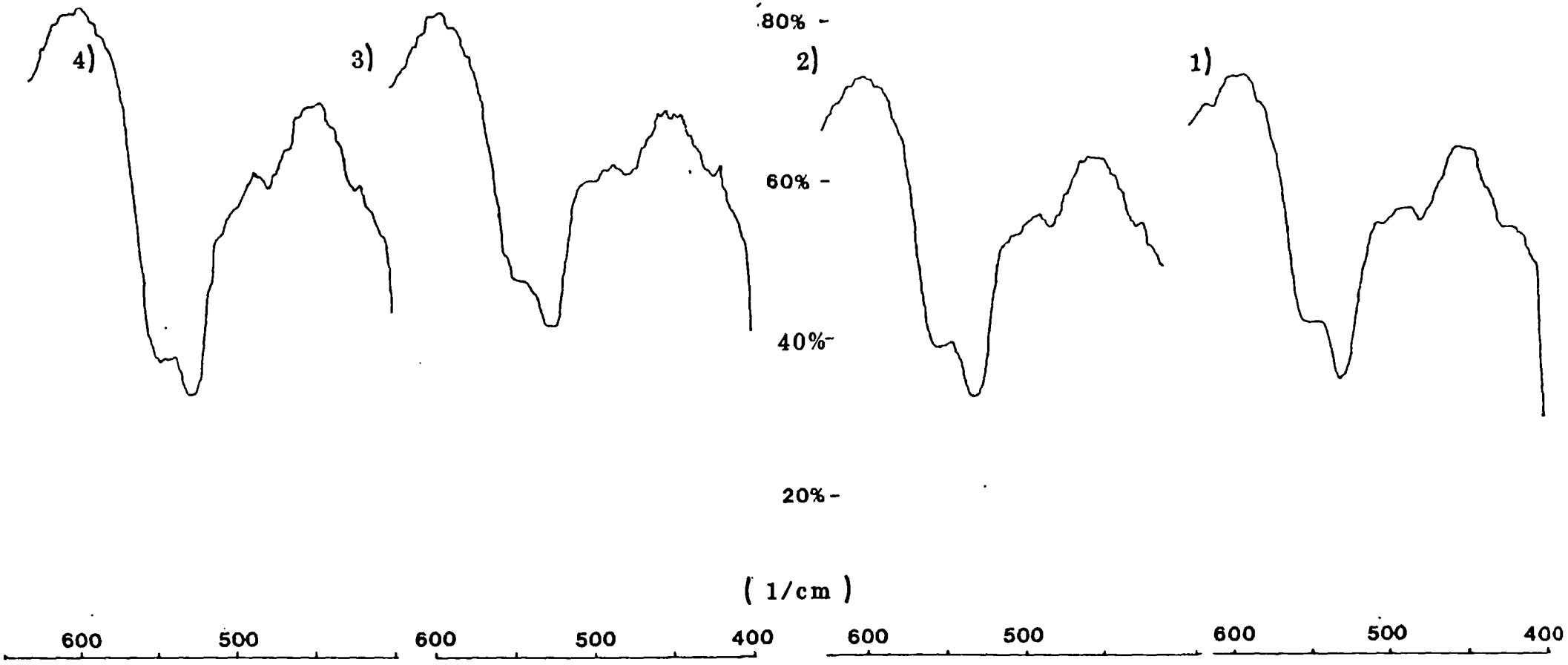

iii) P(-O) Bands

The symmetric and antisymmetric $P(-O)_2$ vibrations are observed in the ir for the studied compounds between 760 - 790 cm^{-1} (ν $P-(O)_2$ sym) and 820 - 860 cm^{-1} (ν $P-(O)_2$ asym) respectively. The band in the infra-red observed at 855 cm^{-1} in butyl DDPA is a doublet whilst the methyl, ethyl DDPA's (characterised by Nyquist), iso-propyl and octyl DDPA's (characterised here), are singlets. This band is not observed as a doublet in the butyl derivatives of DDDiS and TDTP. An ir temperature-variation study, (the ν $P-(O)_2$ asym is too weak in the Raman) showed the higher frequency band to be favoured at a higher temperature, possibly identifying this as belonging to conformer (a), (see fig. 5.1.14), however only a tentative ΔH value was calculated because the two components are not well resolved. It is difficult to explain the absence of doublets at around 850 cm^{-1} for other DDPA's and dialkyl monothiochlorophosphates, and therefore it is possible that one of these bands may have another assignment, but this is unlikely, because explanation for the temperature variation is otherwise not evident.

Conclusions

The precision of the determination of ΔH (see table 5.1.2), is not high (perhaps $\pm$20%), but some trends in the values are apparent. The energy difference between conformers is largest in the case of n-octyl DDPA. The ΔH values estimated from the ir and Raman P=S results agree well in both cases for butyl and iso-propyl DDPA. Most interestingly, the ΔH values calculated from the ν(P-S) bands agree remarkably well with those calculated from the ν(SH) bands: this lends support to the interpretation of the isomerisation in terms of two concerted rotational processes about the P-S and P-O bonds. Nyquist stated (1), that "Rotational isomers have also been reported for the $(CH_3O)_2P=S(Cl)$ molecule, as the result of rotation about the P-O bond. Because the ir spectra for the basic structure of $(CH_3O)_2$ P=S(SH) and $(CH_3O)_2P=S(Cl)$ are similar and rotation occurs about the P-O bonds in both molecules, it seems likely to us that the geometric positions of the S-H groups are affected by the geometric positions of the $O-CH_3$ groups."

"This effect, we suggest, results in two stable rotational isomers such as (a) and (b), but where the O-R groups are also in different geometric positions relative to the S-H groups."

Table 5.1.2 ΔH Values for Equilibrium kJ mol^{-1}

R	ν(S-H)a	ν(P-S)a	ν(P-S)b	ν(O-P-O)b
Pr-i	2.7	2.1	2.3	
Bu-n	3.4	2.4	3.1	3.5
Oct-n	4.5			

(a) = from Raman spectra, (b) = from ir spectra.

See Fig. 5.1.5 for plots of In (I_a/I_b) versus 1/T(°K)

Fig 5.1.14 Infrared spectra of 20% n-butyl DDPA in tetradecane (700-900 1/cm) 1)40 2)50 3)60 deg C

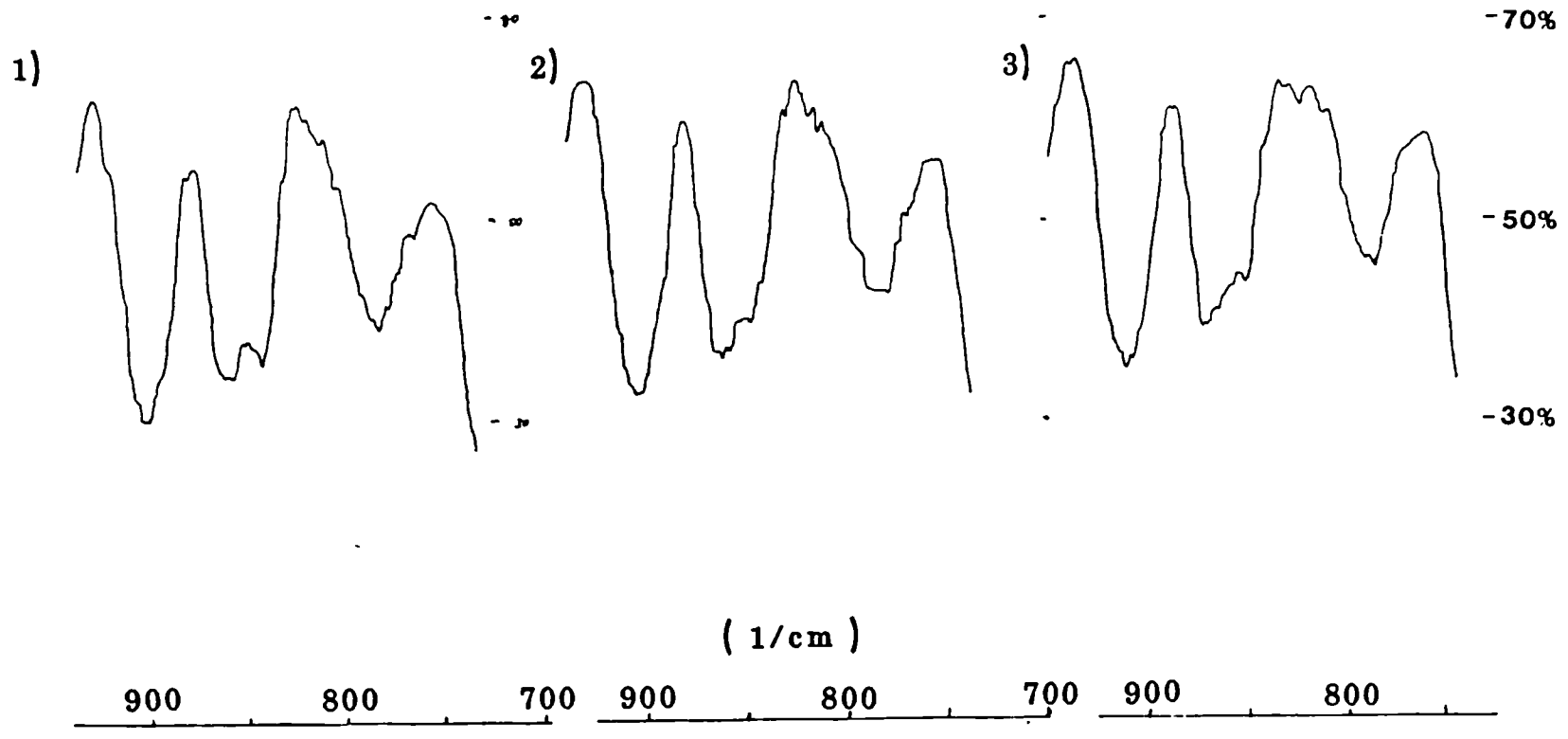

Fig 5.1.15

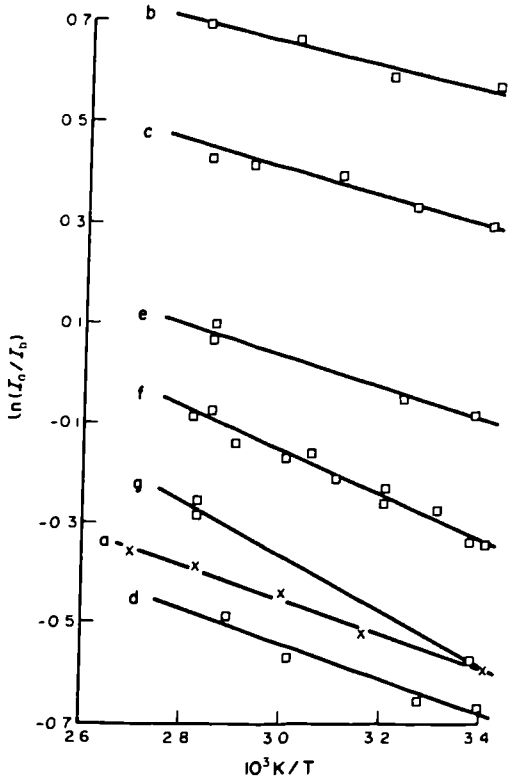

Plots of ln (I_a/I_b) against T^{-1} for ν(S–H) and ν(P–S) band pairs: 20% solutions in *n*-tetradecane. (a) $(Pr^iO)_2P(:S)SH$, ν(S–H) from Raman spectra. (b) $(Pr^iO)_2P(:S)SH$, ν(P–S) from Raman spectra. (c) $(Pr^iO)_2P(:S)SH$, ν(P–S) from i.r. spectra. (d) $(Bu^nO)_2P(:S)SH$, ν(S–H) from Raman spectra. (e) $(Bu^nO)_2P(:S)SH$, ν(P–S) from Raman spectra. (f) $(Bu^nO)_2P(:S)SH$, ν(P–S) from i.r. spectra. (g) $(Oct^nO)_2P(:S)SH$, ν(S–H) from Raman spectra.

5.2 The Behaviour of n-Butyl DDPA in Different Solvents as Studied by Raman Spectroscopy

It has already been discussed that n-tetradecane breaks down the hydrogen bonding between DDPA molecules. More of conformer (a) are involved in intermolecular hydrogen bonding because of their higher availability than the intramolecularly hydrogen bonded conformer (b). On heating or dilution the higher frequency νP-S or νSH bands of the conformer (a) increase in intensity, hence proving this point. The νSH region in the Raman spectrum of 30% DDPA in solvents of high donor number (acetone or methyl acetate),is similar in appearance to the Raman spectrum of the neat acid. A broad band (2450 cm^{-1}) is observed that is characteristic of a ν SH vibration involved in hydrogen bonding to the solvent preferentially, rather than to other DDPA molecules. However, bands at 2590 cm^{-1} are distinguishable confirming the presence of conformers (a) and (b). A basic solvent such as DMA dissociates the acid to give a solvated proton and a DDP- anion; the $\nu(PS)_2$ sym band of the DDP- anion is observable at 560 cm^{-1} and is strong in the Raman. However, the presence of weaker bands present at 530 cm^{-1} ν(P-S) and 650 cm^{-1} ν(P=S), and 2550-90 cm^{-1} ν(SH) bands show that DMA does not completely dissociate the acid.

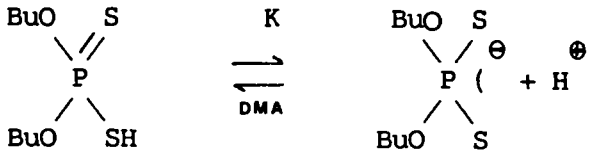

ν(P-S) 530,550 cm^{-1}
ν(SH) 2550,2590 cm^{-1}

$\nu_{(sym)}PS_2$ 560 cm^{-1}

The Raman spectrum of 30% DDPA in nitromethane reveals an interesting phenomenon, (fig 5.2). Nitromethane eliminates the intermolecular hydrogen bonding but contrary to solution in tetradecane, no band at 2590 cm^{-1} is observed. A broader band is distinguishable as a shoulder on the sharp 2550 cm^{-1} band. Nitromethane has a small donor number but a small interaction with the conformer (a) SH proton (free from intramolecular hydrogen bonding), may reduce the SH frequency of conformer a) or possibly an interaction with the SH proton of conformer b) may broaden the S-H band hence mask the SH band of conformer a). It is possible that this phenomenon may be caused by the large dieletric constant of nitromethane.

Fig 5.2 Raman spectrum of 30% n-butyl DDPA in nitromethane (SH and PS regions)

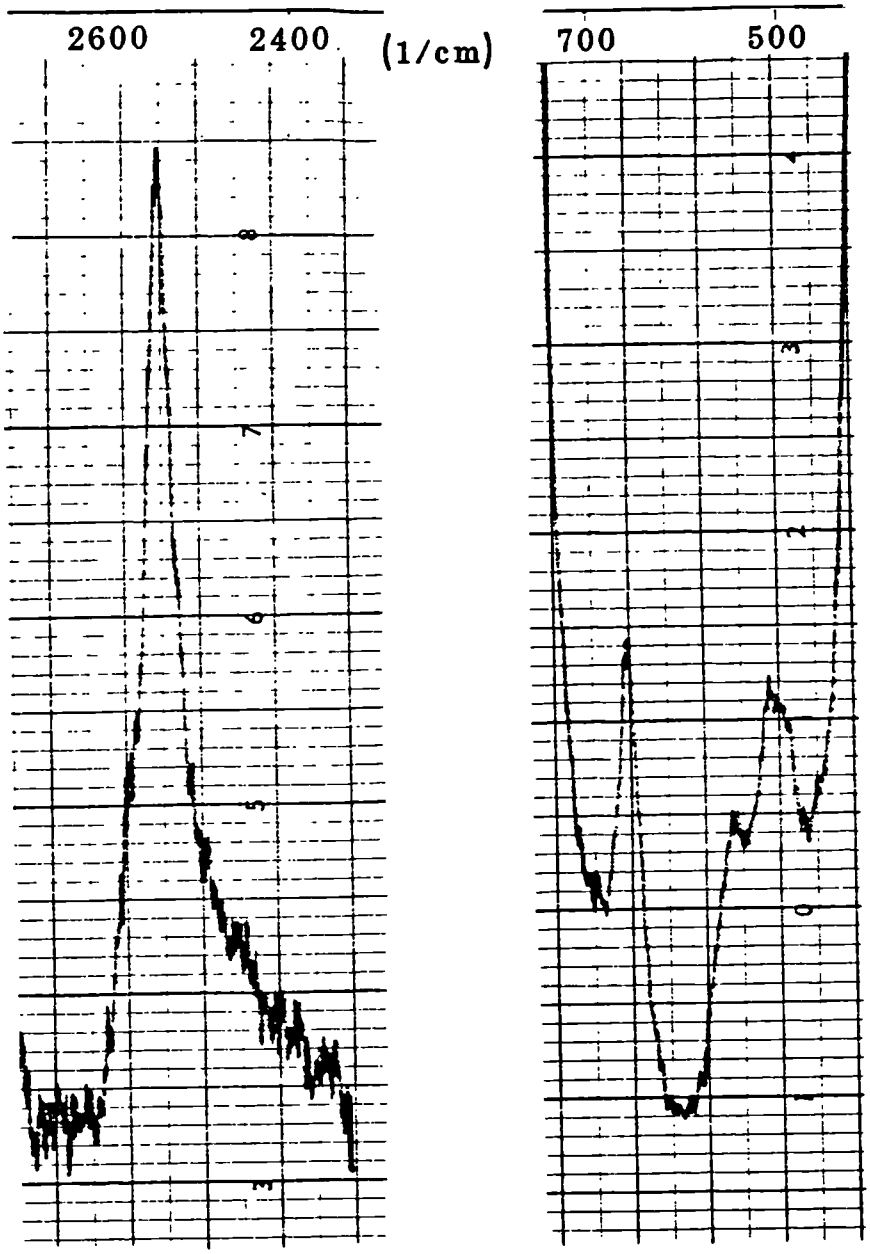

Chapter 5

1) Nyquist R.A., Spectrochim. Acta 1969, Vol. 25A, 47.

2) Thomas L.C., Interpretation of the vibrational spectra of organophosphorus compounds, Heyden, London, 1974.

3) Nyquist R.A., Spectrochim. Acta 1966, Vol 22A, 1563-1569.

4) Nyquist R.A., Spectrochim. Acta 1963, Vol. 19A, 713.

5) Nyquist R.A., Spectrochim. Acta 1967, Vol. 23A, 2505.

6) Nyquist R.A., and Muelder W.W., Spectrochim. Acta, 1968, Vol. 24A, 187.

7) Waters D.N., and Paddy J.L., Proc. 10th Internat. Conf. Raman Spectroscopy, P 14-26 (edited by Peticolas and Hudson B.), Univ. Oregon Press, Eugene, Or. (1986).

8) Popov E.M., Kabachruik M.I. and Mayants L.S., Russian Chem. Rev. 1961, 30, 362.

CHAPTER 6

The Study Of The Relative Antioxidant Capacities Of Zinc Dialkyldithiophosphates And Their Most Important Hydrolysis, Oxidation And Thermal Degradation Products By Differential Scanning Calorimetry - (D.S.C.)

6.1 Introduction

Differential Scanning Calorimetry is a method intensively used to characterise the oxidative stability of lubricating oils, for example, formulated lubricating oils and virgin and re-refined lubricating base stocks, (1-5). Oxidative stabilities of lubricating oils containing different antioxidant mixtures or concentrations can be compared with the aid of DSC. Samples of less than 2mg are used in a high pressure atmosphere of air or oxygen; therefore experimentation is carried out under thin film conditions, simulating in this respect actual engine conditions. Oxidation onsets are determined either isothermally (onset times), or dynamically (onset temperatures at a given heating rate). This section discusses the application of thin layer high pressure DSC and compares the oxidation stabilities of solutions of various antioxidants at different concentrations in 'an academic' oil, squalane ($C_{30}H_{62}$), which was selected due to its favourable viscosity and boiling point. An original technique is also devised and employed to compare a wider range of organophosphorus antioxidants. This method has the following differences with respect to the thin layer technique.

1) Bulk solutions are used, typically between 30 - 40 µl.
2) Oxygen is present in the form of a hydroperoxide rather than gaseous oxygen.
3) The atmosphere is inert and is between 100-500 psi nitrogen.
4) The exotherms observed isothermally or dynamically represent the reaction of the antioxidant or an antioxidant-derived species with a hydroperoxide, not the oxidation of the oil. The "bulk solution" DSC results described in this chapter reflect the hydroperoxide decomposition capacities of the respective antioxidant. The thin-layer DSC technique gives an indication of the autoxidation inhibiting properties of the antioxidant.

6.1.1 Differential Scanning Calorimetry

The term "differential scanning calorimetry" has become a source of some confusion in thermal analysis the past several years. This is because there are two quite different types of instruments which use the same name. These two types of instrument are based on different principles and a brief discription follows:-

a) Heat Flux Differential Scanning Calorometer

This system arguably resembles a DTA calorimeter, (6). It employs thermocouple systems of varying degrees of complexity , the essential feature being that the output from the thermocouple system is relatable to the energy change. The heat flux through a solid body with a defined thermal resistance between the calorimeter system and the surroundings can be made entirely dependent on the temperature difference measured at the said thermal resistance. On these grounds a record of the time course of this local temperature difference provides a means for the measurement of heat fluxes if a specific calibration factor (apparatus factor) is known.

b) Power Compensation DSC

In power compensation DSC the difference in energy inputs required to maintain the sample and reference material continuously at the same temperature (ie. $\Delta T=0$) is measured. This is effected by continuous monitoring of ΔT by a resistance thermocouple system and automatic regulation of the power supplied to independent heaters provided for the sample and reference material.

6.1.2 The DuPont 990 DSC System

The DuPont 990 DSC is a heat flux differential scanning calorimeter. A characteristic feature of the design of this device is that one of the components of the differential thermocouple represents a suitably shaped sheet which ensures favourable heat conditions between the furnace and the sample container placed on the sheet. The second component of the differential thermocouple, a chromel disc, is welded to the sample and reference support. Chromel-alumel thermocouples serve for measuring the temperature of the sample and reference pans. The recorder indicates the sample temperature or time on the x axis and the temperature difference or heat change on the y axis. Operating temperatures extend from 80 to 1000 deg K but depend on the type of sample pans used, and heating rates from 0.5 to 100 deg K/min. The sample mass has to be less than 50mg. Experiments may be conducted in the isothermal or dynamic mode.

The Dynamic Mode

Samples can be linearly heated at a rate between 0.5 and 100 deg/min to a limit temperature. The system can be held at this limit temperature or allowed to cool to ambient temperature and if placed on cycle mode re-warmed up to the limit temperature at the required heating rate. To achieve good heating rate linearity a high proportional band and low rate mode is selected , (60-70% pb and 0% rm).

The Isothermal Mode

The sample and reference pans are heated to the required isothermal temperature (limit temperature), at a maximum heating rate (100 deg K/min). The system is then switched into the isothermal mode which maintains the system at the limit temperature. Heat output at time (t) is measured on the recorder. A higher rate mode value is required to help prevent limit temperature overshoot when pre-heating the sample to the isothermal temperature. The DuPont 990 DSC cell can be operated under conditions of high pressure, (up to 1000 psi).

6.1.3 Calibration of the Cell

The calibration coefficient (E), was determined using indium and tin which are metals with known heats of fusion and melting points in the region of interest. The calibration coefficient varies with atmosphere and pressure, (7). E was determined at atmospheric pressure and 500 psi, in "white spot" nitrogen.

The equation given below yields E:

$$E = \frac{\Delta H.m}{60.A.B.\ q}$$

ΔH = heat of fusion, (mcal/mg)

M = sample mass (mg)

A = peak area (in^2)

B = time base setting (min/in)

q = Y-axis range (mcal/sec/in)

Sample calculation (atmospheric pressure)

ΔH = 6.79 cal/g for indium

M = 8.2 mgs

A = 11 sq ins

B = 0.2 min/in

q = 1 mcal/in/sec

Therefore E = 0.52

Table of Calibration Coefficients

	ΔH(mcal/mg)	T_M deg C	E(N_2 atm.)	E(N_2 500 psi)
Indium	14.14	156.6	0.59	0.52
Tin	6.79	231.9	0.52	0.47

The accuracy of the thermocouples is tested by comparing the melting point of indium (T_M), observed experimentally with the literature value, (156.6 deg C).

The Calculation of ΔH

The peak area is used to calculate the ΔH value by substitution into the following equation:

$$\Delta H \text{ (mcal/mg)} = \frac{A}{m} 60 \text{ E.B. q}$$

The values are converted into Joules/gram.

6.2 Dynamic Thin Layer Oxidation of Squalane Containing Varying Concentrations of n-Octyl DDDiS, DDPA, ZDDP and iso-Octyl ZDDP (Commercial)

Thin layer high pressure DSC performed on a Dupont 990 system was used to compare the antioxidant capacities of n-octyl DDDiS, DDPA and ZDDP, and a commercial iso-octyl ZDDP.

Method

Approximately 0.5mg of squalane containing varying amounts of antioxidant were oxidized in an atmosphere of 500 psi air at a heating rate of 9.1 degs/min. Aluminium open top sample pans were used to contain the sample, and an empty aluminium pan was used as a reference. Comparisons of the antioxidant capacities were determined from the onset of oxidation temperatures which are calculated by extrapolating the base line and leading edge of the peak, the intersection being the onset temperature. The heats of reaction for the oxidation were also monitored and compared. The y axis setting was 5mcal/sec/in and the x axis setting was 20 deg/min, therefore a time base conversion was required to determine the ΔHr values (B = 2.2 min/in). A calibration coefficient of 0.52 (500 psi tin value), was considered to be the most appropriate figure to use because the observed temperature range of the exotherms is closest to the melting point of tin.

Results Tables 6.2.1-6.2.4

n-Octyl ZDDP (Lab prepared)

See figures 6.2.1 to 6.2.4

Conc Moles/dm^3	T onset deg C	Wt mg	A sq in	ΔHr J/g
0.08	244.5	0.45	0.67	2138
0.06	231.0	0.50	0.91	2614
0.04	226.75	0.43	1.09	3644
0.02	217.0	0.50	1.67	4797
0.01	211.0	0.53	2.18	5912
0.005	202.5	0.42	1.81	6193
0.0025	196.2	0.40	1.85	6646

Commercial iso-Octyl ZDDP

Conc Moles/dm^3	T onset deg C	Wt mg	A sq in	ΔHr J/g
0.08	249	0.395	0.626	2278
0.06	243	0.60	0.964	2309
0.04	236	0.54	1.328	3533
0.02	225	0.48	1.469	4395
0.01	219	0.62	2.12	4953
0.005	208	0.455	1.885	6224
0.0025	197	0.45	1.928	6088

n-Octyl DDDiS

Conc Moles/dm^3	T onset deg C	Wt mg	A sq in	ΔHr J/g
0.08	233.8	0.5	1.231	3654
0.06	227.5	0.32	0.867	3892
0.04	223	0.58	1.640	4060
0.02	213	0.45	1.57	5011
0.01	205.5	0.43	1.928	6439
0.005	200	0.5	2.058	5909
0.0025	197.5	0.48	2.181	6529

Fig 6.2.1 DSC traces displaying the oxidation of squalane containing different n-octyl ZDDP concentrations

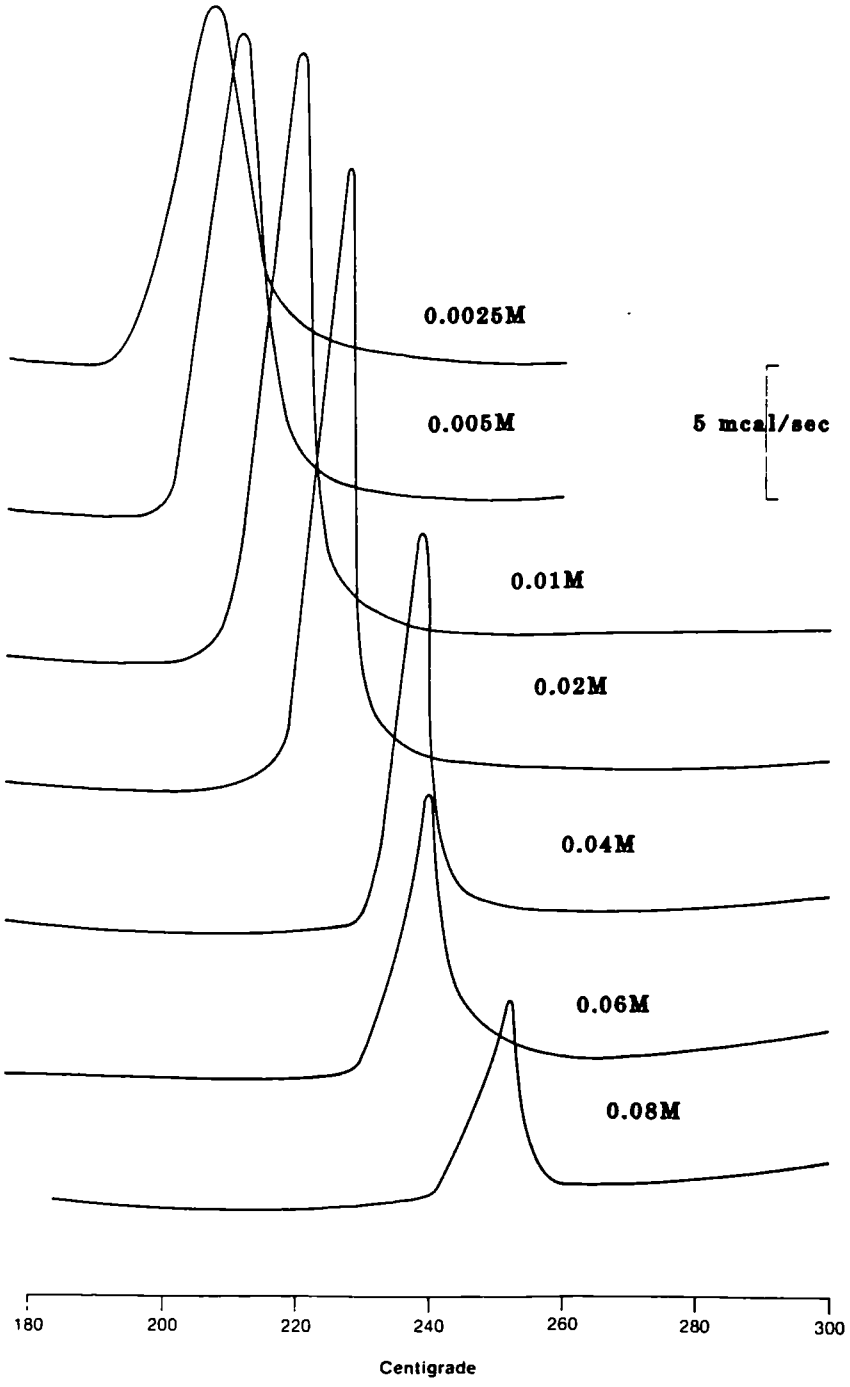

Fig 6.2.2 DSC traces displaying the oxidation of squalane containing different commercial iso-octyl ZDDP concentrations

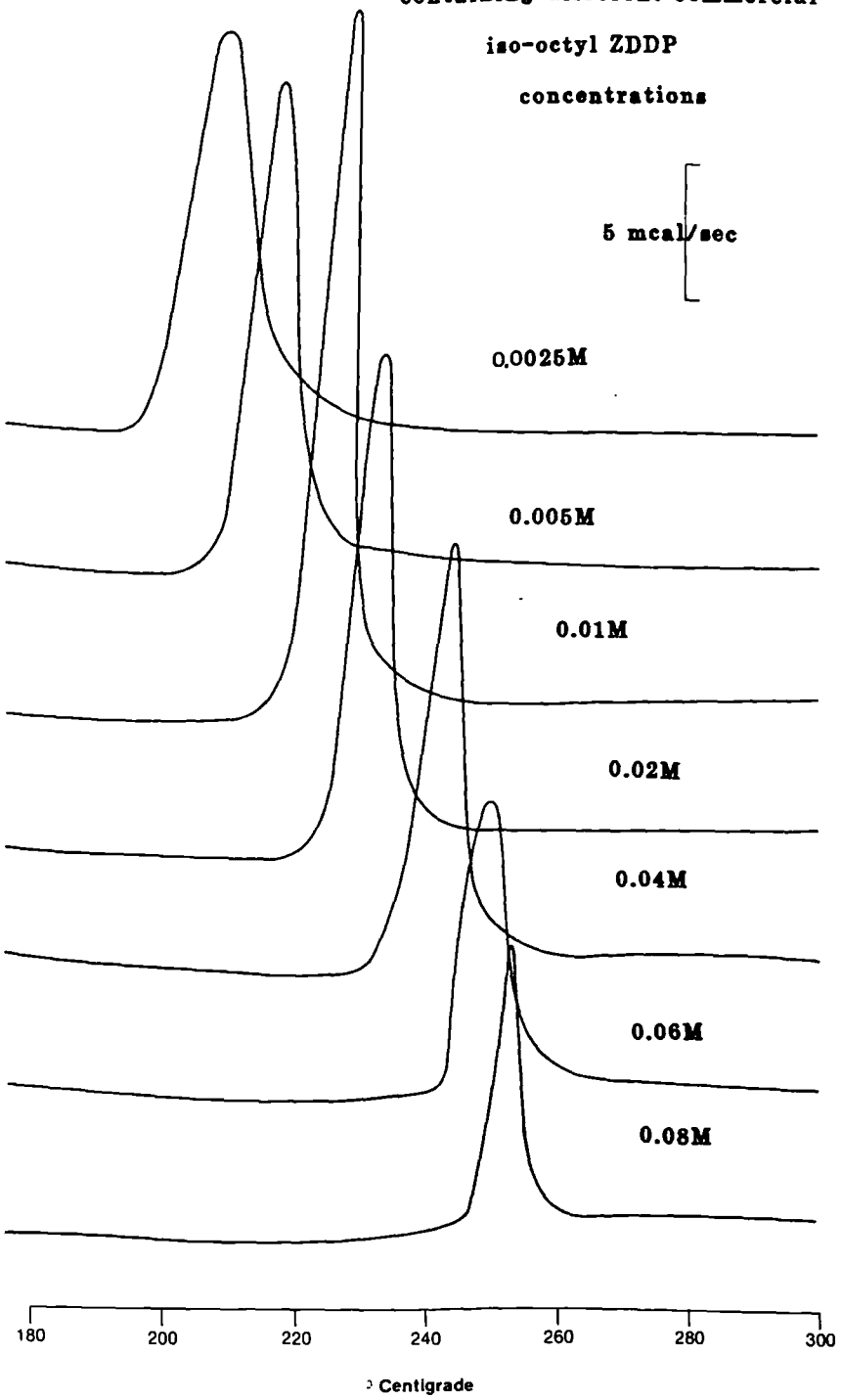

Fig 6.2.3 DSC traces displaying the oxidation of squalane containing different n-octyl DDDiS concentrations

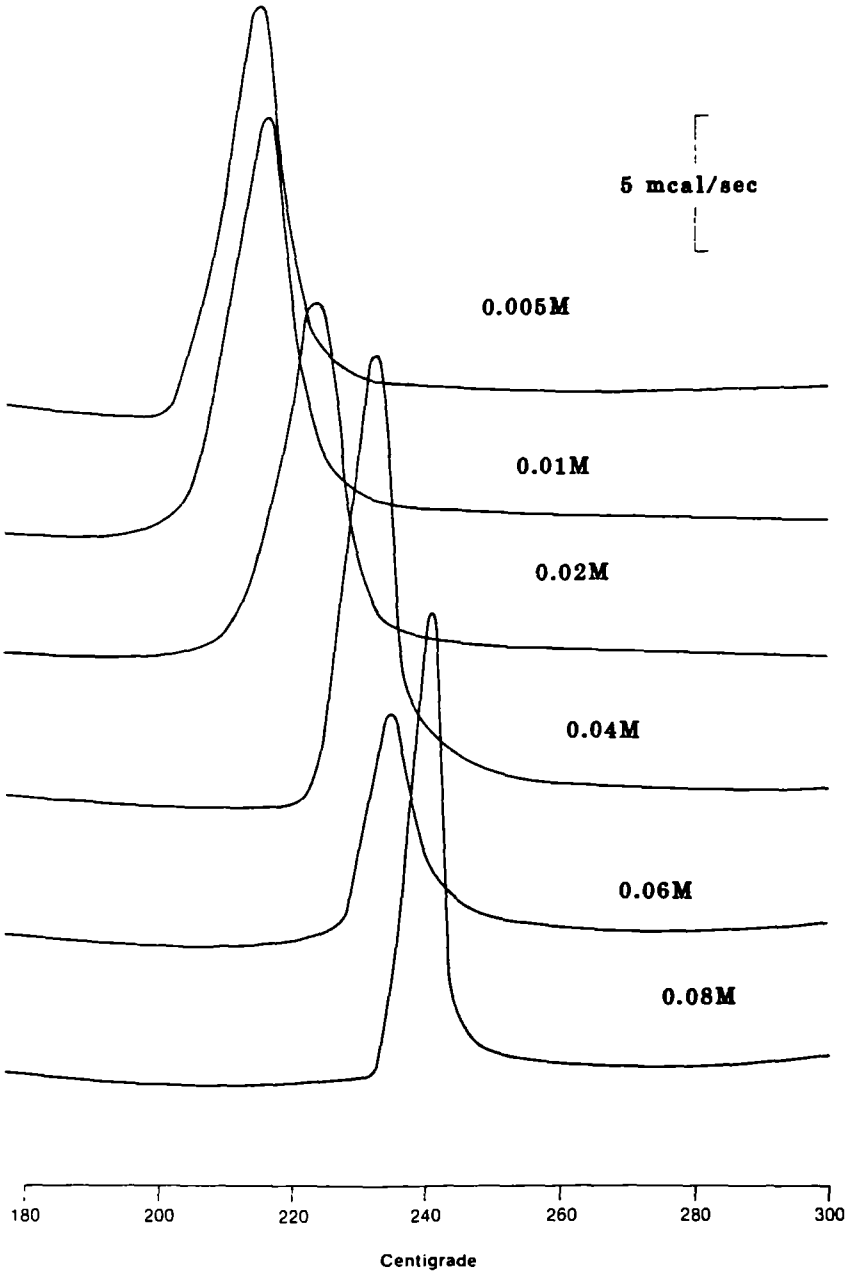

Fig 6.2.4 DSC traces displaying the oxidation of squalane containing different n-octyl DDPA concentrations

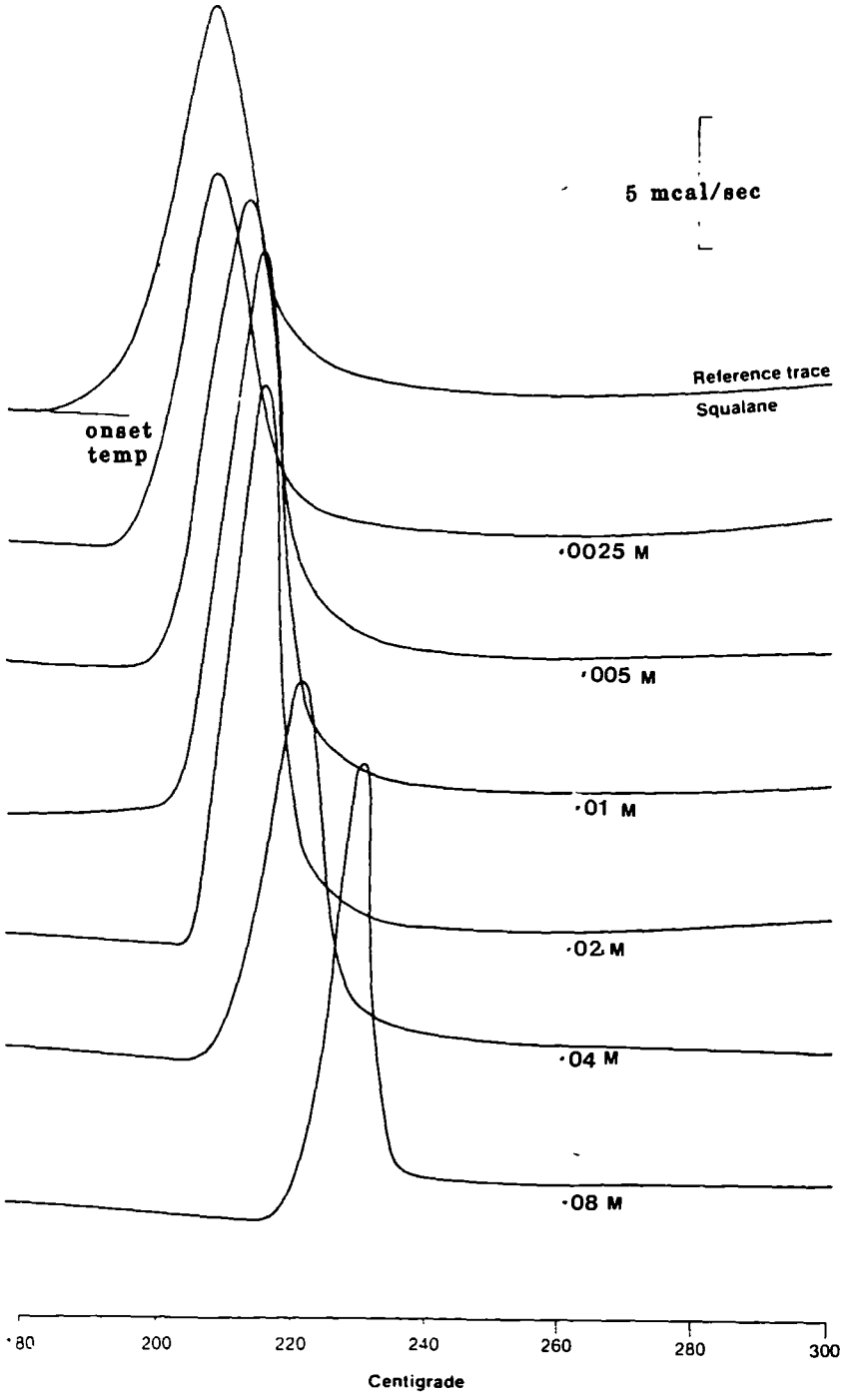

n-Octyl DDPA

Conc Moles/dm^3	T onset deg C	Wt mg	A sq in	ΔHr J/g
0.08	220	0.45	1.438	4590
0.04	211	0.45	1.58	5281
0.02	206	0.58	2.2	5448
0.01	204	0.61	2.404	5659
0.005	200	0.5	2.33	6708
0.0025	197.6	0.44	1.90	6217
Squalane Ref	195	0.5	2.39	6860

Conclusions

This technique is similar to that employed by Noel, (1,2). Noel determined the relative antioxidant capacities of a phenolic antioxidant, a ZDDP and an aromatic disulphide. The following trend was deduced for the relative effectiveness of these antioxidants:

Phenolic > ZDDP > Aromatic disulphide

The antioxidant quality increased with concentration for both ZDDP and phenolic antioxidant; however a point was reached when additional aromatic disulphide produced no change in the onset temperatures.

The following trend for the antioxidant capacity of the analysed antioxidant is derived from the onset temperatures:

Commercial iso-octyl ZDDP > n-octyl ZDDP > n-octyl DDDiS > n-octyl DDPA.

Not only is the onset temperature lowered by reducing the antioxidant concentration but the heat of reaction increases tending towards the value observed for pure squalane. A simple T.G. experiment was performed on a thin film of squalane. The sample was weighed before and after a DSC scan at 500 psi in nitrogen and the percentage loss determined. Three flushes to 500 psi N_2 were performed to ensure freedom from oxygen contamination. The sample was allowed to cool to room temperature before the second weighing was performed. The results are displayed in the table overleaf.

*T deg C	Wt prior to DSC scan	Wt post	% weight loss
195	0.34	0.33	3%
235	0.36	0.275	24%
255	0.35	0.185	43%

*The limit temperature to which the sample is heated at 10 deg/min at 500 psi N_2 and then cooled to ambient temperature.

Evaporation therefore accounts for the reduction of the ΔH value when the antioxidant concentration is increased. For example, 0.08M n-octyl DDPA with an onset temperature of 220 deg C, is oxidised in the temperature range analysed by the T.G. method. The observed heat of reaction is lower by a factor of 1.5 than the value for pure squalane, this corresponds to a 34% weight loss which is a similar figure to the range determined from the T.G. analysis, viz 22% - 43%. Analysis of the cooling curve indicates that the rate of cooling is faster than the heating rate (approximately 20 deg/min); therefore the heating process contributes mainly to the evaporation of the sample. Therefore the actual weight loss in the DSC experiment is probably near the middle of the stated range.

6.3 The Comparison of the Antioxidant Capacities of n-Butyl ZDDP and some of its Major Hydrolysis, Oxidation and Thermal Decomposition products by the DSC Bulk Solution Oxidation Method

High pressure DSC in an inert nitrogen atmosphere (500 psi) was used to compare the hydroperoxide decomposition reactions of n-Butyl ZDDP and the following related compounds:-

	Mode of Formation from ZDDP
n-Butyl Disulphide	Decomposition
n-Butyl Thiol	Decomposition
n-Butyl Sulphide	Decomposition
DDDiS	Oxidation
TDTP	Decomposition
TTetTP	Decomposition

Experimental

n-Butyl disulphide, sulphide, and thiol were obtained from Aldrich Ltd., (purity between 96-98%). Distillations were performed to improve further their purities. n-Butyl ZDDP, DDDiS, TDTP and TTetT were synthesised by methods previously discussed and their purities checked by G.L.C and H-1, C-13 and P-31 NMR techniques. Cumene hydroperoxide was selected to provide the oxygen source because it is a relatively stable hydroperoxide thereby reducing the risk of an explosion. The hydroperoxide was purified via the sodium salt (8), to remove any cumene contamination. Squalane was used as a solvent for the reaction as it gives a reproducible DSC baseline, and has a manageable viscosity necessary to produce good mixing. Solutions of 0.126 M cumene hydroperoxide and 0.08 M antioxidant in squalane (chromatography pure) were prepared and equal aliquots mixed to give a solution 0.063 M with respect to hydroperoxide and 0.04 M with respect to antioxidant. Measurements were performed using a DuPont 1090 DSC with an attached thermal analyser computer and a DuPont 990 DSC with a thermal analyser (not computerised). Calibration coefficients were determined for each instument and therefore a viable comparison of the determined results could be made. Dynamic DSC scans at varying heating rates were performed on a known aliquot of the prepared solution, (typically 30 ul) in aluminium sample pans ,in an atmosphere of 500 psi white spot nitrogen. The cell was flushed three times before scanning to expel any oxygen from the system.

Results

Fig 6.3.1 displays the squalane baseline at a heating rate of 10 deg/min whilst fig 6.3.2 displays the decomposition of .126M cumene hydroperoxide in the absence of antioxidants, in squalane, at a heating rate of 10 deg/ min. Figs 6.3.3- 6.3.9 depict the various observed exotherms for the reaction of the respective antioxidants with cumene hydroperoxide at varying heating rates. The results are summarised in table 6.3.1.

The ASTM E698-79 standard method for calculating Arrhenius kinetic constants (9) was employed to determine the respective kinetic parameters for the decomposition of cumene hydroperoxide by an antioxidant. This method is based on work performed by T. Ozowa, (10). Kinetic parameters are obtained from the Tmax variation with heating rate. The method is often used in assessing kinetic parameters of thermally unstable materials.

Theory

The method assumes that the reaction is Arrhenius in character, $k = Z\exp(-E/RT)$ where k is the specific rate constant in reciprocal minutes for first order reactions, Z is the pre-exporential factor in reciprocal minutes, E is the activation energy in J/mol, R is the gas constant (8.314 J/mol K) and T is the temperature in Kelvin. The general rate law is assumed: $-dC/dt=k(1-C)^n$ where C is fractional conversion of CHP, t is the time in minutes and n is the reaction order. The kinetic parameters are determined using the peak maxima temperature from the following expression :

$$E = -2.3\ R[d \log_{10} Q/d\ (1/T\ max.)]$$

Q = heating rate (deg C/min)

T max = peak maximum temperature (Kelvin)

The pre-exponential factor was calculated from the following equation.

$$Z = QE\exp(E/RT)/RT^2$$

First order behaviour is assumed to calculate the half life time from the specific rate constant at a particular temperature, $t_{1/2} = 0.693/k$.

Activation energies are therefore calculated from a plot of $\log_{10} Q$ versus 1/T max for the various listed antioxidants (.04M) reacting with cumene hydroperoxide (.063M) , (see table 6.3.2).

Fig 6.3.1

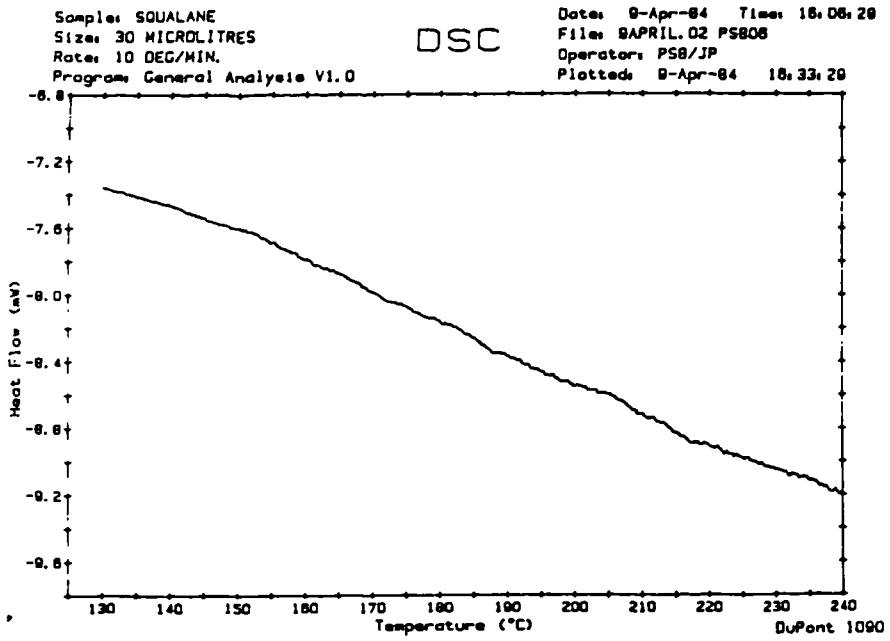

Fig 6.3.2

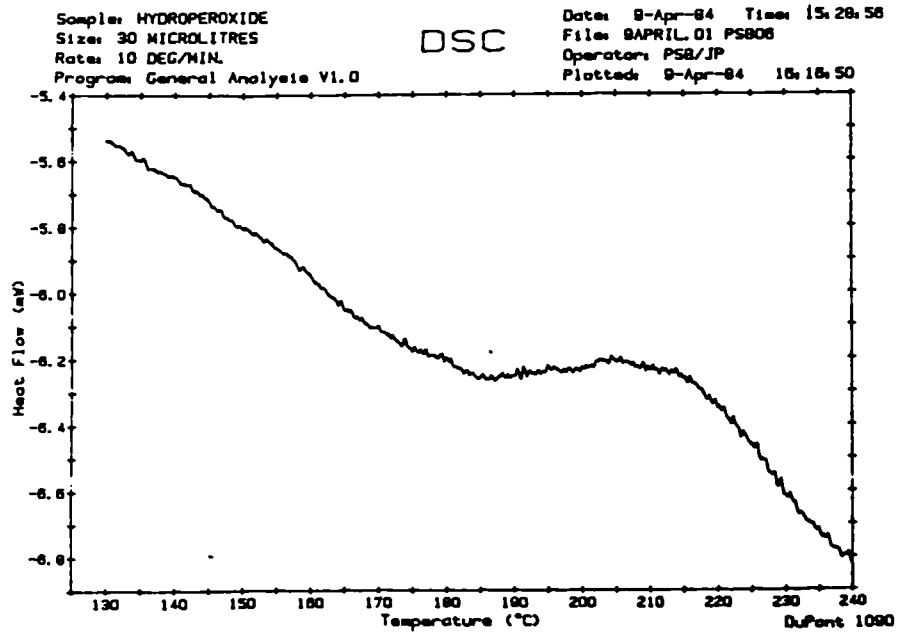

Fig 6.3.3(a)

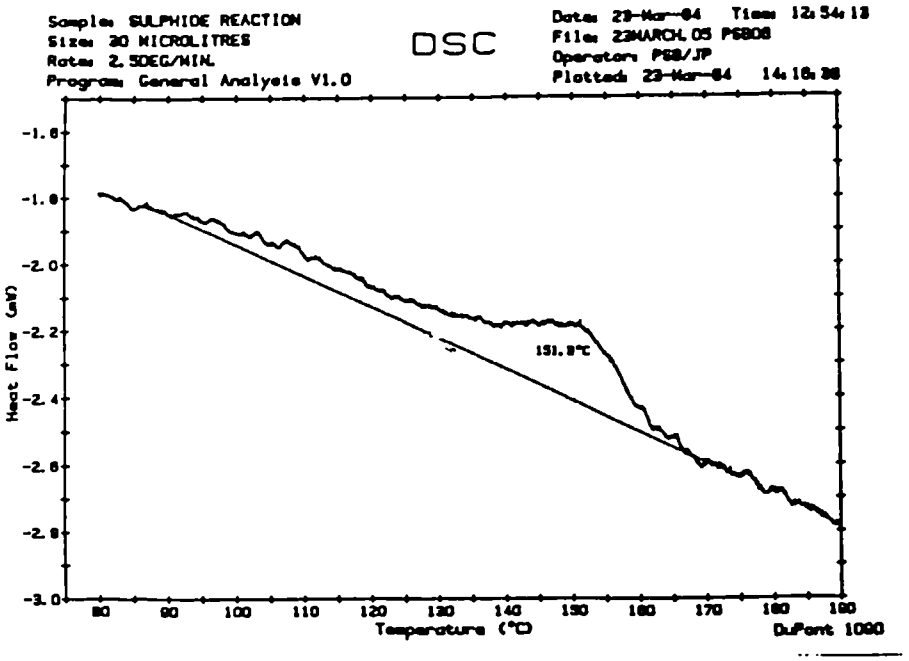
Sample: SULPHIDE REACTION
Size: 30 MICROLITRES
Rate: 2.5DEG/MIN.
Program: General Analysis V1.0
DSC
Date: 23-Mar-94 Time: 12:54:13
File: 23MARCH.05 PS806
Operator: PSB/JP
Plotted: 23-Mar-94 14:16:36
Heat Flow (mW)
-1.6
-1.8
-2.0
-2.2
-2.4
-2.6
-2.8
-3.0
151.8°C
80 90 100 110 120 130 140 150 160 170 180 190
Temperature (°C)
DuPont 1090

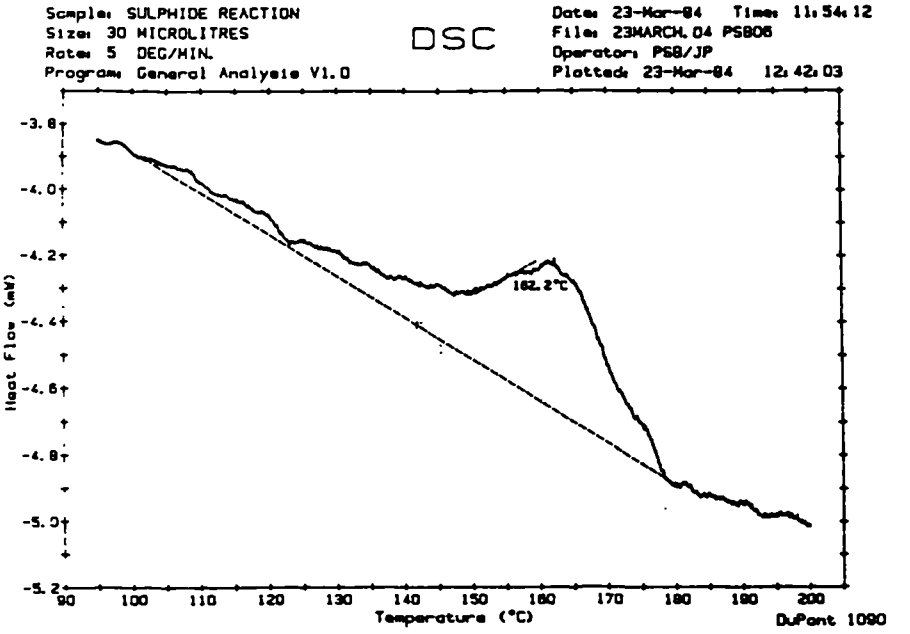
Sample: SULPHIDE REACTION
Size: 30 MICROLITRES
Rate: 5 DEG/MIN.
Program: General Analysis V1.0
DSC
Date: 23-Mar-94 Time: 11:54:12
File: 23MARCH.04 PS806
Operator: PSB/JP
Plotted: 23-Mar-94 12:42:03
Heat Flow (mW)
-3.8
-4.0
-4.2
-4.4
-4.6
-4.8
-5.0
-5.2
162.2°C
90 100 110 120 130 140 150 160 170 180 190 200
Temperature (°C)
DuPont 1090

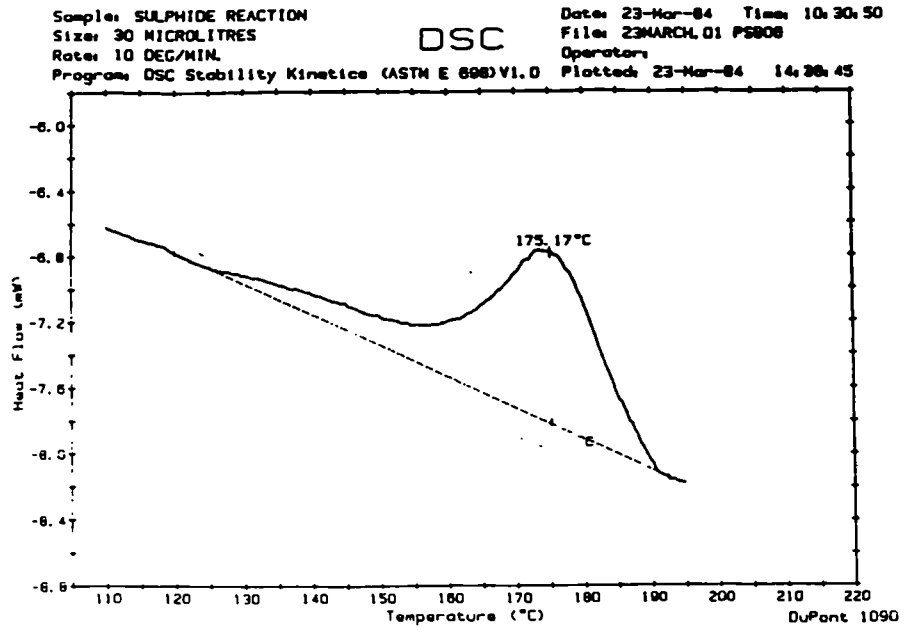
Sample: SULPHIDE REACTION
Size: 30 MICROLITRES
Rate: 10 DEG/MIN.
Program: DSC Stability Kinetics (ASTM E 698)V1.0
DSC
Date: 23-Mar-94 Time: 10:30:50
File: 23MARCH.01 PS806
Operator:
Plotted: 23-Mar-94 14:38:45
Heat Flow (mW)
-6.0
-6.4
-6.8
-7.2
-7.6
-8.0
-8.4
-8.8
175.17°C
110 120 130 140 150 160 170 180 190 200 210 220
Temperature (°C)
DuPont 1090

Fig 6.3.3(b)

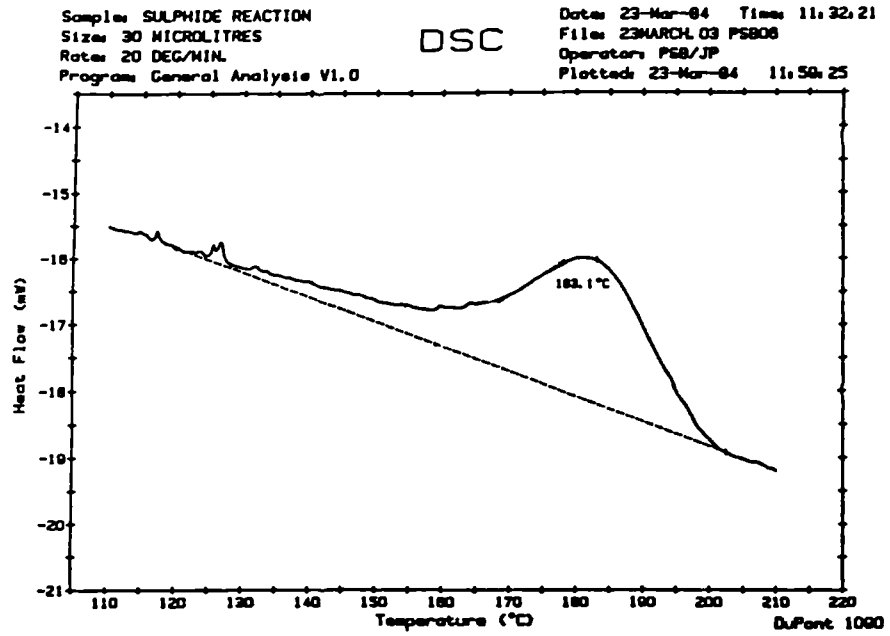
Sample: SULPHIDE REACTION
Size: 30 MICROLITRES
Rate: 20 DEG/MIN.
Program: General Analysis V1.0
DSC
Date: 23-Mar-84 Time: 11:32:21
File: 23MARCH.03 PS808
Operator: PSB/JP
Plotted: 23-Mar-84 11:50:25
183.1°C
Heat Flow (mW)
Temperature (°C)
DuPont 1090

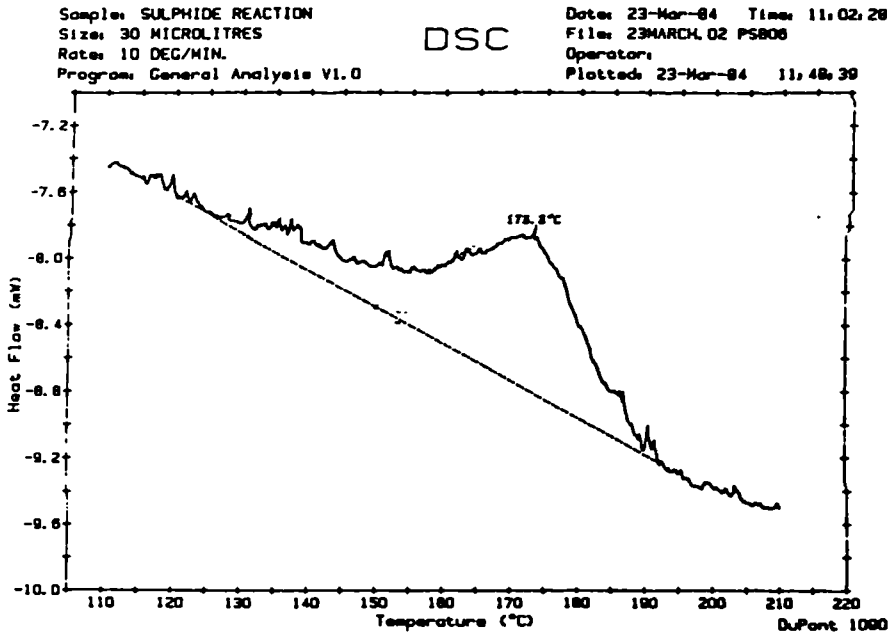
Sample: SULPHIDE REACTION
Size: 30 MICROLITRES
Rate: 10 DEG/MIN.
Program: General Analysis V1.0
DSC
Date: 23-Mar-84 Time: 11:02:28
File: 23MARCH.02 PS808
Operator:
Plotted: 23-Mar-84 11:48:39
178.8°C
Heat Flow (mW)
Temperature (°C)
DuPont 1090

Fig 6.3.4

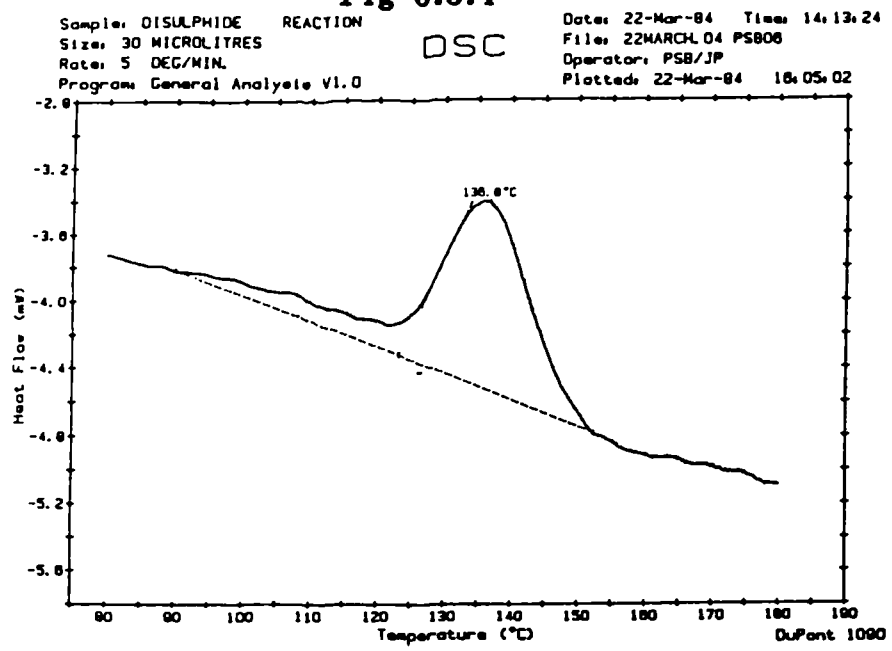
Sample: DISULPHIDE REACTION
Size: 30 MICROLITRES
Rate: 5 DEG/MIN.
Program: General Analysis V1.0
DSC
Date: 22-Mar-84 Time: 14:13:24
File: 22MARCH.04 PSB06
Operator: PSB/JP
Plotted: 22-Mar-84 16:05:02
136.6°C
Heat Flow (mW)
Temperature (°C)
DuPont 1090

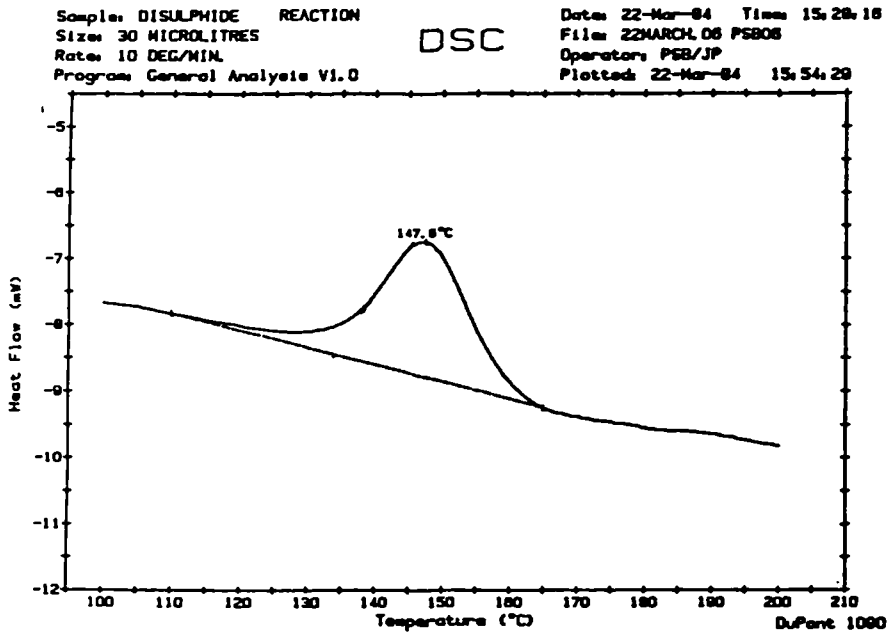
Sample: DISULPHIDE REACTION
Size: 30 MICROLITRES
Rate: 10 DEG/MIN.
Program: General Analysis V1.0
DSC
Date: 22-Mar-84 Time: 15:28:16
File: 22MARCH.06 PSB06
Operator: PSB/JP
Plotted: 22-Mar-84 15:54:29
147.8°C
Heat Flow (mW)
Temperature (°C)
DuPont 1090

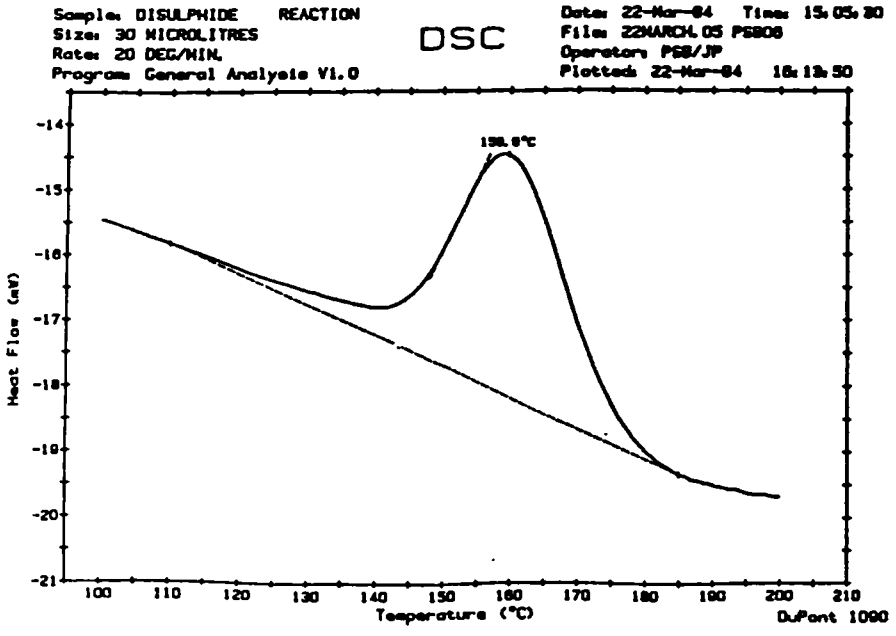
Sample: DISULPHIDE REACTION
Size: 30 MICROLITRES
Rate: 20 DEG/MIN.
Program: General Analysis V1.0
DSC
Date: 22-Mar-84 Time: 15:05:30
File: 22MARCH.05 PSB06
Operator: PSB/JP
Plotted: 22-Mar-84 16:13:50
158.6°C
Heat Flow (mW)
Temperature (°C)
DuPont 1090

Fig 6.3.5

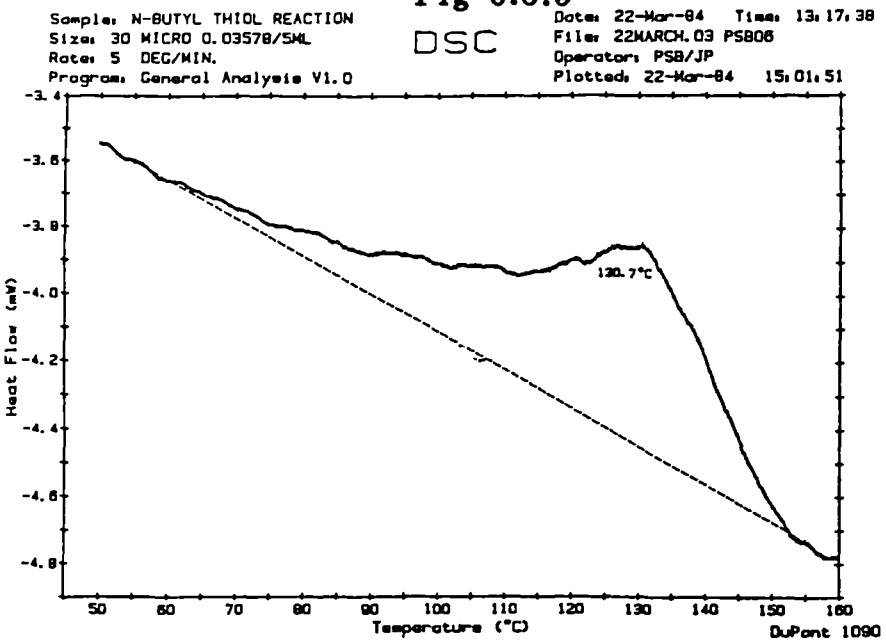
Sample: N-BUTYL THIOL REACTION
Size: 30 MICRO 0.03578/5ML
Rate: 5 DEG/MIN.
Program: General Analysis V1.0
DSC
Date: 22-Mar-84 Time: 13:17:38
File: 22MARCH.03 PSB06
Operator: PSB/JP
Plotted: 22-Mar-84 15:01:51
130.7°C
Heat Flow (mW)
Temperature (°C)
DuPont 1090

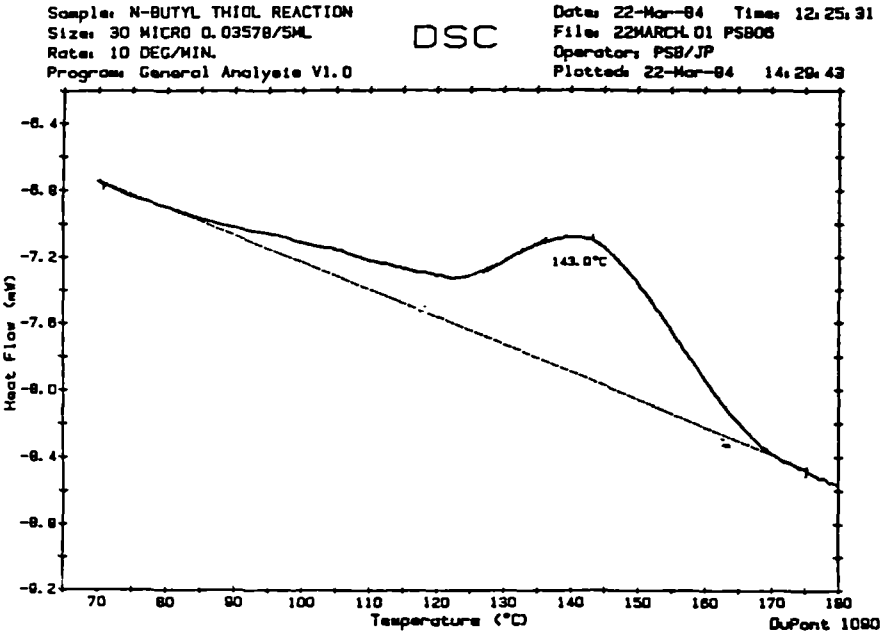
Sample: N-BUTYL THIOL REACTION
Size: 30 MICRO 0.03578/5ML
Rate: 10 DEG/MIN.
Program: General Analysis V1.0
DSC
Date: 22-Mar-84 Time: 12:25:31
File: 22MARCH.01 PSB06
Operator: PSB/JP
Plotted: 22-Mar-84 14:29:43
143.0°C
Heat Flow (mW)
Temperature (°C)
DuPont 1090

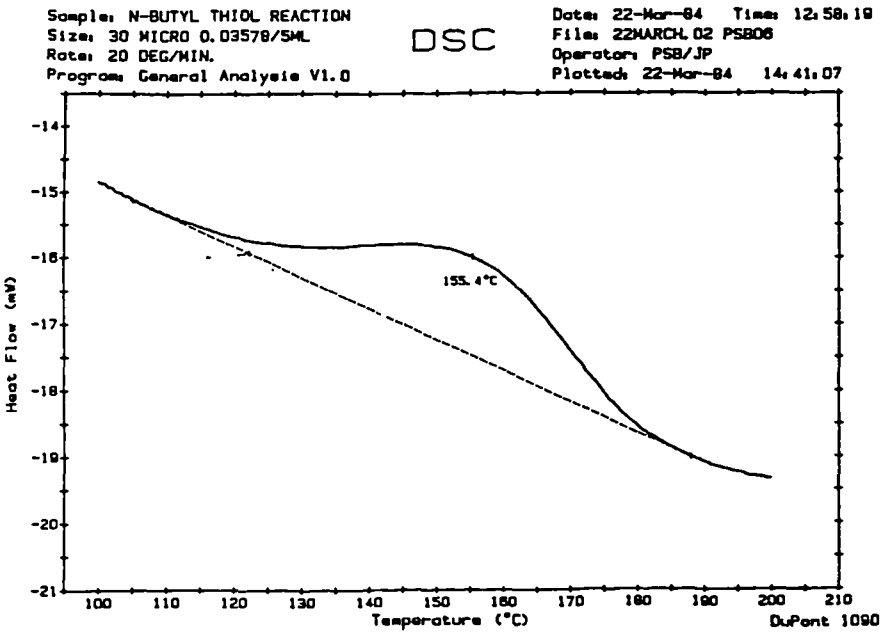
Sample: N-BUTYL THIOL REACTION
Size: 30 MICRO 0.03578/5ML
Rate: 20 DEG/MIN.
Program: General Analysis V1.0
DSC
Date: 22-Mar-84 Time: 12:58:19
File: 22MARCH.02 PSB06
Operator: PSB/JP
Plotted: 22-Mar-84 14:41:07
155.4°C
Heat Flow (mW)
Temperature (°C)
DuPont 1090

Fig 6.3.6

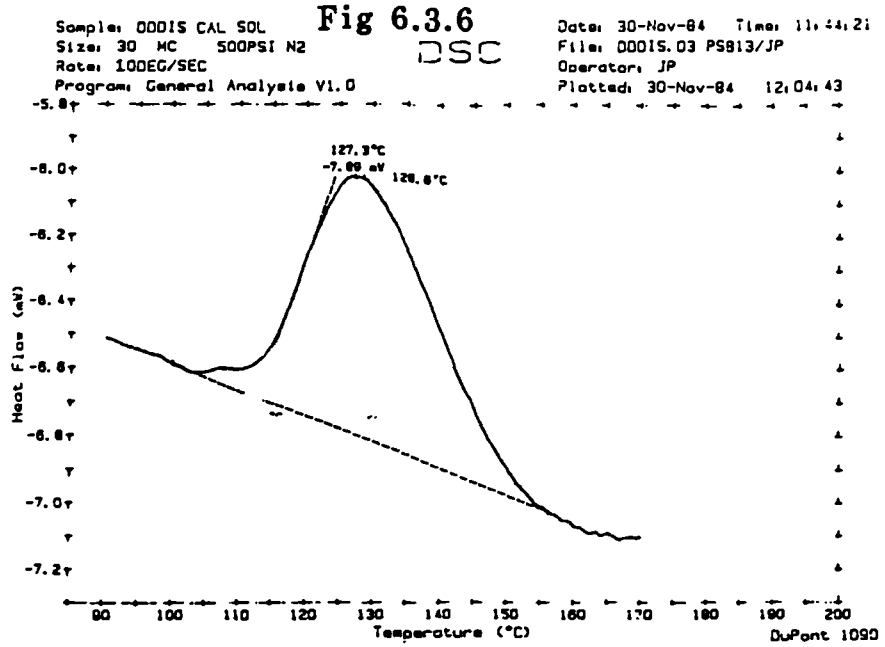
Sample: 0001S CAL SOL
Size: 30 MC 500PSI N2
Rate: 100EG/SEC
Program: General Analysis V1.0
DSC
Date: 30-Nov-84 Time: 11:44:21
File: 0001S.03 PS813/JP
Operator: JP
Plotted: 30-Nov-84 12:04:43
127.3°C
-7.09 mW
128.6°C
Heat Flow (mW)
Temperature (°C)
DuPont 1090

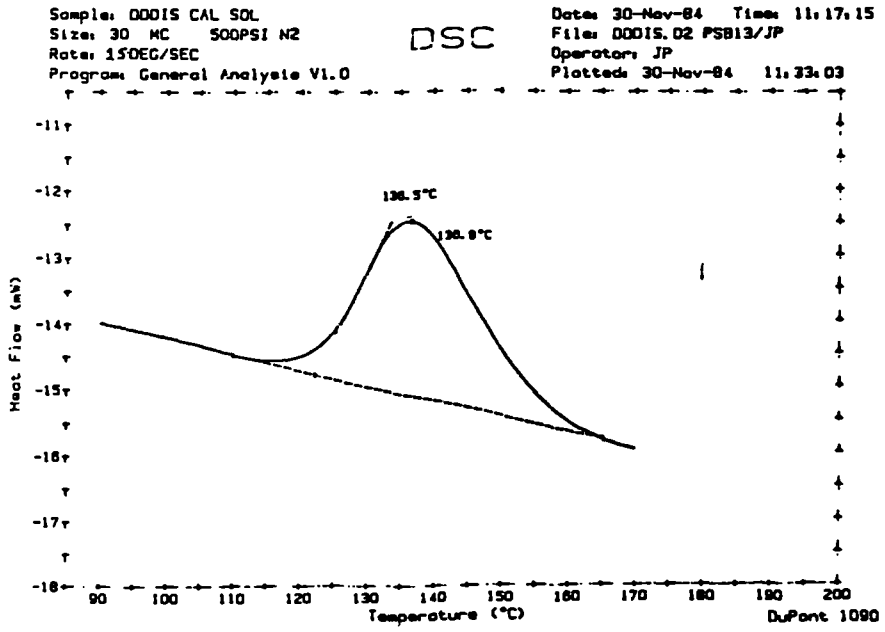
Sample: 0001S CAL SOL
Size: 30 MC 500PSI N2
Rate: 150EG/SEC
Program: General Analysis V1.0
DSC
Date: 30-Nov-84 Time: 11:17:15
File: 0001S.02 PS813/JP
Operator: JP
Plotted: 30-Nov-84 11:33:03
136.5°C
138.8°C
Heat Flow (mW)
Temperature (°C)
DuPont 1090

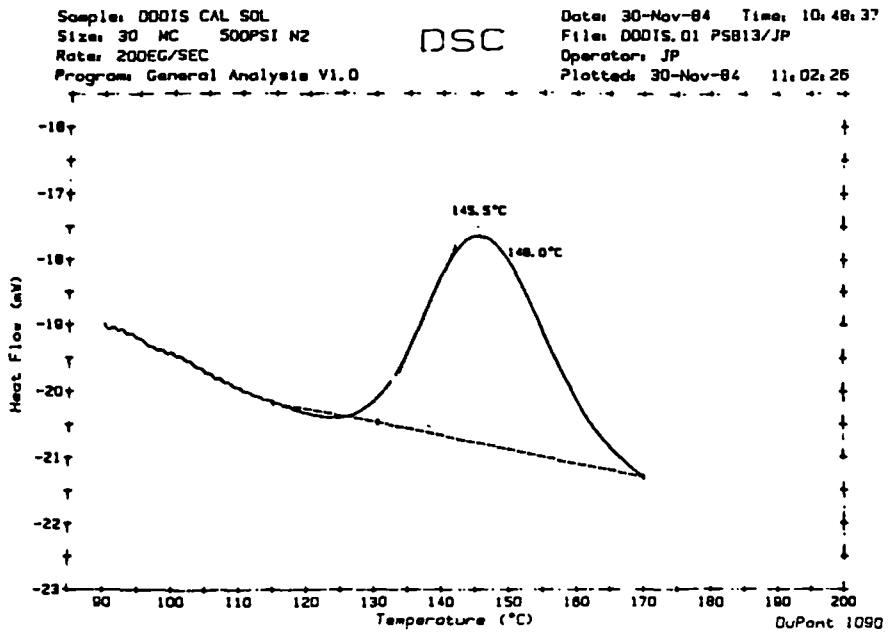
Sample: 0001S CAL SOL
Size: 30 MC 500PSI N2
Rate: 200EG/SEC
Program: General Analysis V1.0
DSC
Date: 30-Nov-84 Time: 10:48:37
File: 0001S.01 PS813/JP
Operator: JP
Plotted: 30-Nov-84 11:02:26
145.5°C
148.0°C
Heat Flow (mW)
Temperature (°C)
DuPont 1090

Fig 6.3.7 TDTP reaction

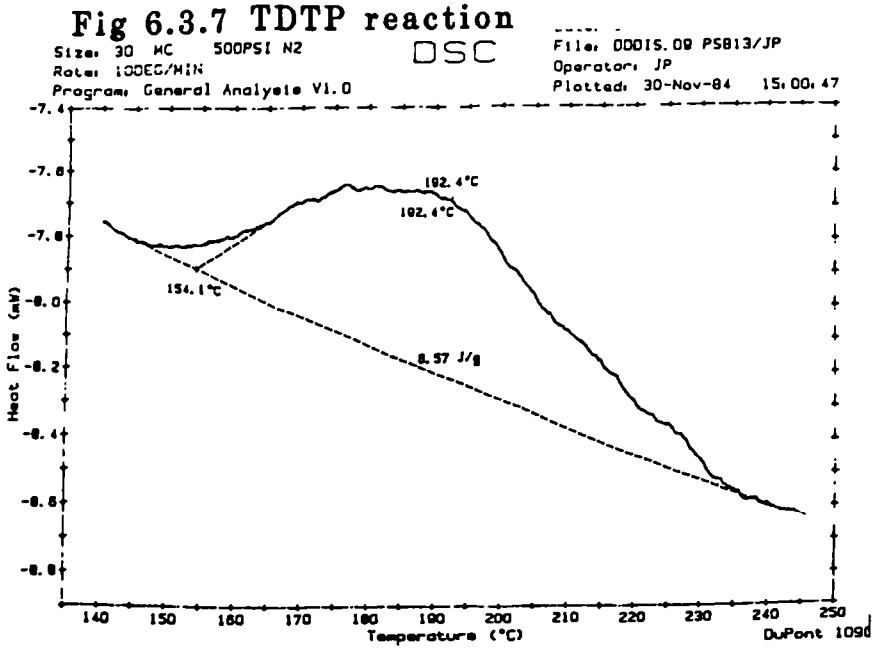

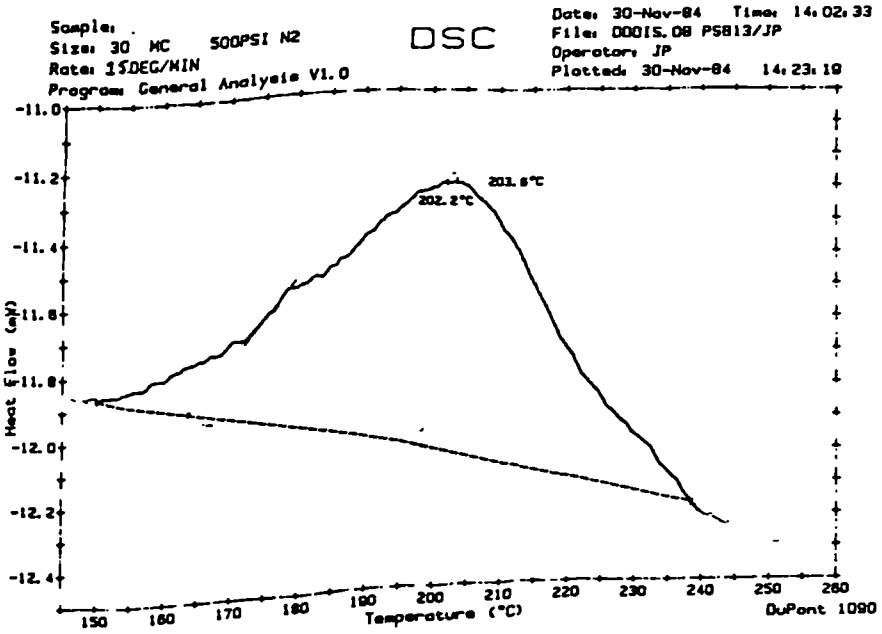

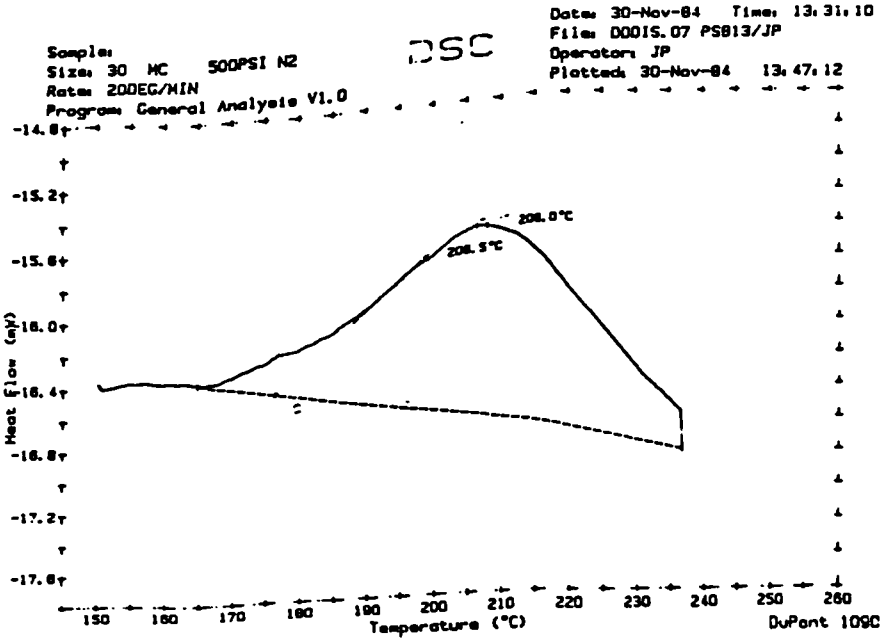

Fig 6.3.8

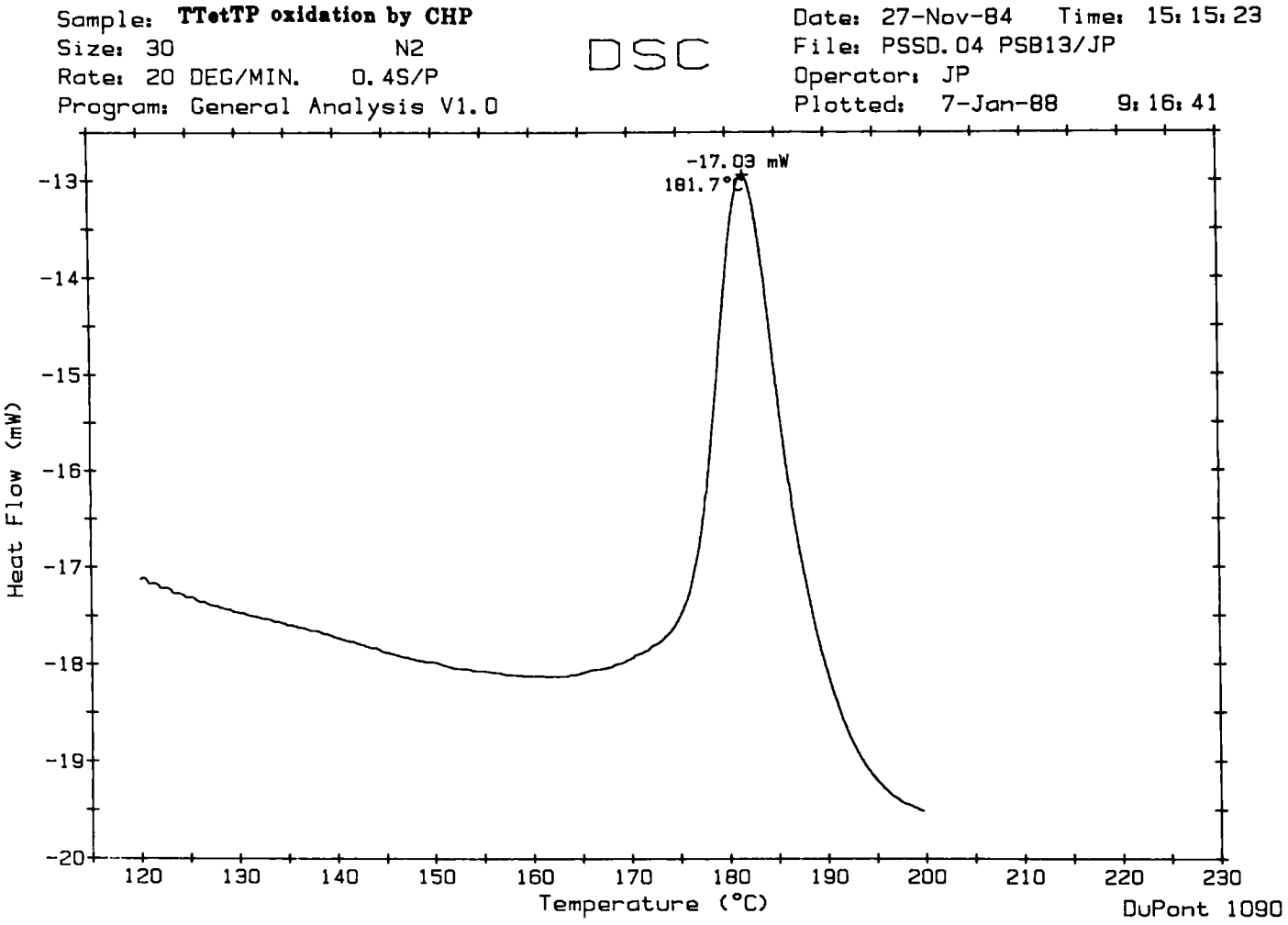
Sample: TTetTP oxidation by CHP
Size: 30
N2
Rate: 20 DEG/MIN. 0.4S/P
Program: General Analysis V1.0
DSC
Date: 27-Nov-84 Time: 15:15:23
File: PSSD.04 PSB13/JP
Operator: JP
Plotted: 7-Jan-88 9:16:41
-17.03 mW
181.7°C
-13
-14
-15
-16
-17
-18
-19
-20
Heat Flow (mW)
120
130
140
150
160
170
180
190
200
210
220
230
Temperature (°C)
DuPont 1090

Fig 6.3.9

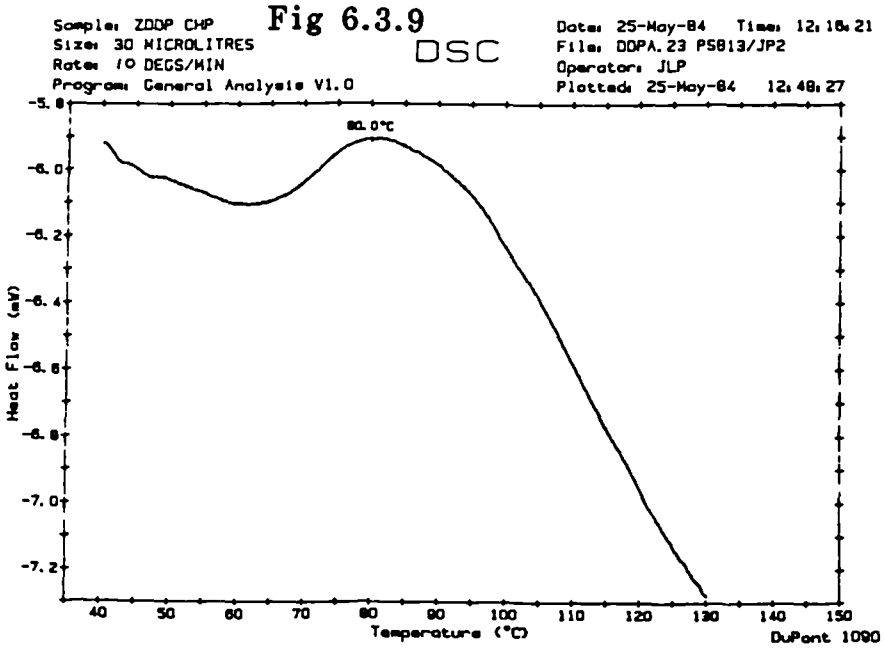
Sample: ZDOP CHP
Size: 30 MICROLITRES
Rate: 10 DEGS/MIN
Program: General Analysis V1.0
DSC
Date: 25-May-84 Time: 12:16:21
File: DOPA.23 PS813/JP2
Operator: JLP
Plotted: 25-May-84 12:48:27
80.0°C
Heat Flow (mW)
Temperature (°C)
DuPont 1090

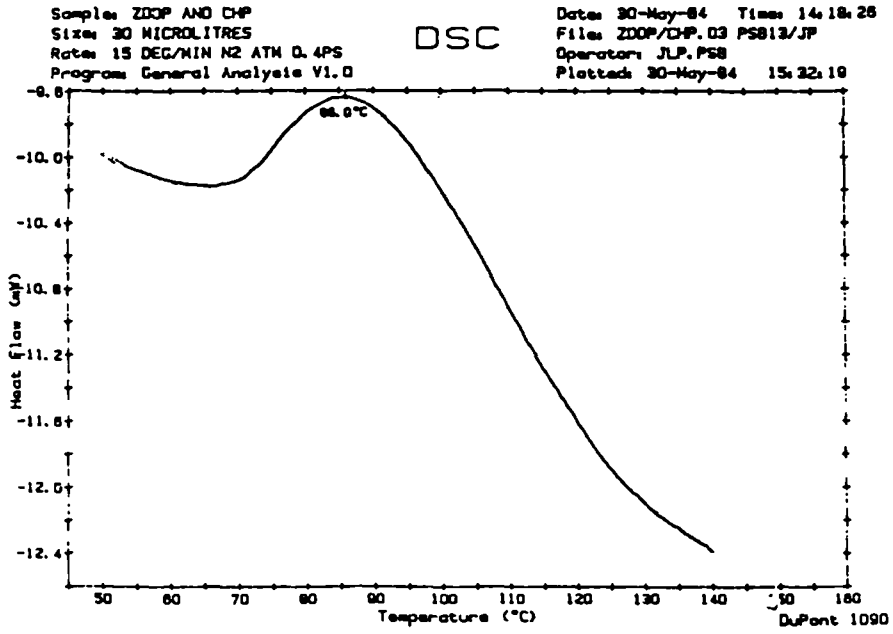
Sample: ZDOP AND CHP
Size: 30 MICROLITRES
Rate: 15 DEG/MIN N2 ATM 0.4PS
Program: General Analysis V1.0
DSC
Date: 30-May-84 Time: 14:18:26
File: ZDOP/CHP.03 PS813/JP
Operator: JLP.PS8
Plotted: 30-May-84 15:32:10
88.0°C
Heat Flow (mW)
Temperature (°C)
DuPont 1090

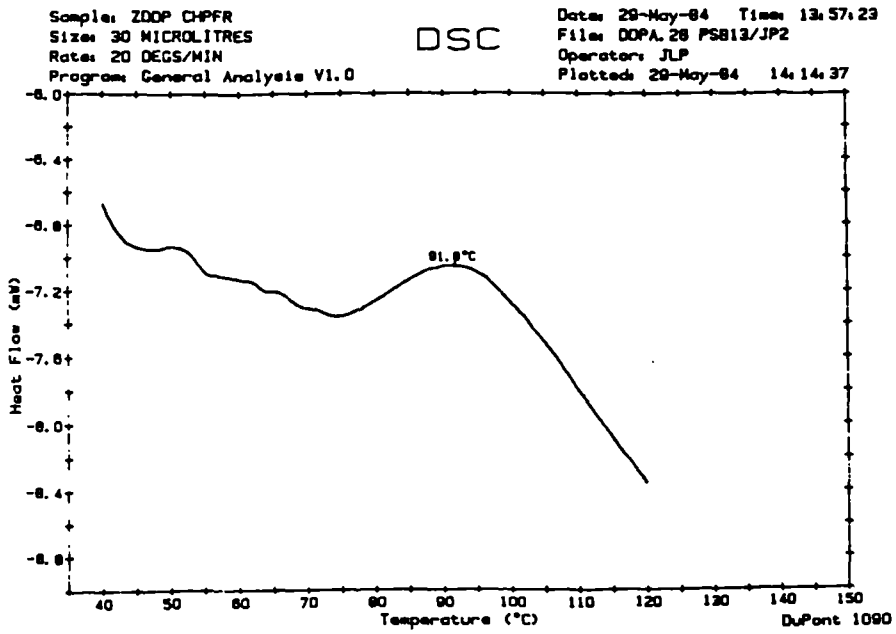
Sample: ZDOP CHPFR
Size: 30 MICROLITRES
Rate: 20 DEGS/MIN
Program: General Analysis V1.0
DSC
Date: 29-May-84 Time: 13:57:23
File: DOPA.28 PS813/JP2
Operator: JLP
Plotted: 29-May-84 14:14:37
81.9°C
Heat Flow (mW)
Temperature (°C)
DuPont 1090

Table 6.3.1 ΔHr and Tmax values of DSC exotherms produced from the reaction of 30 microlitres of 0.04M antioxidant and 0.063M CHP in squalane

Heating rate Q (°C/min)	Antioxidant															
	Bu_2S		Bu_2S_2		BuSH		DDDiS		TDTP		TTetTP		ZDDP		in the absence of antioxidant	
	T max °C	ΔHr J/g	T max °C	ΔHr J/g	T max °C	ΔHr J/g	T max °C	ΔHr J/g	T max °C	ΔHr J/g	T max °C	ΔHr J/g	T max °C	ΔHr J/g	T max °C	ΔHr J/g
2.5	151.3	5.8	-	-	-	-	-	-	-	-	-	-	-	-	-	-
5	162.2	4.8	136.8	8.2	130.7	8.9	-	-	-	-	-	-	-	-	-	-
10	175.2 173.3	5.3	147.6	7.1	143.0	6.1	127.3	7.6	192.4	5.3	167	5.6	80.0	3.5	212	2.4
15	-	-	-	-	-	-	136.5	7.9	203.5	4.9	174.2	5.8	86.0	-	-	-
20	183.1	6.3	159.9	8.1	155.4	5.4	146.0	6.9	206.5	4.8	181.6	6.4	91.8	-	-	-

Note: ΔHr values are quoted in joules per gram of squalane

(see figs. 6.3.2 - 6.3.9).

Table 6.3.2

Kinetic parameters determined by the ASTM E698-79 technique

	E(kJ mol^{-1})	T max 10 deg/min °C	Z (1/min)	k (130°C) min^{-1}	$t^{1}/2$ (130°C) (min)
DDDiS	60.3±2	127.3	$3.34x10^{7}$	0.51	1.36
BuSH	79 ±2	143	$4.56x10^{9}$	0.26	2.67
Bu_2S_2	88.5±2	147.6	$5.90x10^{10}$	0.20	3.47
TTetTP	93 ±3	167	$6.35x10^{10}$	0.056	12.38
Bu_2S	103±3	174	$6.75x10^{11}$	0.03	23.1

Z values are determined from T max values for when B = 10°C/min

Conclusions and Observations

The trend in reactivity is reflected both by the calculation of the half-life time at 130 deg C and a comparison of the Tmax values of the respective exotherms, at a heating rate of 10 deg/min. ZDDP is omitted from the kinetic parameter calculation because the ZDDP peak temperatures are difficult to determine accurately because they are close to the warm up period. The trend of reactivity with respect to the reduction of cumene hydroperoxide is ZDDP > DDDiS > BuSH > Bu_2S_2 > TTetTP > Bu_2S > TDTP. The results convey that the antioxidant sulphur content is important and in general it can be deduced that the higher the sulphur content the more effective the antioxidant is at decomposing hydroperoxides. The presence of an antioxidant reduces the hydroperoxide decomposition temperature when scanning dynamically.

6.4 The Kinetics of Hydroperoxide Decomposition by Dialkyldithiophosphoryl Disulphide Determined from DSC Measurements

Dialkyldithiophosphoryl disulphide is an important ZDDP oxidation product. n-Butyl DDDiS is a reactive antioxidant and readily decomposes hydroperoxides, (see section 6.3). This section analyses the effect of the change of n-octyl DDDiS and hydroperoxide concentration on the rate of reaction, employing DSC as the experimental technique.

6.4.1 Variation of Cumene Hydroperoxide Concentration

Experimental

High pressure (500 psi N_2) DSC scans using a Dupont 990 DSC, were performed on 40 ul aliquots of squalane solutions containing (a) 0.06M CHP and 0.04M n-octyl DDDiS and (b) 0.12M CHP and 0.04M n-octyl DDDiS at the same heating rate, (approx. 18 deg/min).

Results

The exotherms are displayed in fig 6.4.1 and table 6.4.1 summarizes the data calculated from the exotherms.

Table 6.4.1

	Tmax	ΔHr
Solution (a) 0.06M CHP	167 deg C	7.22 J/g
Solution (b) 0.12M CHP	159 deg C	14.4 J/g
0.04M Butyl DDDiS and 0.06M CHP*	146 deg C	7.5 J/g

*previously determined at a heating rate of 20 deg/min

Deductions

i) The Heats of Reaction

Halving of the concentration of the hydroperoxide present halves the ΔH of reaction. The heat of reaction calculated for solution (a) is very similar to the value determined for the reaction between 0.063M CHP and 0.04 n-butyl DDDiS.

ii) The Tmax Values

From the Tmax values displayed in table 6.4.1 it can be deduced that n-butyl DDDiS reacts faster with cumene hydroperoxide than n-octyl DDDiS. The concentration of hydroperoxide significantly affects the rate of reaction and thus must be incorporated any postulated rate expression.

Fig 6.4.1 DSC traces displaying the reduction of 1) 0.12M CHP 2) 0.06M CHP induced by 0.04M n-octyl DDDiS in squalane

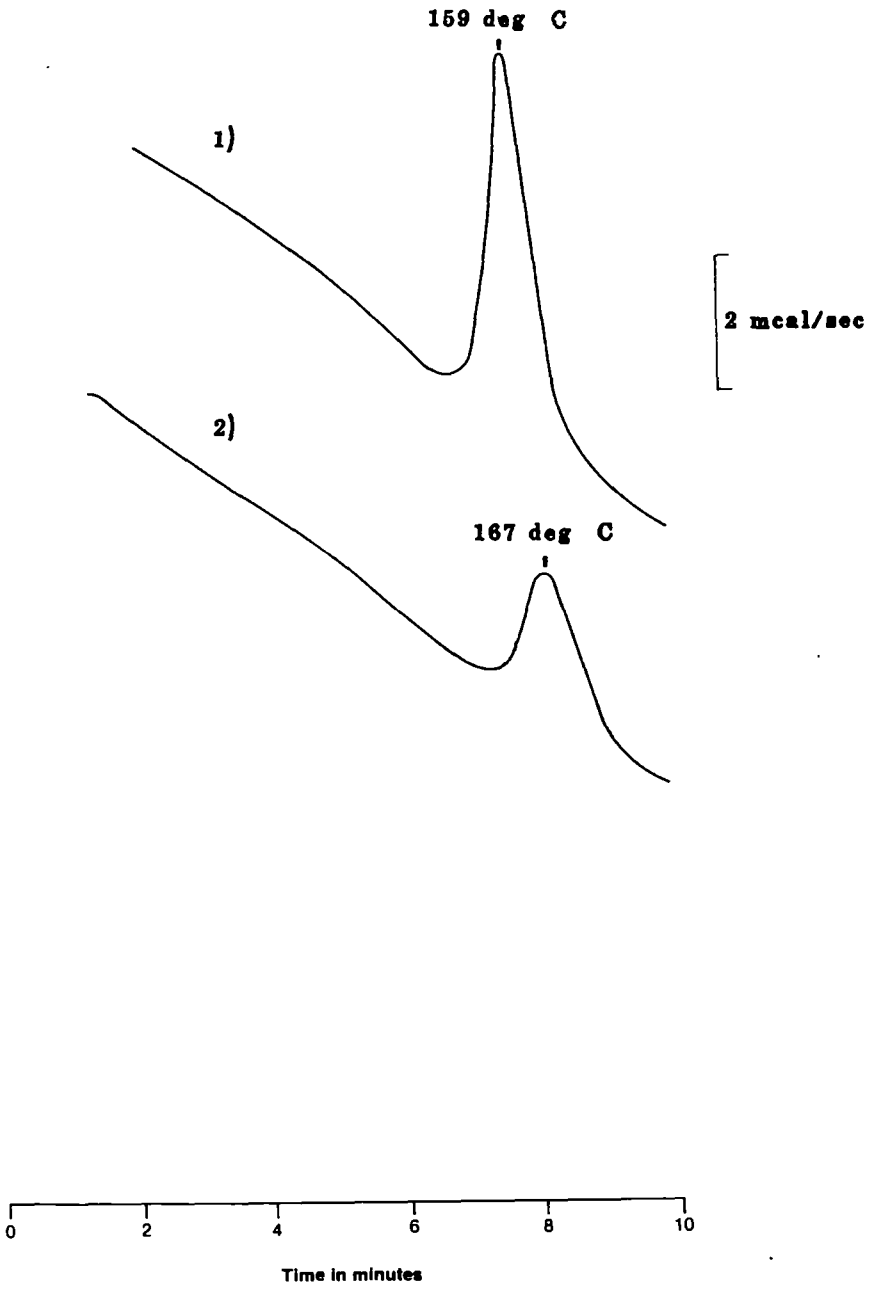

6.4.2 Variation of the Concentration of Antioxidant (n-Octyl DDDiS)

Experimental

A Dupont 990 Differential Scanning Calorimeter was used to study the exothermic reaction between octyl DDDiS and cumene hydroperoxide in squalane. DSC scans of 30 ul samples of 0.12M CHP and differing octyl DDDiS concentration were performed with the instrument in the dynamic mode (heating rate = 18 deg/min), in an atmosphere of nitrogen (500 psi). Two flushes of nitrogen up to 500 psi were carried out to expel oxygen from the DSC cell . Similar DSC scans were performed on solutions of 0.12M CHP in fluorube, with and without the presence of DDDiS (0.02M).

Results (see figs 6.4.2 and 6.4.3)

Table 6.4.2 displays the change of the Tmax and ΔH values resulting from reductions in the n-octyl DDDiS concentration.

Table 6.4.2

Molarity of n-octyl DDDiS in squalane		ΔH (J/g)	T max (°C)
i)	$4x10^{-2}$	13.5	156.5
ii)	$2x10^{-2}$	12.3	162.5
iii)	$1x10^{-2}$	13.2	170
iv)	$5x10^{-3}$	11.6	175
v)	$2.5x10^{-3}$	9.3	186.3
vi)	$4x10^{-4}$	7.9	217.5
vii)	$2x10^{-4}$	7.7	223.8
viii)	0	6.7	233.8
Molarity of n-octyl DDDiS in Fluorube			
ix)	$2x10^{-2}$	11.1	129
x)	0	-	210

Fig 6.4.2 DSC traces displaying the reduction of 0.12M CHP in squalane induced by different n-octyl DDDiS concentrations

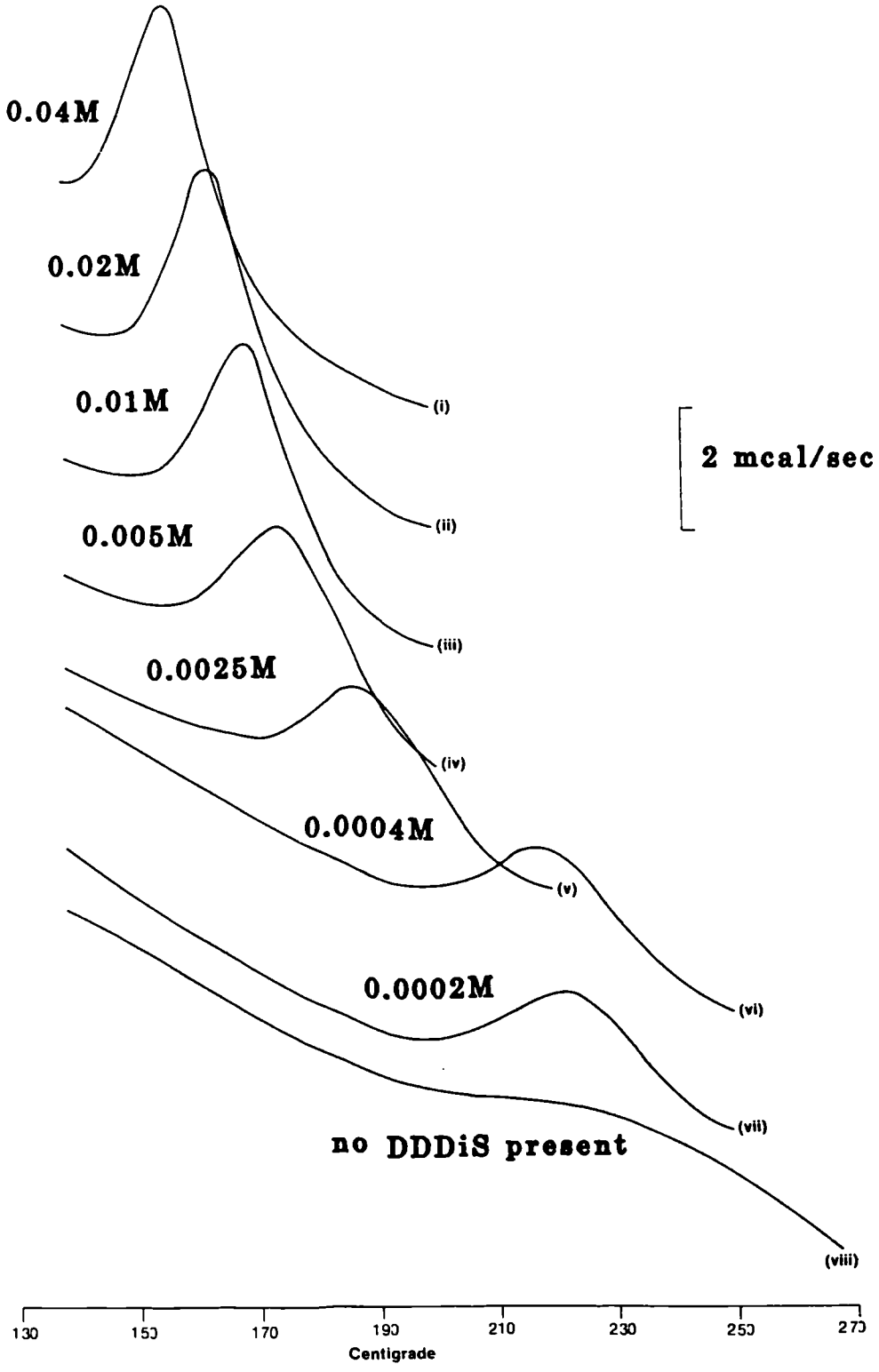

Fig 6.4.3 DSC traces displaying the decomposition of 0.12M CHP in fluorube (ix) induced by 0.02M n-octyl DDDiS (x)with no DDDiS present

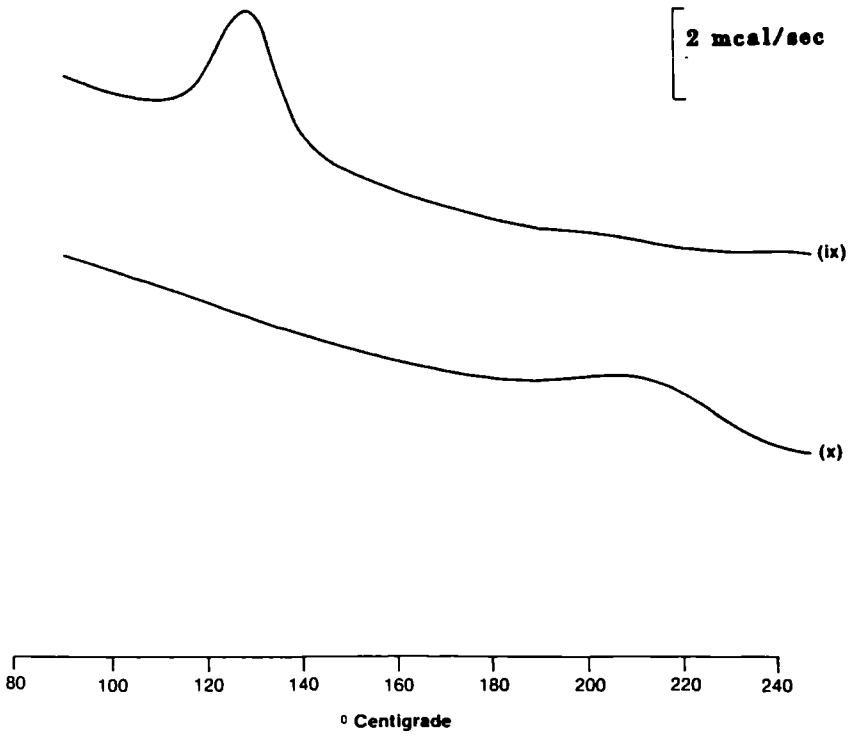

Observations and Deductions

The measured heats of reaction are not directly proportional to the concentration of DDDiS. A halving of the DDDiS concentration does not produce a halving of the heat of reaction. A sixteen-fold dilution of 0.04 molar n-octyl DDDiS produces only a 31% reduction in the heat of reaction.

Raman spectroscopy was used to quantify the extent of the possible reduction of the respective ΔHr magnitudes that may occur as a result of evaporation of hydroperoxide, when scans are performed on DDDiS solutions of increased dilution. The Tmax values of the reaction between the hydroperoxide and the DDDiS shift to higher temperatures as the DDDiS concentration is reduced thereby producing a relatively larger amount of evaporation of hydroperoxide.

Dynamic DSC scans (18 deg/min) were performed on solutions solely 0.12M CHP in squalane at 500 psi N_2. The scans were terminated between temperatures of 140 - 260 deg C. The system was allowed to cool whilst the thermal analyser plotted the cooling curve.

Raman spectra were run on the cooled samples . The intensities of a vibration at 1000 cm^{-1} attributed to the aromatic ring of cumene hydroperoxide was compared to the intensity of a squalane vibration. Comparing the intensity ratios of the aromatic band to the internal standard establishes the hydroperoxide loss (or aromatic loss if the hydroperoxide has in fact decomposed), at different termination temperatures. The contribution of the cooling process to the hydroperoxide evaporation must be estimated in order to determine the loss on heating from the overall loss. The rates of cooling from 255 to 50 deg C are approximately 27 deg/min from 255 deg C to 196 deg C, 16.8 deg/min from 196 to 122 deg C and 6 deg/min from 122 to 50 deg C. It is reasonable to assume therefore, that approximately the same amount of evaporation occurs on cooling as in heating.

Table 6.4.3 tabulates the respective overall and heating evaporation losses as percentages at different termination temperatures between 100 deg C and 255 deg C.

Table 6.4.3

Temperature of Termination (deg C)	Overall % Loss	Heating % Loss
100	7	3
140	15	7
160	17	8
180	23	11
200	36	18
220	37	18
255	41	20

From a plot of % heating losses versus termination temperature, the % loss range can be determined from the onset and completion exotherm temperatures. This range of % loss can be roughly compared to the % change in the ΔH values for the exotherms of different DDDiS concentrations with respect to the exotherm of the 0.04M n-octyl DDDiS and 0.12M CHP reaction ΔH, see table 6.4.4.

Table 6.4.4

Conc (M) DDDiS	Exotherm Range deg C	Predicted Heating Loss Range	Change in ΔH w.r.t 0.04M DDDiS
0.04	130-180	5 - 11%	
0.02	140-188	7 - 13%	9%
0.01	140-192	7 - 13%	11%
0.005	150-200	8 - 14%	14%
0.0025	160-210	9 - 15%	31%
0.0004	190-250	13 - 20%	41%
0.0002	194-250	13 - 20%	43%
NO DDDiS	210-260	16 - 20%	50%

The following points can be deduced from comparisons of the determined evaporation losses, change in ΔH's and Tmaxs for the respective DDDiS concentrations in squalane and fluorube:

1) A concentration change from 0.04M through to 0.005M produces a % difference in the ΔH values which are in the same range as the % losses due to hydroperoxide evaporation.

2) The ΔH values are not directly proportional to the concentration of DDDiS ie. a halving of the [DDDiS] does not produce a halving of the ΔH.

3) A reduction in the DDDiS concentration increases the Tmax value of the exotherm; however very low concentrations of DDDiS still induce hydroperoxide decomposition at a higher rate than when no antioxidant is present.

4) The reaction between the antioxidant and hydroperoxide is more exothermic than the decomposition of hydroperoxide in the absence of antioxidant.

5) Considering the points discussed above it can be concluded that the reaction between n-octyl DDDiS and CHP is autocatalytic. The products from the initial reaction between n-octyl DDDiS and cumene hydroperoxide can also decompose hydroperoxides.

6) The results indicate that hydroperoxide decomposition occurs in fluorube both in the presence and absence of DDDiS. Fluorube is a highly inert fluorocarbon, and therefore the observed reactions are due to the reaction of DDDiS or a related oxidation product with cumene hydroperoxide, or, if no DDDiS is present, the thermally induced decomposition of cumene hydroperoxide. The similar argument therefore applies to the exotherms obtained in squalane, the exotherms are not the result of a reaction between the hydrocarbon and the hydroperoxide, (unlike the thin layer higher pressure technique). The exotherm Tmax values of the hydroperoxide decomposition in fluorube are lower than in squalane implying that the CHP decomposition reaction occurs more readily in fluorube. A possible explanation for this is that the hydroperoxide is destabilised (ie. of a higher energy) with respect to the transition state in fluorube thereby reducing the activation energy of the hydroperoxide decomposition. The heat evolution was similar in fluorube to squalane but the ΔH value in J/g is smaller because of the high density of fluorube relative to squalane (fluorube = 1.9 g/ml, squalane = 1.22 g/ml).

6.5 Calculation of Kinetic Parameters by Dynamic DSC for the Reactions of n-Octyl DDDiS with Cumene Hydroperoxide in Squalane

Experimental

The ASTM E698 method for determining the kinetics of decomposition of thermally unstable materials was used to study the kinetics of decomposition of CHP induced by n-octyl DDDiS.

Dynamic DSC was performed at different heating rates in a nitogen atmosphere (500 psi) to observe the reactions occurring in 40µl aliquots of the following solutions: a) 0.04M n-octyl DDDiS and 0.12M cumene hydroperoxide, and b) 0.004M n-octyl DDDiS and 0.12M cumene hydroperoxide in squalane.

In order to test the reproducibility of the exotherms, three sets of data were recorded following reaction (a), on different days using freshly made solutions. Reaction (a) was also studied at differing nitrogen pressures.

Results

Tables 6.5.1 to 6.5.4 list the Tmax and ΔHr values of the three sets of data for reaction (a) and one for reaction (b). Figs 6.5.1 and 6.5.2 display the exotherms of set 1 reaction (a) and the recorded exotherms of reaction (b). For nitrogen pressures above 100 psi the ΔH values were found to be independent of the nitrogen pressure. However at atmospheric nitrogen pressure a 40% reduction of the ΔH for the reaction was observed, (8.5 J/g at atmospheric pressure compared to 17.5 J/g at 500 psi). The determined Tmax values proved to be satisfactorily reproducible. Nitrogen pressures between 100 psi and 500 psi thus appear to inhibit hydroperoxide evaporation.

6.5.2 The ASTM E698-79 Method of Determining Kinetic Parameters for Reactions a) and b)

The gradient from the plot of ln Q (Q = heating rate, °K/min) versus 1/Tmax (°K) denotes the E/R value of the respective reaction where E = the activation energy and R the gas constant. The application of the following equations gives the various required kinetic parameters assuming first order reaction behaviour:

1) $Z = [QE \exp (E/RT)]/RT^2$
2) $k = Z \exp (-E/RT)$
3) $t_{\frac{1}{2}} = 0.693/k$

The calculated kinetic parameters are displayed in table 6.5.5 for the reaction of (a) 0.04M n-octyl DDDiS and (b) 0.004M n-octyl DDDiS with 0.12M CHP. The table lists rate constants and reaction half lives at the same temperatures as isothermal analysis performed on the reaction mixtures, (see section 6.7).

Fig 6.5.1 DSC traces displaying Tmax shifting induced by heating rate variations for reaction a) (set 1)

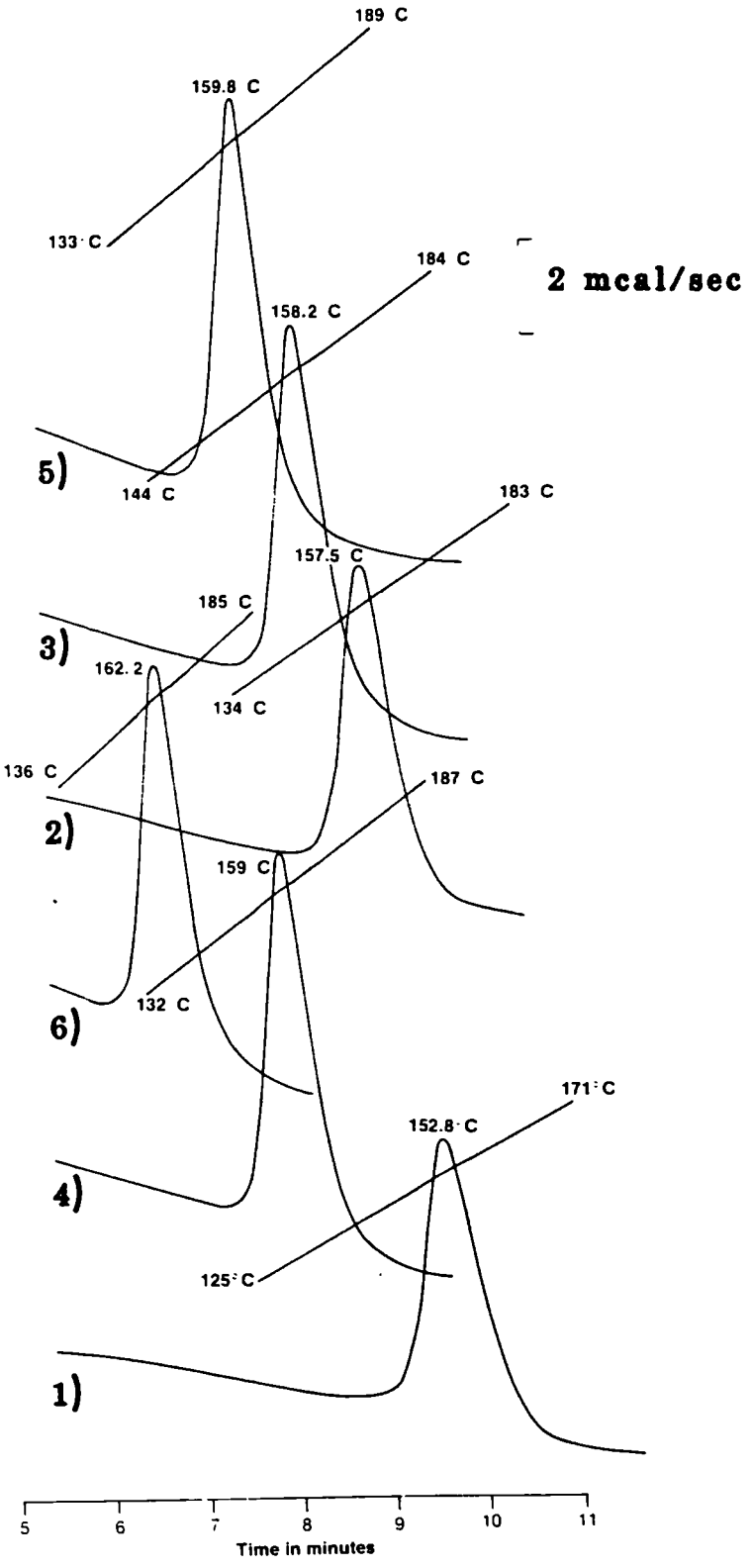

Fig 6.5.2 DSC traces displaying Tmax shifting induced by heating rate variations for reaction b)

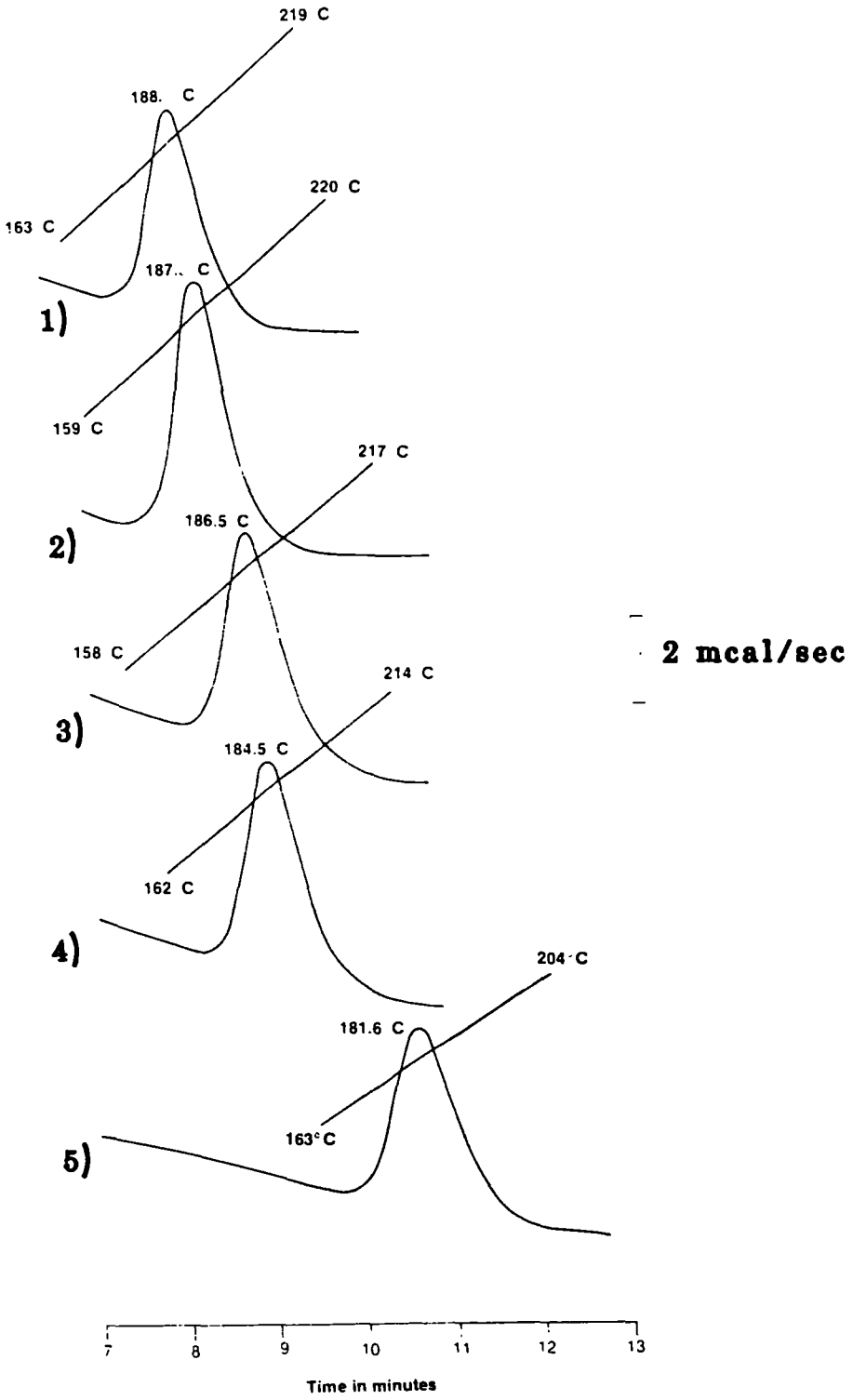

Tables 6.5.1 - 6.5.4

Reaction a) 0.04M n-octyl DDDiS and 0.12M CHP

Set 1

Q(°C/min)	T max (°C)	ΔH (J/g)	1/T max(°K)x10^{-3}	ln Q
11.84	152.8	11.74	2.349	2.471
13.89	157.5	12.34	2.323	2.631
16.10	158.2	13.73	2.319	2.779
17.26	159.0	12.4	2.315	2.848
18.00	159.8	14.49	2.311	2.890
21.84	162.2	11.69	2.300	3.084

mean ΔH = 12.73, σ (%) = 8

Reaction a)

Set 2

Q(°C/min)	Trace (°C)	ΔH (J/g)	1/T max(°K)x10^{-3})	ln Q
8.73	148.1	12.34	2.375	2.167
9.03	148.14	12.19	2.375	2.2
14.05	153.3	12.19	2.346	2.643
18.49	159.0	12.07	2.315	2.917

mean ΔH = 12.19, σ (%) = 1

Reaction a)

Set 3

Q(°C/min)	Trace (°C)	ΔH (J/g)	1/T max(°K)x10^{-3})	ln Q
4.15	138.9	12.85	2.428	1.423
8.19	149.1	12.64	2.370	2.103
8.19	148.2	12.37	2.374	2.103
16.92	159.9	12.31	2.310	2.828
16.92	159.9	11.6	2.310	2.828

mean ΔH = 12.34, σ (%) = 1

Reaction b) 0.004M n-octyl DDDiS and 0.12M CHP

Q(°C/min)	Trace (°C)	ΔH (J/g)	1/T max(°K)x10^{-3})	ln Q
14.15	181.6	9.93	2.200	2.650
18.22	184.5	10.43	2.186	2.903
18.66	186.5	10.58	2.176	2.926
20.24	187.0	11.42	2.174	3.008
21.64	188	9.45	2.169	3.074

mean ΔH = 10.36, σ (%) = 6

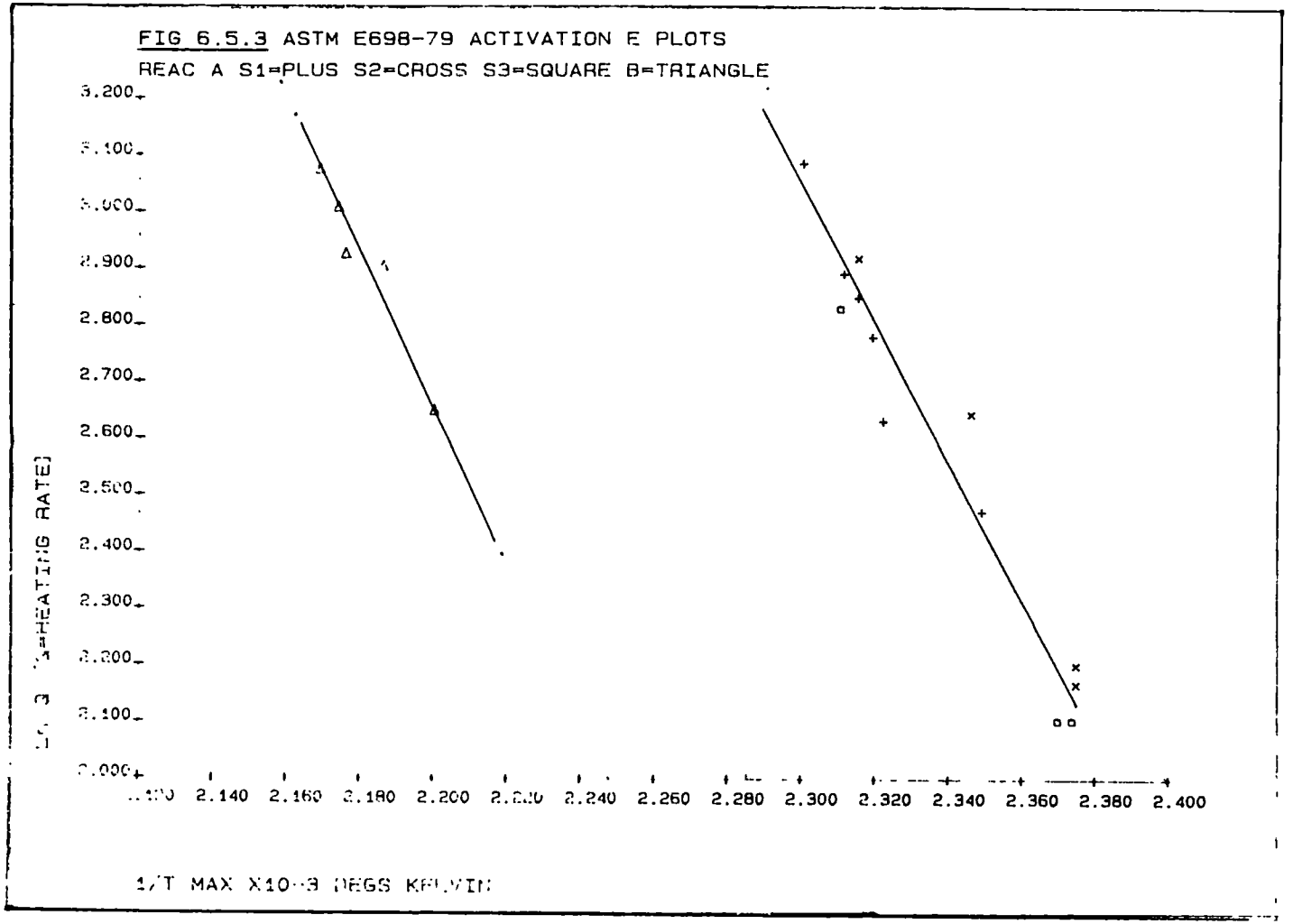
FIG 6.5.3 ASTM E698-79 ACTIVATION E PLOTS
REAC A S1=PLUS S2=CROSS S3=SQUARE B=TRIANGLE
3.200
3.100
3.000
2.900
2.800
2.700
2.600
2.500
2.400
2.300
2.200
2.100
2.000
2.120
2.140
2.160
2.180
2.200
2.220
2.240
2.260
2.280
2.300
2.320
2.340
2.360
2.380
2.400
1/T MAX X10-3 DEGS KELVIN

Table 6.5.5

Kinetic parameters of reactions a) and b)

determined by dynamic DSC

For reaction a) $E = 100kJ\ mol^{-1}$ and $Z^* = 1.35x10^{12}\ min^{-1}$

	116°C	112.4°C	105.7°C	97°C
$k(min^{-1})$	$5.\ x10^{-2}$	$3.9x10^{-2}$	$2.2x10^{-2}$	$1.x10^{-2}$
$t^1/_2$ (min)	13.9	17.8	31.5	69.3

For reaction b) $E = 108kJ\ mol^{-1}$ and $Z = 3.5\ x10^{12}\ min^{-1}$

	140°C	135°C	130°C	125°C
$k\ (min^{-1})$	$7.7x10^{-2}$	$5.2x10^{-2}$	$3.5x10^{-2}$	$2.3x10^{-2}$
$t^1/_2$ (min)	9.05	13.3	19.7	29.6

*Z is calculated from a run which lies on the line of best fit on the plots of lnQ versus $^1/T\ max$ ie for reaction
a) $lnQ = 2.779$ and $^1/T\ max = 2.319x10^{-3}$ and reaction
b) $lnQ = 2.65$ and $^1/T\ max = 2.2x10^{-3}$

Deductions

These results indicate that a tenfold dilution of 0.04 M n-octyl DDDiS increases the exotherm Tmax value produced by the decomposition of 0.12 M CHP in squalane, however only a 18% ΔHr reduction is observed. It can be deduced therefore that the mechanism of CHP decomposition induced by n-octyl DDDiS is autocatalytic and the rate of CHP decomposition depends on the initial n-octyl DDDiS concentration. The ASTM E698-79 method is commonly used to follow the kinetics of decomposition of thermally unstable materials, for example peroxides, and it assumes first order reaction kinetics: strictly the application of the method for the work performed here or an autocatalytic reaction described elsewhere is inappropriate and therefore has only a qualitative value.

6.6 Mechanism of Antioxidant Action of the n-Butyl Sulphide, n-Butyl Disulphide, Tri-n-Butyl Tetrathiophosphate and (OOS) Tri-n-Butyl Dithiophosphate and their Relevance to the DSC Results

The ability of certain organic sulphides and disulphides to decompose hydroperoxides and thus function as preventative antioxidants has been related to their conversion to sulphoxides and thiosulphinates, (11,12). The instability of the sulphoxide or thiosulphinates appears to be an important requirement for activity as an oxidation inhibitor .

The following reaction mechanism has been postulated (11,12), for the antioxidant function of disulphides and sulphides.

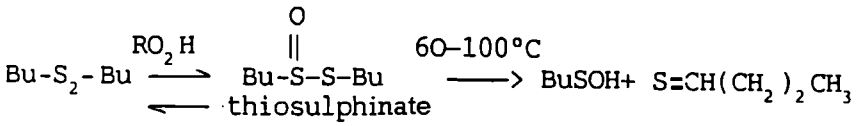

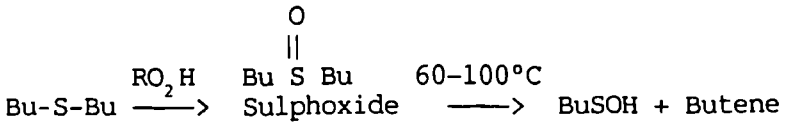

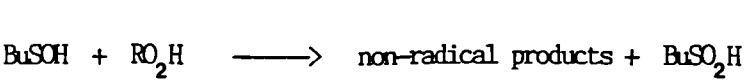

BuSOH oxidation products eg. $BuSO_2H$ and SO_2 may also decompose hydroperoxides.

Holcik et al (13), considered the following mechanism to describe the antioxidant function of trialkyldithiophosphates.

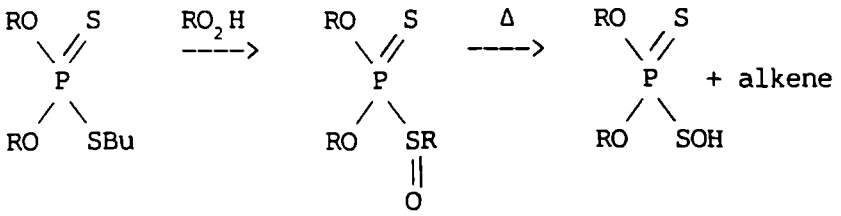

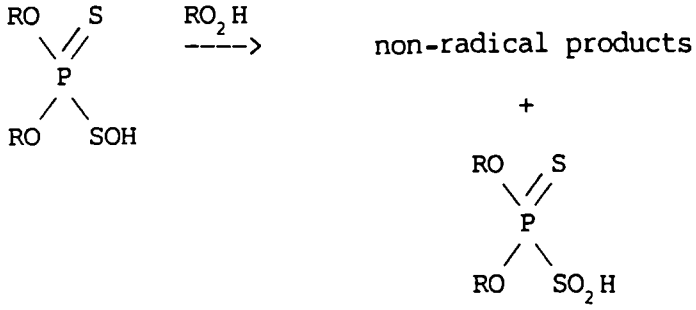

Further organophosphorus sulphenic acid oxidation products may also decompose hydroperoxides. DSC data indicated that the trend of reactivity with respect to hydroperoxide decomposition is as follows:

n-butyl disulphide > TTetTP > n-butyl sulphide > TDTP

Either or both of the following factors may contribute to this observed trend:

i) The trend reflects the relative rates of formation of the respective sulphoxides or thiosulphinates.

ii) The trend reflects the relative stabilities of the sulphoxides or thiosulphinates. Less energy is required to cleave the S-S bond of a thiosulphinate than the C-S bond of a sulphoxide. The main hydroperoxide decomposition occurs on the formation of the sulphenic acid.

6.7 Isothermal DSC Study of the Oxidation of n-Octyl and n-Butyl DDDiS by Cumene Hydroperoxide

Experimental

A 35 µl sample (for example 0.04M octyl DDDiS and 0.12M CHP in squalane) was pipetted into a DuPont DSC aluminium pan. The pan was placed on the sample thermocouple whilst an empty reference pan was mounted on the reference thermocouple. The cell was flushed twice with nitrogen to a pressure of 500psi and then repressurised to a similar pressure. The cell is heated to a "hold at limit" temperature at the maxiumum heating rate (100 deg/min). On reaching the "hold at limit" temperature the instrument is switched into the isothermal mode and the heat flow was monitored against time. Solutions studied were a) 0.12M CHP and 0.04M n-octyl DDDiS, b) 0.02M n-octyl DDDiS and 0.12M CHP, c) 0.04M n-octyl DDDiS and 0.06M CHP, d) 0.04M n-butyl DDDiS and 0.12M 0.12M CHP, e) 0.004M octyl DDDiS and 0.12M CHP, in squalane.

Analysis of Reaction Exotherms

The observed isothermal exotherms were integrated to produce the respective ΔH values for the studied reactions. The isothermal curves were analysed by applying an autocatalytic model, (14). The DSC ordinate is proportional to the rate of reaction. The exotherm shapes indicate that the reaction rate increases to a maximum and then decays symmetrically. This property and the presence of an induction period suggest that the reaction is autocatalytic.

The rate equation for an autocatalytic reaction is as follows:-

$$\frac{dx}{dt} = k\,[A]o^{n+m-1}\,(1-x)^{n}\,x^{m}$$

where: x is the fraction reacted at time t

k is the rate constant

[A]o is the initial concentration of A

n and m are rection orders

The DSC ordinate y is proportional to the multiple of the rate of change of x and the initial concentration of A.

Therefore $y = q[A]o\ dx/dt = q\ k\ [A]o^{n+m}(1-x)^n x^m$

considering the derivative dy/dt:

$$dy/dt = q\ k[A]o^{n+m}\{mx^{m-1}(1-x)^n - nx^m(1-x)^{n-1}\}\ dx/dt$$

The DSC curve exhibits a maximum at the value of x given by $(1-x)/x = n/m$
The areas under the DSC curve to the left and right respectively, of the ordinate drawn through the maximum are proportional to x and 1-x. The ratio n/m is therefore easily obtained. Moreover, for cases n=m, a DSC curve results which is symmetrical about the ordinate through the maximum.

The rate equation for a n=m=1 case is, $dx/dt = k[A]o\ (1-x)x$
Therefore $\ln\{x/(1-x)\} = k[A]ot+C$

C is a constant of integration, whose value may be regarded as defining the origin of the time scale. It is convenient to put $\tau = t+C/(k[A]o)$ thereby defining a new time scale, so that $\ln\{x/(1-x)\} = k[A]o\tau$
The defining equation for the DSC curves follow as:

$$y = qk[A]o\ dx/dt$$

$$= qk[A]o^2 \exp(k[A]o\tau)/\{1+\exp(k[A]o\tau)\}^2$$

The points τa and τb, which correspond to the one half maximum ordinates are calculated to be

$$k[A]o\,\tau a = \ln\{3-8^{1/2}\} = -1.763$$

$$k[A]o\,\tau b = \ln\{3+8^{1/2}\} = +1.763$$

The ratio of the area between the ordinate τa and τb to the area under the whole curve is given by:

$$Qab = 2^{1/2}/2 = 0.7071$$

The rate constant is obtained from the time interval $\tau b - \tau a$, as follows:

$$k[A]o\ (\tau b - \tau a) = \ln\{3+8^{1/2}\} - \ln\{3-8^{1/2}\} = 3.5255$$

Results

The ratios of the areas between the ordinate τa and τb to the area under the whole exotherms were determined for reactions a) to e) and were found to be close to the value expected for n=m=1 case. Rate constants were calculated using the following expression $k[A]o\ (\tau a - \tau b) = 3.5255$ where [A]o is the initial concentration of cumene hydroperoxide.

The exotherms for reactions a) to e) at different temperatures are displayed in figures 6.7.1 - 6.7.4, whilst the reaction temperature and the calculated heats of reaction, $\{\tau b - \tau a\}$ values, Qab values and rate constants are given in table 6.7.1. The Arrhenius plot for reactions a), c) and e) are featured in fig. 6.7.5. The activation energies and pre-exponential factors determined from these plots are listed in table 6.7.1.

Deductions

The following deductions can be made from the analysis of the isothermal DSC data:

i) n-Butyl DDDiS induces hydroperoxide decomposition more repidly than n-octyl DDDiS.

ii) A halving of the concentration of CHP produces a reduction in the ΔH of the reaction by a factor of two, however, a similar reduction in the concentration of DDDiS causes only a minimal ΔH decrease, (approx. 2%).

iii) There is good agreement between the ΔH values determined by the isothermal and dynamic DSC techniques implying that very little or none of the hydroperoxide is decomposed in the warm up period.

iv) The determined activation energies and pre-exponential factors determined from a plot of ln k versus 1/T follow the trend reaction a) < c) < e). The rate of reaction is more dependent on the CHP concentration than the DDDiS concentration.

v) The hydroperoxide decomposition reactions induced by DDDiS are autocatalytic. The isothermal DSC curves indicate that an induction period is present. This period occurs whilst the concentration of a reaction seed builds up and then hydroperoxide decomposition occurs more effectively. A tentative step towards a prediction of a reaction scheme might be as follows:-

$$\text{CHP} + \text{DDDiS} \xrightarrow{\text{CHP}} \text{P1 (=catalyst)} \longrightarrow \text{P2}$$

Fig 6.7.1 Isothermal DSC scans of reaction A at 1) 116 2) 110.1 3) 105.1 and 4) 97 deg C

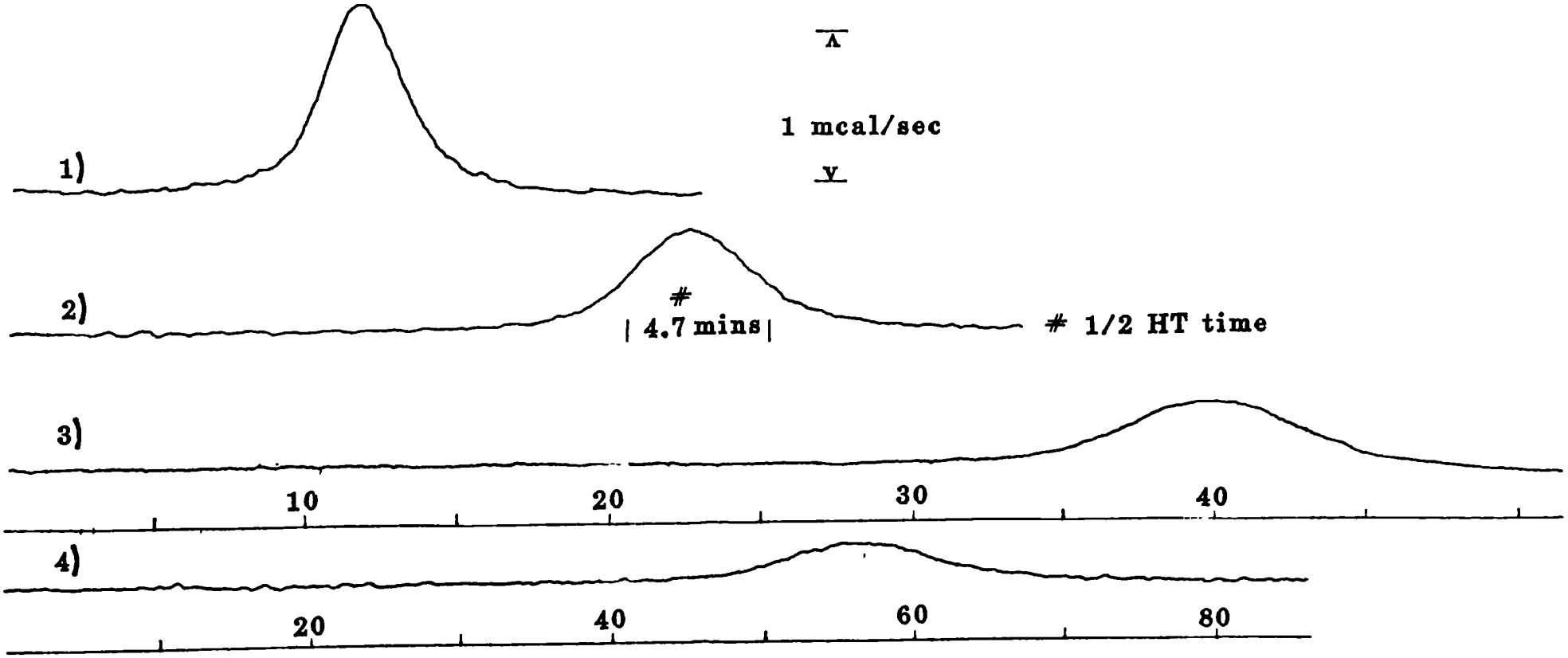

Fig 6.7.2 Isothermal DSC scans of

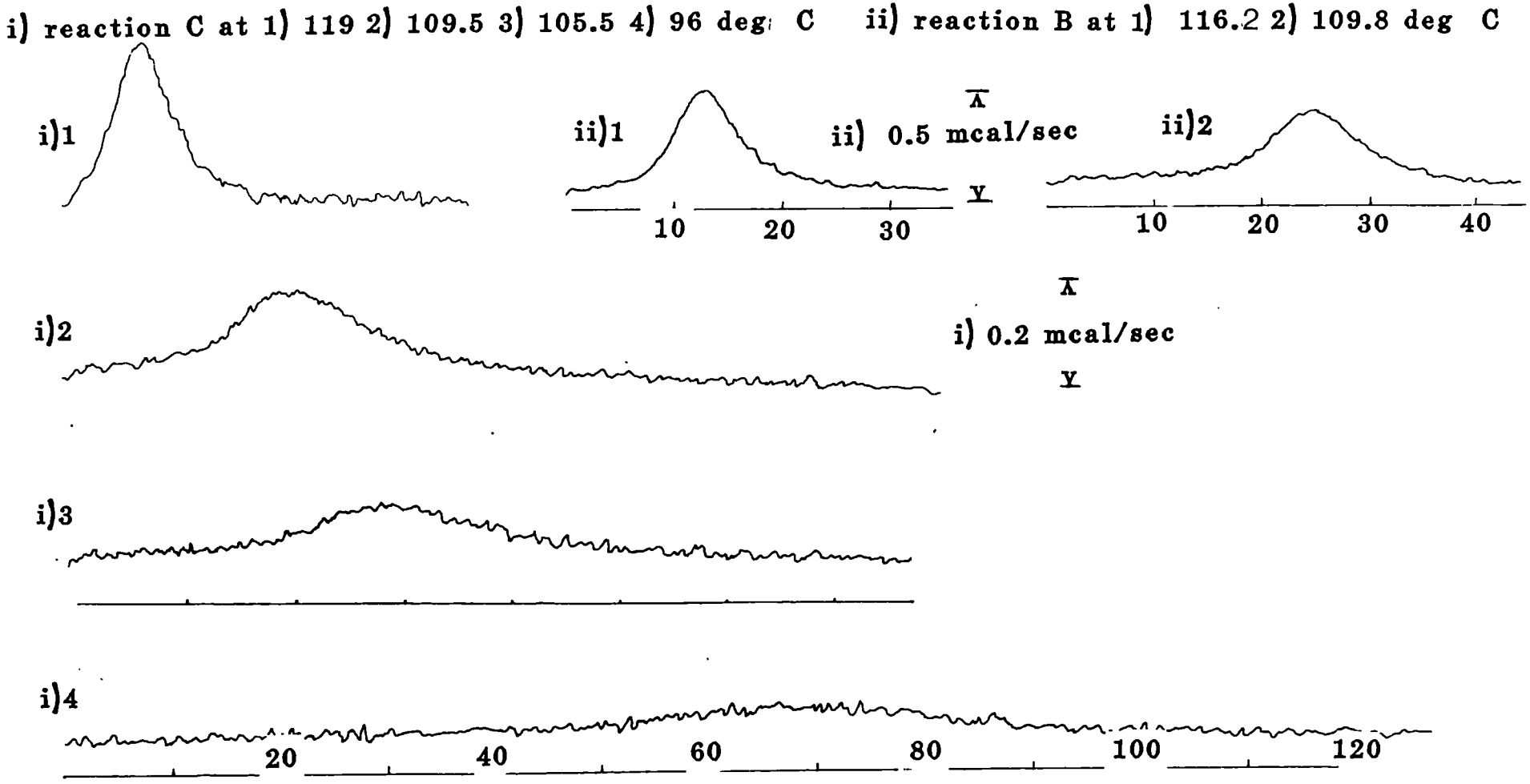

Fig 6.7.3 Isothermal DSC scans of reaction D at 1) 117 2) 108.5 and 3) 105.8 deg. C

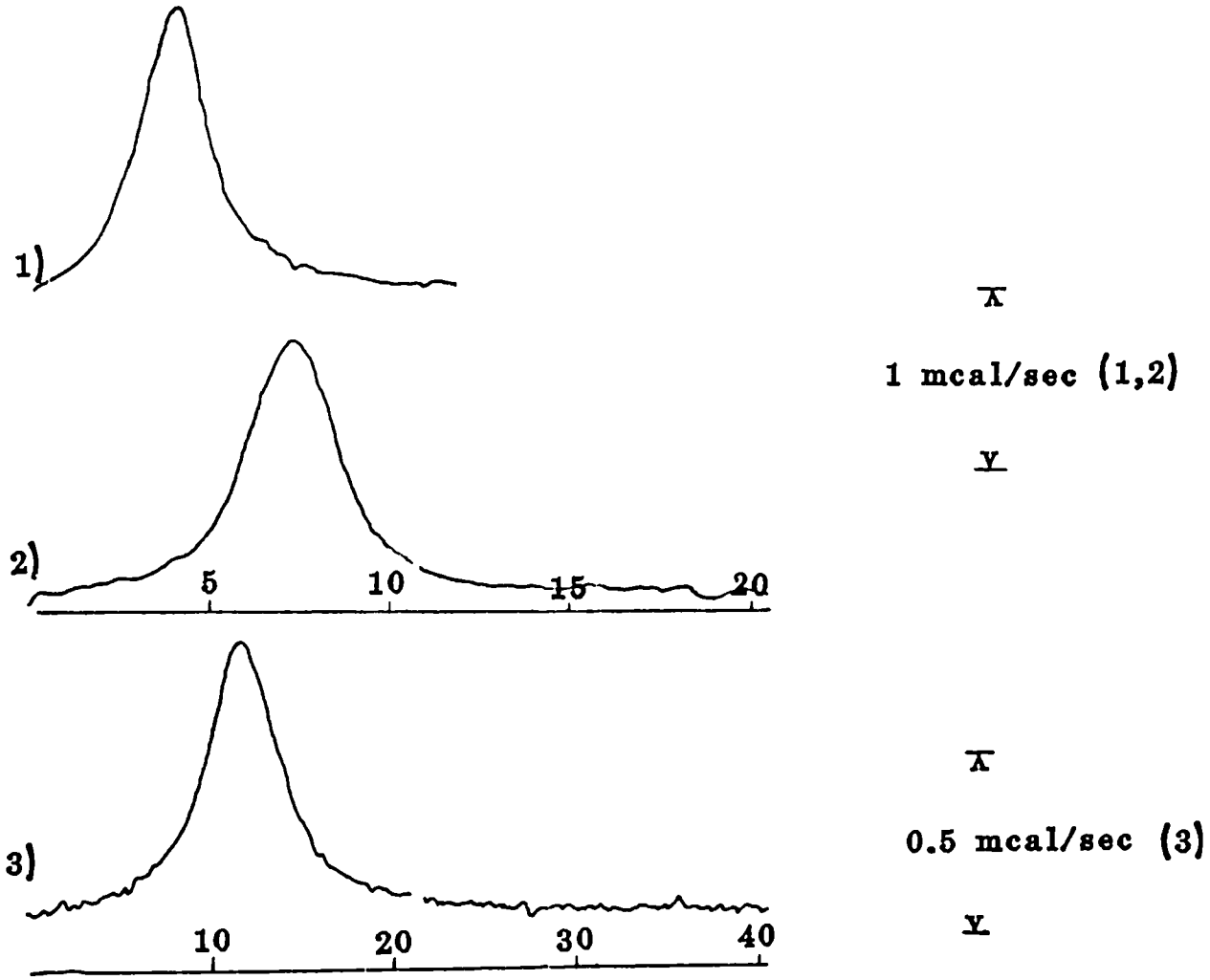

Fig 6.7.4 Isothermal DSC scans of reaction E at 1 and 2) 140 3) 135 4) 130 deg C

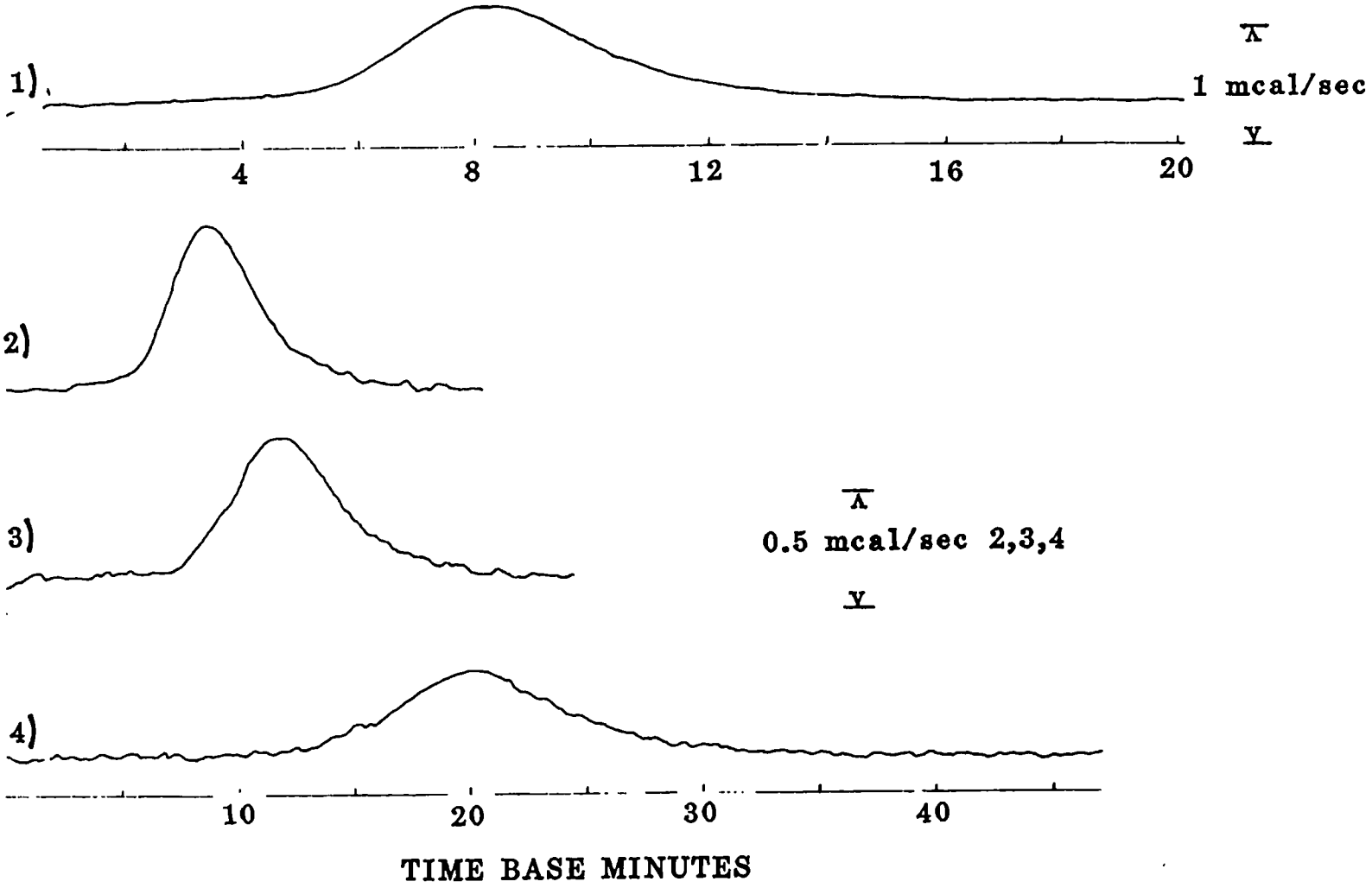

Table 6.7.1

Reaction a) 0.04M n-octyl DDDiS with 0.12M CHP in squalane	isothermal Temp. (Kelvin)	Δ Hr J/g	$(\tau_b - \tau_a)$ min	Qab	k $mol^{-1}dm^3s^{-1}$	Ink	I/T $X10^{-3}$
	389	12.4	3.15	0.70	0.157	-1.85	2.57
	383.1	11	4.72	0.72	0.103	-2.27	2.61
	378.1	11.7	6.1	0.68	0.08	-2.53	2.64
	370	13.2	10.43	0.71	0.047	-3.06	2.703
Activation energy = 82.5 kJ mol^{-1} Pre-exponential factor = 1.1 x 10^{12} min^{-1} dm^{-3} mol							
Reaction b) 0.02M n-octyl DDDis with 0.12M CHP in squalane	389.2	12.2	6.5	0.70	0.15		
	382.8	11.7	9.4	0.71	0.10		
Reaction c) Θ 0.04 n-octyl DDDiS with 0.06M CHP in squalane	392	6.0	6.3	0.72	0.155	-1.86	2.55
	387	5.5	8.7	0.71	0.113	-2.18	2.58
	382.5	5.94	13.0	0.70	0.075	-2.59	2.61
	378.5	5.3	18.1	0.69	0.054	-2.92	2.64
	369.0	-	32.7	-	0.03	-3.52	2.71
Activation energy = 99.3 kJ mol^{-1} Pre-exponential factor = 1.56 x 10^{13} min^{-1} dm^{-3} mol							
Reaction d) 0.04M n-butyl DDDiS with 0.12M CHP in squalane	390	14	2.0	0.69	0.245		
	381.5	16.9	3.15	0.715	0.155		
	378.8	15	4.72	0.70	0.104		
Reaction e) 0.004M n-octyl DDDiS with 0.12M CHP in squalane	413	11.1	3.94	0.71	0.124	-2.09	2.42
	413	8.5	4.52	0.72	0.108	-2.23	2.42
	408	9	5.12	0.68	0.096	-2.34	2.45
	403	8.6	7.68	0.70	0.064	-2.75	2.48
Activation energy = 92 kJ mol^{-1} Pre-exponential factor = 3.1 x 10^{12} min^{-1} dm^{-3} mol							

Θ Note: this experiment was conducted using varying amounts of solution, (30-45 microlitres)

FIG 6.7.5 ARRHENIUS PLOTS FROM ISOTHERMAL DSC DATA

REACTION A=PLUS, C=CROSS, E=SQUARE

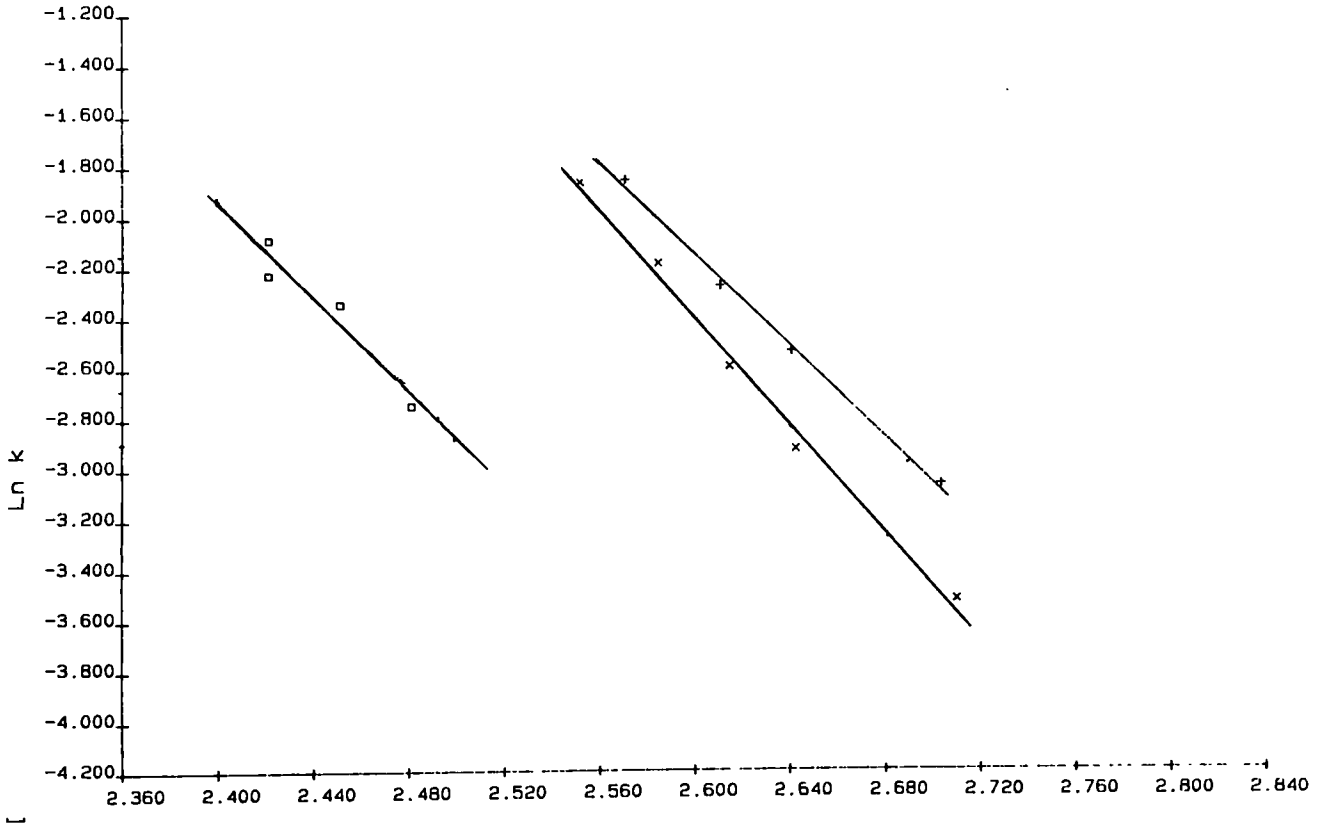

The concentration of DDDiS remains fairly constant throughout the course of the reaction and therefore it is the catalyst P1 or an oxidation product P2 that produces the main hydroperoxide decomposition. A sequence of reaction products is envisaged, of which P1 (the catalytic product) is only the first (or an early member). This is consistent with the mechanism proposed by Al-Malaika and Scott, (15).

Sulphur dioxide, a probable DDDiS oxidation product (15), itself catalyses hydroperoxide decomposition, (16,17). However it is possible that there is another step in the reaction profile, a formation of a thiosulphinate.

Holcik et al (13), suggested that the formation of a sulphoxide was the first reaction in the oxidation sequence of pentaerythritol dithiophosphates by cumene hydroperoxide. The authors remarked on the presence of an induction period before the main hydroperoxide decomposition occurred whilst the concentration of sulphoxide built up. The thermal decomposition of the sulphoxides produced sulphenic acids (P-S-OH) which catalytically decomposed the hydroperoxide. The thiosulphinates produced from the oxidation of the disulphide (DDDiS) must break down or react with CHP to produce the compounds that Al-Malaika observed by ir spectroscopy, which cause more effective hydroperoxide decomposition.

The catalytic model may well be an oversimplification of a very complex reaction. However, it seems a more correct mechanistic simulation than is implied by the ASTM E698 heating rate variation technique which assumes first order behaviour. The model takes into account the autocatalytic nature of the decomposition of cumene hydroperoxide and second order rate constants are evaluated. It is worth noting that the activation energies and pre-exponential factors calculated by both methods are similar. This is probably coincidence but is encouraging because the ASTM technique is often used to calculate the kinetic parameters of thermally unstable compounds (that may even decompose autocatalytically). The ASTM method, even though it makes incorrect assumptions (ie that the order of the reaction is 1) may possibly be used as a rule of thumb technique to determine reation halflives.

Table 6.7.2

	ASTM - E698 (Dynamic)	Autocatalytic Model (Isothermal)
a)	E 100 kJ mol^{-1}	82.5 kJ mol^{-1}
	Z 1.29×10^{12} min^{-1}	1.11×10^{12} $min^{-1} dm^{-3} mol$
e)	E 108 kJ mol^{-1}	92.0 kJ mol^{-1}
	Z 3.5×10^{12} min^{-1}	3.1×10^{12} min^{-1} $dm^{-3} mol$

a) reaction between 0.12M CHP and 0.04 octyl DDDiS

e) reaction between 0.12M CHP and 0.004M octyl DDDiS.

Chapter 6

1) Noel F., J. Inst. Petrol. 1971, 57, 354-358.

2) Noel F. and C Ranton G.E., Amer. Chem. Soc. Sym. 1974 April, 305-320.

3) Walker J.A. and Tsang W., S.A.E. Technical Paper No 801383 1980, 1-8.

4) Blaine R.L. American Laboratory, January 1974.

5) Lovaslz O., Erdol u. Kohle 1977, 30(5), 219-223.

6) Hemminger W. and Holme G., "The Fundamentals of Calorimetry", Verlag Chemie Florida 1984, Chapter 8, 225-227.

7) Instruction Manual for Du Pont 990 Thermal Analyser, 3-8.

8) Fordham and Williams, Can. J. Res. 1949, 27b, 943.

9) ASTM E698-79,Standard Test Method for Arrhenius kinetic Constants for Thermally Unstable Compounds.

10) Ozawa T., J. of Therm. Anal. 1970, 2, 301-324.

11) Shelton J.R. and Davies K., Int. J. Sulphur Chem., 1973, 8(2), 197-220.

12) Shelton J.R., Rubber Chem. and Technology 1974, 47, 949.

13) Holcik J. et al., Polymer Degradation and Stability 1983, 5, 373-397.

14) Waters D.N. and Paddy J.L., Anal. Chem. 1988, 60, 53-57.

15) Al-Malaika, and Scott G., Polymer 1982, Vol. 23. 1711-1712.

16) Armstrong C., Husbands M.J. and Scott G., Euro. Poly. J. 1979, Vol. 15, 241-248.

17) Husbands M.J. and Scott G., Euro. Poly. J. 1979, Vol. 15, 249-253.

CHAPTER 7

The Application of i) Raman Spectroscopy and ii) P-31 NMR Spectroscopy to the Study of the Kinetics of Oxidation of Normal and Basic Zinc Dialkyldithiophosphates

7.1 Introduction

a) Raman Spectroscopy

This thesis has shown that infra-red and especially Raman spectroscopy are very useful methods for investigating the chemical bonding and structures of ZDDP's and and several of their oxidation, hydrolysis, and thermal degradation products. Raman and infra-red spectroscopy may also be used to detect and distinguish between some of the various ZDDP-related compounds. For example, in the study of the oxidation of DDPA the appearance of the (S-S) band at 480 cm^{-1} can be monitored by Raman spectroscopy. It is well documented in the literature that when ZDDP's are oxidised by hydroperoxides basic ZDDP and DDDiS are the initial products formed, (1-8). The literature, however, does not discuss the rate of this reaction in detail and there is very little investigation of the organophosphorus products produced from the oxidation of basic ZDDP's. Raman spectroscopy can be employed to monitor the rate of formation of DDDiS (ν(S-S) = 480 cm^{-1} and ν(P=S) = 660 cm^{-1}). However, Raman spectroscopy has only a limited application in analysing the oxidation of normal ZDDP to the basic salt because the Raman spectra of basic and normal ZDDP are almost identical. The combined decay of the normal and basic ZDDP salts may be studied by following the reduction of intensity of the $\nu(PS_2)$ band at 550 cm^{-1} in the Raman. Raman spectroscopy is also a useful method to analyse some of the products derived from the antioxidant-induced and thermally induced (no antioxidant present) decomposition of cumene hydroperoxide. It is preferable that the solvent utilized to study the antioxidant oxidations is free of Raman bands in the regions 440 cm^{-1} - 700 cm^{-1} and 1500 - 1700 cm^{-1}.

b) P-31 NMR Spectroscopy

Kinetic studies of the oxidation of ZDDP's performed by P-31 NMR spectroscopy are particularly informative because ZDDP's and their various oxidation products have different P-31 NMR chemical shifts. P-31 NMR for example can distinguish between the basic and normal ZDDP salts. Willeremet and Kandah (9), studied the reaction of n-octyl ZDDP with peroxy radicals using P-31 NMR. The radicals were generated by the decomposition of azo-bis-isobutylnitrile in an oxygenated solution of hexadecane at 90 deg C. Marshall (10), has analysed the ZDDP degradation in oils subjected to engine tests. As the oil aged the chemical shifts of the phosphorus compounds became less positive due to the progressive oxidation of the thiophosphate additives. The author suggested that quantitative analysis could be performed if relaxation times were determined. This chapter studies the oxidation of ZDDP's by hydroperoxides using Raman and P-31 NMR spectroscopy.

7.2 Raman Spectroscopy as a Technique to Characterise the Decomposition Products of Cumene Hydroperoxide Under Conditions of High Pressure Nitrogen DSC.

Experimental

Dynamic DSC runs were performed on solutions of a) 30ul of of 0.24M cumene hydroperoxide in squalane, and b) 30ul of 0.0008M n-octyl DDDiS and 0.12M cumene hydroperoxide, at a heating rate of 20 deg/min in an atmosphere of 500 psi nitrogen. The DSC scans of reaction a) were stopped at different temperatures and allowed to cool to ambient temperature. Decomposition of the hydroperoxide may occur on cooling and analysis of the cooling curves indicated that the heating rate and cooling rates were similar. Both the heating and cooling of the samples therefore contribute approximately equally to the decomposition of the hydroperoxide. The DSC scan of reaction b) was terminated on the completion of the exotherm and the sample was allowed to cool to ambient temperature. Raman spectra were recorded on the cooled samples and the region 1500 cm^{-1} - 1700 cm^{-1} was compared to reference Raman spectra of cumene hydroperoxide, acetophenone, phenol, cumyl alcohol, and methyl styrene.

The bands of the reference spectra between 1500 cm^{-1} - 1700 cm^{-1} are listed in the table below:-

Spectrum	Bands in the Region 1500 - 1700 wavenumbers
Cumene Hydroperoxide	1580 and 1600
Acetophenone	1600 and 1680
Phenol	1600 (doublet)
Cumyl Alcohol	1580 and 1600
Methyl Styrene	1600 and 1640

Attempts were made to record spectra of reactions performed with higher concentrations of DDDiS than in reaction b): however, fluorescence became a problem and made it difficult to record satisfactory spectra.

Results

Fig 7.2.1 displays the Raman spectra of the region 1500 to 1700 cm^{-1} for 0.24M cumene hydroperoxide, after dynamic DSC scans (20 deg/min) to limit temperatures of 100, 150, 200 and 230 deg C. The spectra indicate that no decomposition results from a scan to 100 deg C, whilst small amounts of methyl styrene are formed when the limit temperature was 150 deg C. At higher temperatures, progressively larger quantities of methyl styrene are formed along with acetophenone. Raman spectroscopy cannot easily distinguish between cumyl alcohol and cumene hydroperoxide. The total intensity of the 1600 cm^{-1} band after the decomposition occurs is made up of the various contributions of the decomposition products. Expected contributions from methyl styrene and acetophenone to the observed 1600 cm^{-1} band can be estimated from observed intensities of the 1640 cm^{-1} band for methyl styrene and the 1680 cm^{-1} band of acetophenone, because the 1640 cm^{-1} /1600 cm^{-1} and 1680 cm^{-1} /1600 cm^{-1} ratios are known, (calculated from reference Raman specta). The value thus calculated is close to the actually observed intensity of the 1600 cm^{-1} band for reaction a) when heated to 250 deg C, thus indicating that the main reaction products are probably methyl styrene and acetophenone. However it is possible that contibutions from phenol are masked by stronger acetophenone and methyl styrene bands, thereby masking the detection of phenol. Fig 7.2.2. implies that a major product from the decomposition of cumene hydroperoxide induced by 0.0008M n-octyl DDDiS is methyl styrene. The spectrum is weak; however it does not seem to indicate the presence of cumene hydroperoxide, cumyl alcohol or acetophenone because no bands are observed at 1580 cm^{-1} and 1680 cm^{-1}. It is possible that cumyl alcohol is a reaction product but that it is dehydrated by organophosphorus acids produced from the oxidation of DDDiS by CHP. At high CHP/DDDiS molar ratios, is has been shown that phenol is a major reaction product (15). However in this study, the 1600 wavenumber phenol bands are probably masked by the more intense 1600 wavenumber methyl styrene band.

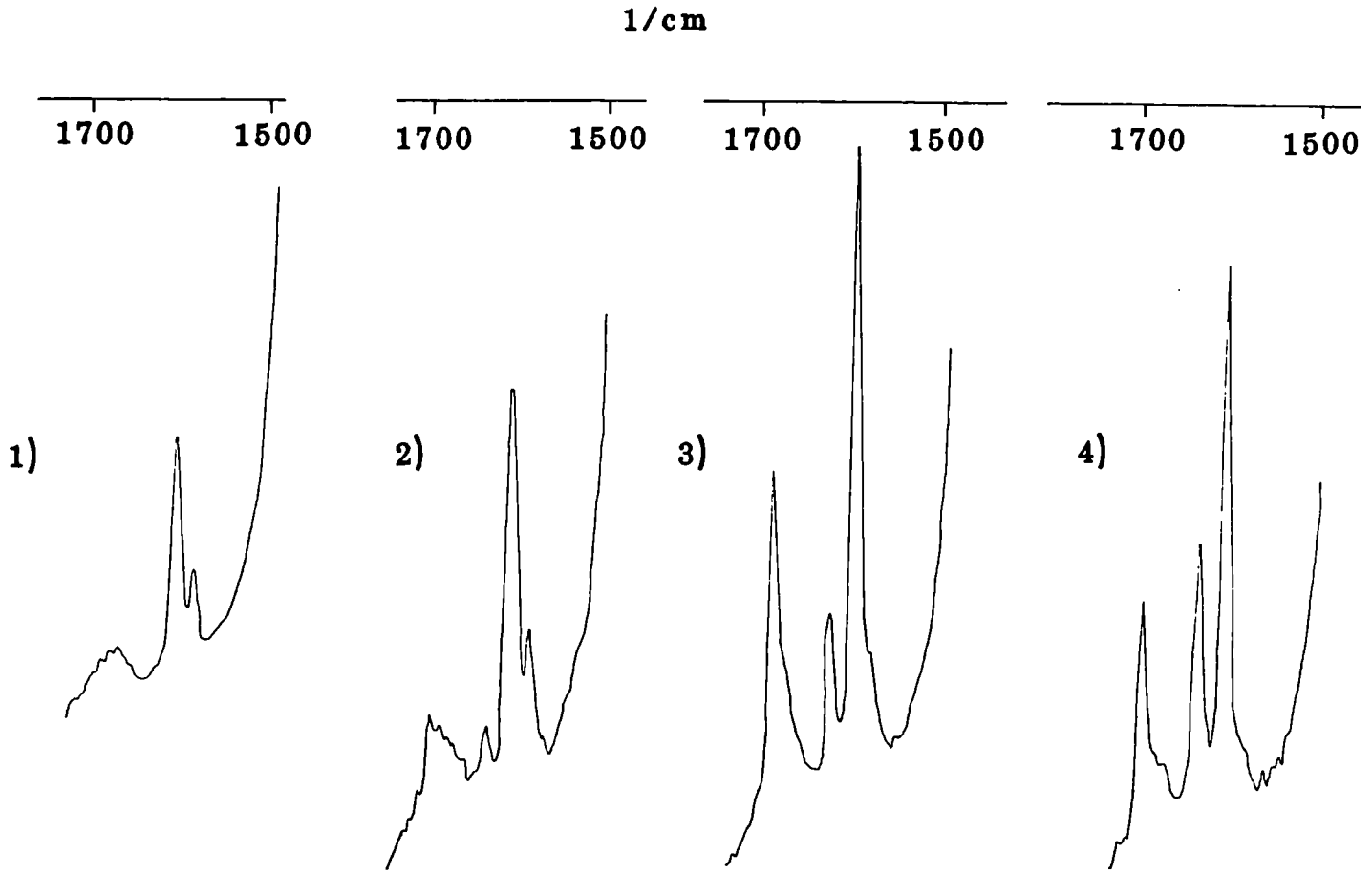

Fig 7.2.1 Raman spectra of .24M CHP in squalane heated to 1)100 2)150 3)200 4)230 deg C at 20 degs C/min then cooled to ambient temperature (500 psi N_2)

Fig 7.2.2 Raman spectrum of reaction B mixture, run after reaction completion

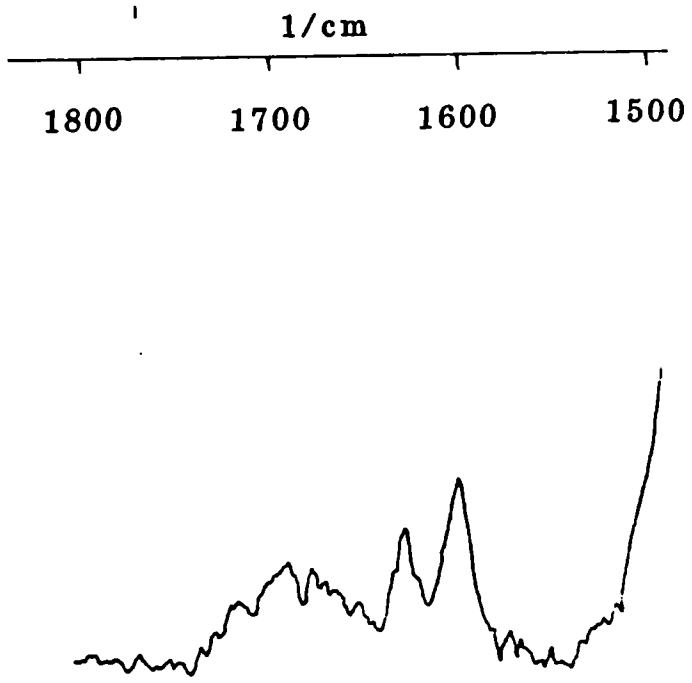

7.3 Kinetic Studies by Raman Spectroscopy of the Oxidation of n-Octyl ZDDP, n-Butyl ZDDP, Basic n-Butyl ZDDP and n-Butyl DDPA

Experimental

Kinetic studies on the reactions listed in the table below were performed using a Raman Spex Ramalab spectrometer (514.5nm excitation line) to follow the course of the reaction.

Table 7.3.1

	Reaction	Solvent	CHP Conc	Bands Studied	Temp °C
a)	0.04M n-octyl ZDDP	Squalane	0.12M	ν(P=S)	30
b)	0.04M n-butyl ZDDP	Cyclohexane	0.12M	ν(S-S)	
				ν(P=S)	24
				$\nu(PS_2)$	
c)	0.01M Basic n-butyl ZDDP	Cyclohexane	0.12M	ν(P=S)	26
				ν(S-S)	
				$\nu(PS_2)$	
d)	0.04M n-butyl DDPA	Squalane	0.12M	ν(P=S)	26

Results

The change of the relative intensities of bands attributed to ν(P=S) at 660 cm^{-1}, ν(S-S) at 480 cm^{-1}), and $\nu(PS_2)$ at 550 cm^{-1} were monitored with respect to an internal standard, either a squalane or an cumyl vibration. For the reactions performed in squalane (a and d), a squalane band at 740 cm^{-1} was used as a reference. A cumyl band at 730 cm^{-1} was selected as a reference for reactions conducted in cyclohexane because of its sharpness and close proximity to the bands of interest. A comparison between a standard 0.12M CHP reference spectrum in the region 300 - 800 cm^{-1} and the reaction spectrum in the region after 240 minutes indicates that, with respect to a 360 cm^{-1} cyclohexane band, the intensity of the 730 cm^{-1} band, used as a reference only, decreases by ca. 10%. Such a decrease is most likely within experimental error for the study. The 730 cm^{-1} reference band is attributed to an aromatic ring vibration. The intensities of the 480 cm^{-1} ν(S-S) vibration and the 550 cm^{-1} $\nu(PS_2)$ vibration were corrected for any contribution resulting from any aromatic or cyclohexane bands obtained from the standard 0.12M CHP in cyclohexane spectrum. There is no such contribution to the ν(P=S) band as the 0.12M CHP in cyclohexane spectrum shows no bands in this region.

Figs 7.3.1-7.3.4 display the change in the Raman spectra of reactions (a)-(d) with time, and figs 7.3.5-7.3.7 show the changes of the band intensity ratios with time. When calculating the band intensity ratios allowance was made for any contribution from CHP and CHP-derived compounds to the band intensities. Reference to reactions a), b) and c) are incorporated in the discussion of the P-31 NMR kinetic studies described later in the text, however, reaction d) is discussed in this section. The oxidation of n-butyl DDPA to produce n-butyl DDDiS reaches completion nearly instantaneously and this is emphasised by table 7.3.2.

Table 7.3.2

Listing Raman Intensity Ratios

	0.08M n-butyl DDPA in squalane	0.04M n-butyl DDDiS in squalane	Reaction d) 0.04M n-butyl DDPA with 0.12M CHP after 12 min at 26°C
$\frac{I\ 480\ cm^{-1}\ \nu(S-S)}{I\ 740\ cm^{-1}\ \nu(Squ)}$	not present	1.26	0.56
$\frac{I\ 660\ cm^{-1}\ \nu(P=S)}{I\ 740\ cm^{-1}\ \nu(Squ)}$	0.36	1.36	0.70

The intensity ratios of the ν(S-S) and ν(P=S) bands of reaction d), after 12 minutes at 26 deg C with respect to the squalane 740 cm^{-1} internal standard band are approximately half the values observed in the 0.04M n-butyl DDDiS standard spectrum, and therefore 0.04M n-butyl DDPA is oxidised to produce 0.02M n-butyl DDDiS by cumene hydroperoxide. By including this result in the trend of reactivity of the various studied antioxidants, with respect to cumene hydroperoxide reduction, previously determined by DSC, the following is obtained (in order of decreasing reactivity):-

DDPA > ZDDP > DDDiS > BuSH > Bu_2S_2 > TTetTP > Bu_2S > TDTP.

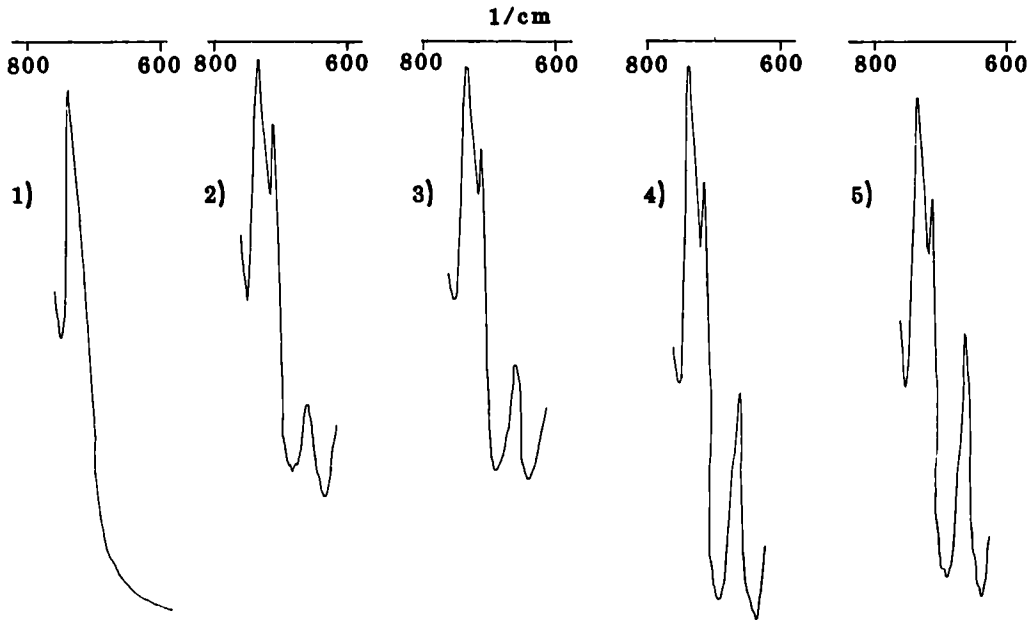

Fig 7.3.1 Raman spectra of reaction A 1)prior to CHP addition and after 2)5 3)20 4)70 5)146 minutes at 30 deg C

Fig 7.3.2 Raman spectra of 1).066 M n-butyl ZDDP in cyclohexane 2).12 M CHP in cyclohexane and 3)-6) reaction B after 10,30,80 and 170 minutes at 24 deg C

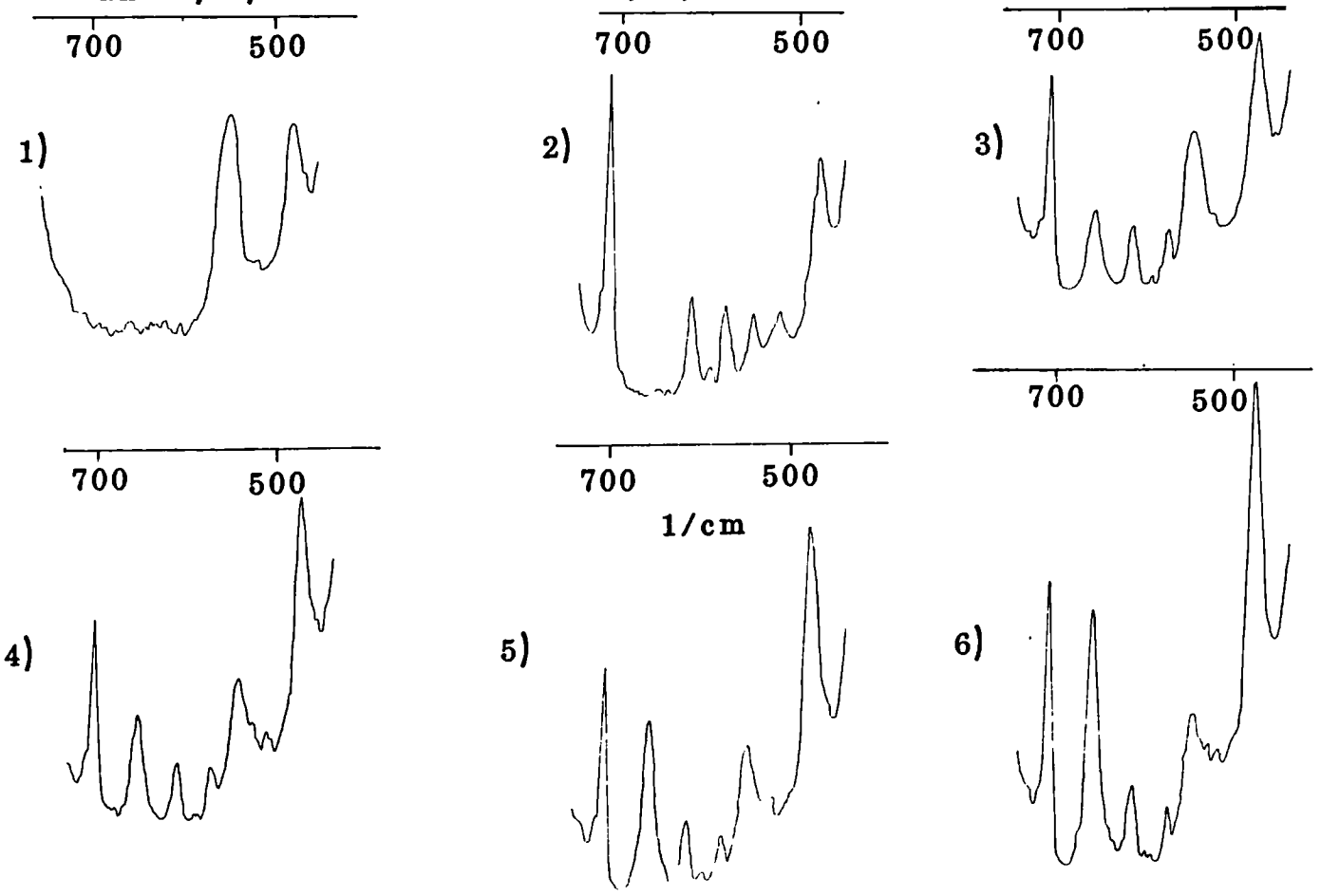

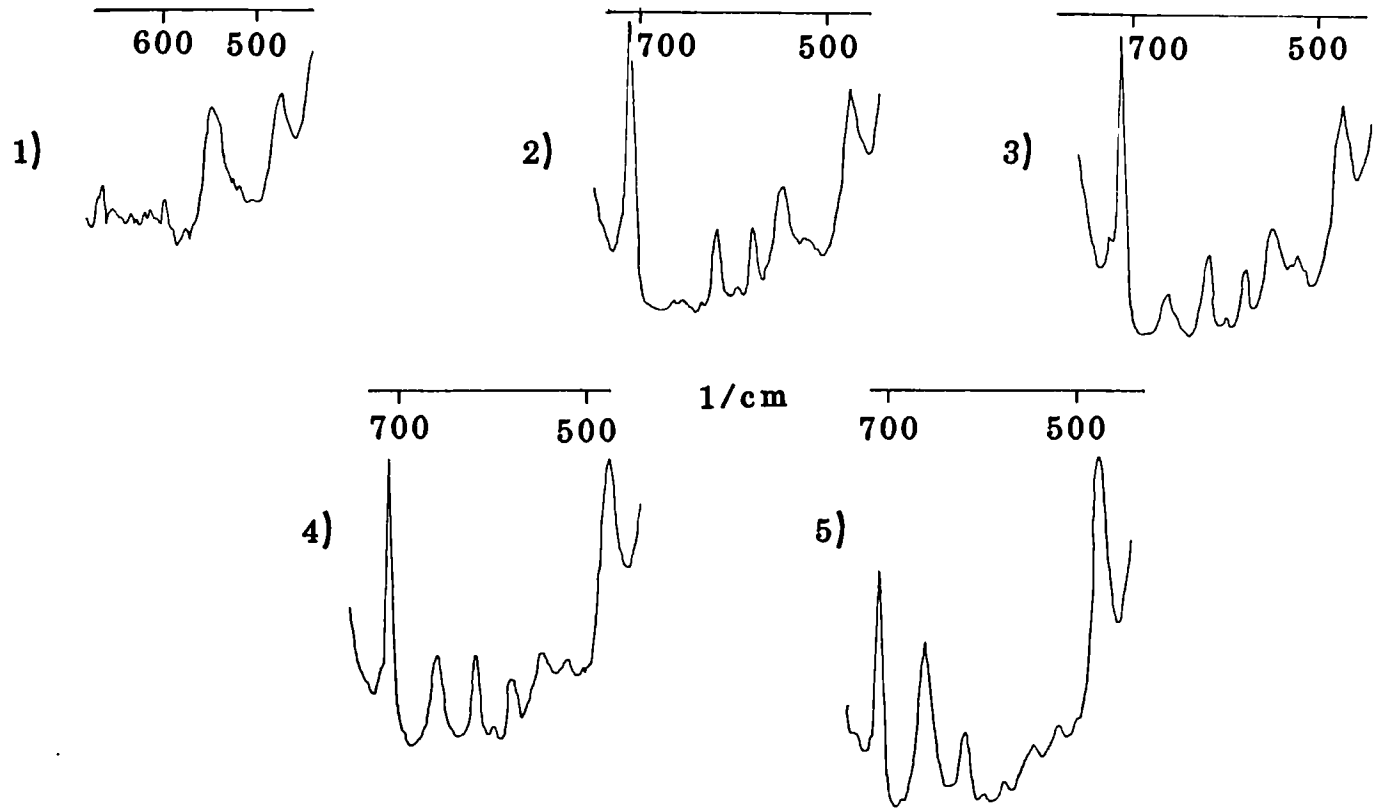

Fig 7.3.3 Raman spectra of 1).02 M basic n-butyl ZDDP in cyclohexane and 2)-5)reaction C after 19,59,120, and 400 minutes at 26 deg C

Fig 7.3.4 Raman spectra of 1) .08 M n-octyl DDPA in squalane and 2) reaction D after 12 minutes at 26 deg C

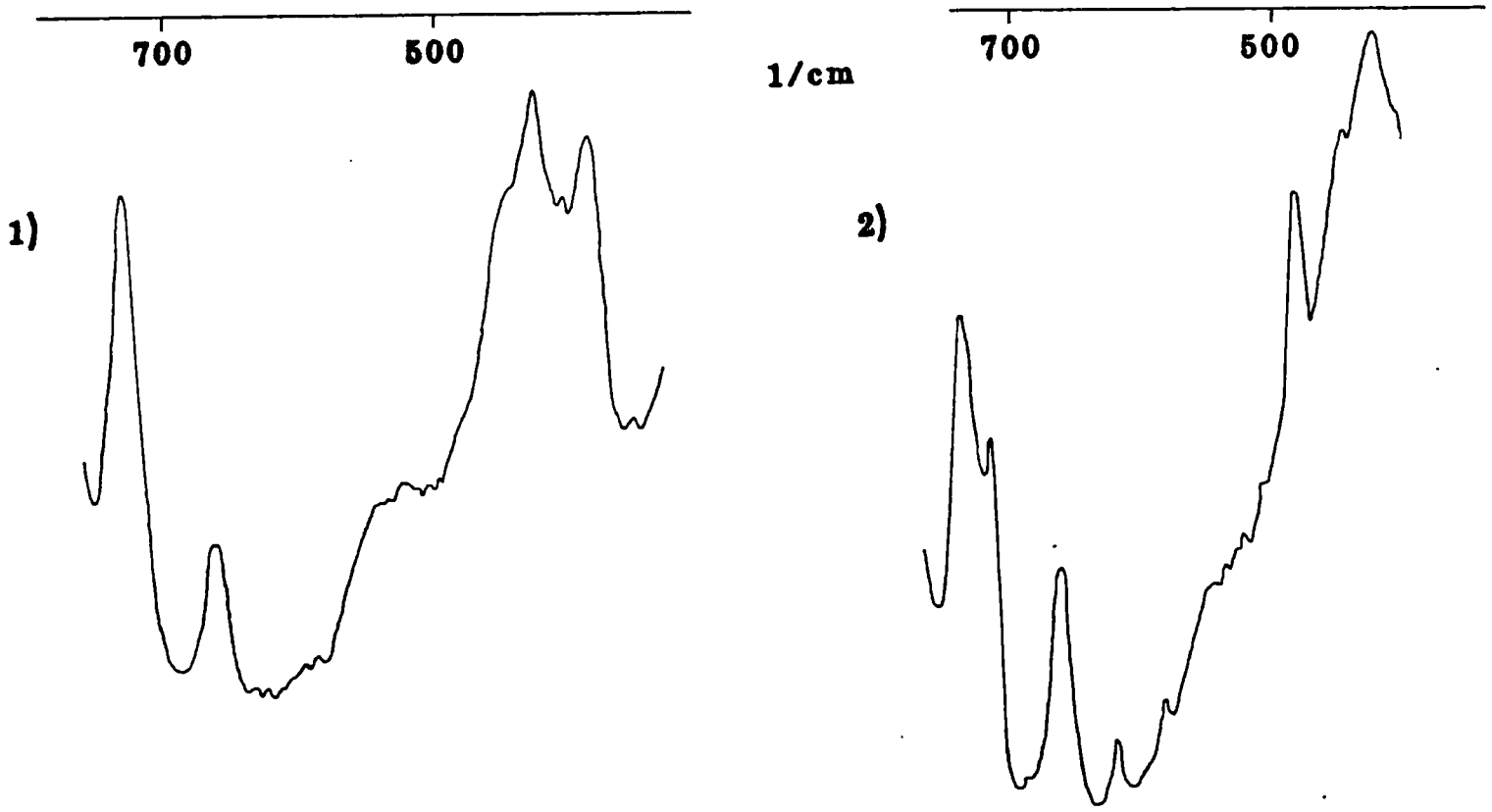

Fig 7.3.5 Raman Kinetic study
Reaction A .04M octyl ZDDP with .12M CHP in squalane

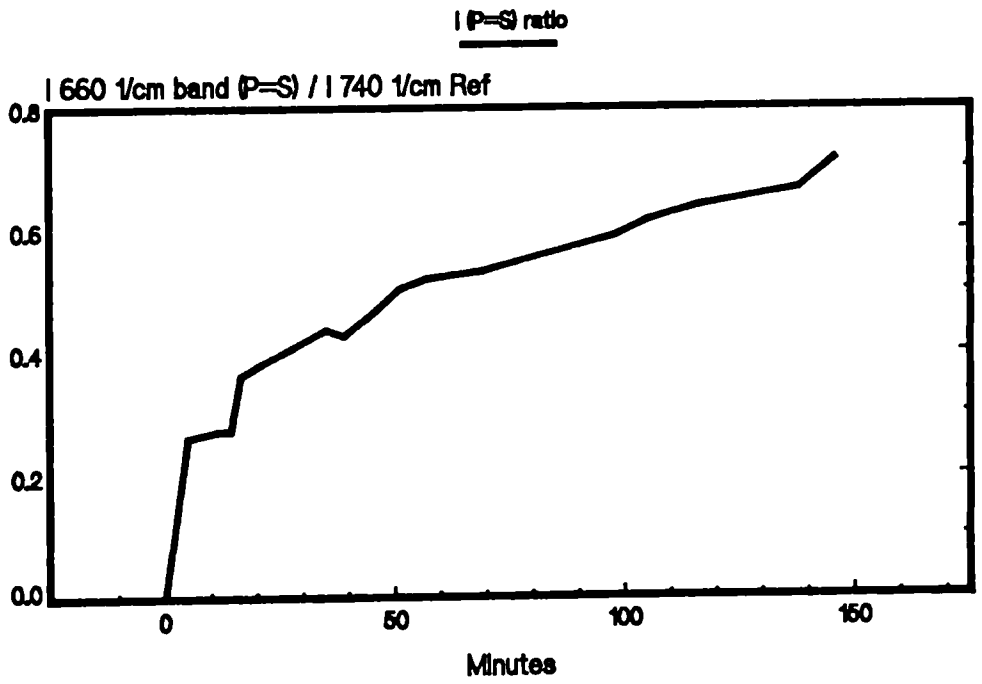

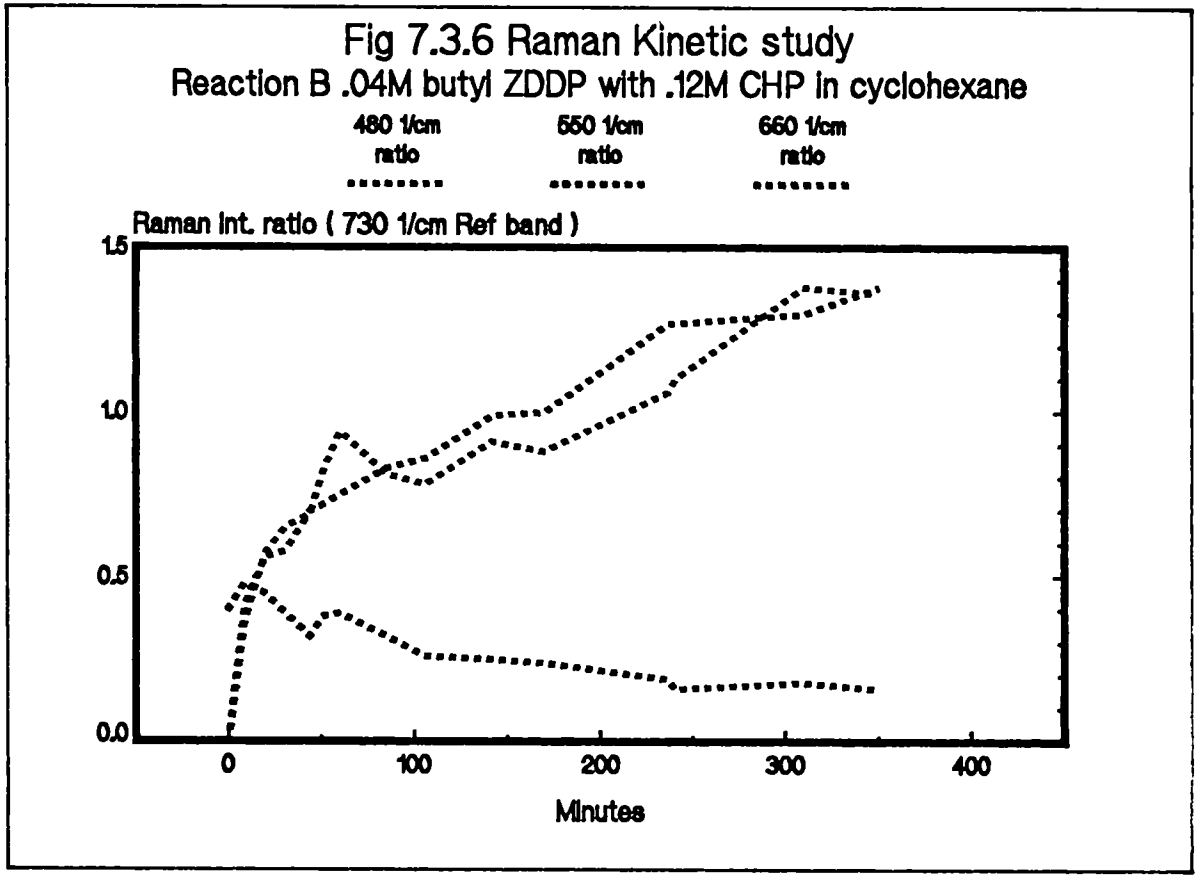
Fig 7.3.6 Raman Kinetic study
Reaction B .04M butyl ZDDP with .12M CHP in cyclohexane
480 1/cm ratio
550 1/cm ratio
660 1/cm ratio
Raman Int. ratio (730 1/cm Ref band)
1.5
1.0
0.5
0.0
0
100
200
300
400
Minutes

Fig 7.3.7 Raman Kinetic study

Reaction C .01M butyl BZDDP with .12M CHP in cyclohexane

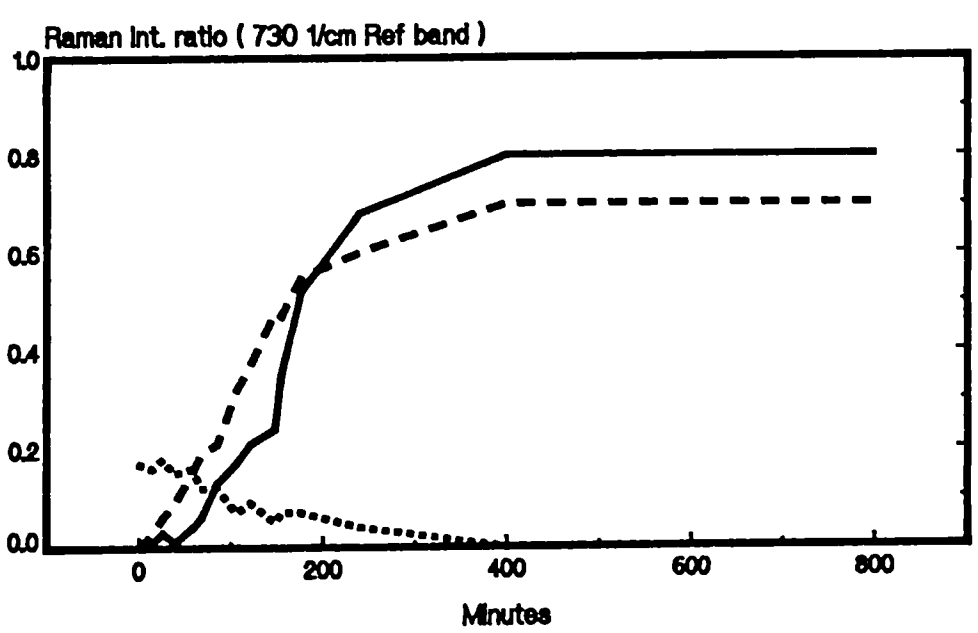

7.4.1 Phosphorus-31 NMR Spectroscopy

Introduction

The table below lists various nuclear magnetic resonance characteristics of phosphorus and compares them with carbon and hydrogen.

Table 7.4.1

	P	C	H
mass Number	31	13	1
Spin Number	1/2	1/2	1/2
Natural Abundance	100%	1.108%	99.985%
Magnetic Moment	17.236	10.705	2.79
Resonance Frequency for 2.3 T Field	40.4 MHz	25.1 MHz	100 MHz
Relative Sensitivity	0.066	0.016	1
Max Nuclear Overhauser Effect	2.24	1.99	0.5

The phosphorus isotope has a NMR detection sensitivity 6.6% of the proton: however, its detection sensitivity compares favourably with carbon. Modern pulsed methods of Fourier transform NMR are capable of obtaining spectra of excellent signal to noise ratio in a reasonable time (4 - 10 mins).

The Nuclear Overhauser Effect

When a nucleus of interest is bound to hydrogen, coupling will occur and normal NMR splitting patterns are produced, sometimes excessively complicating the spectrum. By strongly irradiating the hydrogen nuclei resonance frequency saturation of the energy levels occurs and the splittings that complicate the spectrum disappear. However, a redistribution of spin populations takes place in the energy levels of the nuclei of interest which produce an increased magnetisation. When the nuclei relax via dipole - dipole relaxation mechanisms an enhanced signal intensity is observed. This is known as the Nuclear Overhauser effect (N.O.E.) and is defined as follows, (12):

$$NOE = 1 + \frac{\gamma_H}{2\gamma_x}$$

where γ_H = magnetisation for a proton

γ_x = magnetisation for the nucleus of interest (P-31)

When x = P-31 , the P-31 signal is enhanced 2.24 times (NOE = 2.24) if the Nuclear Overhauser effect is fully operative. However, no protons are directly bonded to phosphorus in the organophosphorus compounds studied in this section, therefore the NOE is likely to be non-operative.

Relaxation Phenomena

The spins of I = 1/2 nuclei, when placed in a magnetic field can be considered to align themselves either parallel or antiparallel to the field with a slight predominance in the former state. There is thus a net magnetic moment (vector sum of those of the individual nuclei) pointing along the magnetic field (z axis).

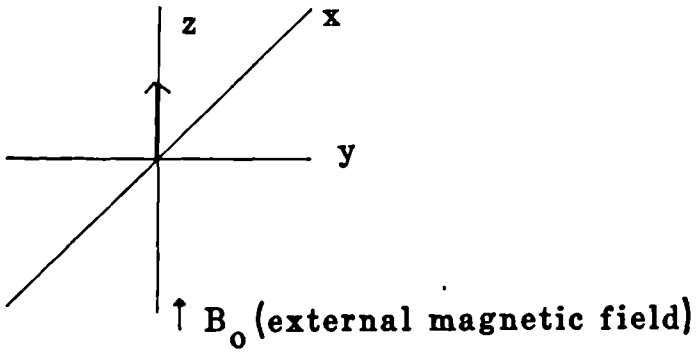

The magnetic moment of a radiofrequency pulse of the requisite length and direction (along the x axis) will disturb the net magnetisation by 90° producing a magnetic moment along the y axis.

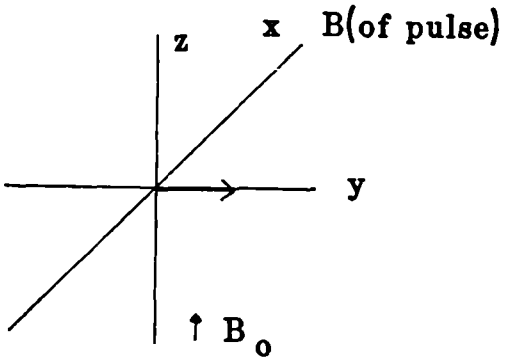

Return to the equilibrium position is slow and takes place by precession of the moment around the z axis. The process is governed by two time constants T_1 and T_2. T_1 describes the return to equilibrium of the magnetic vector in the z direction,

$$\frac{dMz}{dt} = -\frac{(Mz - Mo)}{T_1}$$

Mo = equilibrium magnetisation

Mz = z vector magnetisation at time t

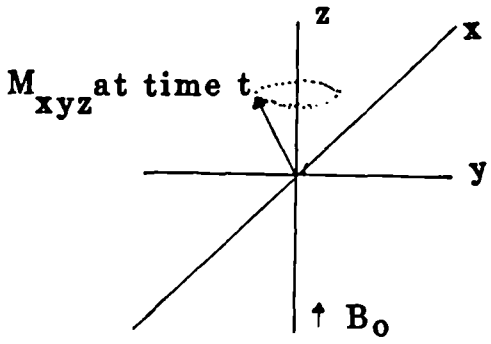

In the z and y directions, T_2 describes the vectors' return to equilibrium,

$$\frac{dMx}{dt} = -\frac{Mx}{T_2}$$

$$\frac{dMy}{dt} = -\frac{My}{T_2}$$

T_1 is the longitudinal relaxation time (spin-lattice). T_2 is the transverse relaxation time (spin-spin) The former governs the interaction of the relaxing nuclei with its surroundings. The probability of spontaneous emission of energy gained after the radio frequency pulse is small and restoration of the equilibrium populations occurs slowly through stimulated emission. Energy exchange occurs between the spin system and the lattice when the systems are mutually coupled via molecular motion. Owing to the random Brownian movements, small fluctuating fields develop in the liquid originating for instance in the neighbouring nuclear magnetic dipoles situated in the vicinity of the spin under consideration. Such local microscopic fields are capable, if they have the correct frequency and phases, of coupling with the spins and "bleeding off" the energy.

T_2 or transverse relaxation time refers to an interaction between the spins themselves. In a magnetic field the nuclear spins precess about the field direction with their phases at random. There is no net magnetisation transverse (Y-axis) to the field. When the radio frequency pulse is applied at the resonance frequency of the precessing spins, the spins precess in phase and a net transverse magnetisation is produced (Mxy). After the pulse is completed, this magnetisation is lost as the spins return to the random phase distribution at equilibrium. This "rate of dephasing" is governed by T_2 . In most cases T_1 approximately equals T_2 and T_1 is normally measured.

The Determination of T_1 Relaxation Times

T_1 relaxation time measurements were performed using the inversion recovery technique, (12) on the P-31 nuclei of the ZDDP's, basic ZDDP's and DDDiS's in cyclohexane and squalane. The results are given and discussed later in the text. The macroscopic spin magnetisation in thermal equilibrium is aligned along the Z axis, ie in the direction of the magnetic field Ho. Application of a 180 degree pulse rotates it onto the -Z axis, and is illustrated overleaf.

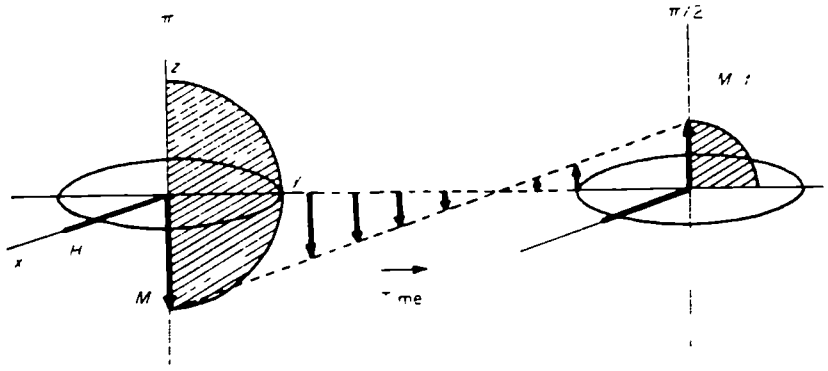

Since return to thermal equilibrium in general is exponential with time and the equilibrium value of $M_z(t)$ is M_∞, the process obeys the differential equation:

$$\frac{dM_z}{dt} = \frac{-M_\infty - M_z}{T_1}$$

which after integrating yields:

$$M_\infty - M_z = Ae^{-t/T_1}$$

For an inversion recovery experiment, $M_z(o) = -M_\infty$ by definition, and thus $A = 2M_\infty$

and hence $M_\infty - M_z = 2M_\infty e^{-t/T_1}$

At a time $t(t \ll T_1)$ after the initial perturbing pulse has elapsed, the magnetisation has partially recovered. If a 90 degree observing pulse is applied the resulting FID is collected and Fourier transformed in the usual manner, the relative intensities of the various lines reflect their individual relaxation times. The experiment is thus characterised by the following pulse sequence:

$(180^\circ - t - 90^\circ - T)n$

Precise data is obtained by varying t and plotting $\ln [M_\infty - M(t)/M_\infty]$ against t, the time interval between the perturbing and observing pulse. The slope of the plot is equal to $1/T_1$. The results of T_1 measurements are given and discussed later, in section 7.4.4.

Quantitative Determination

Both relaxation and nuclear Overhauser effects have to be considered in any quantitative or semi-quantitative determinations involving NMR. The more slowly relaxing nuclear energy levels will become saturated and a reduced signal intensity is observed relative to a species with quicker relaxing species. Both effects may make the normally integrated NMR spectrum unrepresentative of the quantities of nuclei present.

7.4.2 Experimental

The following reactions between ZDDP's or basic ZDDP's and CHP were followed kinetically by P-31 NMR at a probe temperature of 30 deg C:-

a) 0.04M n-octyl ZDDP and 0.12M CHP in squalane.

b) 0.04M n-octyl ZDDP and 0.12M CHP in cyclohexane.

c) 0.04M n-octyl ZDDP and 0.12M CHP in nitrobenzene.

d) 0.01M n-butyl basic ZDDP and 0.12M CHP in cyclohexane.

e) 0.038M n-butyl basic ZDDP and 0.43M CHP in nitrobenzene.

The instrument used was a Joel FX90Q spectrometer with operating conditions as follows:-

	Sample Volume	6 cm
	Tube	10 mm diameter
	Temperature	30 deg C
Observation	(Observation frequency	36.2 MHz
Channel	(Sweep width	74 KHz
Decouple	(Irradiation frequency	89.55 MHz
Channel	(Irradiation sweep width	54.25 KHz
	Pulse	90° (31.5 μ sec)
	Data points	8192 x 2 (Double precision)
	Spectral width	5000Hz
	Filter	2500 Hz
	Number of transients	variable (Typically 100)
	Pulse delay	0.8 secs
	Decoupling mode	complete
	Lock	Deuterium in (5 mm diameter tube suspended in the 10 mm diameter tube)
	Acquisition times	0.41 sec

The samples were run under conditions of complete proton decoupling at all times. The sample tube was sealed to inhibit oxygen diffusion into the system. Tributyl phosphate, dissolved in the deuterated chloroform contained in the 5 mm diameter inner tube of a similar phosphorus content as the ZDDP or basic ZDDP was used as a reference signal. The intensity ratios relative to tributyl phosphate were calculated for the various P-31 signals and were plotted against time. The plotted time is the time corresponding to the mid-point of the accumulation period.

Results

Figs 7.4.1 to 7.4.5 depict the changes in the P-31 NMR signals with time at 30 deg C. The variation of the P-31 NMR signal intensity ratios (relative to tributyl phosphate) with time are plotted in figs 7.4.6 to 7.4.10. During reactions a), b) and d) a white solid precipitated. IR spectroscopy and AA spectroscopy indicated that the white solid was zinc sulphate.

Discussion

P-31 kinetic studies following reactions a) and b) indicate that n-octyl ZDDP is converted very quickly at ambient temperatures to basic ZDDP and DDDiS. Various authors (1-8), have characterised the products of this reaction and postulated the following mechanism :

Reaction 1)

$$4\text{ZDDP} + R^1O_2H \longrightarrow \underbrace{[(RO)_2\ PS_2]_6Zn_4O}_{\text{Basic ZDDP}} + \underbrace{\left[\begin{array}{ccc} RO & & S \\ & \diagdown\!\!\diagup & \\ & P & \\ & \diagup\ \diagdown & \\ RO & & S \end{array}\right]_2}_{\text{DDDiS}} + R^1OH$$

This reaction is observed in the Raman kinetic runs as a fast production of DDDiS ν(P=S) at 660 cm^{-1} and ν(S-S) at 480 cm^{-1}) in the first 40 minutes, (See figs 7.3.5 and 7.3.6). The $\nu(PS_2)$ Raman intensity (relative to an internal standard) goes down slightly during this period,this is consistent with a change from 8 PS_2 groups to 6. The $\nu(PS_2)$ frequencies of basic ZDDP and normal ZDDP essentially are the same.

The half lives of this reaction can be determined by measuring the times during which either half of the ZDDP (normal salt) has been consumed or half the basic ZDDP has been produced. These data can be obtained from a plot of relative P-31 intensity (w.r.t TBP) against time (See figs 7.4.6 - 7.4.10). The half lives are listed in table 7.4.2 for the normal salt oxidation for reactions a) - c).

Table 7.4.2

Reaction with 0.12M CHP	Solvent	Half life (ZDDP determined)	Half life (BZDDP determined)
(a) 0.04M n-oct ZDDP	squalane	10 min	7 min
(b) 0.04M n-oct ZDDP	cyclohexane	5 min	6 min
(c) 0.04M n-oct ZDDP	nitrobenzene	46 min	55 min

Fig 7.4.1(a) P-31 NMR spectra of reaction A

at 30 deg C after 1) 0 2) 16 3) 48 minutes

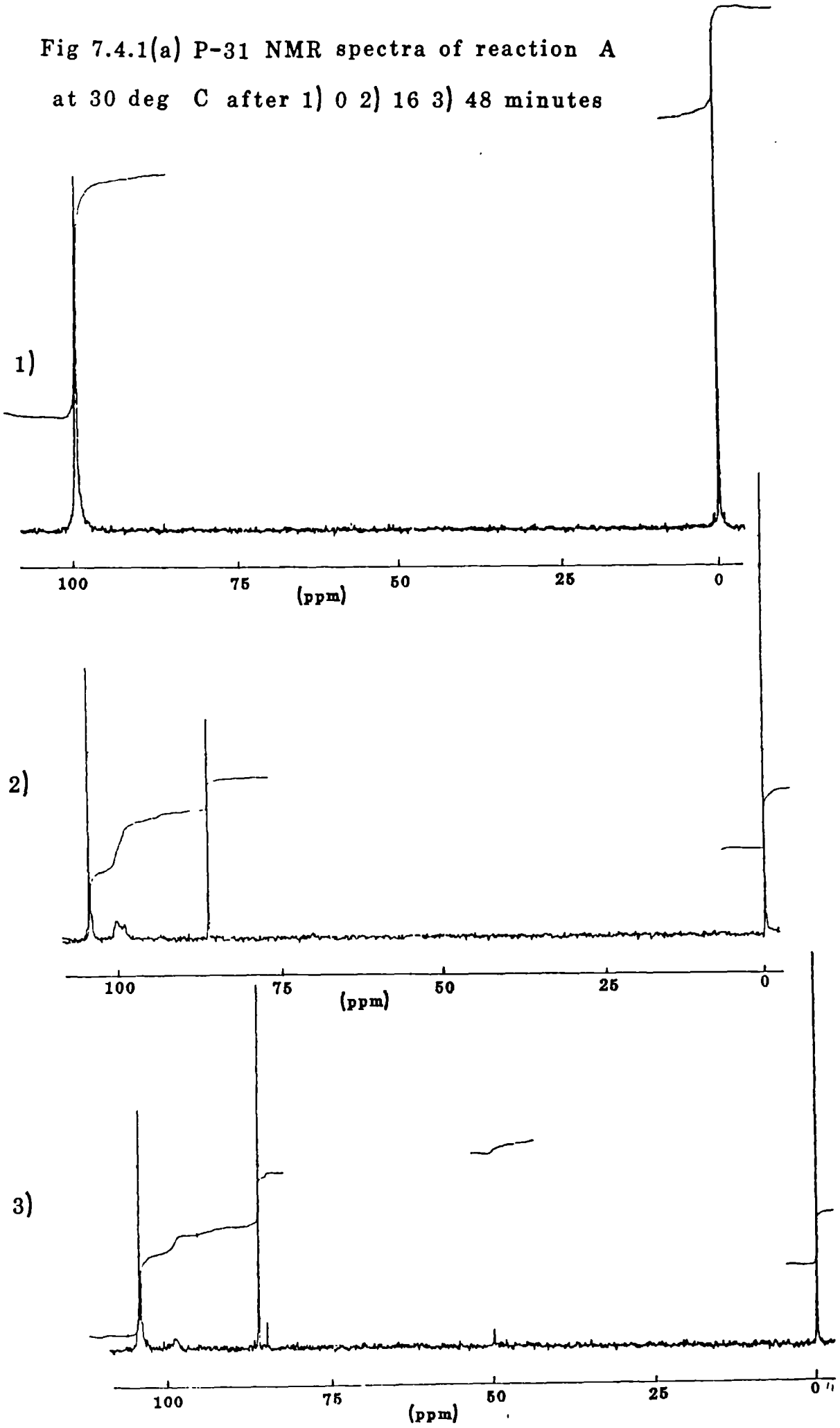

Fig 7.4.1(b) P-31 NMR spectra of reaction A
at 30 deg C after 4) 80 5) 155 6) 290 minutes

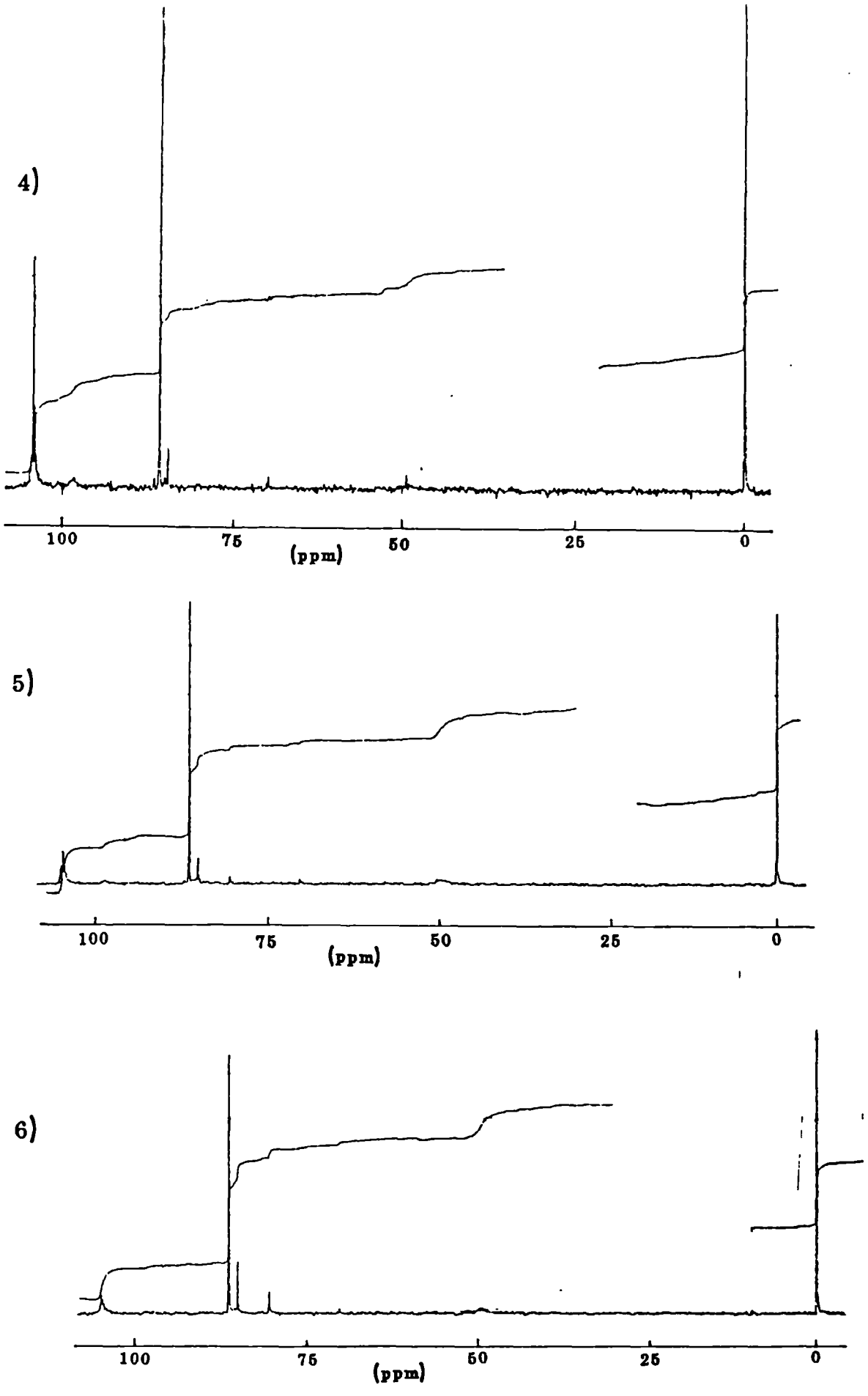

Fig 7.4.2 P-31 NMR spectra of reaction B

at 30 deg C after 1) 0 2) 22 3) 44 4) 71 5) 124 mins

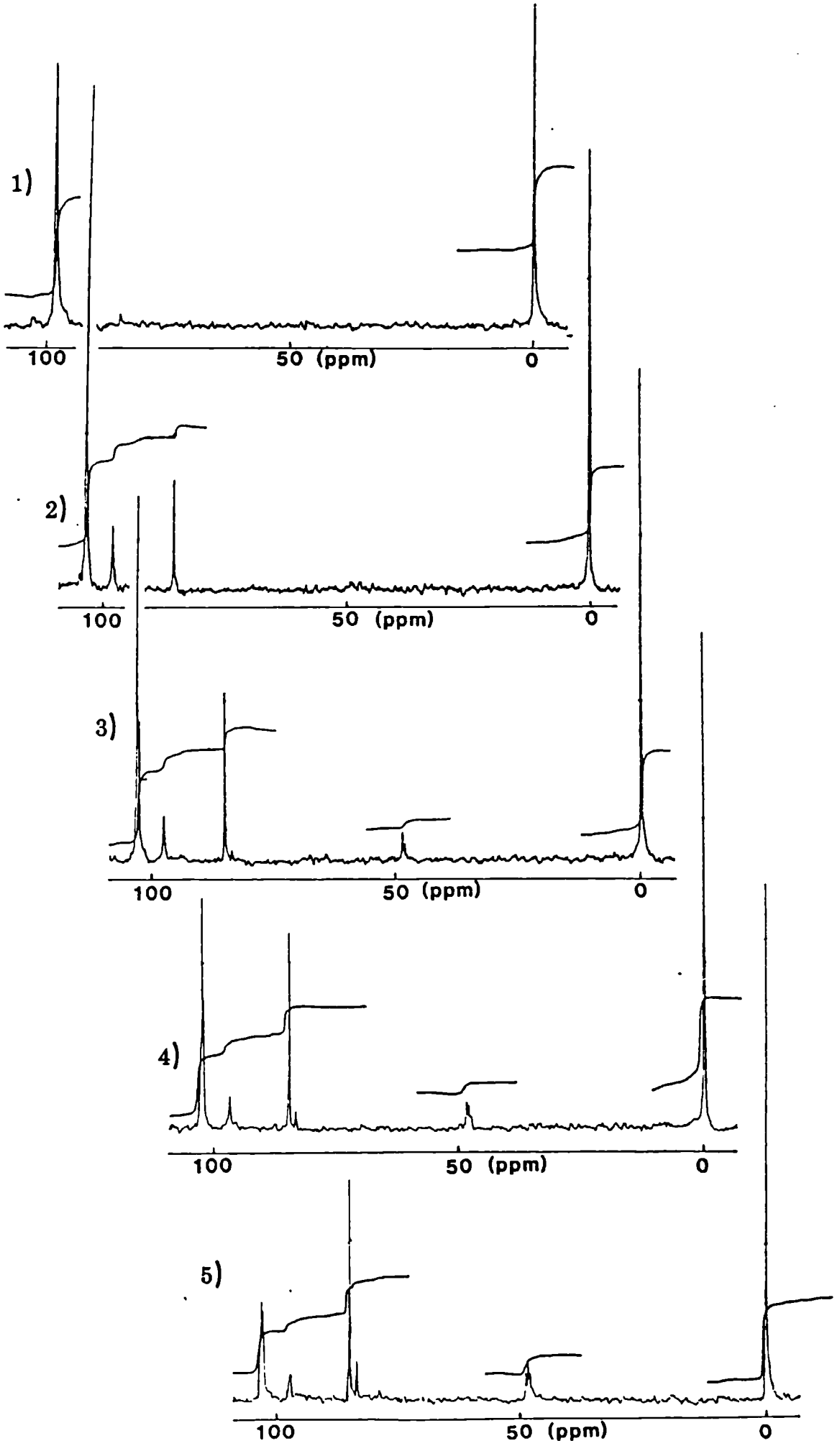

Fig 7.4.3 P-31 NMR spectra of reaction C

at 30 deg C after 1)0 2) 22 3) 44 4) 71 5) 124 mins

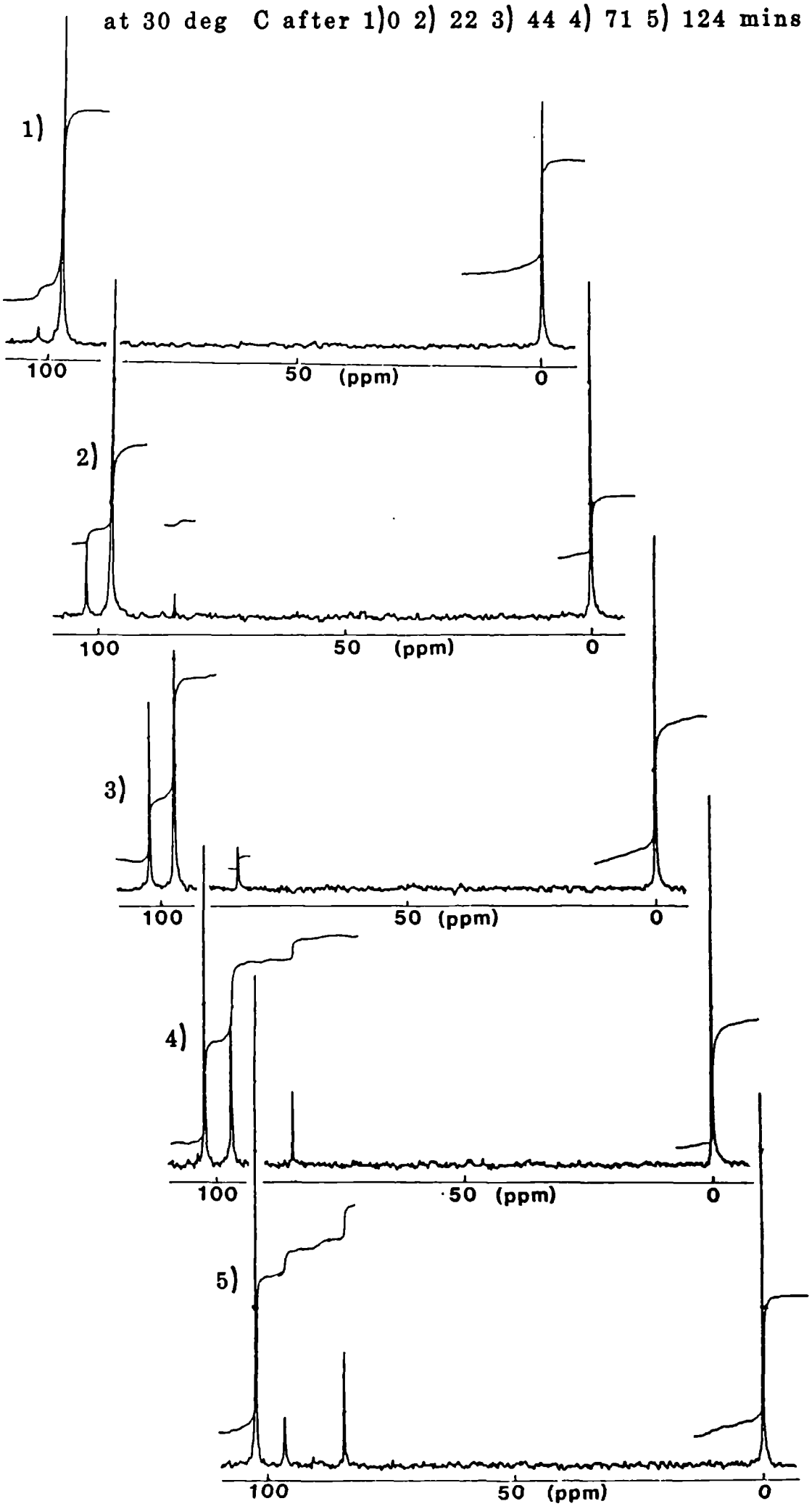

Fig 7.4.4 P-31 NMR spectra of reaction D at 30 deg C after 1)0 2) 17.5 3) 49 mins

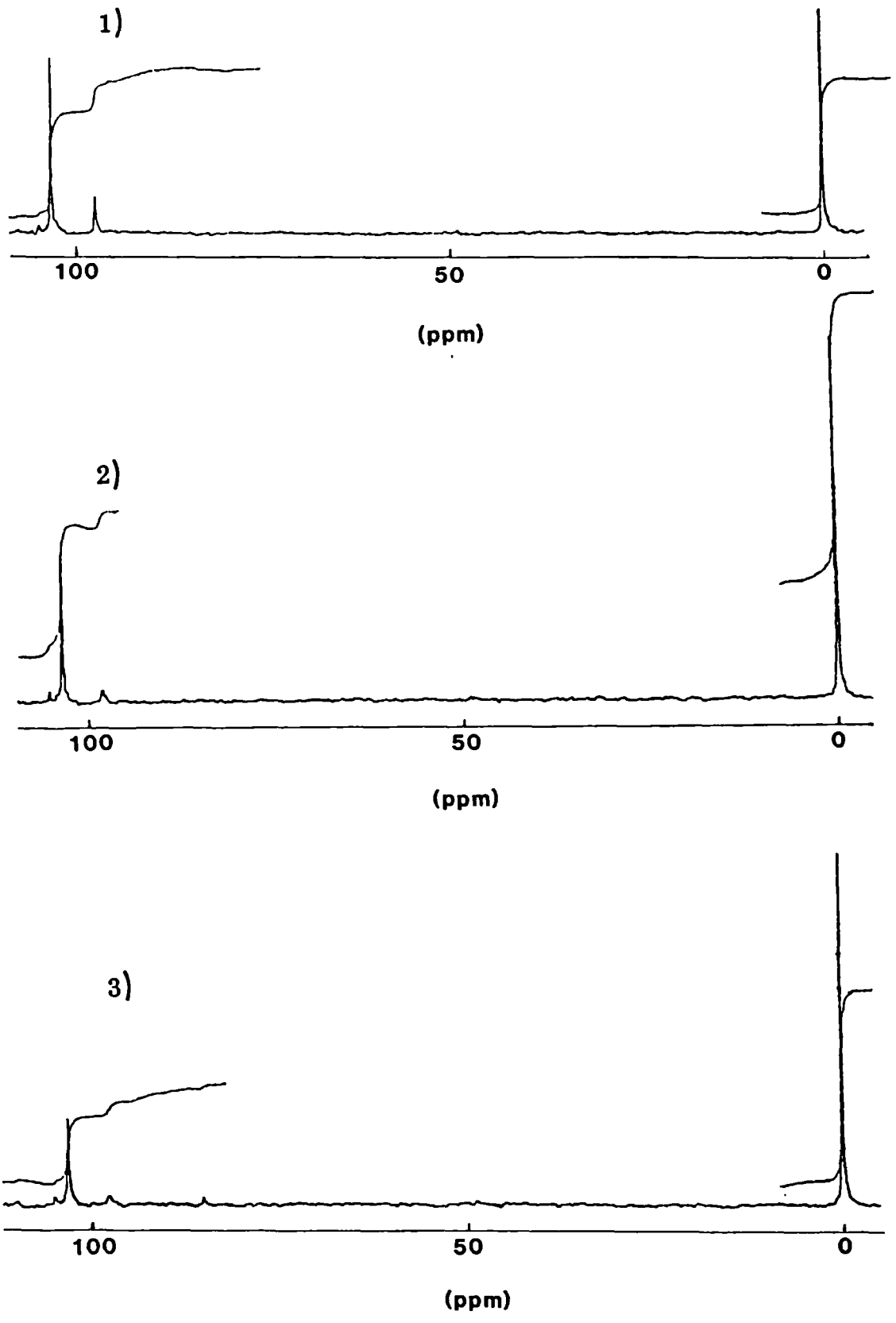

Fig 7.4.4 reaction D after

4) 71 5) 122.5 6) 280 mins

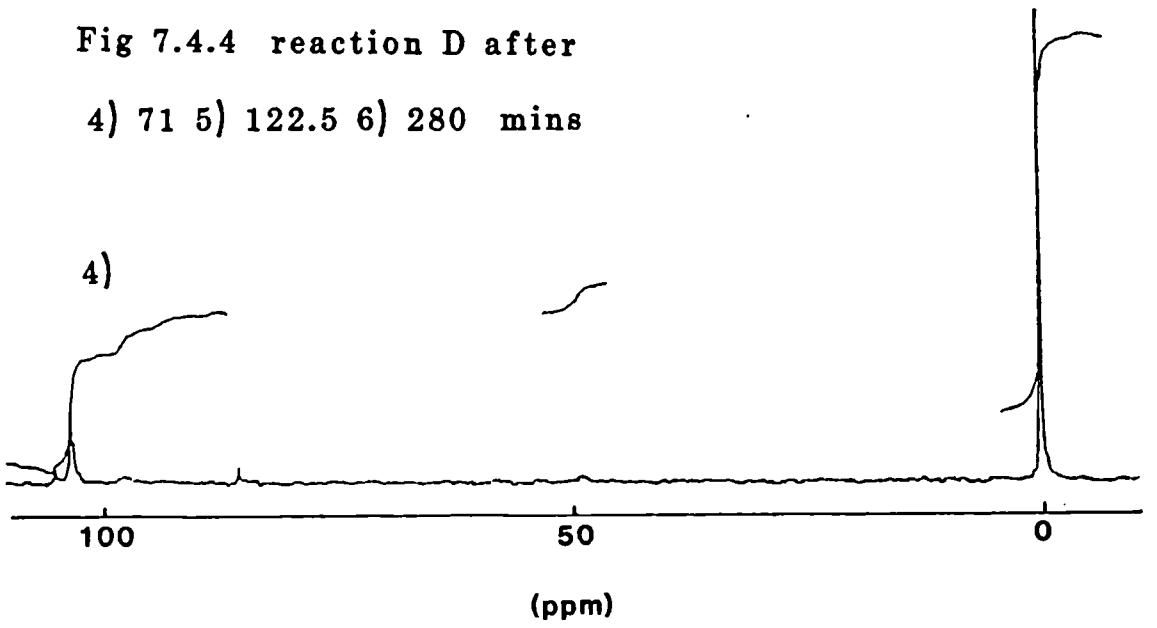

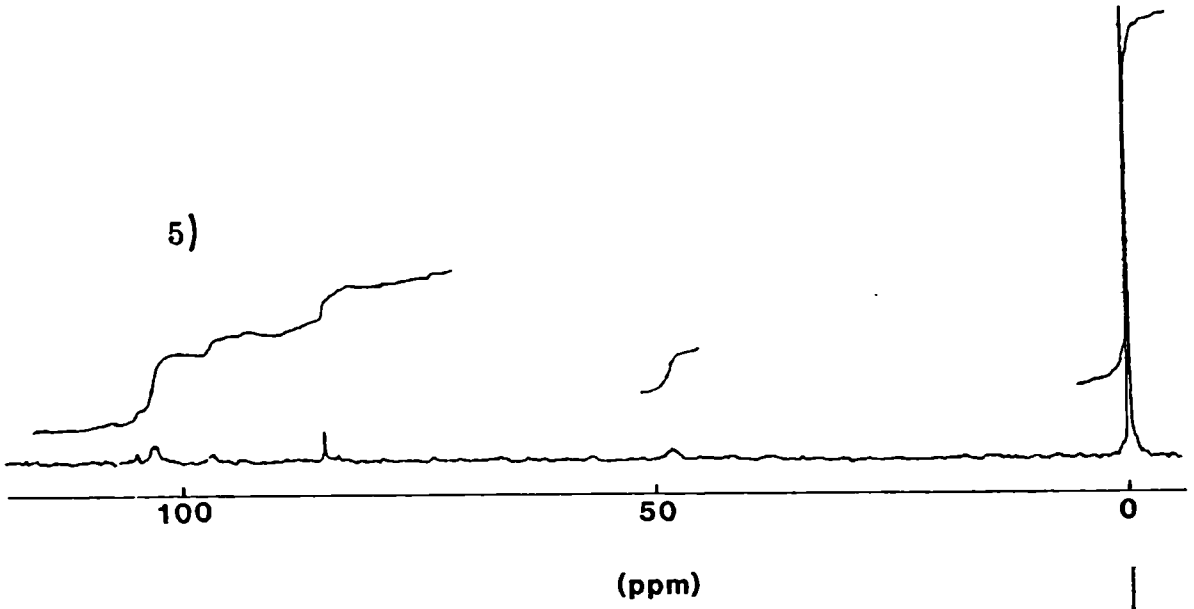

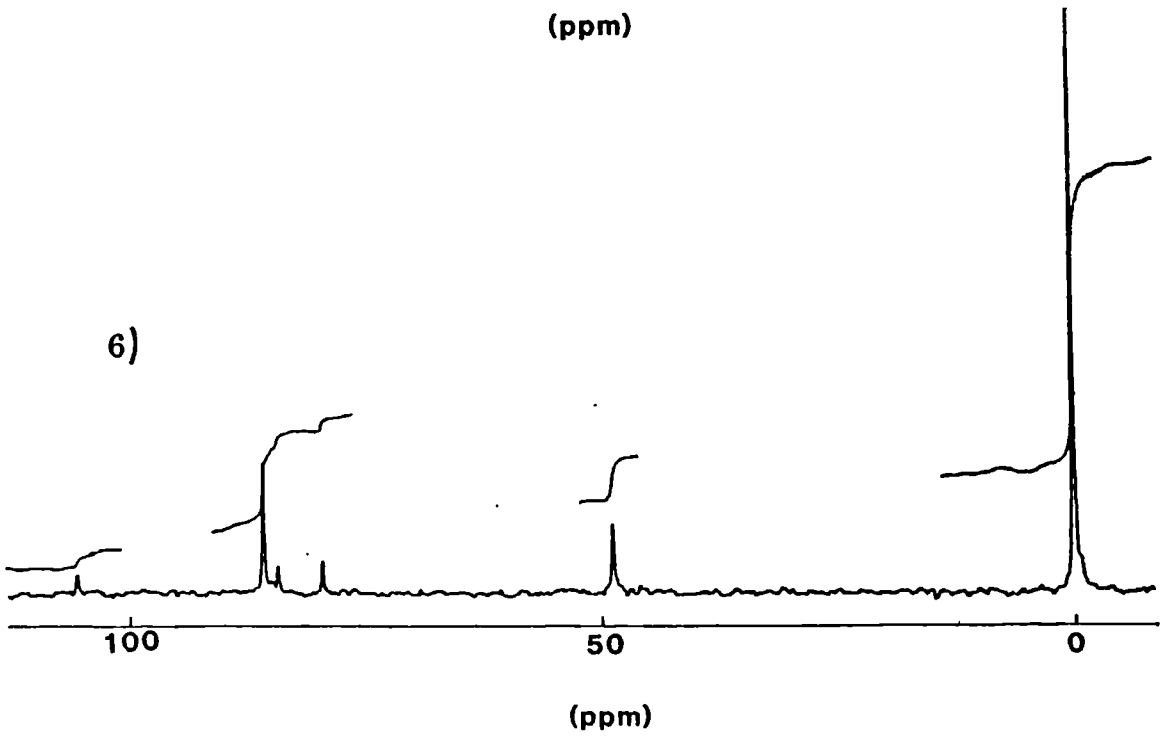

Fig 7.4.5 P-31 NMR spectra of reaction E at 30 deg C after 1)0 2) 62 3) 162 4) 312 5) 762mins

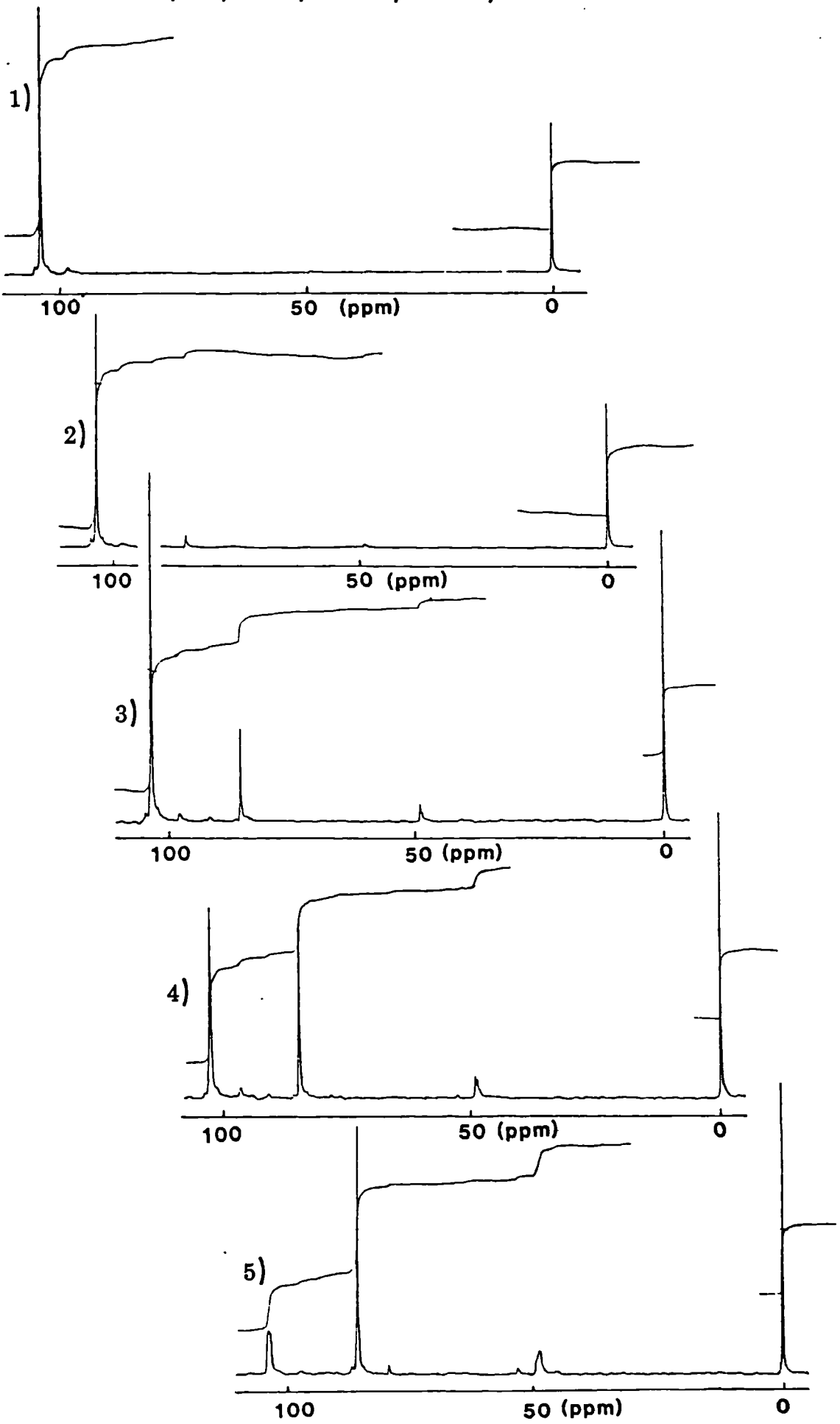

Fig 7.4.6

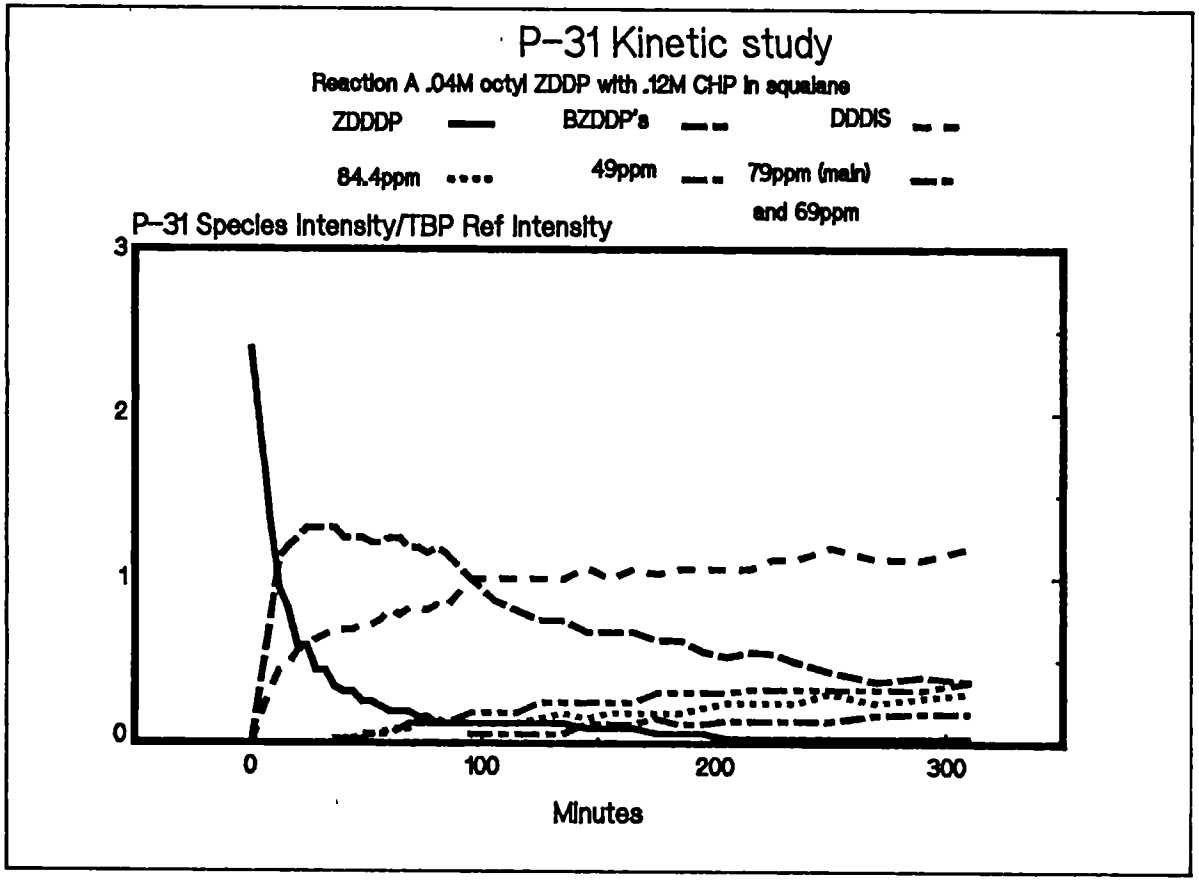
P-31 Kinetic study
Reaction A .04M octyl ZDDP with .12M CHP in squalane
ZDDDP
BZDDP's
DDDIS
84.4ppm
49ppm
79ppm (main) and 69ppm
P-31 Species Intensity/TBP Ref Intensity
3
2
1
0
0
100
200
300
Minutes

Fig 7.4.7

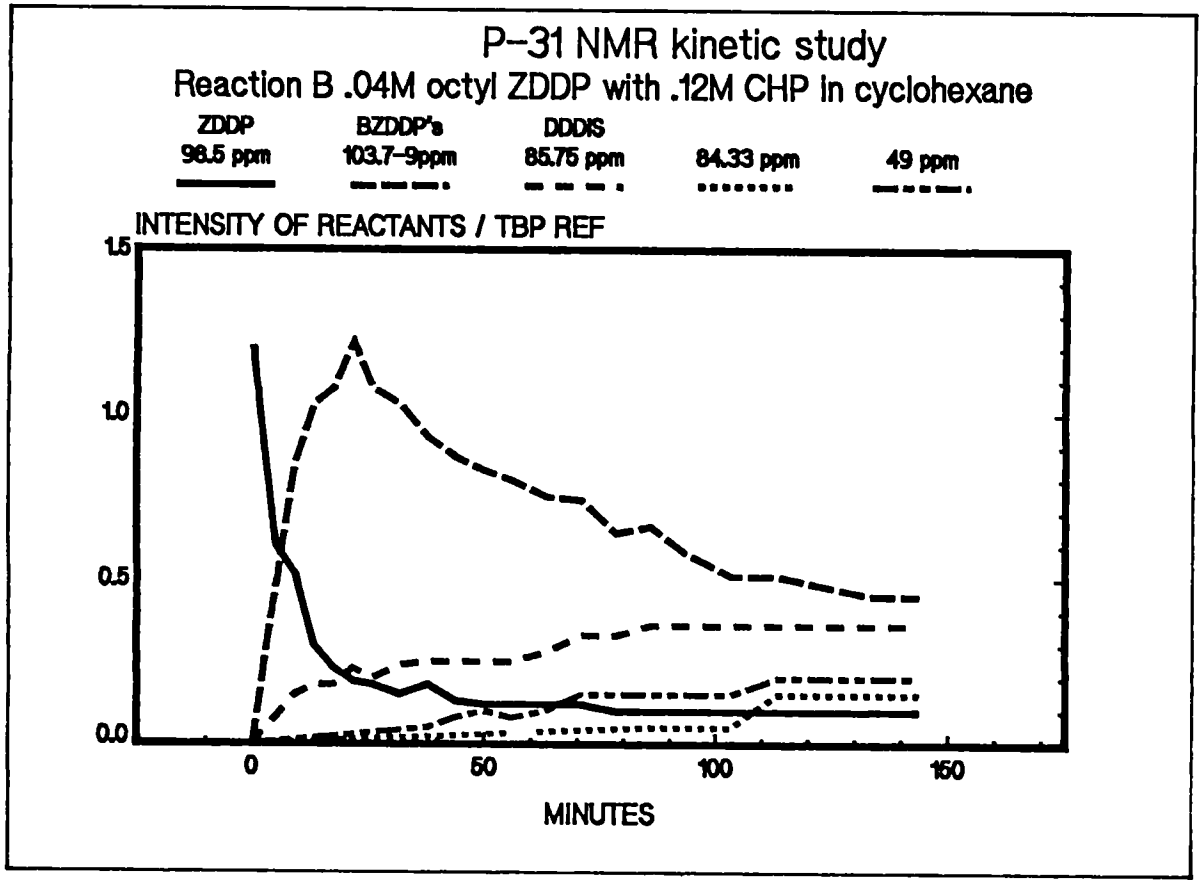
P-31 NMR kinetic study
Reaction B .04M octyl ZDDP with .12M CHP in cyclohexane
ZDDP
98.5 ppm
BZDDP's
103.7-9ppm
DDDIS
85.75 ppm
84.33 ppm
49 ppm
INTENSITY OF REACTANTS / TBP REF
1.5
1.0
0.5
0.0
0
50
100
150
MINUTES

Fig 7.4.8

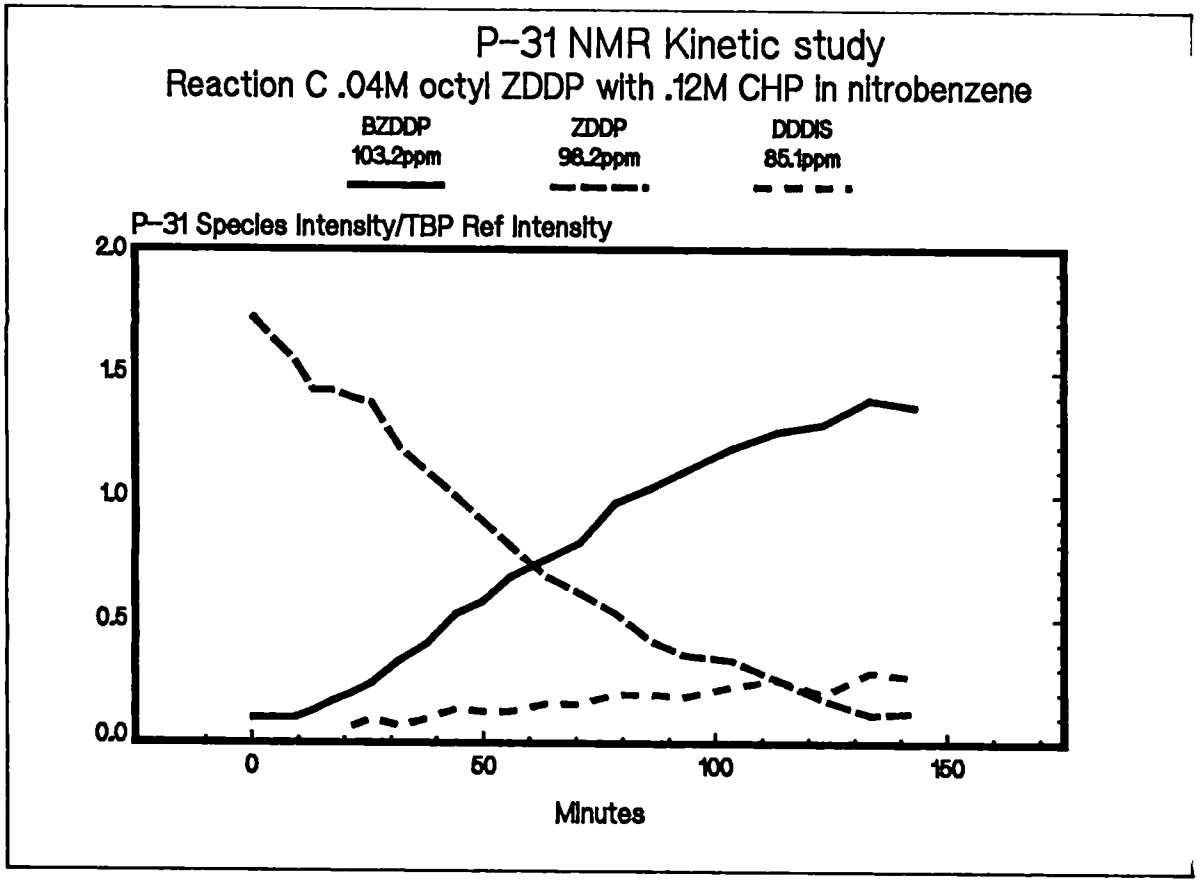
P-31 NMR Kinetic study
Reaction C .04M octyl ZDDP with .12M CHP in nitrobenzene
BZDDP
103.2ppm
ZDDP
98.2ppm
DDDIS
85.1ppm
P-31 Species Intensity/TBP Ref Intensity
2.0
1.5
1.0
0.5
0.0
0
50
100
150
Minutes

Fig 7.4.9

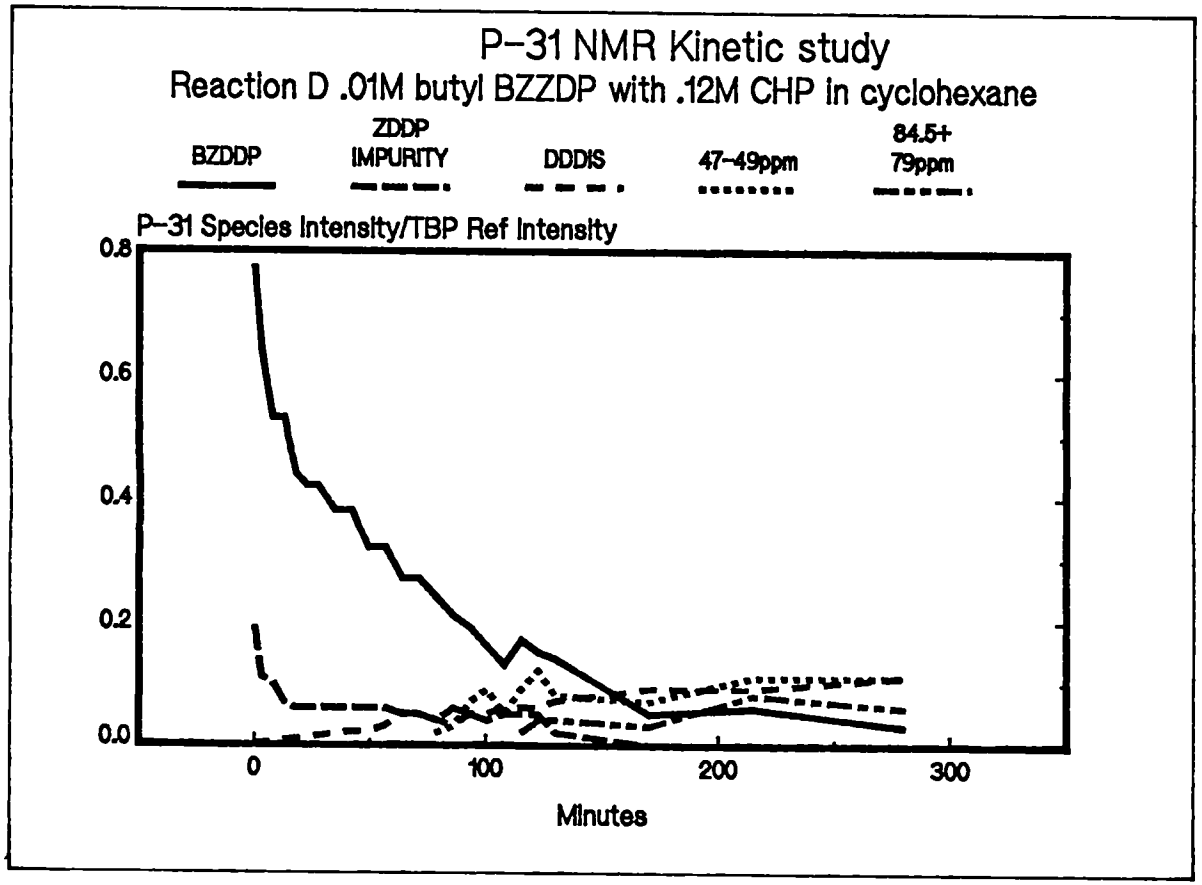
P-31 NMR Kinetic study
Reaction D .01M butyl BZZDP with .12M CHP in cyclohexane
BZDDP
ZDDP IMPURITY
DDDIS
47-49ppm
84.5+ 79ppm
P-31 Species Intensity/TBP Ref Intensity
0.8
0.6
0.4
0.2
0.0
0
100
200
300
Minutes

Fig 7.4.10

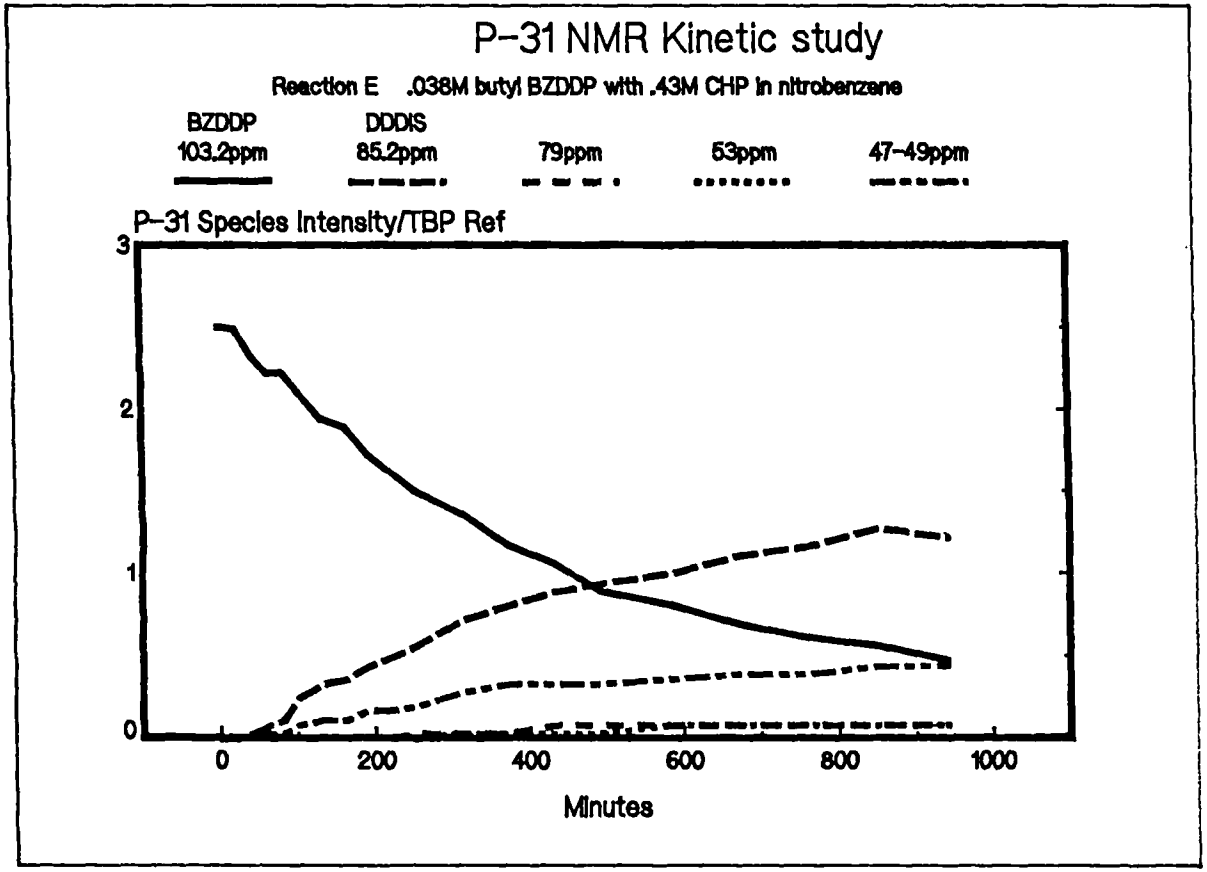
P-31 NMR Kinetic study
Reaction E .038M butyl BZDDP with .43M CHP in nitrobenzene
BZDDP
103.2ppm
DDDIS
85.2ppm
79ppm
53ppm
47-49ppm
P-31 Species Intensity/TBP Ref
3
2
1
0
0
200
400
600
800
1000
Minutes

The oxidation of n-octyl ZDDP is much slower in nitrobenzene than in cyclohexane and squalane. Close examination of the octyl-basic salt P-31 NMR signal reveals that the basic salt gives a doublet (mainly 103.9 ppm but also 103.7ppm) in squalane and cyclohexane whilst the basic salt produced in nitrobenzene gives a singlet (103.2ppm). After the normal salt oxidation, CHP is present in excess and therefore basic salt oxidation occurs. The less prominent basic ZDDP peak (103.7ppm) observed in squalane and cyclohexane is produced by either of the following mechanisms:
Reaction 2) which competes with reaction 1):

$$xZDDP + yR'OOH \longrightarrow \underset{(103.7\ ppm)}{\text{uncharacterized BZDDP}} + DDDiS + R'OH$$

Or Reaction mechanism 3), which is a successive oxidation of BZZDP mechanism

i) $$4ZDDP + R'OOH \longrightarrow \underset{(103.9\ ppm)}{OZn_4[PS_2(OR)_2]_6} + DDDiS + R'OH$$

ii) $$OZn_4[PS_2(OR)_2]_6 + xR'OOH \longrightarrow \underset{(103.7\ ppm)}{\text{uncharacterized BZDDP}} + \text{other organophoshates} + R'OH$$

The species $HOZn[PS_2(OR)_2]$ is a possible candidate for the uncharacterized basic ZDDP because it has a chemical shift of approximately 103 ppm with respect to phosphoric acid (13,14), which is approximately 103.7 ppm relative to tributyl phosphate. In nitrobenzene only one octyl basic ZDDP is observed 103.2 ppm (See fig 7.4.3), reaction (c)). Reaction e) the oxidation of n-butyl basic ZDDP in nitrobenzene indicates that the basic ZDDP signal does not become a doublet throughout the course of the experiment. It is likely therefore, that in nitrobenzene mechanism may be different or the BZDDP products formed have the same P-31 chemical shifts in nitrobenzene.

Table 7.4.3 displays the P-31 chemical shifts relative to tributyl phosphate of the compounds involved in the n-octyl normal salt oxidation in cyclohexane (reaction b) and nitrobenzene (reaction c).

Table 7.4.3

Chemical Shifts (ppm) relative to TBP

	cyclohexane	nitrobenzene
n-octyl BZDDP's	103.9 + 103.7	103.2
n-octyl normal ZDDP	98.7	98.2
n-octyl DDDiS	85.75	85.1

Changes in P-31 chemical shifts due to differences in the polarity of the solvent have been documented for various metal DDP's by Glidewell (15). Because of this change in chemical shift it is not possible to determine which of the basic salts observed in cyclohexane corresponds to the basic salt observed in nitrobenzene.

Table 7.4.4 shows the half lives for the oxidation of basic ZDDP's (combined 103.7 ppm 103.9 ppm signals) determined from the plot of the variation of the ratios of the basic ZDDP intensities (combined) to the tributyl phosphate signal with time for reactions a) - e).

Table 7.4.4

Reaction	Solvent	Half Life
a)	squalane	125 min
b)	cyclohexane	70 min
c)	nitrobenzene	-
	(no depletion of basic ZDDP occurred during the analysis period.)	
d)	cyclohexane	40 min
e)	nitrobenzene	340 min

(half lives were calculated assuming that complete consumption of basic ZDDP occurs).

From the plot,(see fig 7.4.11),of the intensities of the 103.9 ppm basic ZDDP and the 103.7 ppm basic ZDDP for reaction b) against time it is evident that the 103.7 ppm basic ZDDP, because it is more resiliant to oxidation than the 103.9 ppm basic salt, contributes more to the combined basic ZDDP half life.

Summary

The following trends of reactivity have been derived from the P-31 NMR oxidation studies:-

i) cyclohexane > squalane >> nitrobenzene

ii) normal ZDDP > basic ZDDP (103.9 ppm in cyclohexane) > basic ZDDP (103.7 ppm in cyclohexane)

iii) n-butyl basic ZDDP > n-octyl basic ZDDP.

The viscosity of squalane is much higher than that of cyclohexane, thereby possibly reducing the pre-exponential factor, and in turn reducing the rate of reaction (of mechanisms 1) and 2) or 3). The reduction of the rate in nitrobenzene as a solvent, compared to cyclohexane or squalane, may possibly be accounted for in terms of activation process. Thus, the energy of the reactant may be lowered : ie. the reactant may be stabilized by solvation, or alternatively the transition state may be increased in energy (destabilized) relative to the cyclohexane or squalane solvents. In either case the activation energy of the reaction is increased, so that the rate of reaction is lowered.

Fig 7.4.11 Formation and decomposition of basic ZDDP's
In reaction B .04M octyl ZDDP with .12M CHP in cyclohexane

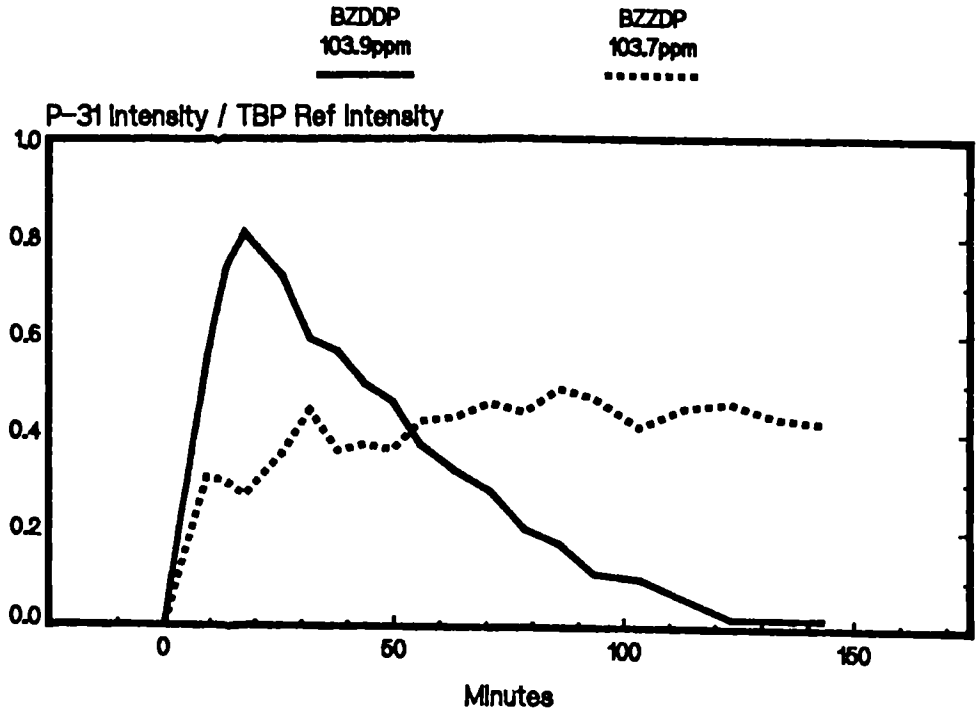

7.4.3 The Assignment of the Products from n-Octyl Basic ZDDP and n-Butyl Basic ZDDP Oxidation Reactions

n-Octyl DDDiS is most certainly an oxidation product from the reaction of n-octyl 103.9 ppm basic ZDDP and cumene hydroperoxide. We can identify DDDiS by observing the ν(S-S) and ν(P=S) bands in the Raman and the 85.75 ppm P-31 signal in cyclohexane. However, the oxidation of n-butyl basic ZDDP (reaction d) in cyclohexane indicates that even when over half of the basic salt has been consumed only a weak DDDiS signal is observable. The Raman kinetic analysis of the oxidation of 0.01 M n-butyl basic ZDDP by 0.12 M CHP in cyclohexane shows that DDDiS formation begins slowly as the basic salt is decomposed and then accelerates . DDDiS is produced from the oxidation of n-butyl basic ZDDP in nitrobenzene. The DDDiS can be identified by a P-31 signal of 85.2 ppm.

The P-31 signals of the compounds formed from the oxidation of the basic ZDDP's are more easily observable in squalane than cyclohexane. Unfortunately, basic n-butyl ZDDP has a low solubility in squalane. The first products formed are most probably derived from the oxidation of the basic n-octyl ZDDP with a P-31 chemical shift of 103.9ppm in reaction a). These compounds have P-31 chemical shifts of 49 and 84.41 ppm respectively and begin to appear after *approximately 40 minutes in reaction a)* along with DDDiS (85.75 ppm). After approximately 90 minutes organophosphorus compounds with chemical shifts of 79 ppm and 69 ppm begin to appear in reaction a). It is difficult to assess which of the two basic ZDDP's (103.9 ppm or 103.7 ppm) the compounds originate from. When considering reaction b) a signal at 49 ppm is detected after approximately 30 minutes and after 80 minutes the P-31 NMR spectrum indicates the presence of a signal at 84.33 ppm. However, bands at 79 ppm and 69 ppm were not observed or were present in quantities too small to be detected above the spectrum baseline.

During the course of the observation period of reaction c) no basic n-octyl ZDDP decomposition occurred. Analysis of the P-31 data of reaction d) indicates that a similar reaction profile is produced but the P-31 signals of the compounds formed are weaker than may be expected.The 49 ppm signal was seen after approximately 70 minutes, however, over half of the basic salt had then been oxidised. Peaks at 84.7 ppm and 79.3 ppm appear after 120 minutes. During the course of the reaction a shoulder on the 104.2 ppm basic ZDDP signal at 103.9 ppm becomes observable: therefore tentively we predict that mechanism 3, a successive BZDDP oxidation, is the correct reaction scheme, in cyclohexane and squalane, in preference to mechanism 2. The observed distribution of organophosphorus compounds produced during reaction e), differs from those formed from the oxidation of n-butyl and n-octyl basic ZDDP's throughout the course of reactions a), b) and d) in the following ways:

1) no shoulder appears on the basic n-butyl ZDDP P-31 signal during the basic ZDDP oxidation.

2) there is no evidence of the production of organophosphorus compounds with chemical shifts of approximately 84 ppm and 69 ppm.

3) a weak signal at 53 ppm is detectable after 200 minutes.

4) the DDDiS P-31 signal (85.2 ppm) is more prominent.

P A Willermet and S K Kandah (9), studied the reaction of n-octyl ZDDP with peroxy radicals. The peroxy radicals were generated by the decomposition of azo-bis-isobutylnitrile (AIBN) in an oxygenated solution of hexadecane at 90 deg C. The products of the reaction of 0.0195M n-octyl ZDDP and radicals generated from the decomposition of between 0.0078M and 0.0197M AIBN, were analysed by P-31 NMR. Deposits of $ZnSO_4$ were produced in the reaction. Table 7.4.5 compares the chemical shifts and assignments of organophosphorus compounds characterised by Willermet and Kandah and those observed in this work.

The studies performed by Willermet and Kandah were carried out at temperatures too high to determine whether any basic ZDDP is formed from the reaction of n-octyl ZDDP with peroxy radicals. With the exception of DDDiS all the compounds we have detected are derived from the oxidation of basic ZDDP's and not from n-octyl ZDDP. There are distinct similarities in the distribution of organophosphorus compounds produced by both the reaction of n-alkyl basic ZDDP's with peroxy radicals and that of basic n-alkyl ZDDP's with hydroperoxides. The probable implication is that the products seen by Willermet and Kandah are associated with the decomposition of basic ZDDP's produced from the oxidation of the normal ZDDP salt by peroxy radicals. In our studies no compound with a chemical shift of 61 ppm was detected. In reactions a), b) and d) a signal at 84.4 ppm was observed unique to our work, having a chemical shift very similar to that of DDPA. This assignment is particularly unlikely because our Raman studies have indicated that DDPA is immediately oxidised by hydroperoxides to give DDDiS. Stothers and Robinson (16)*, stated that the magnitudes of the P-31 chemical shifts decrease (become less positive) in the following order: Ar = Aromatic

$(RO)_2P(O)OAr\rangle$ $(RO)_2P(O)SAr\rangle$ $(RO)_2P(S)(OAr)\rangle$ $(RO)_2P(S)SAr$

Table 7.4.6 displays various organophosphorus compounds which may be disregarded as possible assignments for the compounds with chemical shifts of 49 ppm and 84.41 ppm observed in the kinetic studies. The data reflects the trend discussed by Stothers and Robinson.

* This trend is misquoted by Harris et al (17), and Wittman and Pudmer (13) as:

$$(RO)_2P(O)O^{\ominus} \rangle (RO)_2P(O)S^{\ominus} \rangle (RO)_2P(S)O^{\ominus} \rangle (RO)_2P(S)S^{\ominus}$$

This is probably correct but not representative of work performed by Stothers and Robinson.

Table 7.4.5 P-31 NMR

CHEMICAL SHIFTS OF PRODUCTS FROM THE FOLLOWING REACTIONS

n-oct ZDDP reaction with $RO_2\cdot$ at 90°C in hexadecane (9)	n-oct ZDDP and n-oct basic ZDDP reaction with CHP at 30°C in squalane (this work)	n-Bu basic ZDDP reaction with CHP at 30°C in nitrobenzene (this work)	Possible Assignment
Chemical shift relative to H_3PO_4 (ppm)	Chemical shift relative to TBP (ppm)	Chemical shift relative to TBP (ppm)	
85	85.75	85	$[(RO)_2PS_2]_2$
	84.4	-	unidentified dithiophosphate
79	79.75	79	$[(RO)_2PS]_2S$
68	68.75	-	$(RO)_3P(S)$
61	-	-	$(RS)_3P(O)$
53	-	53	$(RS)_2(RO)P(O)$
47	49	47-49	Unidentified monothiophosphate

Table 7.4.6

Compound R = Octyl	Literature analogue	Chemical shift(ppm)	Ref No
$(RO)_2P(S)SP(O)(OR)_2$	$(C_2H_5O)_2\overset{\alpha}{P}(S)S\overset{\beta}{P}(O)(OC_2H5)_2$	α 78, β 14	18
$(S)P(OR))_2(SR)$	$(S)P(OC_2H_5)_2(S\ C_4H_9)$	95	18
$(O)P(OR)_2(SR)$	$(O)P(SC_2H_5)(OC_2H_5)_2$	26	18
$((RO)_2P(O)OP(S)(OR)_2$	$(C_2H_5O)_2\overset{\alpha}{P}(O)O\overset{\beta}{P}(S)(OC_2H_5)_2$	α−15, β+54	18
$[(RO)_2P(S)]_2O$	$[(C_2H_5O)_2P(S)]_2O$	52	17
$(RO)_2P(O)SZn^{\oplus}$	$(C_9H_{19}-C_6H_4-O)_2P(O)SZn^{\oplus}$	38·3	9
$(RO)(RS)P(O)SZn^{\oplus}$	$(C_9H_{19}-C_6H_4-O)$ \ $P(O)SZn^{\oplus}$ / $(C_9H_{19}-C_6H_4-S)$	95·3	9
$(RO)_2P(S)SZn^{\oplus}$	$(C_9H_{19}-C_6H_4-O)_2O(S)SZn^{\oplus}$	101.4	9
	$(C_4H_9-O)_2P(S)SZn^{\oplus}$	99	19

The following mechanism was proposed by Rossi and Imperato (2), for the reaction of isopropyl ZDDP with cumene hydroperoxide.

$$4ZDDP + R^1O_2H \longrightarrow [(RO)_2PS_2]_6Zn_4O + \text{DDDiS} + R^1OH$$

Basic ZDDP

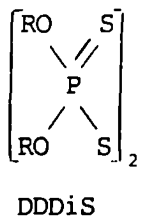

$$\downarrow 15\ R^1O_2H$$

$$1{\cdot}5\ \text{DDDiS} + 1{\cdot}5\ [(RO)_2P(O)S]_2 + Zn\ O + 15R^1OH + 3\ Zn\ SO_4$$

Ivanor and Kateva (20), discovered by monitoring the consumption of a hydroperoxide, that ZDDP's react much more slowly in polar solvents than in non-polar solvents. Our P-31 kinetic studies confirm this observation. The authors (20), argued that in non-polar and polar solvents the reaction proceeds via a hexavalent zinc complex intermediate where "zinc possess Sp^3d^3 hybridization analogous to that observed in its zinc co-ordination compounds with ammonia".

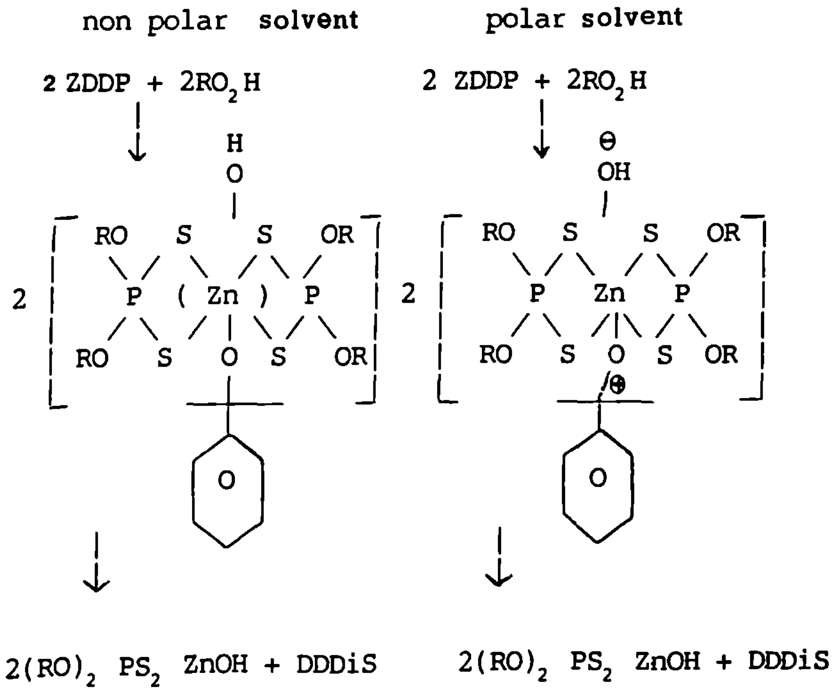

We believe that the mechanisms postulated by Rossi and Imperato (2) and also Ivanor and Ketava (20), are oversimplifications for the reasons listed below:-

1) The P-31 chemical shift of $[(RO)_2P(O)S]_2$ is likely to be very similar to the P-31 signal of 14.8 ppm for the oxygen adjacent phosphorus atom of $(OR)_2P(S)$-S-$P(O)(OR)_2$ however, a signal is not observed in this region.

2) Two basic salts are produced in the reaction sequence (103.9 ppm and 103.7 ppm) with different susceptibilities to oxidation in non-polar solvents.

3) Rossi and Imperato predicted that two compounds are formed from the oxidation of basic ZDDP (DDDiS and $[(RO)_2P(O)S)]_2$; however, the P-31 studies show that more than two compounds are produced, with chemical shifts of 84.41, 79.75, 69,49 and 85.75ppm in cyclohexane or squalane and 85, 79, 53, 49 and 47 ppm in nitrobenzene.

4) The dithiophosphate ligands are much larger than NH_3 molecules: therefore steric hinderance will probably inhibit the formation of a hexavalent intermediate complex.

The following reaction schemes are proposed on the basis of the P-31 kinetic studies:-

1) in squalane R = octyl R' = cumyl

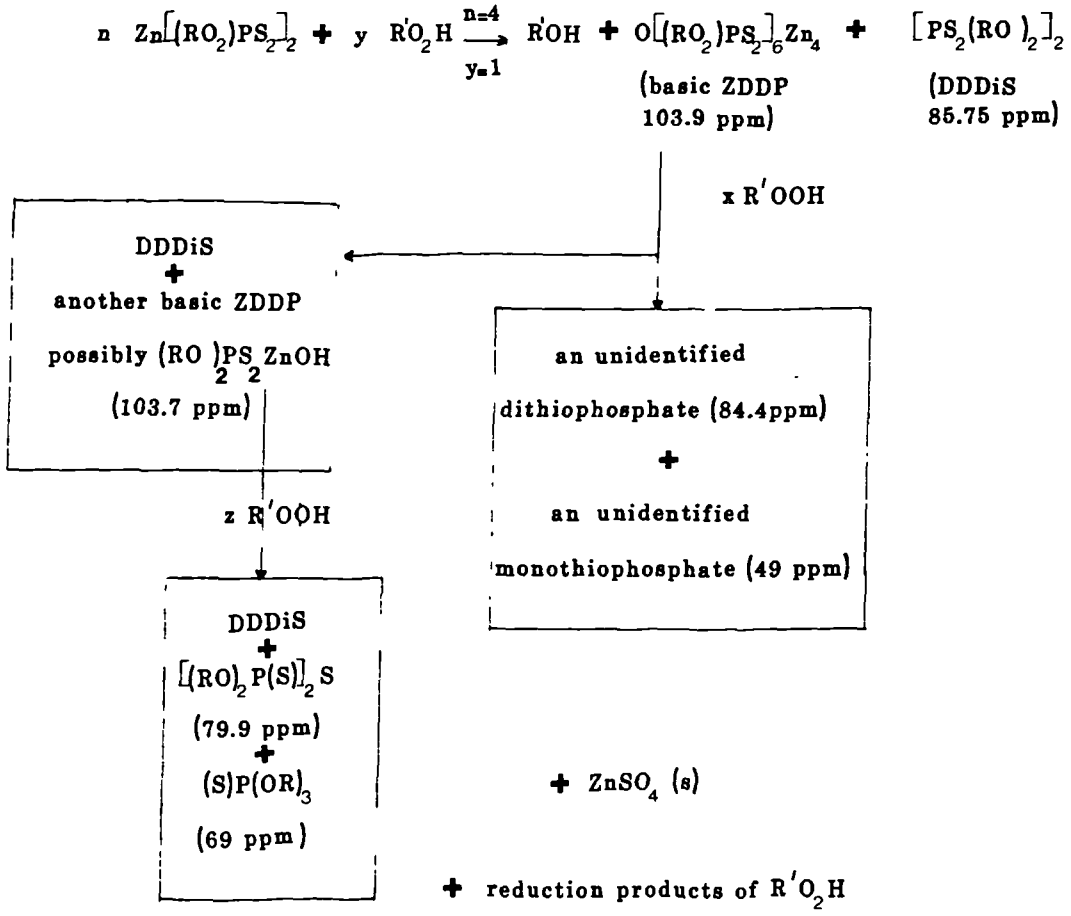

——→ indicates a successive basic ZDDP oxidation mechanism

2) in nitrobenzene R=n-butyl R'= cumyl

the first step is equivalent to reaction mechanism 1)

4ZDDP + R'OOH → basic ZDDP + DDDiS + R'OH

then basic ZDDP + zR'OOH → DDDiS + unidentified monothiophosphates or other basic ZDDP(s)

where z is unknown

(85.2 ppm) (49,47 ppm)

+ also,

small quantities of

$[(RO)_2P(S)]_2S$ + $(RO)(SR)_2P(O)$

(79 ppm) (53 ppm)

+

CHP reduction products

+

$ZnSO_4$ (solvated)

7.4.4 An Assessment of the Quantitative Value of the P-31 NMR and Raman Kinetic Studies

In our P-31 NMR studies we find that the sum of all the relative intensities (w.r.t TBP) remains reasonably constant throughout the course of the reaction, for reaction a), reaction c) and reaction e).

Therefore the assumptions that i) each phosphorus nucleus relaxes at the same rate and ii) the integrated intensity is a direct measure of the concentration of the compounds appear justified. These assumptions are less valid for reactions performed in cyclohexane (reactions b) and d)). During the course of reaction d) (0.01M basic butyl ZDDP reacting with 0.12 CHP) the sum of the relative P-31 NMR intensities decreases by 50%.

Table 7.4.7 (a and b) compares the P-31 NMR and Raman determined molarities of DDDiS after the complete oxidation of the normal ZDDP, and at other listed times during the course of the basic ZDDP oxidation. The results agree well with the stoicheiometry of the first stage of ZDDP oxidation (mechanism 1), ie. approximately 0.01 moles of DDDiS are produced from 0.04 moles of ZDDP. P-31 analysis of the oxidation of 0.01 M n-octyl ZDDP by 0.12 M CHP in squalane and the Raman studies described in section 7.3 indicate that a further quantity of DDDiS, equivalent to a 0.01 M solution,is formed from the basic ZDDP decomposition. This value agrees well with the quantity of DDDiS produced from the oxidation of 0.01 M n-butyl basic ZDDP by 0.12 M CHP in cyclohexane determined by Raman spectroscopic analysis detailed in section 7.3. However an estimation of the amount of DDDiS by P-31 NMR analysis formed from the oxidation of 0.01 M n-butyl basic ZDDP by 0.12 M CHP in cyclohexane is lower by a factor of three. Presently this anomaly cannot be explained.

T_1 relaxation times were calculated for various ZDDP's and ZDDP-related organophosphorus compounds in cyclohexane and squalane by the inversion-recovery technique. Table 7.4.8 on page 115 lists the various determined relaxation times at 30 deg C.

Table 7.4.7a ZDDP oxidation

	Raman studies (26°C)				^{31}P NMR studies (30°C)			
Reaction	Time (min)	[DDDiS]* ν(P=S)calc	[DDDiS] ν(S-S)calc	Time (min)	$I^{31}P$ ZDDP / $I^{31}P$ TBP	$I^{31}P$ DDDiS / $I^{31}P$ TBP	Θ [DDDiS]	$I^{31}P$ BZDDP (at time t) / $I^{31}P$ DDDiS
0.04M n-octyl ZDDP with 0.12M CHP in squalane	0	Θ	-	0	2.4	-	-	
	30	0.013M	-	25	0.6	0.6	0.01M	2.2
	140	0.02M	-	140	0.1	1	0.017M	
	-	-	-	250	0.03	1.1	0.018M	
0.04M n-octyl ZDDP with 0.12M CHP in cyclohexane	not performed			0	1.3	-		
				20	0.19	0.23	0.0073M	5.3
				60	0.12	0.28	0.0086M	
				140	0.1	0.36	0.011M	
0.04M n-octyl ZDDP with 0.12M CHP in nitrobenzene	not performed			0	1.74	-	-	
				140		0.29	0.007M	4.7
0.04M n-butyl ZDDP with 0.12M CHP in cyclohexane	40	0.012M	0.014M		not performed			
	140	0.019M	0.018M					

* The DDDiS concentration was determined by comparing the ν(S-S) and ν(P=S) intensities with a standard DDDiS solution.

Θ The DDDiS concentration was calculated assuming that each ^{31}P nuclus relaxes at the same rate and therefore the initial ZDDP ratio (relative to TBP) corresponds to a 0.08M ^{31}P nuclus solution, as each ZDDP molecule contains two phosphorus atoms.

Table 7.4.7b Basic ZDDP Oxidation

Reaction	Raman studies (26°C) Time (Min)	[DDDiS] ν(P=S) calc	[DDDiS] ν(S-S) calc	^{31}P studies (30°C) Time (min)	$I^{31}P$ BZDDP / $I^{31}P$ TBP	$I^{31}P$ DDDiS / $I^{31}P$ TBP	[DDDiS]	$I^{31}P$ BZDDP(t=o) / $I^{31}P$ DDDiS
0.01M basic butyl ZDDP with 0.12M CHP in cyclohexane	0	0	0	0	0.774			
	58	0.00082M	0.0027M	42	0.38	0.02	0.0009M	
	177	0.01M	0.0083M	170	0.05	0.068	0.0028M	11
0.038M basic butyl ZDDP with 0.43M CHP in nitrobenzene				0	2.5	-		
	not recorded			242	1.7	0.44	0.02M	
				960	0.47	1.22	0.056M	2

Table 7.4.8

Compound	Solvent	T_1 Relaxation Time (Seconds)
n-octyl DDDiS	squalane	2.6
n-butyl DDDis	squalane	3
n-octyl DDDiS	cyclohexane	7
n-butyl DDDiS	cyclohexane	9.2
n-octyl ZDDP	squalane	2
n-butyl ZDDP	squalane	2.6
n-octyl ZDDP	cyclohexane	9
n-butyl ZDDP	cyclohexane	9
n-butyl Basic ZDDP*	squalane	2.1

*low solubility in squalane, however a sufficient P-31 NMR signal was produced to conduct the experiments.

The greater length of the octyl chain enables the octyl derivatives to relax faster than the n-butyl compounds. The P-31 nuclei of large organophosphorus molecules relax faster than smaller molecules, therefore the following trend of relaxation times is observed: Basic ZDDP < ZDDP < DDDiS

The P-31 nuclei relax more quickly in squalane than in cyclohexane because the squalane solvent molecules are "tumbling" more slowly thereby "bleeding off" the energy of the excited nuclei more effectively. It is for this reason that the organophosphorus compounds are more easily detected in squalane than in cyclohexane. This inversion-recovery data indicate that in the same solvent ZDDP's and DDDiS have similar T_1 relaxation times, however the kinetic studies would suggest that DDDiS when compared to basic ZDDP (combined) relax more slowly in cyclohexane than squalane, this is emphasised by the following ratios which relate to corresponding points in the reactions where [bZDDP]/DDDiS are expected to be the same :-

In cyclohexane after 25 minutes, I P-31 n-octyl bZDDP / I P-31 n-octyl DDDiS = 5.2

In squalane after 30 minutes, I P-31 n-octyl bZDDP / I P-31 n-octyl DDDiS = 2.2

The theoretical value obtained from the mechanism proposed by Burn (1), (see p. 103) assuming each P-31 nucleus relaxes at the same rate, should be 3. These differences therefore cannot be completely explained in terms of the T_1 relaxation time measurements, hence the method in its present stage of refinement has to be regarded as semi-quantitative. More accurate quantitative measurements of the studied reactions are needed.

1) Burn A.J., Cecil R. and Young V.O., J. Inst. Petroleum. 1971, 57, 319

2) Rossi E. and Imparato L., Chem. and Ind. (Milan). 1971, 53, 838

3) Ivanor S.K. and Ketava I., Neftekhimiya. 1971, 11, 290

4) Sher V.V., Markova Y.I., Khanakava L.G., Kuzmina G.N. and Sanin P.I., Neftekhimiya, 1973, 13, 876

5) Grishna O.N. and Bashinova V.M., Neftekhimiya, 1974, 14,142

6) Wystrach V.P., Hook E.O. and Christopher G.C.M., J. Org. Chem. 1956, 21, 705

7) Dickert J.J. and Rowe C.N. J. Org. Chem. 1967, 32, 647

8) Brunton G., Gilbert B.C., and Mawby R.J., J.C.S. Perkin II, 1976, 650

9) Willermet P.A. and Kandah S.K., A.S.L.E. Trans. 1984, 27, 1, 67-72

10) Marshall G.L., Appl. Spectrosc. 1984, 38, 4, 522-6

11) Al Malaika and G. Scott, Eur. Poly. J, 1980, 16, 503-509

12) Wehrli F.W. and Wirthlim T, "Interpretation of ^{13}C NMR spectra", Heyden & Sons, Chapter 4, 129-151

13) Wittmans Z. and Pudmer E., A.S.L.E Trans. 1985, 28, 4, 426-430

14) Willermet P.A., Mahoney L.R., Bishop C.M., A.S.L.E. Trans 1980, 23, 2, 217-224

15) Glidewell C., Inorganica Chemica Acta 1977, 25, 159-163

16) Stothers J.B. and Robinson J.R., Canadian J. Chem. 1964, 42, 967

17) Harris R.K. et al, J.Chem.Soc. (A) 1967, 37-40

18) Crutchfield M.M., Dungan C.H., Letcher J.H., Mark J, Van Wazer J.R., "Topics in Phosphorus Chemistry", 1967, 5.

19) Coy R.C. and Jones R.B., A.S.L.E. Trans. 1981, 24, 1, 77-90

20) Ivanor S.K. and Kateva J.D., J. Poly. Sci. Symposium. 1976, No 54, 237-247